# POLITECNICO DI MILANO

Facoltà di Ingegneria Industriale

Corso di Laurea Specialistica in
Ingegneria Aeronautica


# Investigation of physical properties of paraffin based hybrid rocket fuels

Relatore: Prof. Luigi T. DE LUCA

Co-relatore: Ing. Mario KOBALD
DLR – Institute of Space Propulsion

Tesi di Laurea di:

Juri CARISSIMI Matr. 755434

Anno Accademico 2011 - 2012

# Contents

# List of Figures

# List of Tables

# Sommario

La propulsione ibrida combina i vantaggi della propulsione solida e di quella liquida, cioè : sicurezza intrinseca dovuta al separato stoccaggio di ossidante e combustibile, possibilità di accensioni e spegnimenti multipli, modulazione della spinta intervenendo sul flusso di ossidante. Finora lo sviluppo della tecnologia ibrida è stato rallentato dalla bassa velocità di regressione del grano di combustibile solido. Per ovviare a questo problema sono stati utilizzati differenti approcci: chimico basato sull'utilizzo di additivi energetici, fluidodinamico basato su un incremento della turbolenza del flusso, fisico basato sull'entrainment. L'entrainment è quel fenomeno per cui combustibili bassofondenti formano uno strato liquido sulla superficie solida del combustibile. Questo strato fuso, sottoposto ad un flusso tangenziale di ossidante, diventa instabile causando il trascinamento di goccioline nel flusso di ossidante e causando in ultimo un incremento della velocità di regressione.

Il presente lavoro, svolto presso il DLR - Istituto per la Propulsione Spaziale a Lampoldshausen, riguarda combustibili bassofondenti arricchiti con additivi energetici al fine di aumentare l'energia posseduta dal combustibile. Sono utilizzati additivi metallici come l'Alluminio ed additivi organici come Polietilene ed Acido Stearico. Si vuole caratterizzare l'influenza di due importanti proprietà fisiche quali la viscosità e la tensione superficiale sulla velocità di regressione.

La viscosità, in accordo con le ricerche di Karabeyoglu, ha un ruolo importante sulla velocità di regressione: bassi valori di viscosità conducono ad un incremento della velocità di regressione. Per questo motivo viene studiato il comportamento delle differenti formulazioni a partire da 200°C alla temperatura di fusione della paraffina. Si effettua una caratterizzazione in funzione della temperatura al fine di osservare le formulazioni che esibiscono i valori più limitati e le variazioni più marcate. Viene poi effettuata un'analisi in termini energetici delle formulazioni analizzando il comportamento del modulo elastico e del modulo viscoso in funzione della temperatura e della velocità angolare.

La tensione superficiale potrebbe anch'essa avere un ruolo importante che nel passato non è stato considerato. In questo lavoro si caratterizza l'andamento della tensione superficiale in funzione della temperatura, evidenziando la differenza rispetto alle paraffine pure, sia in termini di valori assoluti ad una data temperatura che in termini globali.

Da ultima viene effettuata una stima teorica mediante il software CEA dell'efficienza di combustione, dell'impulso specifico e dell'ammontare dei residui di combustione nel caso dell'impiego di Alluminio in diverse percentuali ed a differenti temperature.

Parole chiave: entrainment, tensione superficiale, viscosità, cere paraffiniche

# Analisi delle proprietà fisiche di combustibili per la propulsione ibrida a base di paraffina

## Introduzione

La propulsione ibrida, caratterizzata dal tentativo di combinare i vantaggi della propulsione liquida e della propulsione solida, ha un grosso limite dato dalla bassa velocità di regressione del combustibile solido. Questo problema non permette alte densità di spinta portando a geometrie del grano complesse e ad un'elevata quantità di residui incombusti.

Diversi metodi sono stati sperimentati per aumentare la velocità di regressione: il primo di questi è stato ridurre il flusso di calore dovuto alla gasificazione, ma l'effetto benefico è ridotto dall'incremento della superficie di soffiamento.

Un metodo differente consiste nell'utilizzare combustibili che fondono presso la superficie di regressione. In questa classe di combustibili sono comprese sostanze liquide o gassose che vengono congelate.

I combustibili solidi possono incorporare additivi energetici di tipo metallico al fine di migliorare le prestazioni e la densità.

Il modello su cui si basa questo metodo è l'entrainment [1].

Test sono stati realizzati presso AFRL ed ORBITEC [2] considerando differenti formulazioni: Pentano, HFI, Isopropanolo e Acetone a differenti flussi di ossidante. I risultati hanno mostrato un'incremento della velocità di regressione di 3-4 volte rispetto ad HTPB.

L'entrainment delle goccioline liquide, responsabile dell'incremento della velocità di regressione, è correlato a quattro quantità:

- pressione dinamica $P_d$
- spessore dello strato di combustibile liquido $h_l$
- viscosità $\mu$ dello strato liquido
- tensione superficiale $\sigma$

secondo la relazione:

$$\dot{m}_{ent} = \frac{P_d^{\alpha} h^{\beta}}{\mu_l^{\gamma} \sigma^{\pi}} \tag{1}$$

Gli esponenti di questa formula empirica differiscono a seconda della fonte, come mostrato in Tabella 1

Tabella 1: Valore esponenti per entrainment

| | $\alpha$ | $\beta$ | $\gamma$ | $\pi$ |
|---|---|---|---|---|
| Gater - L'Ecuyer [3] | 1.5 | 2 | 1 | 1 |
| Nigmatulin et al. [4] | 1 | 1 | - | - |
| Karabeyoglu [2] | 1-1.5 | - | $>\pi$ | $<\gamma$ |

## Analisi ottiche e termodinamica della combustione

Nakagawa ed Hikone [5] hanno analizzato la dipendenza della velocità di regressione dalla viscosità . Sono stati utilizzati slab di paraffina ed ossigeno in un combustore 2D. La viscosità varia additivando il combustibile con etilene-vinil acetato in percentuali del 10% e del 20%. La velocità di regressione misurata ha mostrato un legame con la viscosità del tipo $\mu^{-1/6}$ .

Considerando che generalmente l' entrainment si sviluppa in condizioni ben al di sopra delle condizioni critiche di pressione e temperatura, si hanno difficoltà a trovare un'espressione generale che descriva il fenomeno dell'entrainment. Esistono differenti correlazioni per esprimere le proprietà fisiche, come ad esempio quelle di Marano ed Holder [6], Magoulas e Tassios [7], o Gani. Per cere paraffiniche con numero di atomi di carbonio pari a circa 30 si ricavano una pressione critica di 6.5 bar ed una temperatura critica di circa 840 K.

Karabeyoglu et al [8] hanno predetto l'entrainment in condizioni subcritiche e supercritiche basandosi sulla relazione di Gater e L'Ecuyer ignorando però il contributo della tensione superficiale.

## Idruri metallici

Gli idruri metallici sono di grande interesse per la propulsione ibrida grazie alla loro capacità di immagazzinare elevate quantità di idrogeno. Inoltre sono in grado di incrementare la velocità di regressione mediante due meccanismi: il trasferimento di calore radiativo addizionale, dovuto alla combustione di idruri metallici e la loro bassa temperatura di decomposizione che incrementa la velocità di regressione a causa delle reazioni eterogenee che avvengono in superficie, presso lo strato limite fuso del combustibile.

Gli idruri metallici rivestono grande importanza a causa del loro basso peso molecolare che permette un incremento nei valori di impulso specifico.

## Attività Sperimentale

L'attività sperimentale ha coinvolto l'analisi di due importanti proprietà fisiche delle cere paraffiniche quali la tensione superficiale e la viscosità. Sono stati effettuati test considerando quattro diverse cere paraffiniche prodotte da Sasolwax: 0907, 1276, 6003 e 6805.

Sono state analizzate sia cere paraffiniche pure, sia additivate in percentuali diverse, con additivi metallici e con additivi organici. In particolare sono stati utilizzati: alluminio, polietileneglicole 6000, polietilene co-vinil-acetato, grafite ed acido stearico.

## Tensione Superficiale

Il primo parametro ad essere analizzato è stato la tensione superficiale. Questa proprietà fisica indica la capacità di un liquido di resistere ad una forza esterna applicata. La tensione superficiale è legata alla temperatura da una relazione lineare. Due relazioni teoriche legano temperatura e tensione superficiale: la Legge di Eötvös e la relazione di Guggenheim-Katayama. Nel presente lavoro viene utilizzato un tensiometro Krüss EasyDyne che misura la tensione superficiale all'interfaccia, con un range di misura 1-999 $mN/m$ con accuratezza 0.1 $mN/m$.

La tensione superficiale viene misurata a partire da una temperatura di circa 130°C fino alla temperatura di solidificazione. Generalmente vengono effettuate circa 35-40 misure per ogni test. La relazione lineare temperatura - tensione superficiale è ricavata attraverso una regressione lineare che permette di calcolare i valori di tensione superficiale fino alla $T_{av}$ (temperatura media tra punto di fusione e punto di ebollizione).

La figura Figura 1 mostra gli andamenti dei valori di tensione superficiale per le quattro cere paraffiniche pure, mentre in tabella Tabella 2 si riportano gli scostamenti percentuali in termini di tensione superficiale alla temperatura di 100°C ed alla $T_{av}$.

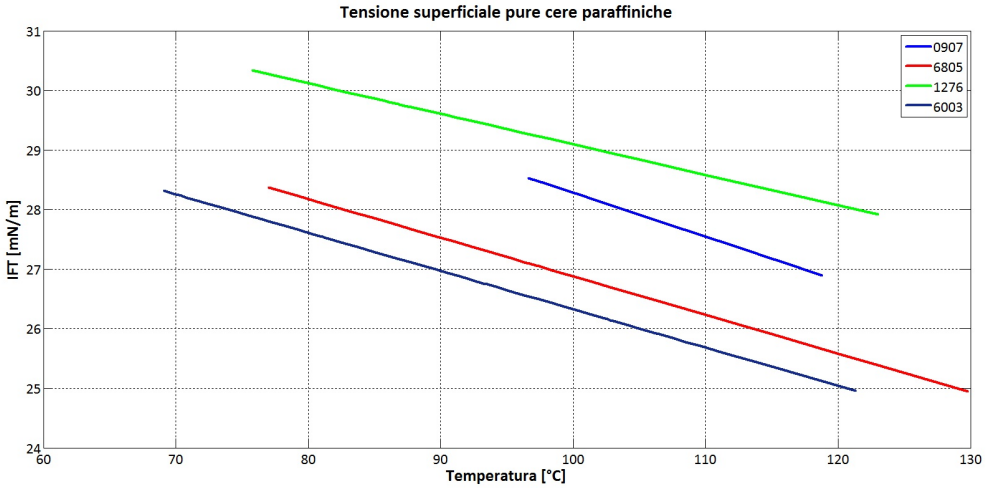


Figura 1: Valori di tensione superficiale per combustibili non additivati

Tabella 2: Confronto tensione superficiale all'interfaccia cere pure a 100°C

| Sasolwax | IFT [mN/m] | $\Delta_{IFT}$ [%] | $\Delta_{IFT}$ at $T_{av}$[%] |
|---|---|---|---|
| 6003 | 26.32 | - | - |
| 6805 | 26.88 | +2.08 | +0.87 |
| 0907 | 28.28 | +6.90 | -31.89 |
| 1276 | 29.09 | +9.50 | +28.18 |

Tabella 3: Coefficienti retta di regressione e valori di tensione superficiale a 100℃

| Formulazione | Coefficiente di pendenza | $\Delta_{slope}$ | $\Delta_{IFT}$ a 100℃ | $\Delta_{IFT}$ a $T_{ave}$ |
|---|---|---|---|---|
| Pure 0907 | -0.0736 | -% | -% | -% |
| 0907 + 2% Carbon Black | -0.0620 | -15.76% | -2.02% | +19.51% |
| 0907 + 10% PEG 6000 | -0.0825 | +12.09% | +0.64% | -17.33% |
| 0907 + 10% PECVA | -0.0755 | +2.58% | -0.53% | -5.44% |
| 0907 + 10% Stearic Acid | -0.0639 | -13.18% | -1.63% | +16.42% |
| 0907 + 10% Aluminum | -0.0677 | -8.01% | -2.09% | +7.17% |
| 0907 + 40% Aluminum | -0.0796 | +8.15% | -1.87% | -17.60% |
| Pure 6805 | -0.0648 | -% | -% | -% |
| 6805 + 1% Carbon Black | -0.0662 | +2.16% | +0.26% | -0.98% |
| 6805 + 10% PEG 6000 | -0.0586 | -9.57% | -0.30% | +5.70% |
| 6805 + 10% PECVA | -0.0612 | -5.56% | +2.42% | +7.60% |
| 6805 + 10% Stearic Acid | -0.0701 | +8.18% | -0.56% | -15.69% |
| Pure 1276 | -0.0512 | -% | -% | -% |
| 1276 + 1% Carbon Black | -0.0523 | +2.15% | -1.31% | -2.65% |
| 1276 + 10% PEG 6000 | -0.0879 | +71.68% | -0.24% | -29.17% |
| 1276 + 10% PECVA | -0.0527 | +2.93% | +0.28% | -0.77% |
| 1276 + 10% Stearic Acid | -0.0675 | +31.83% | -2.75% | -16.63% |
| Pure 6003 | -0.0643 | -% | -% | -% |
| 6003 + 1% Carbon Black | -0.0646 | +0.47% | +0.65% | +0.5% |
| 6003 + 10% PEG 6000 | -0.0629 | -2.18% | +1.06% | +3.09% |
| 6003 + 10% PECVA | -0.0624 | -2.95% | +4.29% | +8.83% |
| 6003 + 10% Stearic Acid | -0.0698 | +8.55% | +0.11% | -5.19% |
| 6003 + 10% Aluminum | -0.0622 | -3.27% | +0.49% | +2.84% |

Le cere paraffiniche 6003 e 6805 hanno la medesima pendenza negativa con una differenza nei valori di di tensione superficiale all'interfaccia pari al 2.08% , mentre Sasolwax 0907 presenta una pendenza negativa più marcata di Sasolwax 6003. Sasolwax 1276 ha una pendenza negativa debolmente superiore che causa un incremento dei valori di tensione superficiale del 9.5% a 100℃ e del 28.18% alla $T_{av}$.

Successivamente i test effettuati con cere paraffiniche pure sono ripetuti utilizzando additivi metallici ed organici come riportato in Tabella 3

Dalla Tabella 3 è possible notare come l'utilizzo di alcuni additivi, quali polietileneglicole, acido stearico ed in maniera più contenuta alluminio, causi una percettibile variazione della pendenza della curva di regressione. Generalmente l'acido stearico ha un effetto positivo, abbassando i valori di tensione superficiale del 5-15%, mentre la grafite ha un effetto trascurabile. Il polietileneglicole ha un effetto benefico particolarmente marcato nel caso di Sasolwax 0907 e 1276.

## Viscosità

La viscosità è stata misurata con un reometro rotazionale RheoStress 6000 con geometria plate-plate, avente range di misura $10^{-7} - 1500\ min^{-1}$ a sforzo costante ed

anche a rotazione costante. Il range di frequenza è $10^{-5} - 100$ Hz.

Il primo passo è stata la misurazione della viscosità in funzione della temperatura a partire da 200°C fino alla temperatura di solidificazione, come si vede in Figura 2.

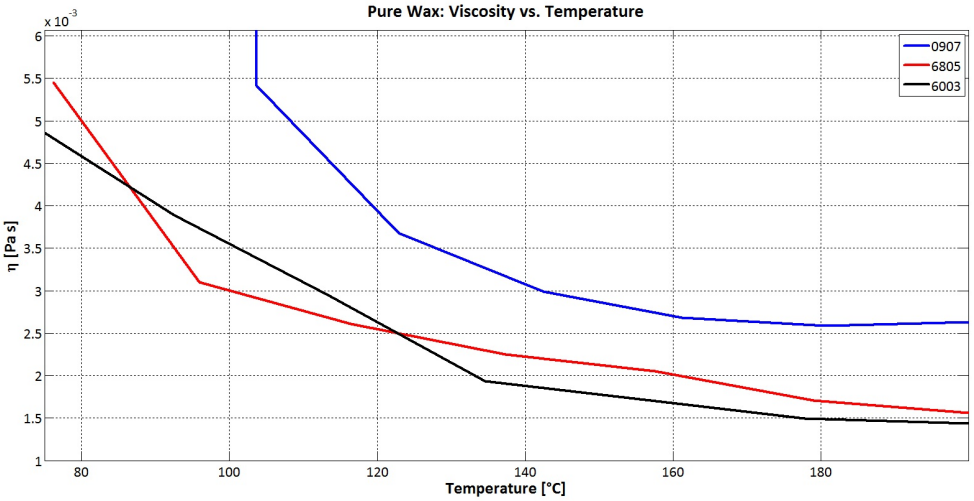


Figura 2: Viscosità Sasolwax pure

Dalla Tabella 4 si nota come la Sasolwax 1276 abbia valori di viscosità circa 70 volte più elevati della 6003. Sasolwax 6805 e 0907 hanno valori più alti rispettivamente del 19.4 e 60.9% rispetto alla 6003.

Tabella 4: Viscosità delle Sasolwax pure a 150°C

| Sasolwax | $\eta$ [Pa s] | $\Delta_\eta$ [%] |
|---|---|---|
| 6003 | 0.001779 | - |
| 6805 | 0.002125 | +19.4 |
| 0907 | 0.002863 | +60.9 |
| 1276 | 0.1205 | +6773.0 |

In Tabella 5 si rappresentano le variazioni di viscosità nel caso di utilizzo di additivi rispetto al caso di paraffina pura.

Successivamente sono stati analizzati il modulo elastico ed il modulo viscoso. I risultati in Figura 3 mostrano come allo stato liquido il modulo viscoso abbia valori più elevati del modulo elastico, mentre dopo la solidificazione i dati mostrano fluttuazioni. Questo comportamento allo stato solido è dovuto ad una solidificazione non uniforme della cera paraffinica, che quindi causa variazioni nei valori di viscosità e di modulo. Il comportamento delle Sasolwax 6003 e 6805 è molto simile, mentre nel caso della Sasolwax 1276 il modulo viscoso prevale in maniera netta nella fase liquida. Nel caso di Sasolwax 6003 e 6805 si registrano disomogeneità ad alte temperature, dovute ai bassi valori di viscosità registrati. Un parametro complessivo che ci permette di percepire in

Tabella 5: Valori di viscosità a 150C

| Formulazione | Viscosità a 150℃[Pa s] | $\Delta_\eta$ |
|---|---|---|
| Pura 0907 | 0.002863 | -% |
| 0907 + 1% PECVA | 0.004585 | + 60.15% |
| 0907 + 5% PECVA | 0.006746 | + 135.63% |
| 0907 + 10% PECVA | 0.028000 | + 878.00% |
| 0907 + 10% PEG | 0.007219 | + 152.15% |
| 0907 + 5% Acido Stearico | 0.003973 | + 38.77% |
| 0907 + 10% Acido Stearico | 0.004175 | + 45.83% |
| 0907 + 5% 1276 | 0.005096 | + 78.00% |
| 0907 + 10% 1276 | 0.005359 | + 87.18% |
| 0907 + 1% Grafite | 0.005542 | + 93.57% |
| 0907 + 10% Alluminio | 0.005950 | + 107.82% |
| Pura 6805 | 0.002125 | -% |
| 6805 + 1% PECVA | 0.002946 | + 38.64% |
| 6805 + 5% PECVA | 0.003999 | + 88.19% |
| 6805 + 10% PECVA | 0.028500 | + 1241.18% |
| 6805 + 10% PEG | 0.003157 | + 48.56% |
| 6805 + 5% Acido Stearico | 0.002487 | + 17.04% |
| 6805 + 10% Acido Stearico | 0.002587 | + 21.74% |
| 6805 + 5% 1276 | 0.002939 | + 38.31% |
| 6805 + 10% 1276 | 0.003466 | + 63.11% |
| 6805 + 1% Grafite | 0.003613 | + 70.02% |
| 6805 + 10% Alluminio | 0.008460 | + 298.12% |
| Pura 1276 | 0.120500 | -% |
| 1276 + 1% PECVA | 0.036900 | - 69.38% |
| 1276 + 5% PECVA | 0.097700 | - 18.92% |
| 1276 + 10% PECVA | 0.317700 | + 163.65% |
| 1276 + 10% PEG | 0.103800 | - 13.86% |
| 1276 + 5% Acido Stearico | 0.088600 | - 26.47% |
| 1276 + 10% Acido Stearico | 0.081000 | - 32.78% |
| 1276 + 1% Grafite | 0.020900 | - 82.66% |
| 1276 + 10% Alluminio | 0.096900 | - 19.59% |
| Pura 6003 | 0.001779 | -% |
| 6003 + 1% PECVA | 0.002763 | + 55.31% |
| 6003 + 5% PECVA | 0.005274 | + 196.46% |
| 6003 + 10% PECVA | 0.057300 | + 3120.91% |
| 6003 + 10% PEG | 0.004708 | + 164.64% |
| 6003 + 5% Acido Stearico | 0.002136 | + 20.07% |
| 6003 + 10% Acido Stearico | 0.002285 | + 28.44% |
| 6805 + 5% 1276 | 0.002550 | + 43.34% |
| 6805 + 10% 1276 | 0.003246 | + 82.46% |
| 6805 + 1% Grafite | 0.002471 | + 38.90% |
| 6805 + 10% Alluminio | 0.004185 | + 135.24% |

maniera nitida le differenze tra le varie cere paraffiniche è il modulo complesso, che è mostrato in Figura 4.

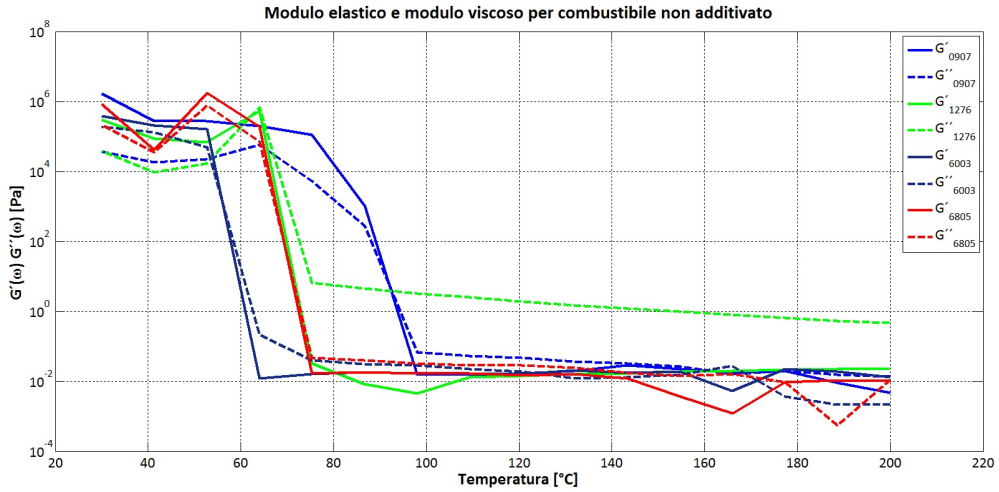


Figura 3: Modulo elastico e modulo viscoso per combustibile non additivato

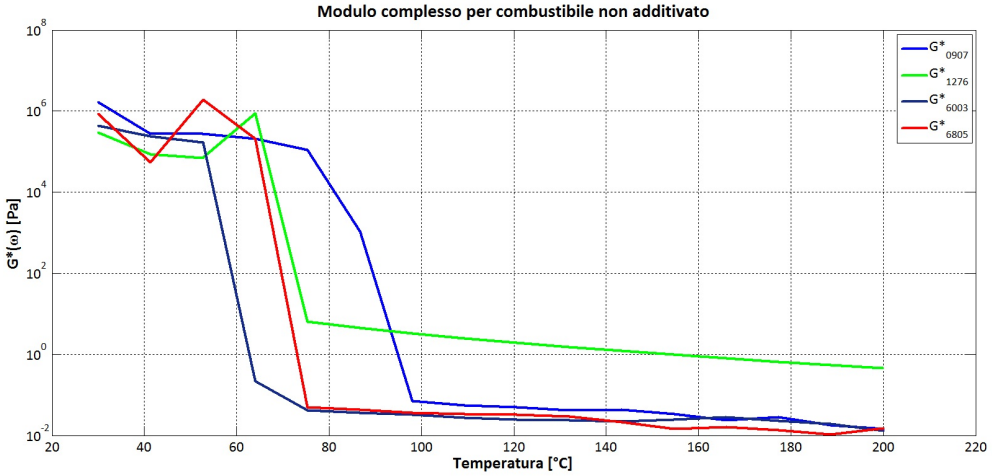


Figura 4: Modulo complesso per combustibile non additivato

## Banco prova e stima teorica dei residui di combustione

Presso il complesso M11 del DLR a Lampoldshausen sono stati già svolti test con la camera di combustione [9], che verrà utilizzata in una fase successiva per verificare il legame tra velocità di regressione e le proprietà fisiche del combustibile indagate nel presente lavoro di tesi.

Ovviamente è stato necessario un rinnovo importante dell'apparato sperimentale. La camera di combustione può essere considerata come suddivisa in due parti: una

prima parte in cui avviene la rettificazione del flusso di ossidante ed una seconda parte in cui è posizionato lo slab di combustibile ed avviene la combustione. L'alimentazione dei gas in camera di combustione avviene con tre differenti linee. Una prima linea adduce idrogeno ed ossigeno necessari all'ignizione, la cui portata può essere variata agendo sulla pressione a monte. Una seconda linea di ossidante permette la combustione, la portata è regolata attraverso un flussimetro. Infine una terza linea fornisce l'azoto necessario ad assolvere due funzioni: mantenere pulita la finestra attraverso cui vengono effettuate le riprese video durante la combustione e raffreddare la camera di combustione dopo i test. Le valvole sulla linea vengono azionate mediante un sitema di controllo remoto predisposto da Siemens. Per le riprese video viene utilizzata una videocamera ad alta velocità Photron.

Per l'analisi dei residui condensati di combustione è previsto l'utilizzo di un sistema di campionamento usato in precedenza. I residui solidi potranno essere trattati chimicamente con processi come la titolazione.

## Conclusioni e sviluppi futuri

In questo lavoro sono state analizzate le proprietà reologiche di combustibili paraffinici puri e additivati, indagando il comportamento del modulo elastico, di quello viscoso e della viscosità in funzione della temperatura. E' stato inoltre indagato il comportamento della tensione superficiale. Si è notato come mediante l'utilizzo di additivi queste proprietà possano cambiare anche in maniera marcata.

I passi successivi da compiere sono quindi test di combustione utilizzando tecniche ottiche che permettano di osservare l'entrainment delle goccioline, ciò al fine poi di verificare il tipo di legame sussistente tra velocità di regressione e proprietà fisiche del combustibile. Un altro ambito di indagine consiste nel verificare i legami tra proprietà meccaniche del combustibile e moduli elastico e viscoso. Ovviamente alle formulazioni utilizzate in questo lavoro se ne potrebbero aggiungere altre, in particolare metalli ed idruri metallici.

L'analisi dei residui di combustione, qui stimata a livello teorico, permette di ricavare informazioni riguardo la qualità della combustione.

# Acknowledgements

I want to thank my supervisor, Prof. De Luca, and Ing. Toson for their support and help in the revision of this thesis. I would to thank Ing. Kobald and Dr. Ciezki for the opportunity to work at DLR.

# Abstract

Hybrid propulsion combines the advantages of liquid and solid propulsion. In particular its main characteristics are: safety thanks to oxydant and fuel stored separately, possibility of multiple shut on/off, thrust modulation regulating the oxidant mass flow. Hybrid systems have specific impulse higher than solids, but the main reason that up to now has delayed the development of hybrid technology is the low regression rate of the fuel. The most promising fuels are those that melt forming a thin liquid layer over the solid fuel, leading to entrainment of droplets effect. For this reason in this work done at DLR - Institute of Space Propulsion in Lampoldshausen, paraffin based fuels, which are liquefying hybrid fuels, are considered.

Performances can be enhanced also chemically by using additives capable of increasing the energetic content of the fuel. In this work two different types of additives are used: organic additives as Polyethylene and Stearic Acid and metal additives like Aluminum.

The purpose is to characterize different formulations by a rheological point of view. Two main properties are supposed to influence regression rate of paraffin based fuels: surface tension and viscosity. Viscosity behavior is analysed as function of temperature, from 200°Cto the melting temperature. The mechanical properties of the formulation concerning on storage and loss modulus are also characterized, in particular it is interesting the behavior across the melting point. Surface tension, a parameter that is generally neglected, is investigated basing on Karabeyoglu researches which consider surface tension an important parameter in determining the regression rate. The behavior of surface tension with increasing temperature for different kind of waxes and additives is investigated.

The last part that needs to be delved is the analysis of combustion products: the amount of metal collectable (a mixture made of wax and Aluminum is considered) , the specific impulse and combustion efficiency are estimated theoretically. Tests involving different formulations should be done to get experimental results.

Keywords: entrainment, surface tension, viscosity, waxes

# Chapter 1

# Introduction

Chemical rocket propulsion systems can be classified basing on the physical state of reactants in: solid, liquid and hybrid. Liquid systems main advantage is the high specific impulse value but these systems are quite complex. Solid technology is cheaper and less complex than liquid one, but specific impulse values are low. Hybrid systems role is to combine advantages of liquid and solid systems. This kind of propulsion is based on fuel and oxidizer stored separately and in different physical states.

## 1.1 Theoretical background

Despite his safety and cost advantages hybrid systems have a great limit: the low fuel regression rate. This limit does not allow high fuel loading, high thrust densities, resulting in a complex grain design and a large amount of residuals.

For this reason different methods have been experimented in order to increase the fuel regression rate.

The first is to reduce the gasification heat flux, but the effectiveness of this method is reduced by the increased blowing surface.

A different approach is based on using propellants which melt at the regression surface. In this propellants class, substances like gases or liquids that are frozen to be solid are included. Examples of these propellants are $O_2$, hydrocarbons or liquid amines. Solid cryogenic propellants have been used at AFRL and ORBITEC [2].

Solid fuels can incorporate energetic metals in order to increase performance and density.

The regression rate model for these class of propellants is based on entrainment [1].

In the tests made at AFRL the space-time averaged regression rate, defined as:

$$\bar{\dot{r}} = \frac{R_f - R_i}{t_b} \tag{1.1}$$

is calculated.

The experiments involve different propellants formulations: Pentane, HFI, Isopropanol and Acetone at different mass flow rate. Test results show that pentane regression rate is 3-4 times higher than HTPB, as shown in Figure 1.1.

Instantaneous regression rate can be split in three different parts: the maximum value is reached in the first one, in the third one the regression rate drops down rapidly.

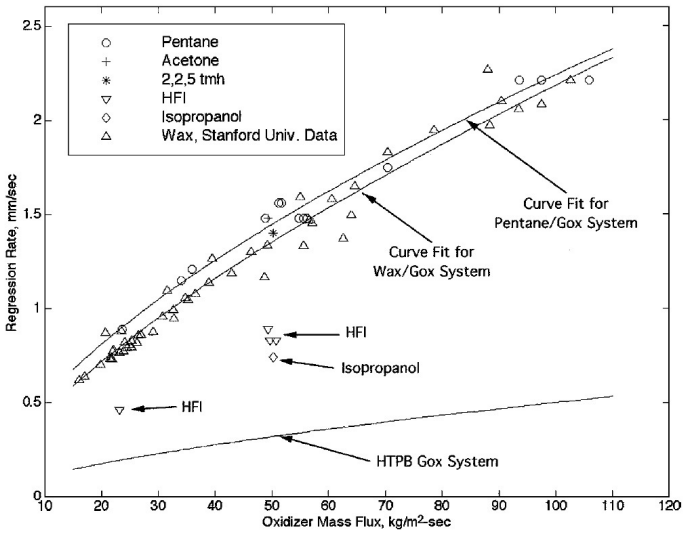


Figure 1.1: Regression rate as a function of oxidizer mass flux

The second third gives a reasonable representation of the steady state regression rate law.

The phenomen associated with cryogenic hybrids is articulated in three different aspects:

- requirements for the formation of a melt layer on the regression surface
- melt layer linear stability under strong shear caused by a gas flow
- classical theory extension to liquid droplet entrainment

Entrainment increases fuel regression rate without increasing blowing parameter. The thickness of melt layer is related with energy transfer in both solid and liquid phase. In the gaseous phase temperature ranges from 1500 to 2000 K. The radiation is high where there is a great presence of solid particles in the gaseous flux.

The heat that is required to vaporize the material transported by entrainment is zero.

Karabeyoglu [2] considers two opposite situations related with $R_l$ , that is the ratio of thermal thickness and radiative penetration thickness in the liquid layer:

in the first one, $R_l >> 1$ , the radiation absorption in the liquid layer is very large and all the radiative heat is absorbed at the liquid-gas interface. The thickness is:

$$h = \delta_l ln(1 + C_l \Delta T_1 / h_m) \tag{1.2}$$

where

- $\delta_l$ is the thermal thickness in the liquid phase
- $C_l$ is the specific heat in the liquid phase
- $\Delta T_1$ is the temperature difference between vaporization and melting

This case is related with propellants loaded with absorbing materials as carbon black.

In the second case $R_l << 1$ the absorption of the radiation in the liquid phase is small and the thermal layer is smaller than radiative thickness in the liquid phase. For this reason all the radiative flux is absorbed in the solid.

The melt layer thickness is directly proportional to $\delta_l$ and inversely proportional to the regression rate.

Another parameter that can influence melt layer thickness is the environment temperature $T_a$, the higher $T_a$ the higher the thickness. The highest melt layer thickness is achieved when $T_a$ is the melting temperature $T_m$.

The linear stability of liquid layer requires a non linear investigation, for this reason Karabeyoglu, Altmann and Cantwell [2] have developed empirical relations.

The liquid mass flow rate in the melt layer per unit width is:

$$\overline{\dot{m}_l} = \frac{P_d C_f h^2 \rho_l}{2\mu_l} \tag{1.3}$$

This relation allows to state that the effect of gas dynamic pressure is destabilizing, while viscosity and surface tension are stabilizing.

The empirical expression for entrainment of liquid droplets is:

$$\dot{m}_{ent} = \frac{P_d^{\alpha} h^{\beta}}{\mu_l^{\gamma} \sigma^{\pi}} \tag{1.4}$$

with the values for the exponents reported in Table 1.1

Table 1.1: Exponent values

| | $\alpha$ | $\beta$ | $\gamma$ | $\pi$ |
|---|---|---|---|---|
| Gater - L'Ecuyer | 1.5 | 2 | 1 | 1 |
| Nigmatulin et al. | 1 | 1 | - | - |
| Karabeyoglu | 1-1.5 | - | $>\pi$ | $<\gamma$ |

In hybrid application the viscosity role is assumed to be more important than surface tension in establishing entrainment mass transfer rate.

Boundary layer classical law are modified by entrainment:

- the ratio between enthalpy difference and heat of gasification is altered because the heat of gasification is reduced by mechanical entrainment
- the blocking factor $\frac{C_H}{C_{H0}}$ is modified by two phase flow
- ripples on the liquid layer surface increase surface roughness and heat transfer

Surface roughness decreases increasing gas flow dynamic pressure.

The regression rate increase because of:

- entrainment
- reduced gasification
- reduced blocking effect

Paraffin and waxes are not cryogenic propellants but they have high rates of entrainment of liquid droplets . The extra mass transfer generated by entrainment can lead to an increase in regression rate of an order of magnitude.

Melt layer thickness can be hundreds of microns for typical operative conditions in hybrid rockets.

**Liquid layer stability** The liquid layer stability is influenced by a wide range of parameters. If dynamic pressure increases, both maximum amplification and the most amplified wave number increase. Blowing has a small stabilizing effect on the film. Increase in viscosity and in surface tension stabilizes the film.

Classical hybrid materials are viscous, so they cannot sustain the film thin instabilities.

In hybrid rocket typical conditions the body force has a negligible effect if compared with shear force caused by gas flow.

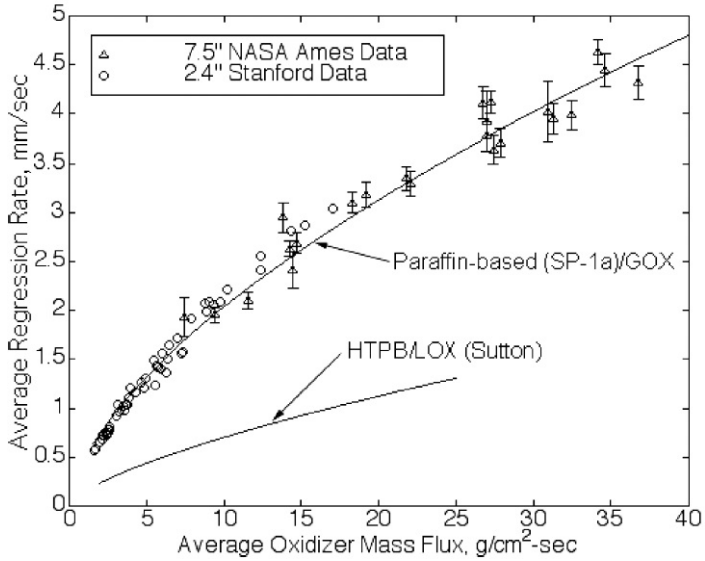


Figure 1.2: Regression rate as a function of oxidizer mass flux: Paraffin vs. HTPB

In Figure 1.2 it is possible to notice that [10]

$$\dot{r}_{paraffin} = 3 \div 5 \dot{r}_{HTPB} \tag{1.5}$$

## 1.2 Motivations and objectives

As stated in the previous section, hybrid systems have many advantages if compared with solid or liquid systems, but hybrid systems have a great disadvantage that till now as not allowed a complete development of this technology: the low regression rate of the fuel.

The entrainment of droplets of the fuel is a promising way to increase the regression rate.

According to Karabeyoglu et al. [2] entrainment mass flow rate depends on four different parameters: dynamic pressure, melt layer thickness, surface tension and viscosity. Each parameter has an exponent that has been investigated in some researches as shown in 1.4. According to this relation, high values of surface tension and viscosity reduce entrainment, while dynamic pressure and melt layer thickness have a destabilizing effect, increasing entrainment.

Considering that melt layer thickness (that can be be recorded by a video camera) and dynamic pressure can be investigated only with combustion tests, the aim of this work is to investigate the behavior of viscosity and surface tension of the liquid fuel. The variation of these two properties as function of temperature is investigated for different types of mixture.

Four different waxes are used: Sasolwax 0907, Sasolwax 6805, Sasolwax 1276 and Sasolwax 6003. Different types of additives are used: Aluminum, Stearic Acid, Carbon Black, Poly Ethylene Co Vinyl Aceate and Poly Ethylene Glykol.

Surface tension is investigated with a heatable tensiometer, in this way surface tension values are experimentally obtained from a temperature of 130°Cto the melting temperature of the wax. Data obtained are plotted in a mean curve allowing a comparison of the variation of surface tension values and a comparison of these values at a given temperature.

Viscosity is investigated with a rotational rheometer as a function of shear rate and as a function of temperature from 200°Cto the solidification temperature. Viscosity values of different mixtures at fixed temperatures are obtained allowing an analysis of the effect of the additives on viscosity.

Complex, storage and loss modulus of some mixtures are investigated in order to show the behavior of these parameters in the liquid phase, in the solid phase and in the transition.

In this way, when combustion tests will be done, it shall be possible to find a relation between physical properties of the fuel and fuel burning rate.

Further developments should be the investigation of dynamic pressure and melt layer thickness (the other two influencing parameters, as mentioned above) and the analysis of combustion parameters like specific impulse and combustion efficiency.

## 1.3 Description of the thesis

The thesis is organized in five chapters:

- Chapter 1: Introduction. A general overview on liquefying hybrid propellants and a description of entrainment phenomenon and parameters is presented. Motivations and objectives are shown.

- Chapter 2: Alkanes. A general overview of the properties of alkanes is presented. Some methods that allow the calculation of crictical properties of alkanes (critical pressure and critical temperature) are shown. Results of a research made by Karabeyoglu, Stevens and Cantwell [8] are presented. This research shows the importance of carbon number on some parameters like blowing parameter, surface tension and viscosity.

- Chapter 3: Paraffin based fuels. A general overview of additives effect on paraffin based fuels is presented. Different types of hydrides are described and the effect

of some of them on performances is presented. In the last paragraph a research that investigates temperature and concentration behavior [11] is shown.

- Chapter 4: Surface tension. Surface tension and some methods of measurement are briefly theoretically described. Surface tension behavior as a function of temperature is investigated for the four waxes. Then, the effect of additives on waxes is investigated.
- Chapter 5: Viscosity. A general overview of viscosity and different types of viscometer and rheometer are presented. Pure waxes and waxes with additives are investigated as function of shear rate and temperature. Storage, loss and complex modulus behavior of some mixtures is investigated as function of temperature.
- Chapter 6: Some analysis for future developments. A general overview on renewed combustion test facility at DLR is presented and a possible sampling probe system for combustion products is briefly described. Some analysis are done with CEA in order to obtain a theoretical estimation of some parameters like specific impulse and combustion efficiency.

# Chapter 2

# Alkanes

In a work realized by Marano and Holder [12] the asymptotic behavior correlations are presented. The most important part related with our researches is the one concerning on correlations for thermal and transport properties. The general formula for asymptotic behavior correlation is:

$$Y = Y_{\infty} - \Delta Y_0 exp(-\beta(n \pm n_0)^{\gamma}) \tag{2.1}$$

where:

$$Y_{\infty} = Y_{\infty,0} + \Delta Y_{\infty}(n - n_0) \tag{2.2}$$

Internal energy, enthalpy, entropy and free energy are asymptotically proportional to carbon number. Ideal gas enthalpy, free energy of formation, ideal gas heat capacity and liquid heat capacity are type II properties. Type I properties approach a finite value for large carbon numbers. Type II properties are additive in nature, the limit is linear with carbon number. Enthalpy of vaporization for the lattice fluid can be expressed as

$$\Delta H = \Delta E_n + RT \tag{2.3}$$

Enthalpy of vaporization at fixed temperature is a type II property, in fact the theory predicts its linearity with carbon number. Surface tension is a type I property. Logarithm of viscosity is a type II property as it can be seen in Figure 2.1.

At critical carbon number there is transition in the flow behavior of polymer melted. Increasing carbon number, the viscosity rate of increase declines and viscosity assumes a non-Newtonian behavior. Transition is connected with chain entanglement concept. An increase in carbon number means that molecules become more entwined, in this way a long range motion require motion of other molecules, increasing viscosity. Below the critical carbon number the bulk flow is due to motion of individual molecules, while above, it is due to the motion of entangled chains. As stated in previous lines, below the critical carbon number (assumed to be 286) the logarithm of viscosity is linear with carbon number (type II property) . Above 286 a non-Newtonian behavior raises. Error distribution is a function of carbon number and temperature. Errors obtained with ABC are higher than errors obtained with other methods.The highest error per temperature unit is obtained with the most viscous material. There is a linear dependence between the logarithm of Newtonian viscosity and the logarithm of molecular weight.

The behavior of viscosity with molecular weight is presented in Figure 2.2.

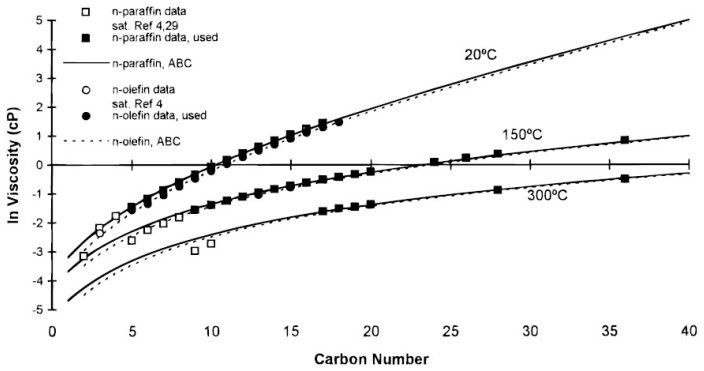


Figure 2.1: Viscosity as a function of carbon number

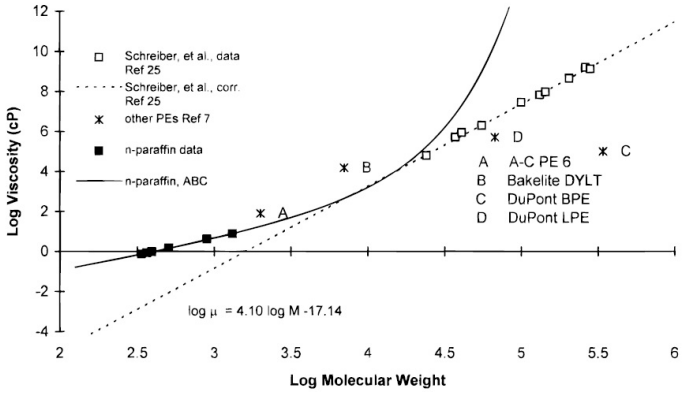


Figure 2.2: Viscosity as a function of molecular weight

Surface tension data are limited at a carbon number below 20 for n-olefins and n-paraffins as showed in Figure 2.3. For n-olefins data are limited below 100 ℃, for n-paraffin data are limited below 150 ℃. Surface tension is a type I property. There is a little difference in surface tension values for n-olefins and n-paraffins at any carbon number. Branching reduces surface tension.

## 2.1 Normal alkanes as hybrid rocket fuels

Normal alkanes is a group of fully saturated straight chain hydrocarbons formulated as $C_nH_{2n+2}$ , where n can range from 1 to values higher than 300. A large fraction of fast burning liquefying fuels are pure normal alkanes or mixtures of n-alkanes (for example paraffin waxes).

Surface temperature is an important parameter because thermophysical properties of the fuel depend on the temperature of the melt layer. In the subcritical phase temperature is determined by a physical process controlled by phase change, while in the supercritical phase the process depends on pyrolysis.

Critical properties like critical temperature and critical pressure can be determined in the present case with different methods:

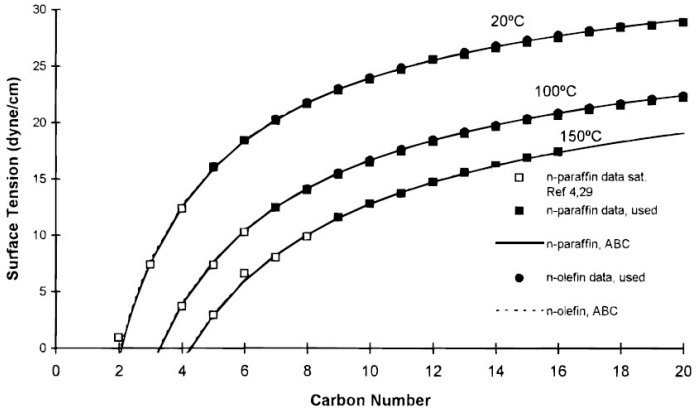


Figure 2.3: Surface tension as a function of carbon number

- Magoulas and Tassios [7]

$$ln(p_c) = 4.3398 - 0.3155N_c^{0.6032} \tag{2.4}$$

$$ln(959.98 - T_c) = 6.81536 - 0.211145N_c^{2/3} \tag{2.5}$$

- Teja

$$ln(p_c - 0.84203) = 1.75059 - 0.196383N_c^{0.890006} \tag{2.6}$$

$$ln(1143.8 - T_c) = 7.15908 - 0.303158N_c^{0.469609} \tag{2.7}$$

- Hu

$$p_c = \frac{10}{0.19694 - 0.059777N_c^{0.5} + 0.46718N_c} \tag{2.8}$$

$$T_c = \frac{0.38106 + N_c}{0.0038432 + 0.0017607N_c^{0.5} + 0.00073827N_c} \tag{2.9}$$

- Gani

$$p_c = (\sum n_i \Delta p_{c1i} + 0.10022)^{-2} + 1.3705 \tag{2.10}$$

$$T_c = 181.128 * ln(\sum n_i \Delta T_{c1i}) \tag{2.11}$$

where $N_c$ is the number of carbon atoms in the molecular structure, $n_i$ the number of groups of the i group, $p_{c1i}$ and $T_{c1i}$ the pressure and temperature coefficient related with i group.

In Figure 2.4 the phase diagram is shown and it can be noted that above critical pressure and critical temperature the fluid is in supercritical conditions [13].

Moderate to high carbon number normal alkanes such as paraffin waxes have low critical pressures, working in supercritical conditions for all practical operating engines. In this case there is not a surface separating the liquid phase from the vapor phase and

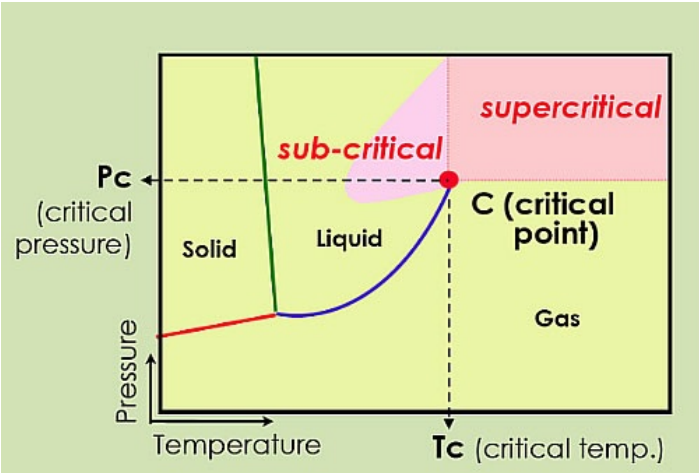


Figure 2.4: General phase diagram

the surface tension is not well defined. For this reason the law for entrainment mass transfer is:

$$\dot{m}_{ent} = K'' \frac{C_f a_t^{\beta} \rho_l}{\mu_l} \frac{G^{2\alpha}}{\dot{r}^{\beta}} \tag{2.12}$$

Total regression rate can be considered as result of two different contributes:

$$\dot{r} = \dot{r}_v + \dot{r}_{ent} \tag{2.13}$$

Thickness has a logarithmic dependence on the energy terms, so the effect of reduced liquid phase heating is small at moderate entrainment.

It is introduced Fr parameter that takes into account the increased heat transfer by wrinkling of the liquid surface. Surface roughness decreases with increasing dynamic pressure of the gas flow.

Entrainment component of the regression rate increases rapidly with growing entrainment parameter. The increase in non-dimensional entrainment regression slows down as $R_{ent}$ increases. If entrainment parameter has a large value, the entrainment component of regression rate dominates vaporization.

$R_{ent}$ is a strong function of the material properties and it depends weakly on local flux and axial location. Fuel solid density and blowing parameter strongly depend on the particular fuel used.

The classical regression rate for an arbitrary carbon number $n$ can be written as:

$$\phi_{cl} = \frac{(\rho_s)_{ref}}{\rho_s} \frac{BC_{B1}}{(BC_{B1})_{ref}} \tag{2.14}$$

The behavior of entrainment with carbon number is presented in Figure 2.5.

### 2.1.1 Pure n-alkanes

Calculation of regression rate of normal alkanes requires to know the fuel properties over a wide range of temperatures and carbon numbers. ABC equations are used to predict the properties of homologous series, particularly for those fuels that have moderate to high molecular weight.

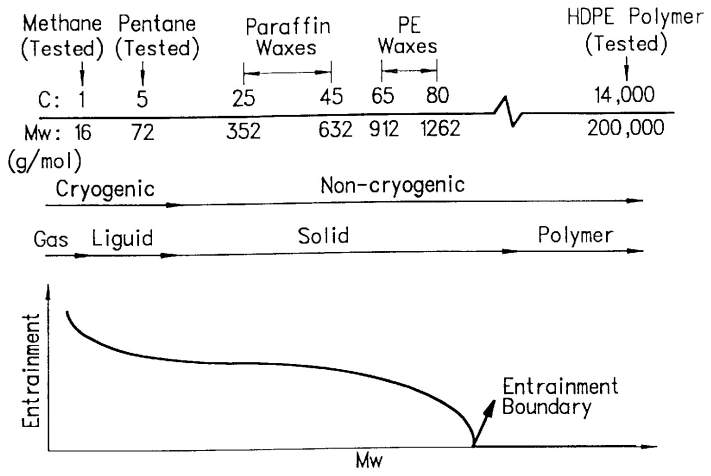


Figure 2.5: Entrainment as a function of carbon number

### Critical conditions

Critical pressure drops with increasing carbon number: for infinite carbon number the critical pressure asymptotes to zero as predicted by many of the state equations for long chain molecules. Large part of hybrid systems using paraffin based fuels are operating in supercritical conditions, making the distinction between the liquid and vapor phase to disappear. Critical temperature increases with molecular weight and asymptotes to 1020.7 K. Viscosity can be calculated with the following set of equations:

$$Y = Y_{\infty,0} + \Delta Y_{\infty}(n - n_0) - \Delta Y_0 exp[-\beta(n - n_0)^{\gamma}] \tag{2.15}$$

$$\Delta Y_0 = A_0 + \frac{B_0}{T} + C_0 lnT + D_0 T^2 + \frac{E_0}{T^2} \tag{2.16}$$

$$\Delta Y_{\infty} = A_{\infty} + \frac{B_{\infty}}{T} + C_{\infty} lnT + D_{\infty} T^2 + \frac{E_{\infty}}{T^2} \tag{2.17}$$

and

$$\mu_l = exp(Y) \tag{2.18}$$

This method becomes inaccurate for a carbon number lower than 11. The accuracy of this method reduces with increasing molecular weight for carbon numbers larger than 70.

It exists also another method to estimate viscosity of liquids composed of large n-alkanes molecules at a specified temperature T, implemented by Bicerano [14]. Bicerano predicts a critical molecular weight corresponding to a carbon number of 254: at this value the viscosity behavior with increasing carbon number changes dramatically. This behavior is due to extra restrictions on molecular motion induced by entanglement of long molecules. The rate of viscosity increases with decreasing carbon number above entanglement molecular weight.

Liquid density can be predicted correctly with ABC method for carbon number larger than 11:

$$Y = Y_{\infty,0} + \Delta Y_{\infty}(n + n_0) - \Delta Y_0 exp[-\beta(n + n_0)^{\gamma}] \tag{2.19}$$

and

$$\rho_l = 1000\frac{M_w}{Y} \tag{2.20}$$

### 2.1.2 Mixture of n-alkanes

Many paraffin fuel systems are not pure n-alkanes, but they are mixtures of strain chain molecules. An accurate estimation of viscosity of mixtures is calculated using weight averaged carbon number.

It is very important the PD parameter (polydispersity), that is defined as the ratio of weight averaged carbon number and number averaged carbon number. Polydispersity is an index of broadness of molecular weight distribution in a mixture. For this reason the most important parameters are PD and $n$.

In order to estimate the condensed phase temperature field, three temperatures are needed: ambient temperature, melting temperature and surface temperature. Ambient temperature is the bulk temperature of bulk solid grain. Melting temperature can be estimated as:

$$Y = Y_{\infty} - (Y_{\infty} - Y_0)exp[-\beta(n - n_0)^{\gamma}] \tag{2.21}$$

and

$$T_m = Y \tag{2.22}$$

Surface temperature determines the effective melt layer temperature at which the critical fluid properties (especially density and viscosity) should be evaluated. These fluid properties influence the stability of the fluid layer and govern the entrainment mass transfer. If the partial pressure of the fuel is less than the critical pressure, evaporation determines the surface temperature. This behavior is expected for light members of the series with high critical pressure or for moderate carbon numbered members if chamber pressure is very low. If surface partial pressure is higher than critical pressure, the distinction between liquid and gas phase is lost and the fluid heat is dictated by pyrolysis process of the fuel molecules. In this condition the surface temperature is the temperature at which a certain amount of fuel is thermally decomposed in smaller molecules.

**Kinetic theory** If the partial pressure of vapor is less than critical pressure of the fuel, the temperature is determined by an evaporation process. In order to know the surface temperature it has to be determined the variation of internal degrees of freedom. For carbon numbers larger than 20 the accuracy of surface temperature prediction is not important because fuel systems with high carbon number operate at supercritical regime and so surface temperature is not determined by evaporation process. The mass fraction of the fuel increases as the enthalpy ratio increases.

**Thermal analysis** Assuming to be in supercritical conditions and that the phenomenon is governed by pyrolysis, the solid fuel slab can be divided in three zones:

- **Pyrolysis zone** that is a thin layer next to the surface in which pyrolysis reactions take place. In this zone the mass fuel fraction reduces from one to a low value, due to the thermal cracking of the original n-alkane molecules that form the fuel bulk. If the activation energy is high, the thickness of radiation zone is small. Radiative terms can also be ignored if there is a very large absorptivity (radiation and convection) or a very small absorptivity (convection term only). Fixed the regression rate, the surface temperature increases slightly with decreasing fuel mass fraction at the surface.
- **Liquid zone** that is an area where there are no reactions.
- **Solid zone** that is an area where there are no reactions too.

In this tests, made by Karabeyoglu, Stevens and Cantwell [8], have been used Paraffin Wax FR4045, Polyethylene Wax (Marcus 200), Polyethylene Wax (Polyflo 200) and High Density Polyethylene Polymer (HPDE). All formulations have the same flux exponent and the regression rate is only determined by mass flux coefficient. HPDE is the slowest burning alkane with a burn rate around 20% of SP-1a regression rate, as it can be noted in Figure 2.6.

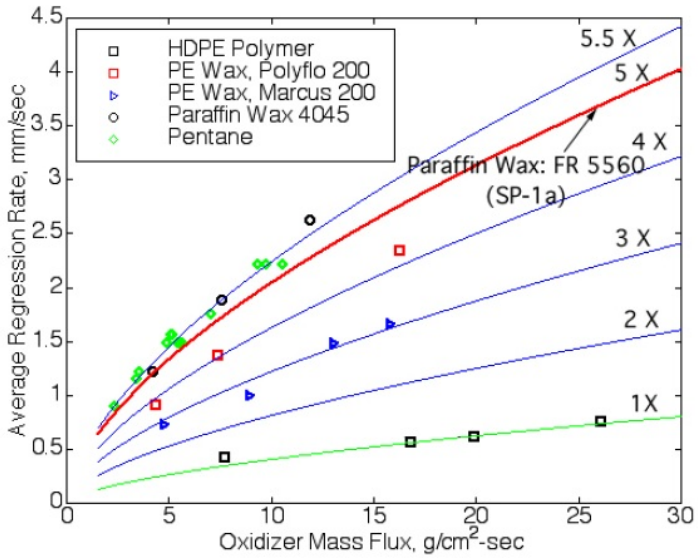


Figure 2.6: Regression rate of some alkanes vs. GOX

Regression rate is assumed to be constant in order to estimate the surface temperature at the beginning of the entrainment process. Activation energy is based on expected surface temperature and it is assumed to be constant for all members of the series. Each fuel is assumed to be a pure n-alkane with the corresponding carbon number. Melting temperature increases monotonically with carbon number, the rate of increase decreases with increasing carbon number. The same behavior is followed by critical temperature. Surface temperature has different behaviors: in subcritical

conditions it increases with increasing carbon number. Critical pressure decreases with the carbon number and at a certain $n$ the partial pressure of the vapor at surface becomes equal to the critical pressure for this particular n-alkane. This is the $n$ at which the distinction between liquid and gas disappears and supercritical operations starts (Figure 2.7).

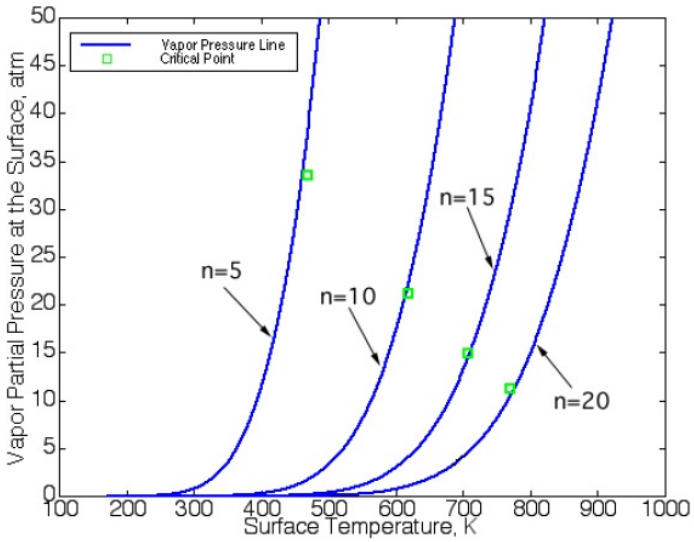


Figure 2.7: Vapor pressure of alkanes as a function of temperature at different carbon number

At critical carbon number there is a jump in surface temperature: surface temperature in pyrolysis condition is much higher than at evaporation condition. In supercritical regime the surface temperature decreases with increasing carbon number. Normal alkane molecules become less resistant to thermal decomposition as they become longer. Fluid layer temperature increases at low $n$ and it has constant values from moderate to high $n$. At this temperature fluid properties are evaluated in order to estimate entrainment parameters. Heat of gasification increases in subcritical conditions and it has a jump at critical $n$, decreasing slowly at supercritical conditions. Heat of vaporization is nonzero in subcritical regime, while heat of pyrolysis is nonzero in supercritical regime. The blowing parameter decreases from a value of 13 in subcritical regime to a value of 5 in supercritical regime (Figure 2.8).

Viscosity increases with increasing carbon number as shown in Figure 2.9.

Entrainment parameter $R_{ent}$ is low in subcritical conditions, it jumps at critical $n$ and after it starts to decrease increasing carbon number (Figure 2.10). Effect of blowing parameter on the classical regression rate and entrainment regression rate compensate each other, for this reason there is a smooth transition in the total regression rate $\dot{r}$ passing from subcritical to supercritical operations.

For a pure n-alkane the polidispersity is one and it increases as the distribution of molecular weight in the mixture broadens. If polydispersity increases it comprises the improvement in regression rate. For this reason the best fuel at a specified melting point is the one with the narrowest molecular weight distribution.

In subcritical region, if pressure increases, the latent heat of vaporization reduces and surface temperature increases. Pressure shifts the critical carbon number. In

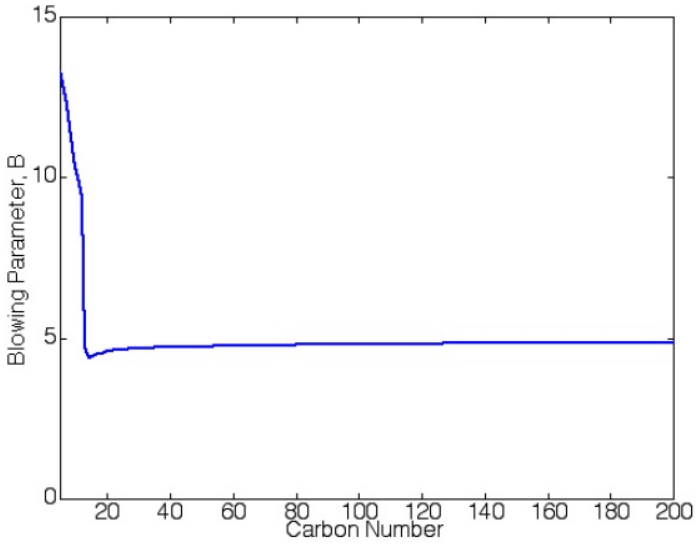


Figure 2.8: Blowing parameter as a function of carbon number

supercritical conditions the pressure has no effect.

Surface tension has small changes in subcritical carbon number, in supercritical case surface tension is zero because the surface is defined by pyrolysis process (see Figure 2.12).

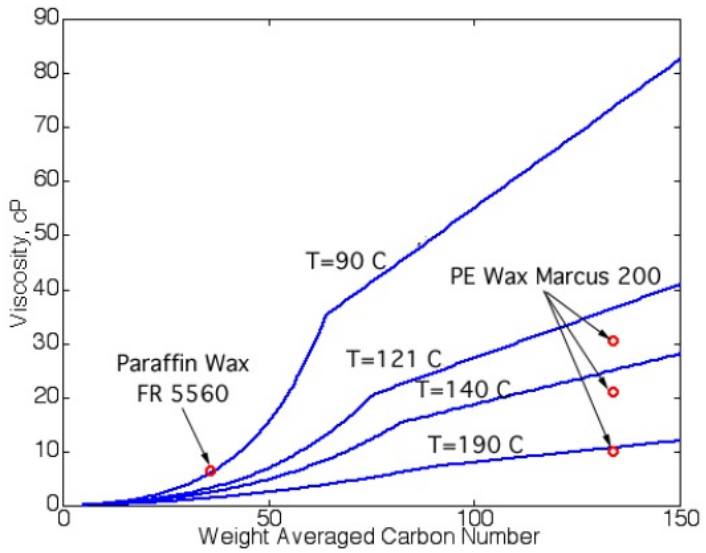


Figure 2.9: Viscosity of n-alkanes at different temperatures as a function of carbon number

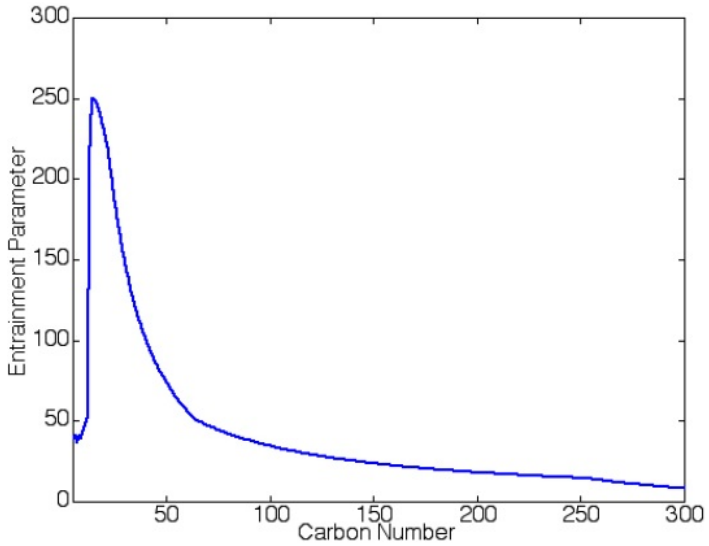


Figure 2.10: Entrainment parameter of n-alkanes as a function of carbon number

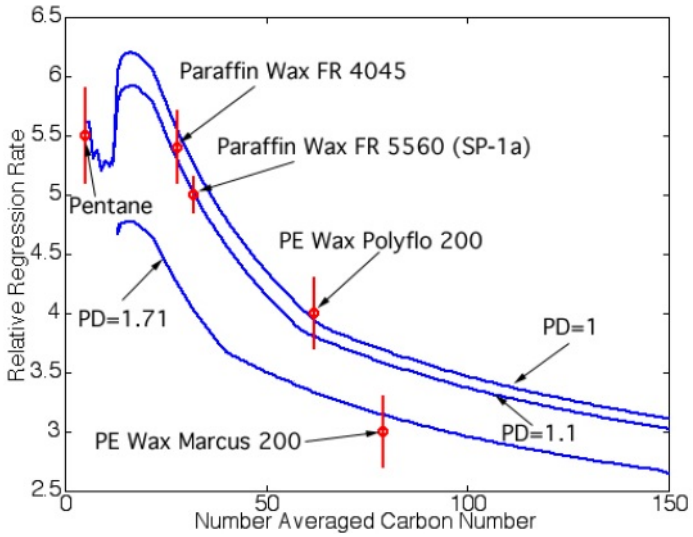


Figure 2.11: Regression rate of n-alkanes with respect to regression rate of HDPE polymer as a function of carbon number at different polydipersity

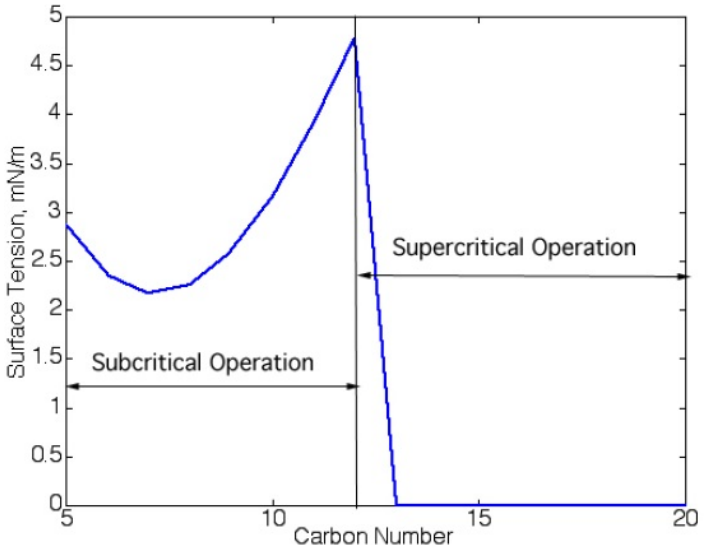


Figure 2.12: Surface tension of n-alkanes as a function of carbon number

# Chapter 3

# Paraffin based fuels

Paraffin regression rate is 4 times the HTPB regression rate. Low values in viscosity and in surface tension generate entrainment. Nakagawa and Hikone [5] change the paraffin based fuel viscosity by adding ethylene-vinyl acetate copolymer (Figure 3.1).

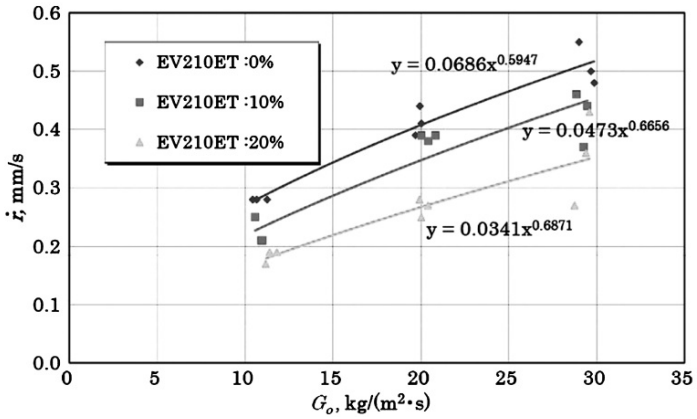


Figure 3.1: Regression rate vs. GOX at different percentage of EVA

They use a paraffin based on $CO$ and $H_2$ and they add it with different percentage of EVA (ethylene-vinyl acetate) in order to change the fuel viscosity. Results reported in Figure 3.2 show that the highest regression rate is achieved using fuel without EVA. The lowest value are obtained with the fuel added with 20% EVA.

If the viscosity increases, the regression rate decreases. $r_f$ increases proportionally to $\mu^{-1/6}$.

The heat transfer coefficient is given by:

$$h = 0.332 k^{2/3} C_{pl}^{1/3} \sqrt{\frac{u_\infty \rho_l}{x}} \mu^{-1/6} \tag{3.1}$$

where:

- $k$ is the thermal conductivity
- $C_{pl}$ is the specific heat of the melted fuel at constant pressure

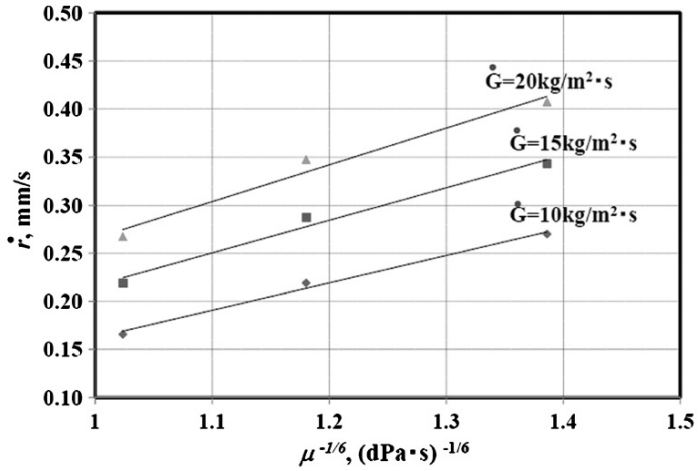


Figure 3.2: Regression rate as a function of viscosity at different GOX

- $u_\infty$ is the melted fuel general flow velocity
- $\rho_l$ is the melted fuel density
- $x$ is the distance from the forward edge
- $\mu$ is the viscosity coefficient

In this work the pressure is atmospheric, so it is demonstrated that the entrainment of droplets takes place also at atmospheric pressure.

A study made by Karabeyoglu, Zilliac, Cantwell, DeZilwa and Castellucci [10] show the feasibility of the mentioned approach with grain bigger than usually used in laboratory tests.

Their study, using SP-1a propellant, is focused on four areas: regression rate law, motor efficiency, ignition characteristics and motor stability.

**Regression rate** Regression rate shows a mass flux exponent of 0.62, a bit smaller than the one recorded for classical hybrid propellants. A smaller exponent reduces the extent of the O/ F shift during motor operation and improve $I_{sp}$ efficiency. On the other side, in these experiments, effects caused by chamber pressure on the regression rate are not observed. In the same way the grain length has not effect on regression rate. The formula used for the determination of $r_f$ can be used reasonably for O/F between 1.7 and 2.3. For mixture ratio with different values the formula needs to be modified.

**Efficiency** Efficiency increases with:

- increasing L*
- increasing mass flux

- increasing motor O/F

Motor efficiencies increase with increasing the mixture ratio. At O/F where $I_{sp}$ is maximized, the motor efficiency is around 85-90%.

The increase in efficiency with increasing L* means that larger motors would run at higher efficiencies.

**Grain integrity** The fuel used in tests shows structural stability also at high chamber pressures. Low heat conductivity and radiation absorption help structural stability.

Fuel tested in this study shows $r_f$ three times larger than the one of HTPB based fuel. The entrainment mechanism still works at high chamber pressure, at large fluxes (as tested in this study) and for grain length that are seven times longer than used with Stanford University motor.

Higher fluxes mean that droplets size is smaller.

Also in this study any dependence by pressure or grain length on $r_f$ was not observed.

## 3.1 Hydrides

Hydrides can be used as energetic additives to increase $I_{sp}$ and $\dot{m}_f$.

A hydride is a chemical compound in which hydrogen is combined with another element: one or more hydrogen centres have nucleophilic, reducing or basic properties.

Types of bond between hydrogen and other elements range from highly covalent to ionic. Hydrides can be distinguished in three main groups basing on the chemical bond: ionic ( saline), metallic and covalent. A further group is the polymeric hydride (like boranes). Hydrides can be components of molecules, oligomers, polymers, ionic solids and other materials. Hydrides usually reacts as Lewis bases or reducing agents. Some metal hydrides behave as hydrogen-atom donors and as acids. Aluminum, beryllium and copper are nonconductors. Hydrides are thermally unstable and under certain conditions some of them can explode with air or moisture.

Hydrides can be used in different ways:

- as reducing agents in chemical synthesis: examples of this kind of hydride are sodium borohydride and lithium aluminum hydride.
- as strong bases in organic synthesis like sodium hydride or potassium hydride
- as desiccants, in order to remove trace of water from organic solvents.
- as a means of hydrogen storage
- as catalyst and catalytic intermediate in catalytic cycles like hydrogenation and hydrodesulfurization catalysts.

**Ionic hydrides** In this kind of hydride hydrogen has a negative charge (ion $H^-$) [15]. Generally ionic hydrides include alkali metals and alkaline-earth metals. These metals react with hydrogen. These hydrides are white crystalline solids, but because of impurities they are generally gray. The hydride ion in saline hydrides is a strong base. They react strongly with water liberating large amounts of hydrogen, making these substances useful for hydrogen storage. Ionic hydrides are used as heterogeneous bases and reducing reagents in organic synthesis. Typical solvents for this kind of reaction are ethers.

**Metallic hydrides** Interstitial hydrides usually exist within metals or alloys and their bonding is considered metallic. This kind of hydride has a strong electrical conductivity [15]. These hydrides have variable physical properties: some are more brittle, some are harder than respective metal. They are intermediate between salts and alloys. Metallic hydrides are made of protons and metal atoms in an electron sea. Electrical conductivity is due to the relative freedom of electron movement in the hydride. These systems are usually non-stoichiometric with variable amounts of hydrogen in the lattice.

Metallic hydrides are obtained heating hydrogen gas with metal or its alloy. They are reactive as the metal, stable in air at ambient temperature but reactive when heated or with acidic compounds. They are grayish black solids. They can be used as reducing agents.

Transition metal hydride complexes include compounds that can be classified as covalent hydrides. This kind of hydride features a single bond between the hydrogen center and the transition metal.

**Covalent hydrides** Covalent hydrides involve all other compound containing hydrogen. In this category hydrides that exist as discrete molecules, polymers or oligomers and hydrogen that has been chemically absorbed to a surface are included . An important part of covalent hydrides is formed by complex metal hydrides, soluble hydrides used in synthetic procedures.

### 3.1.1 Hydrides in rocket propulsion

Hydrogen is often used in space systems. It needs to be stored below 21 K at 1 atm. The use of hydrides is a safer, denser and more convenient way to store hydrogen.

Researches are done on hydrides as additives in propellants because of higher specific impulse and regression rate and lower metal agglomeration. Theoretically hydrides give higher specific impulse.

Maintenance of hydrides is an unsolved problem because of unknown aging process and stability conditions. Many hydrides don't decompose above 100°C but some of them are not much compatible with space propulsion ingredients. Dehydrogenation can take place if storing conditions are not optimal.

$H_2$ can have negative effects on the upper part of atmosphere.

Some hydrides, that can be used in space propulsion and that are investigated in a work by Maggi, Gariani, Galfetti and DeLuca [16], are:

- $AlH_3$ Aluminum Hydride
- $B_{10}H_{14}$ Decaborane
- LiH Lithium Hydride
- $MgH_2$ Magnesium hydride
- $LiAlH_4$ Lithium Aluminum Hydride
- $Li_3AlH_6$ Lithium Aluminum Hexahydride
- $LiBH_4$ Lithium Boron Hydride
- $Mg(BH_4)_2$ Magnesium Boron Hydride

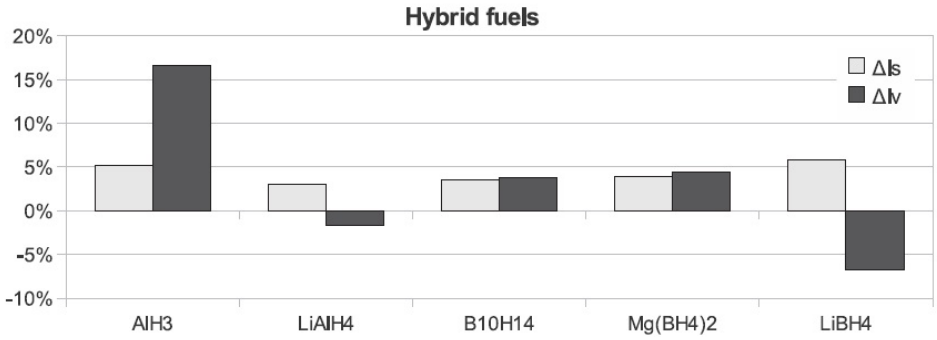


Figure 3.3: Hybrid fuel performance comparison

In the Figure 3.3 optimal $I_s$ and $I_v$ compared to baseline formulation and burning condition [16] are presented (pure HTPB and O/F mass ratio 2.2).

Hydrides main characteristics are low weight and high number of hydrogen atoms per molecule.

Theoretic specific impulse can be computed with thermochemistry. In a classical formulation added with metals the 10% of $I_s$ is lost due to two-phase flow and metal agglomeration. Additives also influence combustion stability, aging and propellant mechanical properties.

Using hydrides in hybrid propulsion $I_s$ increases of 5%. $AlH_3$ is the hydride that gives the best performance with an increase in $I_v$ about 15%. $LiBH_4$ gives an increase in $I_s$ but this good result is limited by its low density. Boron based hydrides give good results thanks to the low molar mass of combustion products, except for decaborane.

Hybrids are also limited by low regression rate, for this reason the use of additives is more focused on improving ballistic properties rather than specific impulse. Hydrides could react with hydroxyl groups of binder, for this reason the mixture process with HTPB can be limited in some cases.

Best performances are achieved with Aluminum Hydride and Lithium Aluminum Hydride. In hybrids propulsion only some hydrides give improvement in performances, but limited. Metallic Al, LiH, $MgH_2$ and $Li_3AlH_6$ cause a decrease of gravimetric specific impulse. Hydride density depresses $I_v$, this happens because part of the oxidizer is replaced by low density hydrides.The only exception is $AlH_3$ that has a density higher than other hydrides analyzed. Metallic aluminum and his hydride give an improvement about 6-12%, while the improvements with other hydrides are limited to few percent.

Condensed combustion products seem to be smaller with hydrides than with metallic additives. In the case of Aluminum Hydride condensed combustion products are similar to the case of metallic aluminum. With other hydrides the quantity of these products is very low or zero.

The analysis of combustion products in formulations with 20% additives allows to infer that the composition is influenced by the choice of oxidizer and solid fuel. The most important combustion products don't change with the additives. The condensed substances are mainly metallic oxides, boron nitride and boron oxide. Alumina decomposes ozone but in a short period it looses its reactivity.

### 3.1.2 Magnesium hydride

Magnesium hydride at standard condition is a powder.
Usually magnesium hydride is obtained with the following reaction:

$$Mg + H_2 \longrightarrow MgH_2$$

It can also be obtained in different ways [17]:

- hydrogenation of magnesium anthracene: anthracene reacts with Mg in THF producing a hydrogenation catalyst that is active under mild conditions. It is reactive and it could be important for hydrogen storage and other applications like reducing and drying agent.
- reaction of diethylmagnesium with litium aluminium hydride: this kind of $MgH_2$ is particularly reactive
- product of complexed $MgH_2$

$MgH_2$ reacts with water forming gaseous hydrogen: $MgH_2 + 2\,H_2O \longrightarrow 2\,H_2 + Mg(OH)_2$

At 300°C magnesium hydride decomposes producing $H_2$.

The properties of magnesium hydride [18, 19] are reported in Table 3.1 .

Table 3.1: Magnesium hydride properties

| | |
|---|---|
| **Molecular weight** | $26.3209 g/mol$ |
| **Phase at standard condition** | solid |
| **Melting point** | 327°C |
| **Density** | $1.45\ g/cm^3$ |
| **Specific heat capacity** $C_p$ | $1.345\ J/(gK)$ |
| **Specific free energy of formation** $\Delta_f G^0$ | -1.364 $kJ/g$ |
| **Specific heat of formation** $\Delta_f H^0$ | -2.861 $kJ/g$ |
| **Specific heat of fusion** | $0.53\ kJ/g$ |

### 3.1.3 Lithium hydride

Lithium hydride is an inorganic compound characterized by low density, high radiation and thermal stability [20]. It reacts with air. It can be transported in an inert atmosphere and it can be produced with fusion or compression. Lithium hydride has a high melting point and it is not soluble in any solvents with which it does not react. It is the lightest ionic compound. Lithium hydride burns not too fast but with an intense heat. It is a white crystalline substance and its density is higher than metallic lithium. Although it is ionic, it is a good electric conductor. Usually LiH is colored with blue-grey.

In contact with external air lithium hydride forms a layer of hydroxide and carbonate. It is the only saline hydride that melts under a pressure of 1 atm or less, without decomposing. Melting implies a 16% volume increase.

Table 3.2: Lithium hydride properties

| | |
|---|---|
| **Molecular weight** | $7.95 g/mol$ |
| **Melting point** | 688℃ |
| **Density** | 0.78 +/- 0.007 $g/cm^3$ |
| **Specific heat of formation** $\Delta H_{f_{25C}}$ | - 90.41 $kJ/mol$ |
| $\Delta H_{hydrolysis_{25C}}$ | - 132.27 $kJ/mol$ |
| **Specific entropy of formation** $\Delta S^0_{25C}$ | 24.7 +/- 2.1 J/(mol ℃) |
| **Specific heat capacity** $C_p$ | 4.307 $J/(gK)$ |
| **Specific free energy of formation** $\Delta_f G^0$ | -70.24 +/- 1.26 $kJ/mol$ |
| **Specific heat of fusion** $\Delta H_{fusion}$ | 20.51 +/- 2.93 $kJ/mol$ |

Table 3.3: Gaseous lithium hydride properties

| | |
|---|---|
| **Specific heat of formation** $\Delta H^0$ | 128.5 $kJ/mol$ |
| **Specific entropy of formation** $\Delta S^0$ | 40.77 e.u. |
| **Specific free energy of formation** $\Delta_f G^0$ | 105.48 $kJ/mol$ |
| **Specific heat capacity** $C_p$ | 29.55 $J/(molK)$ |
| **Specific heat of sublimation** $\Delta H_{sublimation}$ | 217.66 $kJ/mol$ |

If lithium hydride is exposed at air an hydroxide or lithium oxide layer forms on the hydride. Reducing action is weaker than with pure lithium. Melted lithium hydride is a good electric conductor.

The refractive index at 25℃ is $n_D = 1.9847$.

Lithium hydride reacts rapidly in low wet air forming $LiOH, Li_2O, Li_2CO_3$. In wet air it can burn spontaneously forming a thin viscous surface layer that inhibits any further reaction.

The reaction of lithium hydride with water gives as result lithium hydroxide at normal temperatures and lithium oxide at higher temperatures.

Ammonia reacts slowly with lithium hydride at temperatures below 300℃ above this temperature the reaction is fast. Lithium hydride is in equilibrium with alkaline metallic oxides. Lithium oxide could cohabit with lithium hydride without forming water.

Lithium hydride reacts in an irreversible way with lithium hydroxide forming lithium oxide and hydrogen. It reacts strongly with lower alcohols, slowly with upper alcohols and with phenols. It is not compatible with plastics containing hydroxyl, aldehyde, ketone, acids and ester groups. It is reliable that hydrocarbons and ethers are inert.

In the Table 3.2 the lithium hydride characteristics are presented [18, 19].

Lithium hydride in the gaseous state at 25℃ has the properties [20] shown in Table 3.3 .

### 3.1.4 Lithium aluminum hydride

Lithium Aluminum hydride ($LiAlH_4$) is an organic compound used as reducing agent in organic synthesis. At solid state it is highly reactive with water, releasing

gaseous hydrogen.

LAH reacts with water violently:

$$\mathrm{LiAlH_4 + 4\,H_2O \longrightarrow LiOH + Al(OH)_3 + 4\,H_2}$$

This reaction is a good method to obtain $H_2$ in laboratory [21].

$\mathrm{LiAlH_4}$ can be obtained with lithium hydride and an ether solution of aluminum chloride:

$$\mathrm{4\,LiH + AlCl_3 \longrightarrow LiAlH_4 + 3\,LiCl}$$

The industrial synthesis needs to obtain firstly sodium aluminum hydride :

$$\mathrm{Na + Al + 2\,H_2 \longrightarrow NaAlH_4}$$

and after LAH is obtained :

$$\mathrm{NaAlH_4 + LiCl \longrightarrow LiAlH_4 + NaCl}$$

$LiAlH_4$ if heated releases hydrogen in two steps [22]:

$\mathrm{LiAlH_4 \longrightarrow \frac{1}{3}\,Li_3AlH_6 + \frac{2}{3}\,Al + H_2}$

$\mathrm{\frac{1}{3}\,Li_3AlH_6 \longrightarrow LiH + \frac{1}{3}\,Al + \frac{1}{2}\,H_2}$

The two steps could release respectively 5.3 and 2.6 wt.% H relatively to $LiAlH_4$. If heated rapidly $LiAlH_4$ starts melting endothermically at 165-175°C, after it decomposes and recrystallizes with an exothermical reaction forming $Li_3AlH_6$ over the range 175 - 220°C. The second step starts with an endothermic melt reaction over the range 220 - 270 °C forming LiH.

Ti-bearing catalysts eliminate the first melt transformation and lower the temperature of the two reactions, but they cause the loss of hydrogen capacity.

Organic solvent impurities in $LiAlH_4$ play an important role in spontaneous decomposition of the hydride [22]:

- with 3 wt.% carbon, after six years the hydrogen content is only 32% of the initial amount
- after twenty years with 1.86 wt.% carbon, hydrogen content is 67%
- hydrogen is 96% after 18 years with 1.04 wt. % carbon

In Table 3.4 reactions with $\mathrm{LiAlH_4}$ are reported [23, 24].

In [22] the enthalpies of reaction of the following reactions were determined at 298 K :

$\mathrm{Li(s) + Al(s) + 2\,H_2 \longrightarrow LiAlH_4(s)}$

$\Delta H^r_{298} = -113.42 kJ/mol$

Table 3.4: Reactions involving Lithium Aluminum Hydride

| **Reaction** | $\Delta H^0$ [kJ/mol] | $\Delta S^0$ [J/(mol K)] | $\Delta G^0$ [kJ/mol] |
|---|---|---|---|
| $\mathrm{Li(s) + Al(s) + 2\,H_2 \longrightarrow LiAlH_4(s)}$ | -116.3 | -240.1 | -44.7 |
| $\mathrm{Li(s) + Al(s) + \frac{3}{2}\,H_2(g) \longrightarrow LiAlH_4(s)}$ | -25.6 | -170.2 | 23.6 |
| $\mathrm{LiAlH_4(s) \longrightarrow LiAlH_4(l)}$ | 22 | - | - |
| $\mathrm{LiAlH_4(l) \longrightarrow \frac{1}{3}\,Li_3AlH_6(s) + \frac{2}{3}\,Al(s) + H_2(g)}$ | 3.46 | 104.5 | -27.68 |

Table 3.5: Lithium Aluminum Hydride properties

| | |
|---|---|
| **Molecular weight** | $37.954 g/mol$ |
| **Phase at standard condition** | solid |
| **Melting point** | 125℃ |
| **Density** | $0.91\ g/cm^3$ |
| **Solubility** | decomposes in water |
| **Specific heat capacity** $C_p$ | $2.192\ J/(gK)$ |
| **Specific free energy of formation** $\Delta_f G^0$ | -1.178 $kJ/g$ |
| **Specific heat of formation** $\Delta_f H^0$ | -3.064 $kJ/g$ |
| **Flashpoint** | 125℃ |
| **Odor** | odorless |

$\mathrm{LiAlH_4 \longrightarrow \frac{1}{3}\,Li_3AlH_6 + \frac{1}{3}\,Al + H_2}$

$\Delta H^r_{298} = 9.79 kJ/mol$

LAH is metastable at room temperature: during long storage it slowly decomposes to $Li_3AlH_6$ and $LiH$. When LAH is heated, it decomposes in $LiAl$ and $H_2$.

LAH is used in organic chemistry as a reducing agent. It is also used in inorganic chemistry.

The properties of Lithium Aluminum hydride [18, 19] are listed in Table 3.5.

### 3.1.5 Aluminum Hydride

Aluminum hydride (chemical formula $\mathrm{AlH_3}$) is a covalent, binary, colorless and pyrophoric hydride. It contains 10.1 % by weight hydrogen [25]. It is widely used as reducing agents because it gives both high energy thanks to metal oxidation and low molecular weight thanks to hydrogen, resulting in good performances.

There are seven non solvated Aluminum hydride phases: $\alpha$-alane, $\alpha'$-alane, $\beta$-alane, $\delta$-alane, $\epsilon$-alane, $\theta$-alane and $\gamma$-alane

$\mathrm{AlH_3}$ is soluble in tetrahydrofuran and ether. $\alpha\mathrm{AlH_3}$ is the most thermally stable polymorph.

Table 3.6: Aluminum hydride properties

| | |
|---|---|
| **Molecular weight** | $29.99 g/mol$ |
| **Phase at standard condition** | solid |
| **Melting point** | 150℃ |
| **Boiling point** | decomposition |
| **Density** | $1.486\ g/cm^3$ |
| **Solubility** | reactive in water |
| **Specific heat of formation** $\Delta_{f298}H$ | -11.43 ± 0.84 $kJ/mol$ |
| **Gibbs specific energy of formation** $\Delta_{f298}G$ | 46.50 ± 0.96 $kJ/mol$ |

Table 3.7: Aluminum hydride thermodynamic properties

| T [K] | $C_p^o$ | $S^o$ | $(H^o - H_0^o)/T$ | $-(G^o - H_0^o)/T$ |
|---|---|---|---|---|
| 30 | 0.07 | 0.02 | 0.02 | 0.01 |
| 40 | 0.29 | 0.07 | 0.06 | 0.01 |
| 50 | 0.58 | 0.16 | 0.13 | 0.03 |
| 100 | 2.57 | 1.16 | 0.84 | 0.32 |
| 150 | 4.40 | 2.55 | 1.72 | 0.83 |
| 200 | 6.19 | 4.06 | 2.62 | 1.45 |
| 250 | 7.98 | 5.63 | 3.51 | 2.42 |
| 298.15 | 9.61 | 7.18 | 4.36 | 2.82 |

The properties of Aluminum hydride [18, 26] are listed in Table 3.6.

Monomeric $AlH_3$ has been isolated at low temperature showing a planar form.

Aluminum hydride is obtained from lithium aluminum hydride and aluminum tetrachloride with an etheral reaction:

$3\,LiAlH_4 + AlCl_3 \longrightarrow 4\,AlH_3 + 3\,LiCl$

The synthesis is extremely sensitive to desolvating conditions.

Other methods to obtain aluminum hydride are based on $LiAlH_4$ with $BeCl_2$ , $H_2SO_4$ or $ZnCl_2$ .

Aluminum hydride is more reactive than $LiAlH_4$, but they have similar handling properties.

Aluminum hydride can also be produced electrochemically avoiding chloride impurities.

$AlH_3$ reduces aldehydes, ketones, carboxylic acids, anhydrides, acid chlorides, esters, lactones to alcohols and it reduces amides, nitriles and oximes to amines.

The thermodynamic properties [26] of Aluminum hydride are shown in Table 3.7.

In a joint research [27] physical and ballistic properties of aluminum hydride are characterized. It is wanted to replace metallic aluminum with its hydride in combination with HTPB. The first step to be achieved is the stabilization of $AlH_3$. HTPB is not the best binder for aluminum hydride. Aluminum hydride has a relatively low density and a high molecular mass. Density lower than Al implies a very high density for hydrogen storage. Low density makes $AlH_3$ strongly convenient for upper-stage and space applications. All the seven phases of $AlH_3$ tend to dehydrogenate at standard

temperature in a period that ranges from hours to days. $\alpha$- $AlH_3$ is stable for a long period at standard temperature and it starts dehydrogenating above 160°C. Aluminum hydride crystals have been analysed finding that:

- carbon is found in the atomic layer
- with further sputtering alumina is found
- in depth aluminum hydride dominates

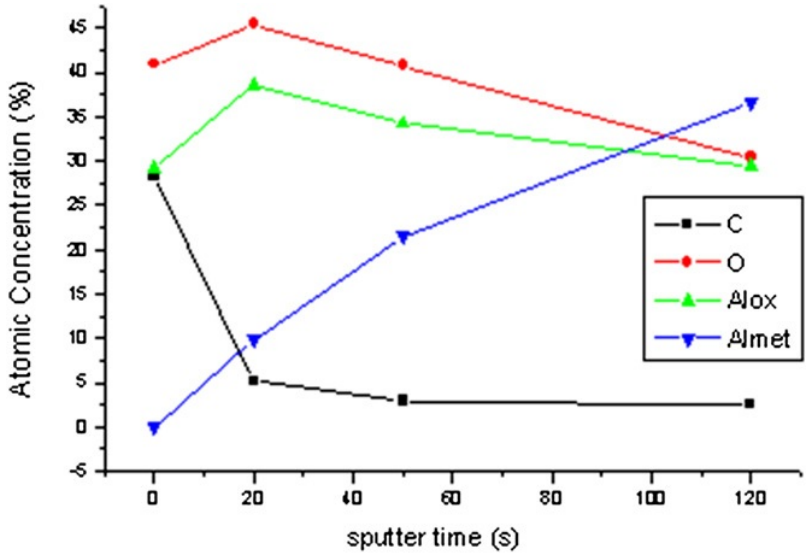


Figure 3.4: X-ray Photoelectron Spectroscopy of $AlH_3$

Aluminum hydride shows a lower flame temperature and a lower mean molecular mass than metallic aluminum. Because of its low density, the effect of $AlH_3$ on volumetric specific impulse is less favorable.

The dehydrogenation global reaction is slightly endothermic at standard conditions.

At 8.5 atm it is observed that dehydrogenation is faster than ignition and the combustion of alane particles with 5-10$\mu m$ diameter takes place. Combustion of dehydrogenated $\alpha$-$AlH_3$ takes place at high temperatures and pressures with combustion times similar to metallic Al. Released $H_2$ burns in the primary flame zone, Al ignites and burns downstream.

Pure Al is inert at low temperatures thanks to oxide coating while $AlH_3$ has coatings depending on the specific stabilization process. This means that $AlH_3$ could burn at temperatures lower than Al, approximately 1450 K. Regression rate and surface temperature show values higher than metallic formulations, while the dependence on pressure is weaker and the ignition is easier with increasing aluminum hydride content.

Flame is very clean allowing to think that there is a small amount of unburnt aluminum that agglomerates. The quality of the flame is strongly superior than in metallic aluminum formulations. The high regression rate favors little agglomeration.

If compared with Al, aluminum hydride shows a higher specific impulse and lower losses. Comparing the two formulations with the same amount of Al, it is found that the mass fraction of alumina in the combustion products is also the same. In the nozzle

the particles diameter increases from symmetry axis to the contour and it decreases going downstream. This distribution between Al and $AlH_3$ changes only quantitatively, not qualitatively. Aluminum hydride burns better because particles at nozzle inlet are smaller with aluminum hydride. Combustion products in the case of $AlH_3$ have a lower percentage of $CO_2$, OH and $H_2O$.

### 3.1.6 Ammonia Borane

Ammonia - Borane can be obtained from Diammoniate of diborane [28]. In absence of any extraneous proton sources the diammoniate in diethyl ether suspension decomposes very slowly at room temperature. Altering the ether environment adding a small quantity of anhydrous ammonia, the rate of hydrogen evolution increased markedly. Ammonia acts as catalyst. The reaction of diammoniate with ammonium chloride can be written as:

$$[H_2B(NH_3)_2][BH_4] + NH_4Cl \longrightarrow [H_2B(NH_3)_2]Cl + H_3NBH_3 + H_2$$

It is believed that two separate and competiting reactions take place to produce ammonia - borane:

the first is a relatively spontaneous decomposition which take place in the presence of ammonia and diethyl ether:

$$[H_2B(NH_3)_2][BH_4] \longrightarrow \frac{1}{n}(H_2NBH_2)_n + H_3NBH_3 + H_2$$

the second is the reaction between the diammoniate and ammonium chloride to produce the chloride salt of the diammoniate cation.

Alton prepared $H_3NBH_3$ through reaction of $NH_4Br$ and $NaBH_4$ in ansul 141 polyether.

Ammonia - borane present the characteristics shown in Table 3.8.

Ammonia - borane is monomeric in dioxane, diethyl ether, liquid ammonia and in the solid state.

Process for preparing ammonia - borane is based on the presence of ether during the reaction between an ammonium salt and a borohydride salt. Reaction of ammonium and borohydride salts in an ether slurry produces ammonia - borane, the decomposition of solid ammonium borohydride does not produce ammonia - borane.

By using a procedure based on that of Schlesinger and Burg [28] the synthesis of ammonia - borane from dimethyl ether - borane is possible:

Table 3.8: Ammonia Borane characteristics

| **Ammonia - Borane characteristics** |
|---|
| Crystalline material with definite X-ray powder pattern |
| Soluble in ether |
| Not readily hydrolized by distilled water |
| Slowly splits out hydrogen at room temperature |
| Reacts with sodium in ammonia to produce $\frac{\frac{1}{2}H_2}{H_3NBH_3}$ |

Table 3.9: Ammonia Borane properties

| | |
|---|---|
| **Melting point** | 110℃- 114℃ |
| **Density** | 0.78 $g/cm^3$ |
| **Molecular weight** | 30.865 g/mol |
| **Boron mass fraction** | 35% |
| **Hydrogen mass fraction** | 19.6% |
| **Nitrogen mass fraction** | 45.4% |
| **Boron atom fraction** | 12.5% |
| **Hydrogen atom fraction** | 75% |
| **Nitrogen atom fraction** | 12.5% |
| **Crystal structure** | orthorombic (T $<$ 200K) |
| | tetragonal ( T $>$ 200K) |
| **Appearance** | colorless solid |

$$(CH_3)_2OBH_3 + NH_3 \longrightarrow H_3NBH_3 + (CH_3)_2O$$

The properties of Ammonia Borane are shown in Table 3.9 [29, 30]

## 3.2 Effect of Boron addition in ramjet motor

The addition of aluminum or boron particles in solid fuels allows building more compact engines. The main problem associated with use of boron is the formation of condensed oxides on the surface of boron particles not allowing a complete boron consumption. This behavior is caused by low melting and boiling points of boron oxide $B_2O_3$ in combination with $B_2O_3$ surface tension. Boron oxide forms thin layers covering boron particles immediately after ignition when temperature is below $B_2O_3$ boiling point. These layers are barriers between the particle surface and oxygen, reducing the rate of chemical reaction. In the study made by Ciezki, Sender, Clauß, Feinauer and Thumann [9] with solid fuel and hot air at 800℃, the derivate of surface tension respect to the temperature $\frac{\partial \sigma}{\partial T}$ is very important, in addition to heat flux. Flow fields and combustion processes of solid fuels added with boron particles are investigated in relevant conditions for ramjet motors.

Measurements are allowed at a range of precise combustion chamber cross section, behind the flame-holding step. Tests are done at ambient pressure. With Schlieren techniques is possible to visualize refractive index gradients in flowfields and combustion processes. In strongly particle-laden flows an intensity reduction due to scattering and absorption by particles is recorded. For this reason results should be analyzed carefully. In this work are also used Mie, PIV and Coherent Anti-Stokes Raman Spectroscopy. A sampling probe system composed by water cooled sampling probe, exchangeable filter housing, remote control valve unit, vacuum pump and exchangeable gas sampling cylinders is used. Sample probe consists of three stainless steel tubes and an outer copper tube. Condensate phase is analyzed with Mammitol method that allows to know the Boron content. Gaseous phase is analyzed with gas chromatography.

In the work different test fuels based on HTPB added with different percentage of Boron or $TiO_2$ are used.

Fuel without addition shows a separation region and a big clockwise recirculating area behind the step, with a length of 5H (H is the step height). At the end of this recirculating area, the flow from this area and the flow from the combustor bottom form a saddle point.Thermal emissions of the investigated test fuels are dominated by soot. A further recirculating zone is located between the upper stage edge, the lower corner and a point approximately at $y/H \approx 1$. Recirculating zone ends approximately at x/H=4.8. U (velocity component in x direction) increases with y/H.

Temperature distribution at y/H=1 is bimodal with an averaged temperature of 850 K and an averaged temperature of 1750 K. At lower y the bimodal distribution is less visible and temperature increases with decreasing y. At low y/H Boron and $TiO_2$ behave as heat sink.

At x/H=8.5, in the boundary layer behind the primary recirculating zone $CO, CO_2, H_2$ and $C_2H_2$ concentrations decrease with increasing y, while $O_2$ concentration increases.

At x/H=14.6 there are irregularities, particularly in $O_2$ and $CO_2$ concentrations revealing an intense mixing with external flow.

$B_2O_3$ concentrations increase with y and with the distance from the step.

In another work made by Ciezki and Schwein [31] it is shown that both crystalline and amorphous particles can be seen on the photographs. Here there are also particles with droplike objects on the surface and bulged areas near the edges of the crystals. These phenomena could be caused by surface processes. The cooling in the probe should stop reactions and combustion in order to get samples of products as they are in the combustion chamber.

### 3.2.1 Effect of Ammonia Borane in hybrid motor

Boranes are made of Boron and Hydrogen. Ammonia borane $NH_3BH_3$ is solid and relatively safe to store and handle. Ammonia Borane releases a consistent amount of hydrogen when it decomposes, so it can lower the molecular weight of combustion process in a rocket motor, increasing $I_{sp}$ and c*. AB has an high $I_{sp}$ and it could be stored in LEO orbit. AB is added to HTPB and PBAN without good results because the grain manufacturing process becomes difficult.

In the research made by Weismiller et al. [32], best performances would be got with pure AB, but it is powder and so it needs a binder. Paraffin shows $T_C$ and c* lower than HTPB, but the addition of AB to paraffin increases $T_C$ and decreases the molecular weight, giving values for both the characteristic velocity and $T_C$ higher than HTPB's. Chamber pressure and thrust decrease slowly because of increasing combustion chamber volume. Thrust profile is in agreement with chamber pressure profile. At high GOX the highest $r_f$ is achieved with 10% AB, the lowest with pure paraffin. At lower GOX the highest $r_f$ is still shown by the formulation added with 10% AB, while the lowest is shown by 20% AB formulation. High quantities of AB produce a condensed phase, that inhibits the diffusion of reactants into the flame and the heat feedback to the un-reacted fuel, reducing the regression rate. $I_{sp}$ increases with increasing AB percentage: the highest value is shown with 50% AB. $I_{sp}$ efficiency is between 0.55 and 0.65 without any dependence from grain length. These low values in efficiency are caused by flow losses and heat losses in the nozzle.

## 3.3 Temperature and concentration behavior

A study made by Schulte, Pein and Högl [11] investigates temperature and concentration behavior in a ramjet with two fuels: polyethylene (PE) and HTPB. Air is heated by combustion of hydrogen and oxygen. Thermocouple and gas-chromatographic techniques are used to obtain temperature and species concentration profiles in the combustion chamber. Standard fuel is polyethylene. Five types of test are done: with an high O/F, with a quasi-stoichiometric mixture ratio, with two different temperature of air at inlet and with HTPB.

The first temperature profile downstream the flameholder shows a fast increase in the inlet air temperature to 1600℃. Going downstream, the peak in temperature approaches the solid wall and the mixing process increases. The combustion process takes place primarily in the shear layer of the incoming air flow and in the recirculation zone. Going downstream both the temperature peak near the wall and the temperature at the center of the port increase. With high air mass flux the region with maximum temperature is 2.5 mm far from the wall, while at lower air mass flux the distance is about 5 mm.

Increasing the air temperature at inlet causes higher values in peak temperature and in the temperature at the center of the combustor. The dependence of $r_f$ on air temperature at inlet is stronger than dependence on air mass flux.

Better mixing in B condition (quasi-stoichiometric condition) causes a radial temperature profile nearly constant. The better mixing in B conditions can be explained by lower velocity in the combustor. In case A (air - rich mixture ratio) mixing is not complete but reactions should be finished. In case B it is reached an higher adiabatic flame temperature but combustion processes should be incomplete. With HTPB, $r_f$ is 85% higher than with PE.

At the beginning of the chamber, in the middle, gas composition is similar to the air while near the wall $O_2$ drop down and the prevailing species become $CO, CO_2, H_2O, N_2$. High CO values indicate rich mixture in the recirculating area. At the end of recirculating area the composition is similar to the air in the middle. Near the wall the concentration of products increases, while $O_2$ and $N_2$ concentrations drop down.

At the transition between recirculating zone and redeveloping boundary layer there are small concentrations of combustion products at the center. CO concentration is maximum at the wall. Going further downstream oxygen concentration decreases, while $H_2O$ and $CO_2$ concentrations increase.

In the last position downstream there is not CO at center. There are higher CO concentrations near the wall. Along the combustor $O_2$ concentration decreases, while $CO_2$ concentration increases. Recirculating zone is homogeneous in concentration but inhomogeneous in temperature (ranging more than 750℃). In order to get a complete mixing and a complete combustion, an afterburner with a sufficient length (or other mixing devices) is needed.

# Chapter 4

# Surface tension: results and discussion

Surface or interfacial tension is the work required to change the shape of a given surface, in other words it is the property of the surface of a liquid to resist an external force and it is caused by the cohesion of similar molecules [33].

Surface tension can be measured as a force per unit length or as energy per unit area: usually surface tension is expressed in $mN/m$ or $dyn/cm$.

Surface tension is caused by the cohesive force between liquid molecules. Considering a liquid, molecules are pulled equally in all directions by adjacent liquid molecules. This does not happen for molecule on liquid surface, which are pulled inwards, creating an internal pressure that force the liquid surface to contract to the minimal area.

By an energetical point of view surface tension tension can be explained in this way: a molecule in contact with a neighbor is in a lower state of energy than if it were alone. Internal molecules have neighbor on every side, boundary molecules don't have neighbor on all sides and so they have a higher energy. The liquid, in order to minimize its energy state, minimizes the number of boundary molecules resulting in the minimization of the surface area.

In order to reduce surface tension values surfactants are used such as TX-100, Cetomacrogol and sodium. In petroleum industry surfactants are used to crack the long chain paraffin molecules which diminish the lifting performance.

## 4.1 Definitions and measurement methods

### 4.1.1 Description of phenomenon

Generally surface tension is represented by the symbol $\gamma$ and it is the force along a line of unit length, where the force is parallel to the surface and perpendicular to the line.

Surface tension can also be defined thermodinamically: it is the energy necessary to create surfaces. The work needed is proportional to the amount of molecules that must be brought to the surface [34].

$$\delta W = \gamma \delta A \tag{4.1}$$

where $\gamma$ is the surface tension and it can be defined as the energy that needs to be supplied in order to increase the surface area by one unit. In this way surface tension is measured in $J/m^2$ or $ergs/cm^2$, giving the same value of force per unit length.

If on one side of the surface there is a pressure different to the pressure of the other side, the difference results in a normal force that is canceled by the surface tension. For this reason a curved surface is needed.

The Young - Laplace equation states that:

$$\Delta p = \gamma(\frac{1}{R_x} + \frac{1}{R_y}) \tag{4.2}$$

where $\Delta p$ is the pressure difference, $R_x$ and $R_y$ are radii of curvature in the axes parallel to the surface and $\gamma$ is the surface tension.

The mean cuvature of the surface is represented by $\frac{1}{R_x} + \frac{1}{R_y}$.

Surface tension is a property of liquid's interface with another medium. Contact angle measures the wetting of a solid by a liquid and it is the angle made by the tangent to the surface and the solid surface [35]. Low values of contact angle mean that the liquid spreads well. Increasing contact angle values, the liquid decreases its property to wet the solid. A zero contact angle implies complete wetting. If the contact angle is below 90 ° the liquid wets the solid, if it is more than 90° the liquid is considered non-wetting. For a couple of substances (liquid/solid) can be found a range of contact angles.

$$\gamma_{la} > \gamma_{ls} - \gamma_{sa} > 0 \tag{4.3}$$

where $\gamma_{ls} - \gamma_{sa}$ is the difference between liquid-solid and solid-air surface tension, $\gamma_{la}$ is the liquid-air surface tension.

At the contact point both the vertical and the horizontal forces must cancel, this point is called 'equilibrium'. The horizontal component of $f_{la}$ is canceled by the adhesive force $f_A$. The vertical component of $f_{la}$ must balance the force $f_{ls}$:

$$f_{ls} - f_{sa} = -f_{la}cos\theta \tag{4.4}$$

resulting in

$$\gamma_{ls} - \gamma_{sa} = -\gamma_{la}cos\theta \tag{4.5}$$

where $\theta$ is the contact angle.

### 4.1.2 Methods of measurement

Surface tension can be measured in many different ways:

- **Du Noüy Ring method**: it is the first method developed to measure surface tension [36]. In this method the liquid is raised until it contacts the surface of the ring. After the sample is lowered stretching the liquid film produced with the ring contact. The maximum pull exerted on the ring by the surface, that is got when the film is stretched, is measured. At this moment the contact angle $\theta$ is 0. Experimentally the distance is increased until the maximum force is reached and crossed. After, the vessel containing the liquid sample is lowered passing again through the maximum force point. In this moment the surface tension is calculated.

- **Du Noüy - Padday method**: the platinum ring used in Du Noüy Ring method is replaced with a rod that measures equilibrium surface tension or dynamic surface tension [36]. The rod is perpendicular to the interface, it is immersed and pulled out of the sample and the maximum force is measured. The diameter of the probe has not any influence, only if it changes there is the need to recalibrate.

- **Wilhelmy plate method**: it's used to check surface tension over long time intervals [36]. A vertical plate of known perimeter is attached to a balance, and the force due to wetting is measured. It is used with liquid - liquid or air - liquid interface. In this method the liquid is raised until the contact between the surface and a perpendicular plate. At the contact, the maximum tension acting on the balance is recorded, avoiding further movements of the sample during tests. Usually the plate is on the order of a few centimetres square and it is made from glass or platinum. The plate is cleaned and attached to a scale or a balance with a thin metal wire. The force on the plate caused by wetting is measured with a tensiometer or microbalance and it is used to obtain the surface tension with the Wilhelmy equation $\gamma = \frac{F}{lcos\theta}$ where $l$ is the wetted perimeter and $\theta$ is the contact angle between the liquid phase and the plate. In general $\theta$ is assumed to be zero.

  This method does not require correction factors, because of assuming the contact angle to be zero. The plate is not moving during measurements, so accurate determination of surface kinetics on a wide range of timescales is allowed. It is not needed to know the density of the liquid as in the ring method. Liquid surface is not pressed avoiding phase mixing. It is a static measurement avoiding the risk of non-equilibrium conditions.

- **Pendant drop method**: the liquid is injected from a needle forming a drop on the tip. Surface tension is calculated observing optically the shape of the drop.

- **Spinning drop method**: it is used with very low surface tension values. A small drop of sample is injected in a thin tube with another liquid. The tube is rotated at high speed: the angular speed of the tube and the shape of the drop allow to obtain the surface tension values.

- **Bubble pressure method**: firstly a capillary tube is immersed in the liquid sample, then constant gaseous flow passes through the tube forming bubbles into the liquid. The surface tension is calculated computing the pressure difference between inside and outside the bubble and the radius of the bubble. This method gives some problem in deviation.

- **Sessile drop method**: it is used for solids and it is a method based on optical contact angle [33]. It is used to measure wetting properties of a region of a solid surface. The angle between the baseline and the tangent at the drop boundary is measured.

- **Oscillating and Expanding Drop method**: it measures the interfacial rheological properties of emulsions and foams [33].

Other types of method that can be used are:

- Drop volume method: the interfacial tension is measured as a function of interface age.

- Capillary rise method
- Stalagmometric method
- Single Fiber Wilhelmy method (solids)
- Dynamic Wilhelmy method (solids)
- Measurement of foamability and stability (for foams and emulsions)
- Vibrational frequency of levitated drops
- Powder Contact Angle Method (solids)

### 4.1.3 Surface tension influencing parameters

**Effect of puddles on a surface**

Pouring water on a surface made of a substance that the water does not adhere to, such as wax, gives a result similar to the mercury poured onto glass: it results in a puddle with a certain thickness.

The thickness of a puddle of liquid, on a surface whose contact angle is 180° , is:

$$h = 2\sqrt{\frac{\gamma}{g\rho}} \tag{4.6}$$

where h is the depth of the puddle (h is a little bit smaller because generally $\theta$ is not 180°).

**Influence of temperature** Surface tension is strongly influenced by temperature. Generally surface tension decreases with increasing temperature, reaching a value of zero at the critical temperature. Surface tension and temperature can be related by:

- **Eötvös rule** that predicts the surface tension of liquid pure substances as function of temperature. At critical point the surface tension is zero.

  Eötvös rule is based on two hypothesis:

  - surface tension depends linearly on temperature
  - temperature dependence of the surface tension can be plotted for all liquids collapsing the data in a single master curve

  The expression is:

  $$\gamma V^{2/3} = k(T_C - T) \tag{4.7}$$

  where k is a constant ($2.1 \cdot 10^{-7} J/(Kmol^{-2/3})$), $V$ is the molar volume and $T_C$ the critical temperature of a liquid, $\gamma V^{2/3}$ is also called 'molar surface tension $\gamma_{mol}$' .

  Considering that the line normally passes the temperature axis 6 K before the critical point:

  $$\gamma V^{2/3} = k(T_C - 6K - T) \tag{4.8}$$

- **Guggenheim - Katayama**:

$$\gamma = \gamma^o \left(1 - \frac{T}{T_C}\right)^n \tag{4.9}$$

where $\gamma^o$ is a constant for each liquid and n is an empirical factor (n=11/9 for organic fluids).

**Influence of solute concentration** The effect of solute on surface tension can be different depending on solute structure.

Another variable is the difference in solute concentration between the bulk liquid and the surface.

### 4.1.4 Surface tension values for some substances

In Figure 4.1 and 4.2 surface tension values of some substances as function of temperature calculated from [37, 38] are shown. Values are obtained knowing the surface tension at a certain temperature and the slope of the surface tension - temperature relation. For all substances this relation is assumed to be linear.

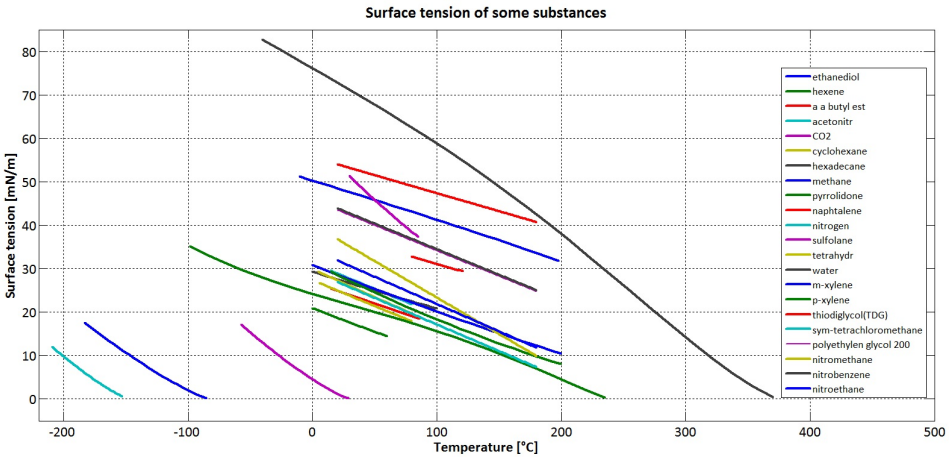


Figure 4.1: Surface tension values for some substances

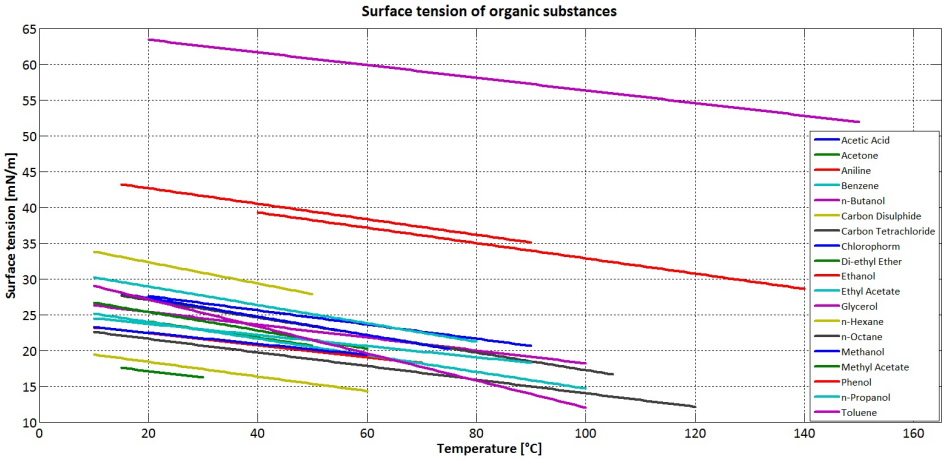


Figure 4.2: Surface tension values for some organic substances

## 4.2 Experimental measurements of surface tension

After this general overview it is possible to start with the experimental activity in the laboratory.

### 4.2.1 Experimental apparatus

For surface tension measurements a Krüß tensiometer [33] is used. The experimental apparatus is formed by:

- the tensiometer composed by:
  - a display where surface tension values, detected temperatures and some other data are shown
  - a hot oil heated balance where the liquid wax is inserted
  - a thermometer that measures directly the temperature in the liquid
  - a Wilhelmy plate
- an oil reservoir electrically heated
- a display where the oil temperature is set and read
- pipes in which hot oil flows heating the tensiometer

Figure 4.3: Surface tension values for some organic substances

Table 4.1: Krüss EasyDyne Tensiometer - Technical data

| **Technical data** | |
|---|---|
| **Operative Range** | |
| Surface tension | 1 - 999 $mN/m$ |
| Density | 1 - 2200 $kg/m^3$ |
| Temperature | -10 - +100 ℃ |
| **Resolution** | |
| Surface tension | +/- 0.1 $mN/m$ |
| Density | 1 $kg/m^3$ |
| Temperature | 0.1 ℃(optional) |
| **Sample system characteristics** | |
| Speed | 2.5 - 14 $mm/min$ |
| Height | 75 $mm$ |
| Ring Correction | Zuidema & Waters, Harkins & Jordan |
| Display | 320 x 240 $pixel$ |
| Interfaces | RS232, USB |
| Power | $15W$ |
| Power | 100 - 240 $VAC$ , 47 - 63 $Hz$ |
| Weight | $11kg$ |
| Dimensions | 270 x 420 x 350$mm$ |

Table 4.2: Wax properties given by Sasolwax GMBH

| Sasol Wax | Congealing point °C | Oil content % | Penetration at 25 °C 1/10mm | Viscosity at 100°C $mm^2/s$ |
|---|---|---|---|---|
| 6003 | 60-62 | 0-0.5 | 17-20 | - |
| 6805 | 66-70 | 0-1 | 16-20 | 6-8 |
| 0907 | 83-94 | 0-1 | 4-10 | 14-18 |
| 1276 | 64-68 | - | 8-13 | 880-920 |

### 4.2.2 Test results - Pure paraffin

The first phase is focused on obtaining surface tension values for pure paraffins. Four different kinds of paraffin, whose properties are shown in Table 4.2, are tested:

- Sasolwax 0907
- Sasolwax 6805
- Sasolwax 1276
- Sasolwax 6003

#### Sasolwax 0907

In Figure 4.4 the experimental data and the mean curve are presented.

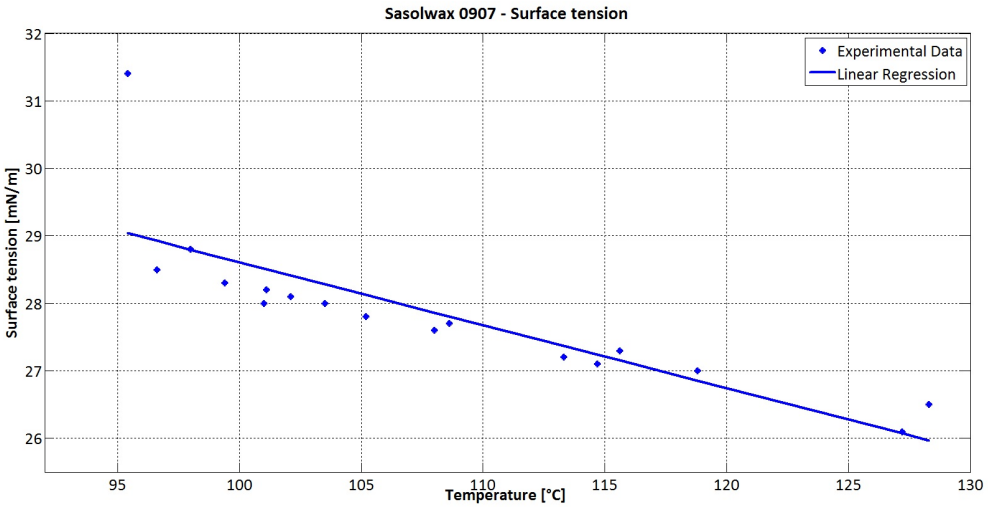


Figure 4.4: Surface tension values for Sasolwax 0907

The coefficient of determination $R^2$, that gives a measure of the fitting of the linear regression curve and the measured points, is calculated. It is the square of the regression coefficient and it can assume values between 0 and 1.

In this case $R^2$ is 0.673. Neglecting the last measured point, that can be influenced by incipient solidification, $R^2$ is 0.952.

### Sasolwax 6805

In Figure 4.5 the experimental data and the mean curve are presented.

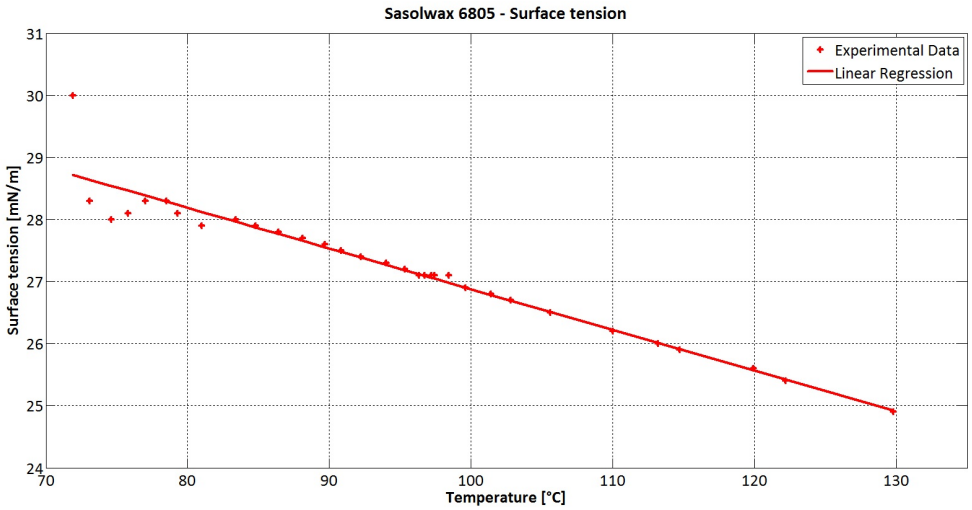


Figure 4.5: Surface tension values for Sasolwax 6805

In this case $R^2$ is 0.930.

### Sasolwax 1276

In Figure 4.6 the experimental data and the mean curve are presented. Temperatures below 75.8℃ don't allow the calculation of surface tension because of solidification.

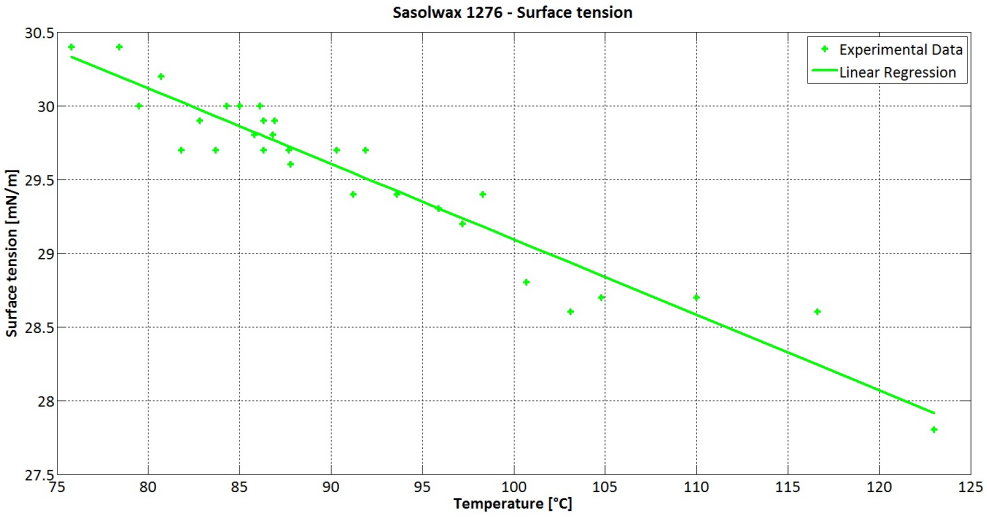


Figure 4.6: Surface tension values for Sasolwax 1276

In this case $R^2$ is 0.920.

### Sasolwax 6003

In Figure 4.7 the experimental data and the linear regression curve are presented. Below 69℃ solidification starts.

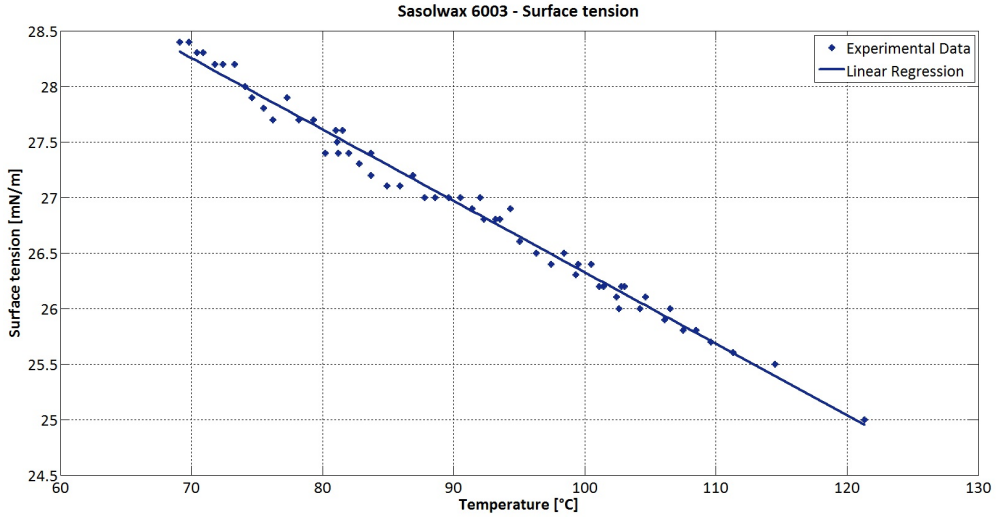


Figure 4.7: Surface tension values for Sasolwax 6003

In this case $R^2$ is 0.987.

Table 4.3: Slope comparison of pure paraffins

| Wax type | Slope Coefficient | $\Delta_{slope}$ calculated on wax 1276 |
|---|---|---|
| Sasol 1276 | -0.0512 | +0% |
| Sasol 6003 | -0.0643 | +25.59% |
| Sasol 6805 | -0.0648 | +26.56% |
| Sasol 0907 | -0.0736 | +43.75% |

### Sasolwax 0907, Sasolwax 6805, Sasolwax 1276 and Sasolwax 6003 surface tension curve comparison

The curves of the different types of paraffin are plotted together in order to show their behavior (Figure 4.8). From this figure it can be inferred that Sasolwax 0907, at the same temperature, has a higher surface tension than Sasolwax 6805. It can also be inferred that the surface tension of Sasolwax 0907 decreases with temperature faster than Sasolwax 6805.

Wax 1276 shows the highest surface tension values, and it has also the lowest slope coefficient. The lowest surface tension values are shown by Wax 6003.

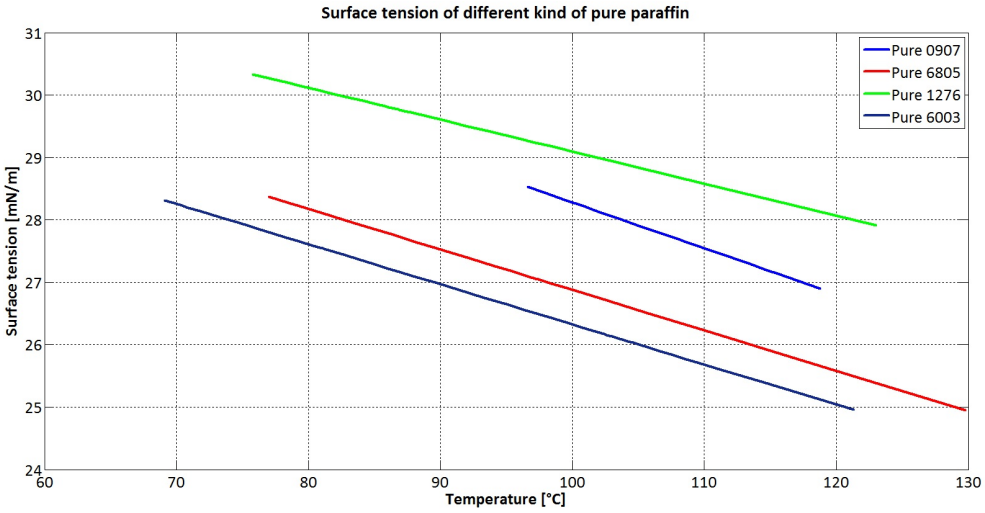


Figure 4.8: Surface tension values for pure paraffin

### Pure paraffin and organic substances comparison

In this paragraph the behavior of surface tension in paraffin and in other organic substances are compared.

The high operative temperatures of pure paraffin can be noted: they range from 75-95°C to 120-130°C. Many organic substances (with the exception of Carbon Tetrachloride, Glycerol, n-Octane and Phenol) have operative temperatures below 100°C.

Another important point is that paraffins, in their temperature range, have surface tension values higher than other substances except for Aniline, Glycerol and Phenol (that are not shown in Figure 4.9). Paraffins show a decrease in surface tension with temperature that is slower than all other substances(Figure 4.9).

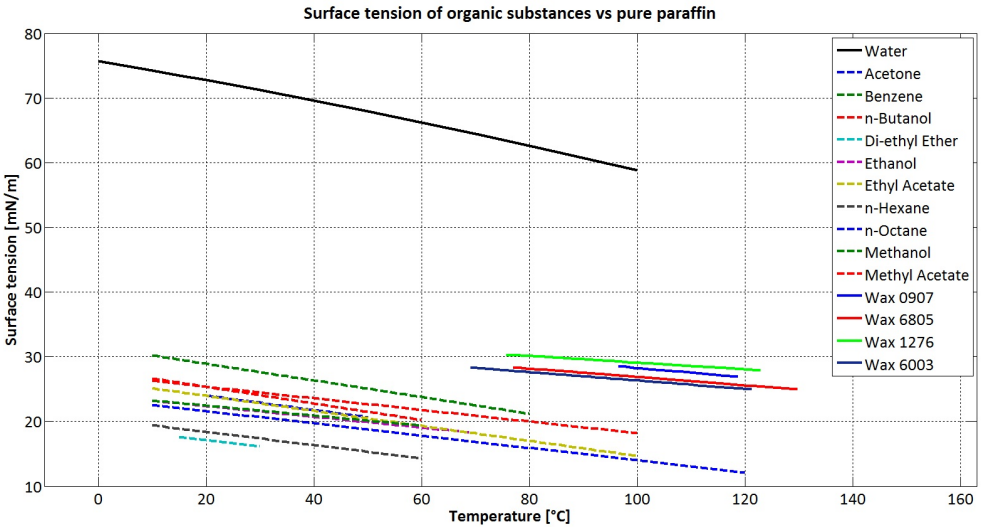


Figure 4.9: Surface tension values: pure paraffins vs. organic substances

### 4.2.3 Test results - Paraffin with additives

After tests done with pure paraffin, some substances are added to pure paraffins.

#### Sasolwax 0907 + 2% Black Carbon

The first sample is a mixture composed by Sasolwax 0907 added with 2% carbon black. Carbon black is not added in order to obtain a modification of the performance, but just to prevent the penetration of the flame in depth in the paraffin.

In Figure 4.10 the experimental data and the mean curve are presented.

In this case $R^2$ is 0.902.

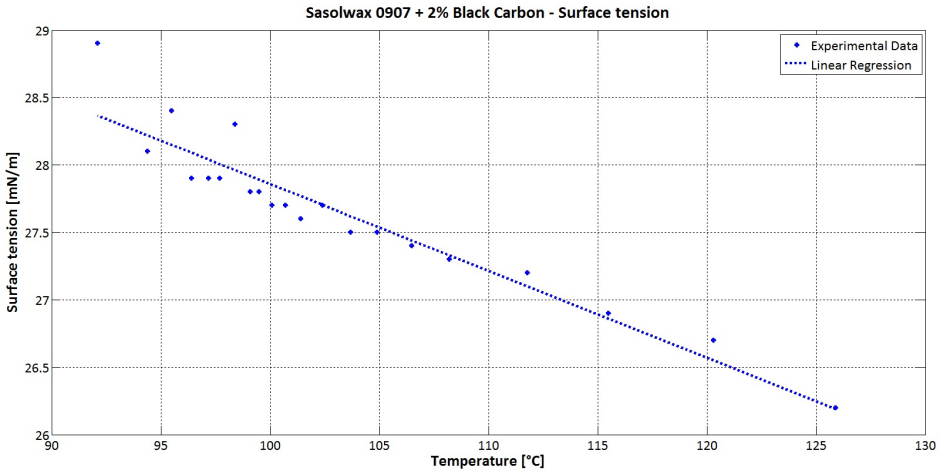


Figure 4.10: Surface tension values for Sasolwax 0907 added with Black Carbon

### Sasolwax 0907 +10% Stearic Acid

In this case a mixture composed by 90% by weight of Sasolwax 0907 and 10% by weight of Stearic Acid is used.

Considering the different characteristics of wax and Stearic Acid it is expected to note a variation in the value of surface tension respect to the case of pure wax Sasolwax 0907.

In Figure 4.11 the data and the mean curve are presented.

In this case $R^2$ is 0.500. Neglecting the last measured points, which can be influenced by incipient solidification, $R^2$ is 0.915.

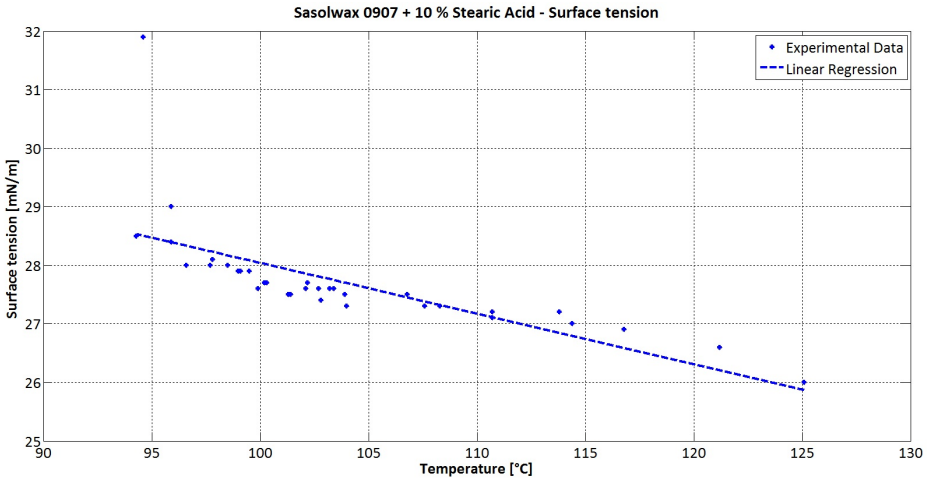


Figure 4.11: Surface tension values for Sasolwax 0907 added with Stearic Acid

### Sasolwax 0907 +10% PEG

A mixture made of 90% by weight of Sasolwax 0907 and 10% of PEG 6000 is tested. In Figure 4.12 the experimental points and the regression curve are shown.

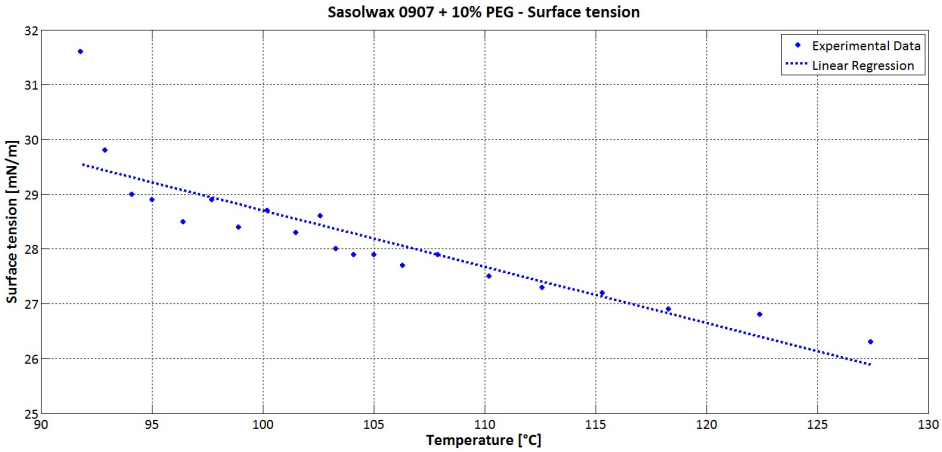


Figure 4.12: Surface tension values for Sasolwax 0907 added with PEG 6000

$R^2$ is 0.770. Neglecting the last measured point $R^2$ is 0.920.

### Sasolwax 0907 +10% PECVA

In this case a mixture composed by 90% by weight of Sasolwax 0907 and 10% by weight of Poly-Ethylene-Co-Vinyl-Acetate is tested.

Considering the different characteristics of the wax and Poly-Ethylene-Co-Vinyl-Acetate it is expected to note a variation in the value of surface tension respect to the case of pure paraffin Sasolwax 0907.

In Figure 4.13 the data and the mean curve are presented.

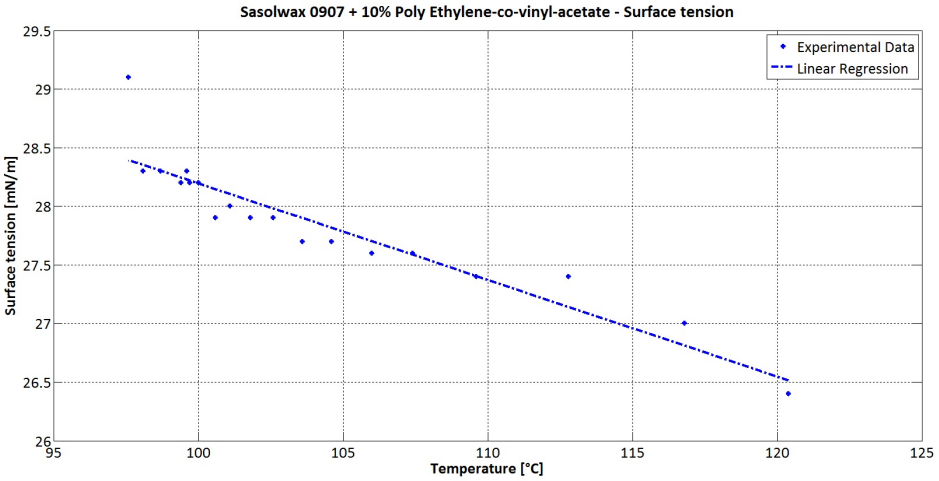


Figure 4.13: Surface tension values for Sasolwax 0907 added with Poly-Ethylene-Co-Vinyl-Acetate

$R^2$ is 0.868.

### Sasolwax 0907 + 10% Aluminum

In this case a mixture composed by 90% by weight of Sasolwax 0907 and 10% by weight of Aluminum is tested.

In Figure 4.14 the data and the mean curve are presented.

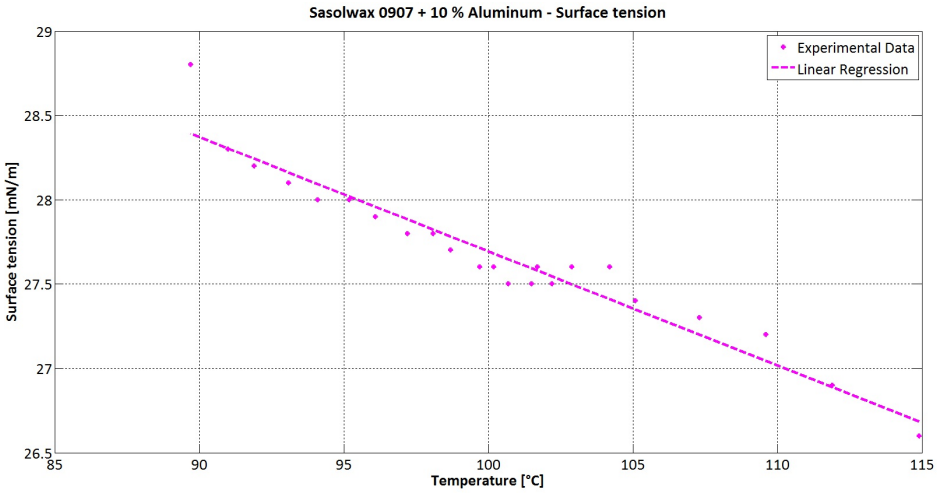


Figure 4.14: Surface tension values for Sasolwax 0907 added with 10% Aluminum

$R^2$ is 0.928.

### Sasolwax 0907 + 40% Aluminum

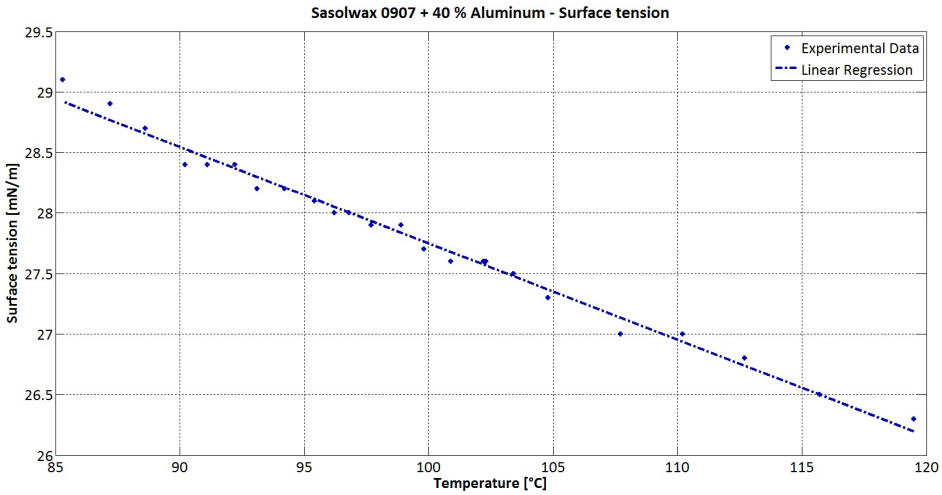


Figure 4.15: Surface tension values for Sasolwax 0907 added with 40% Aluminum

In order to look at the effect of increasing Aluminum percentage, a mixture made of 40% Aluminum is tested.

In Figure 4.15 the data and the mean curve are presented.

$R^2$ is 0.988.

### Comparison of Sasolwax 0907 tests

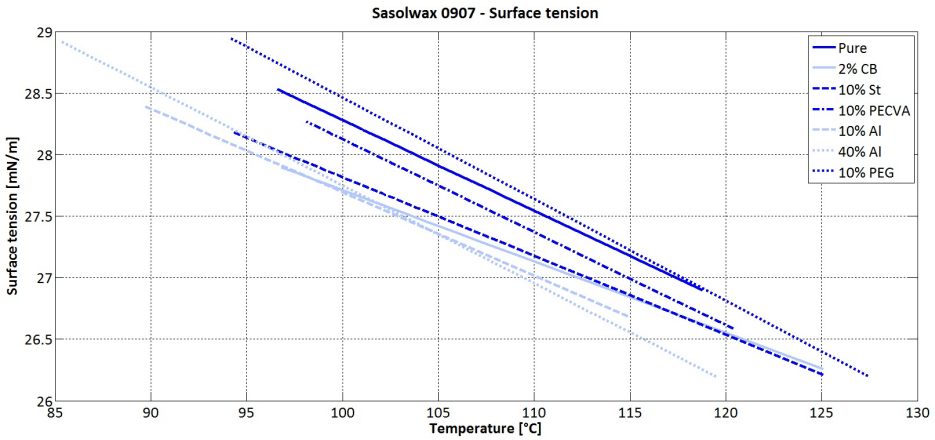


Figure 4.16: Comparison of Sasolwax 0907 tests

As it can be seen in Figure 4.16, there are no great variation in surface tension behavior for Sasolwax 0907 adding some additives such as black carbon or Stearic Acid. The seven curves show that the most different values are obtained adding 10% and 40 % Al. The other curves are quite close one to each other, especially the curve with Black Carbon and the one with Stearic Acid, which are overlapped. Beacuse of the high density of PECVA, an inhomogeneous distribution of the additive in the wax could be present during surface tension tests. This problem is not present while testing waxes mixed with PEG. In this last case curves are close to the pure case.

In the case of Poly-Ethylene-Co-Vinyl-Acetate the values are really close to pure waxes ones. This happens because this additive, when melted, sank like a glue. Considering that the measurement is done at a fixed height of the beker, the contribute of Poly-Ethylene-Co-Vinyl-Acetate could be computed in a percentage lower than 10% by weight.

The lowest values are obtained with 40% Al at high temperatures and with 2% CB and 10% Al at low temperatures.

### Sasolwax 6805 + 1% Carbon Black

A mixture composed by 99% wt. Sasolwax 6805 and 1% wt. carbon black is analysed.

In Figure 4.17 the experimental data and the mean curve are presented.

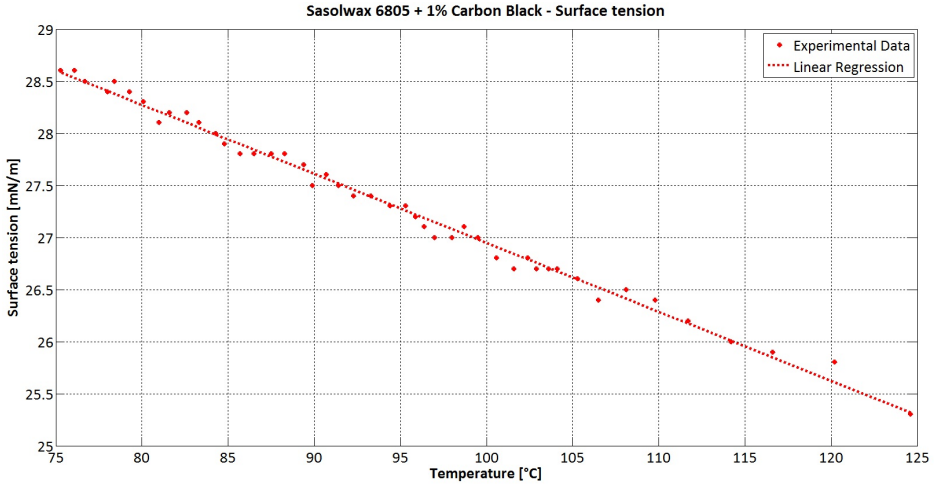


Figure 4.17: Surface tension values for Sasolwax 6805 added with Black Carbon

$R^2$ is 0.992.

### Sasolwax 6805 +10% Stearic Acid

In this case a mixture composed by 90% by weight of Sasolwax 6805 and 10% by weight of Stearic Acid is analysed.

In Figure 4.18 the data and the mean curve are presented.

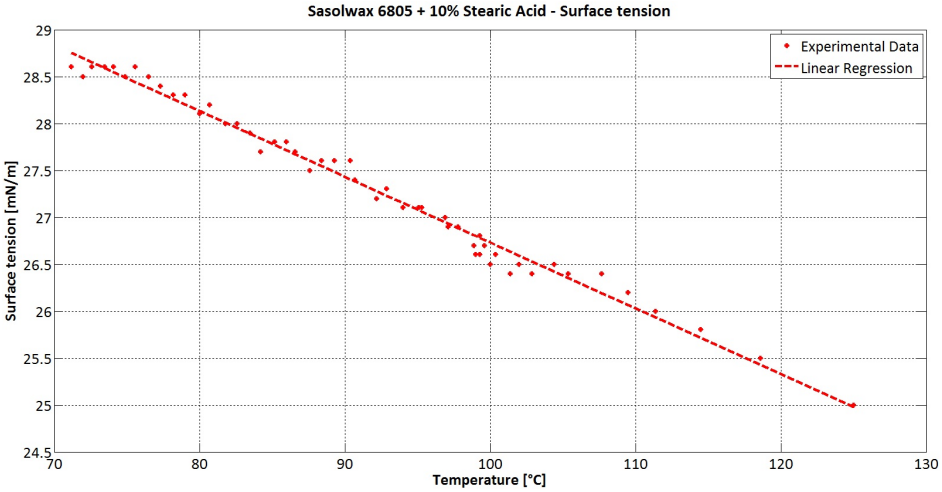


Figure 4.18: Surface tension values for Sasolwax 6805 added with Stearic Acid

$R^2$ is 0.986.

### Sasolwax 6805 +10% PEG 6000

In this case a mixture composed by 90% by weight of Sasolwax 6805 and 10% by weight of PEG (polyethyleneglykol) 6000 is investigated.

Considering the different characteristics of wax and PEG, it is expected to note a variation in the value of surface tension respect to the case of pure paraffin Sasolwax 6805.

In Figure 4.19 the data and the mean curve are presented.

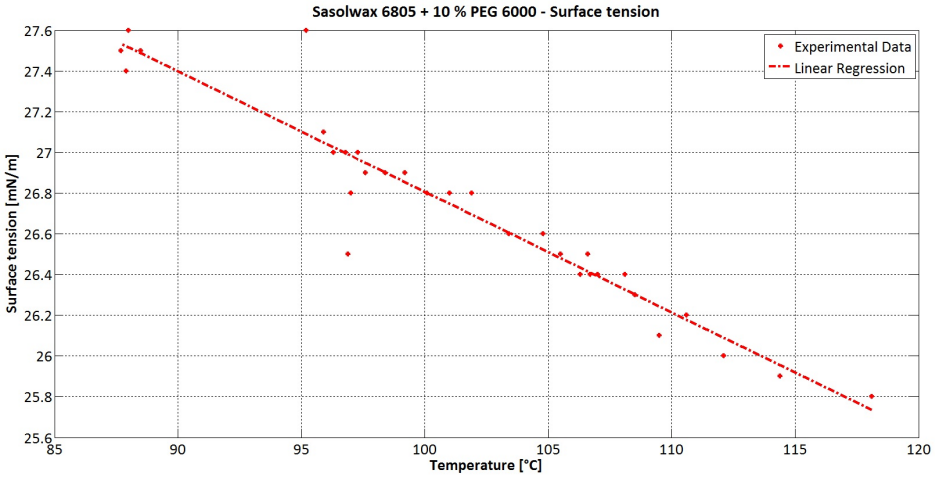


Figure 4.19: Surface tension values for Sasolwax 6805 added with PEG 6000

$R^2$ is 0.911.

### Sasolwax 6805 +10% PECVA

A mixture made by 90% by weight of Sasolwax 1276 and 10% of PECVA is analysed. In Figure 4.20 the experimental point and the regression curve are shown.

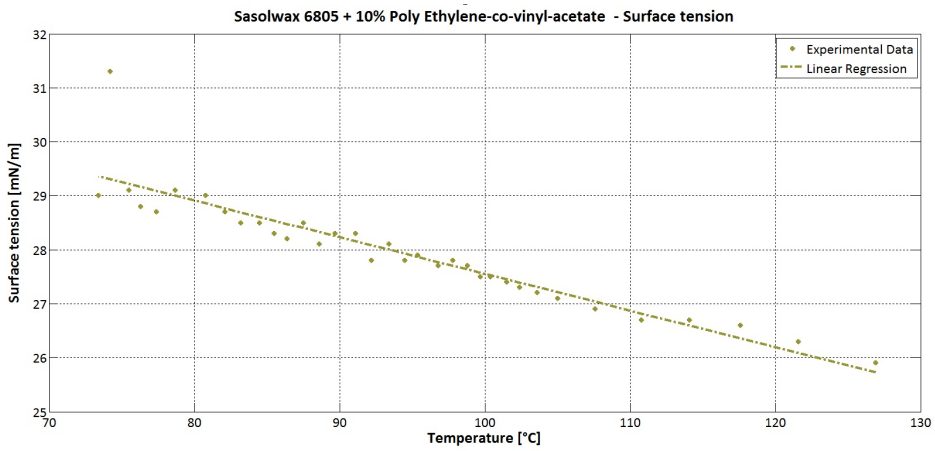


Figure 4.20: Surface tension values for Sasolwax 6805 added with PECVA

$R^2$ is 0.855. Neglecting the last measured points, which can be influenced by incipient solidification, $R^2$ is 0.970.

### Comparison of Sasolwax 6805 tests

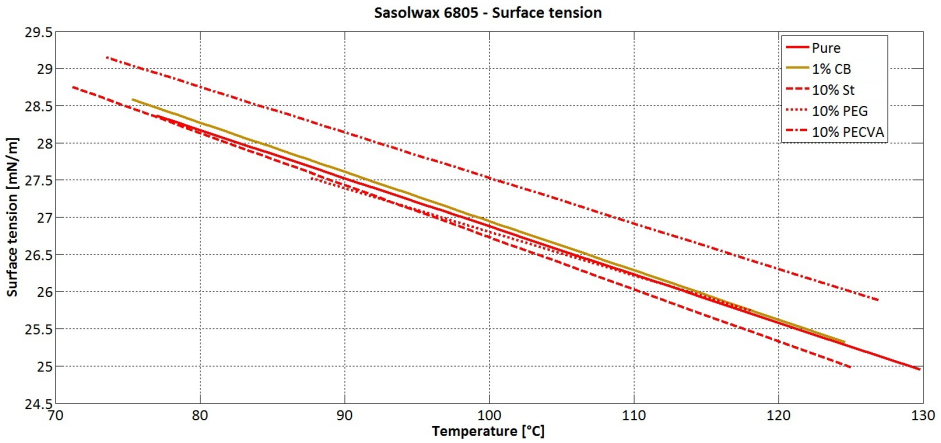


Figure 4.21: Comparison of Sasolwax 6805 tests

As it can be seen in Figure 4.21 there are no great variation in surface tension behavior for Sasolwax 6805 adding some additives such as Carbon Black, Poly-Ethylene-Glykol or Stearic Acid. The four curves are quite close one to each other. The curve that is more different is the one with PECVA that shows the highest surface tension values.The main difference consits in the temperature range: with PEG 6000 the range becomes smaller, with Stearic Acid there is a lowering effect on melting temperature. Carbon Black behaves as Stearic Acid. At high temperatures the lowest surface tension values are obtained with 10% Stearic Acid, while at low temperatures they are got with PEG.

### Sasolwax 1276 + 1% Carbon Black

A mixture composed by 99% wt. Sasolwax 1276 and 1% wt. carbon black is investigated.

In Figure 4.22 the experimental data and the mean curve are presented.

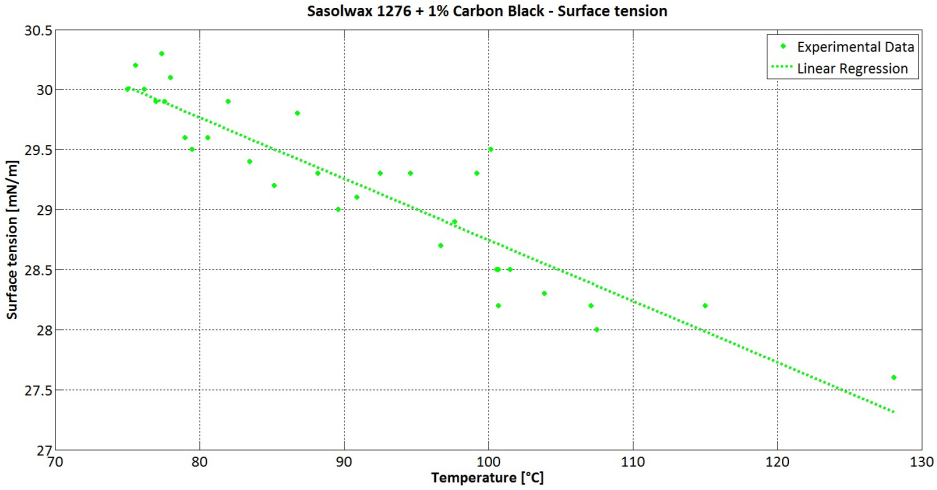


Figure 4.22: Surface tension values for Sasolwax 1276 added with Black Carbon

$R^2$ is 0.840.

### Sasolwax 1276 + 10% Stearic Acid

A mixture composed by 90% wt. Sasolwax 1276 and 10% wt. stearic acid is analysed.

In Figure 4.23 the experimental data and the mean curve are presented.

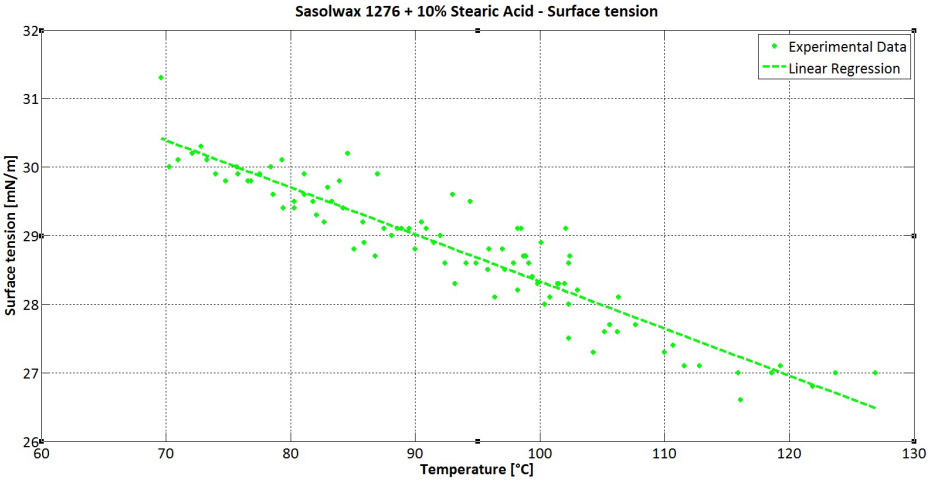


Figure 4.23: Surface tension values for Sasolwax 1276 added with Stearic Acid

$R^2$ is 0.869.

### Sasolwax 1276 +10% PEG

A mixture made of 90% by weight of Sasolwax 1276 and 10% of PEG 6000 is tested. In Figure 4.24 the data and the mean curve are presented.

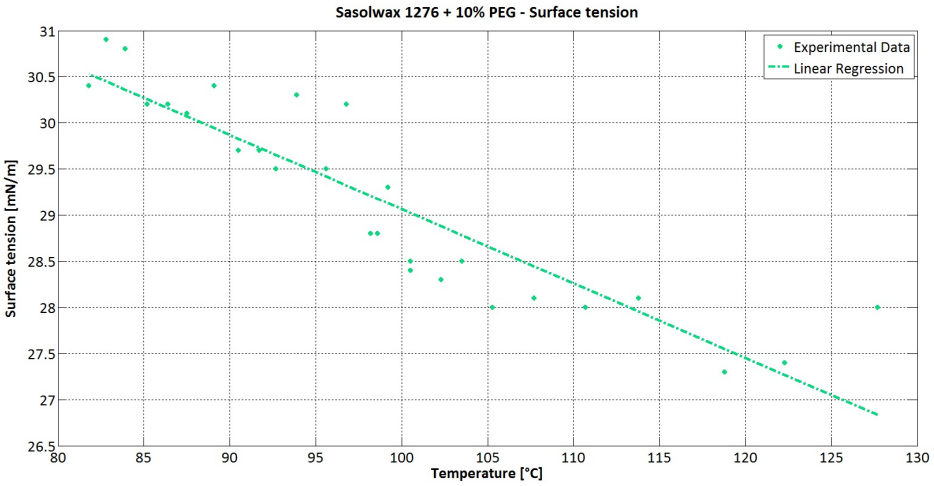


Figure 4.24: Surface tension values for Sasolwax 1276 added with PEG 6000

$R^2$ is 0.820. Neglecting the first measured point, influenced by inhomogeneous temperature in the glass at the beginning of the test, $R^2$ is 0.870.

### Sasolwax 1276 +10% PECVA

A mixture composed by 90% by weight of Sasolwax 1276 and 10% of PECVA is investigated.

In Figure 4.25 the experimental point and the mean curve are shown.

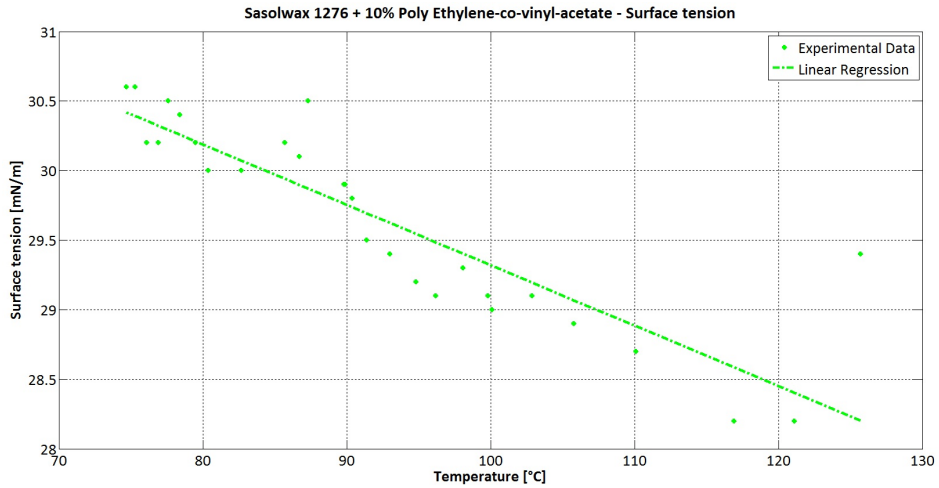


Figure 4.25: Surface tension values for Sasolwax 1276 added with PECVA

$R^2$ is 0.773. Neglecting the first measured point, influenced by inhomogeneous temperature in the glass at the beginning of the test, $R^2$ is 0.917.

### Comparison of Sasolwax 1276 tests

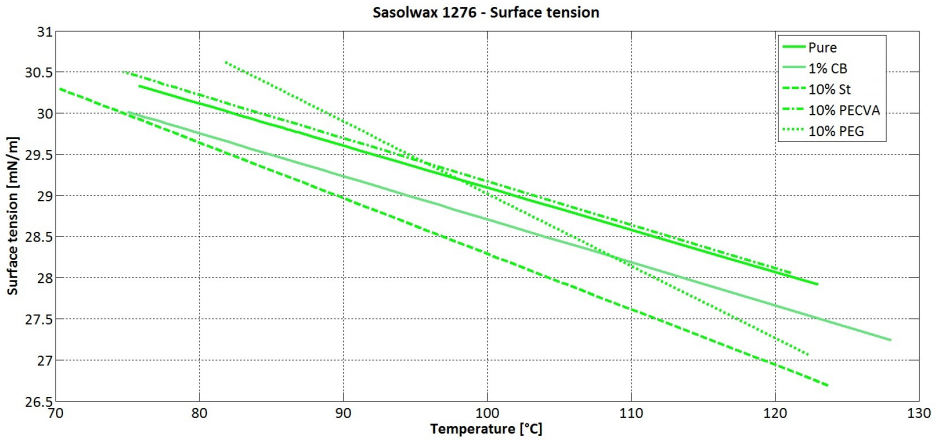


Figure 4.26: Comparison of Sasolwax 1276 tests

As it can be seen in Figure 4.26 there are variation in surface tension values adding Stearic Acid to Sasolwax 1276. Adding Carbon Black the curve does not vary if compared with the pure wax case: it is just shifted. The temperature range is similar for the different formulations: there is just a little change with Stearic Acid. The lowest surface tension values are shown by Stearic Acid, although at high temperature could be better 10% PEG and at low temperature 1% CB. The curve of Sasolwax 1276 added with PECVA is close to the pure wax curve.

### Sasolwax 6003 +1% Carbon Black

In this case a mixture composed by 99% wt. of Sasolwax 6003 and 1% wt. of Carbon Black is tested.

In Figure 4.27 the data and the mean curve are presented.

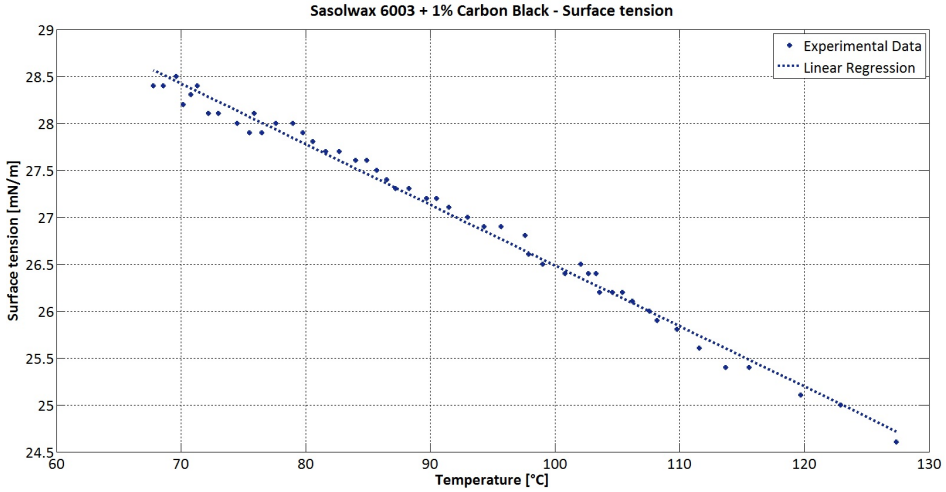


Figure 4.27: Surface tension values for Sasolwax 6003 added with Carbon Black

$R^2$ is 0.990.

### Sasolwax 6003 +10% Stearic Acid

In this case a mixture composed by 90% by weight of Sasolwax 6003 and 10% by weight of Stearic Acid is investigated.

As in other waxes tested with Stearic Acid, it is expected to get a variation in the value of surface tension respect to the case of pure Sasolwax 6003.

In Figure 4.28 the data and the mean curve are presented.

$R^2$ is 0.988.

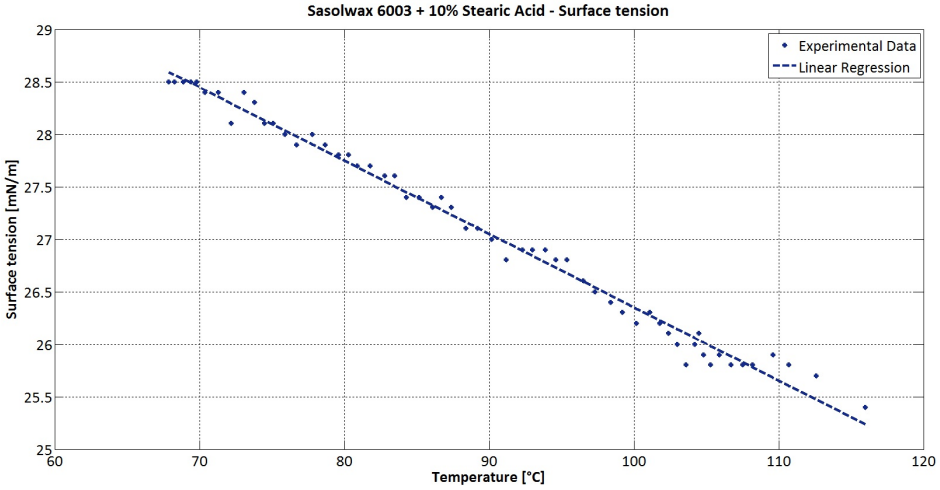


Figure 4.28: Surface tension values for Sasolwax 6003 added with Stearic Acid

### Sasolwax 6003 +10% PEG

A mixture made of 90% by weight of Sasolwax 6003 and 10% of Poly Ethylene Glykol 6000 is analysed.

In Figure 4.29 the data and the mean curve are presented.

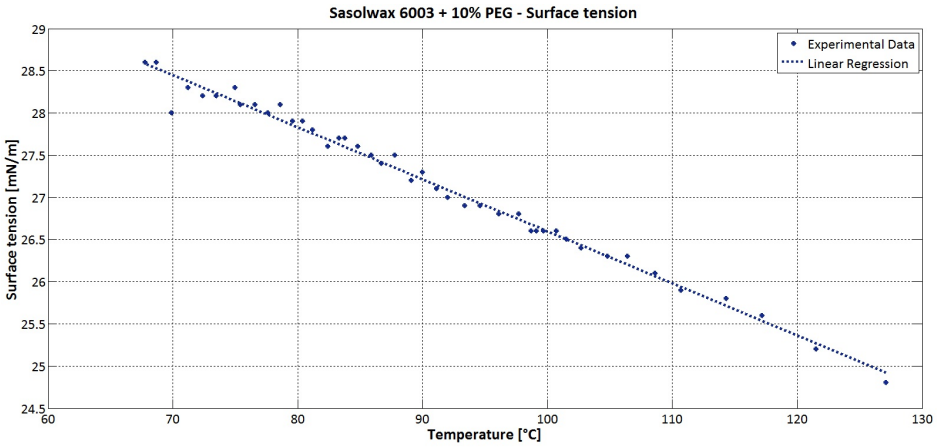


Figure 4.29: Surface tension values for Sasolwax 6003 added with PEG 6000

$R^2$ is 0.988.

### Sasolwax 6003 +10% PECVA

A mixture made of 90% by weight of Sasolwax 6003 and 10% of Poly-Ethylene-Co-Vinyl-Acetate is tested.

In Figure 4.30 the data and the mean curve are presented.

$R^2$ is 0.967.

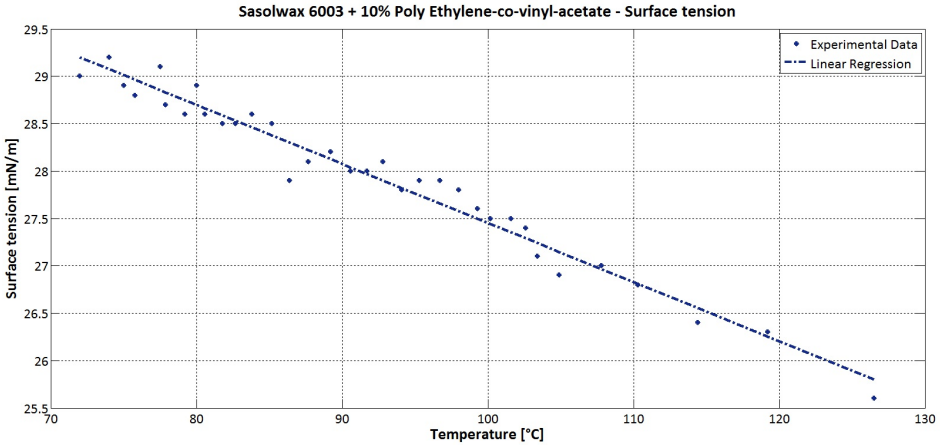


Figure 4.30: Surface tension values for Sasolwax 6003 added with PECVA

### Sasolwax 6003 +10% Aluminum

In this case a mixture composed by 90% by weight of Sasolwax 6003 and 10% by weight of Aluminum is tested.

In Figure 4.31 the data and the mean curve are presented.

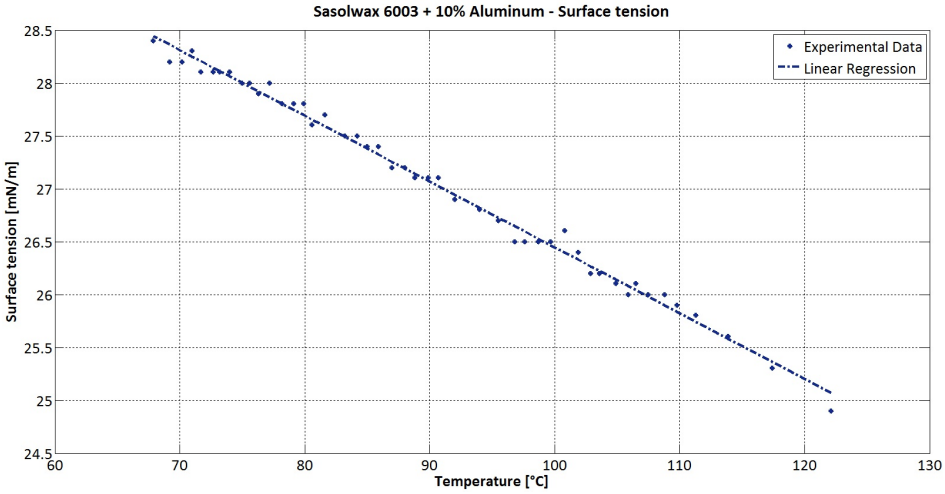


Figure 4.31: Surface tension values for Sasolwax 6003 added with Aluminum

$R^2$ is 0.993.

### Comparison of Sasolwax 6003 tests

As it can be seen in Figure 4.32 there no are variation in surface tension values adding Stearic Acid, Carbon Black or Aluminum to Sasolwax 6003. The temperature range doesn't change. The only curve quite different is the curve of Sasolwax 6003 added with PECVA, that shows higher surface tension values. At low temperature the

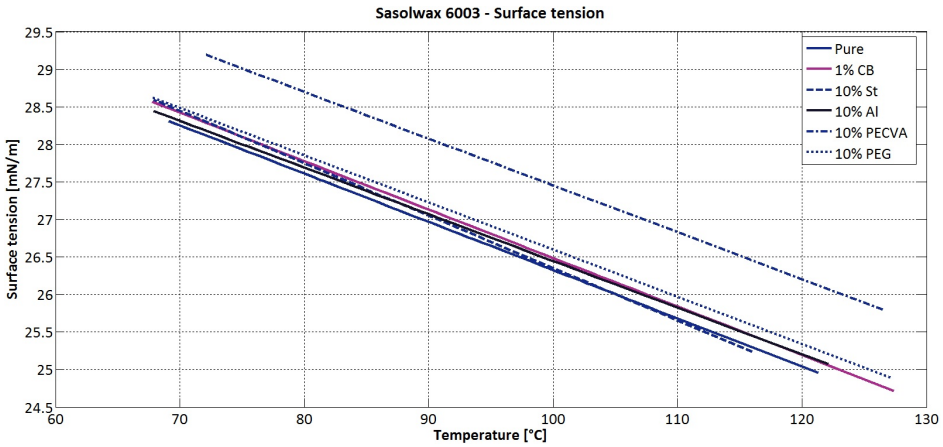


Figure 4.32: Comparison of Sasolwax 6003 tests

lowest values are measured with pure wax, at high temperature they are obtained with 10% Stearic Acid.

### 4.2.4 Comparison of all surface tension tests

In Figure 4.33 there is a comparison of surface tension values got in all tests.

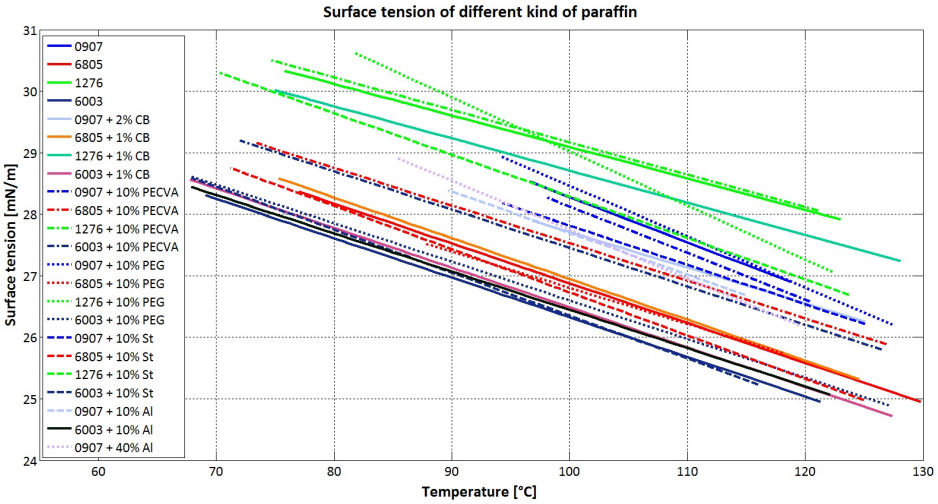


Figure 4.33: Results comparison of tested formulations

In order to understand in a better way the effect of additives, two parameters are investigated: the slope coefficient and the surface tension values at 100°C in mixtures with additives compared with pure waxes.

In Table 4.4 in some cases a perceptible variation in the slope coefficient using additives can be observed . In particular this happens with Stearic Acid, PEG and in a more contained way with Aluminum. The effect of Carbon Black is generally negligible (except the case of Sasolwax 0907). Further tests with PECVA should be done when it will be found a way to mix it in a good way with the waxes (in tests done Poly Ethylene sank at the bottom of the glass, although mixed few seconds before starting the experiment). PEG shows a great effect except the case with wax 6003.

The analysis of surface tension values at 100°C shows that $\Delta_{IFT}$ not always follows $\Delta_{slope}$. This behavior is due to the fact that, while the slope coefficient does not depend on a local parameter, $\Delta_{IFT}$ depends on the temperature at which the curve of mixture with additive crosses the pure wax curve.

The variation in surface tension values at the average temperature ($T_{ave} = \frac{T_b+T_m}{2}$) is also calculated. Boiling and melting temperature are calculated basing on [6] and they are represented in Figure 4.34. In this way it is possible to get the average temperature of the pure wax, that changes changing carbon number. In this way it is possible to calculate the variation in surface tension induced by additives. It is found that generally Stearic Acid has a positive effect, decreasing surface tension of 5-15%, while the effect of Carbon Black is generally negligible. PEG decreases greatly IFT with wax 0907 and wax 1276, while there is a contained increase with wax 6805 and 6003. The effect of PECVA is variable, decreasing or increasing IFT in a range of 5%. A small amount of Aluminum increases the surface tension, while in the only experiment done with 40% Aluminum, surface tension decreases.

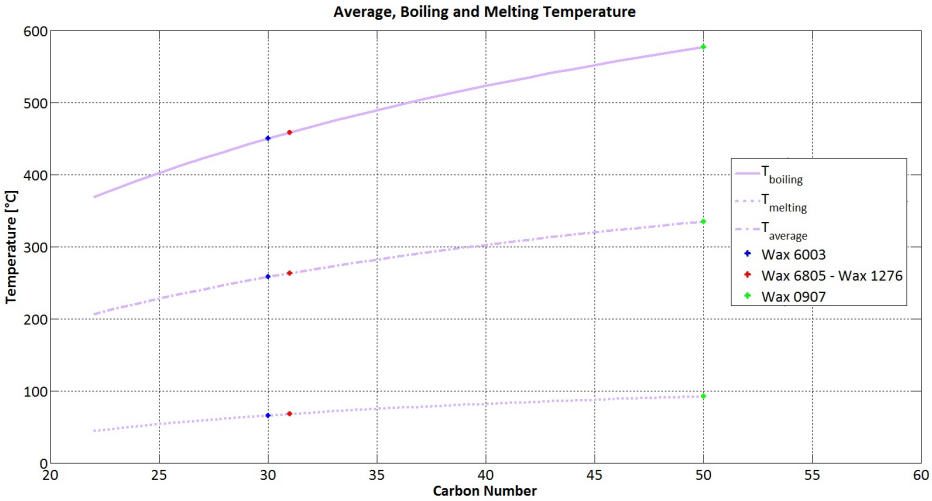


Figure 4.34: Melting, Boiling and Average Temperature according to Marano

Table 4.4: Slope Coefficient and Surface Tension Values at 100°C

| Formulation | Slope Coefficient | $\Delta_{slope}$ | IFT @ 100°C | $\Delta_{IFT}$ @ 100°C | $\Delta_{IFT}$ @ $T_{average}$ |
|---|---|---|---|---|---|
| Pure 0907 | -0.0736 | -% | 28.28 | -% | -% |
| 0907 + 2% Carbon Black | -0.0620 | -15.76% | 27.71 | -2.02% | +19.51% |
| 0907 + 10% PEG 6000 | -0.0825 | +12.09% | 28.46 | +0.64% | -17.33% |
| 0907 + 10% PECVA | -0.0755 | +2.58% | 28.13 | -0.53% | -5.44% |
| 0907 + 10% Stearic Acid | -0.0639 | -13.18% | 27.82 | -1.63% | +16.42% |
| 0907 + 10% Aluminum | -0.0677 | -8.01% | 27.69 | -2.09% | +7.17% |
| 0907 + 40% Aluminum | -0.0796 | +8.15% | 27.75 | -1.87% | -17.60% |
| Pure 6805 | -0.0648 | -% | 26.88 | -% | -% |
| 6805 + 1% Carbon Black | -0.0662 | +2.16% | 26.95 | +0.26% | -0.98% |
| 6805 + 10% PEG 6000 | -0.0586 | -9.57% | 26.80 | -0.30% | +5.70% |
| 6805 + 10% PECVA | -0.0612 | -5.56% | 27.53 | +2.42% | +7.60% |
| 6805 + 10% Stearic Acid | -0.0701 | +8.18% | 26.73 | -0.56% | -15.69% |
| Pure 1276 | -0.0512 | -% | 29.09 | -% | -% |
| 1276 + 1% Carbon Black | -0.0523 | +2.15% | 28.71 | -1.31% | -2.65% |
| 1276 + 10% PEG 6000 | -0.0879 | +71.68% | 29.02 | -0.24% | -29.17% |
| 1276 + 10% PECVA | -0.0527 | +2.93% | 29.17 | +0.28% | -0.77% |
| 1276 + 10% Stearic Acid | -0.0675 | +31.83% | 28.29 | -2.75% | -16.63% |
| Pure 6003 | -0.0643 | -% | 26.32 | -% | -% |
| 6003 + 1% Carbon Black | -0.0646 | +0.47% | 26.49 | +0.65% | +0.5% |
| 6003 + 10% PEG 6000 | -0.0629 | -2.18% | 26.60 | +1.06% | +3.09% |
| 6003 + 10% PECVA | -0.0624 | -2.95% | 27.45 | +4.29% | +8.83% |
| 6003 + 10% Stearic Acid | -0.0698 | +8.55% | 26.35 | +0.11% | -5.19% |
| 6003 + 10% Aluminum | -0.0622 | -3.27% | 26.45 | +0.49% | +2.84% |

# Chapter 5

# Viscosity: results and discussion

Viscosity measures the resistance of a fluid under a shear or tensile stress. It can be defined as the resistance of a fluid to any irreversible positional change of its volume elements. If a fluid has a low viscosity its movements are easier. Viscosity describes the internal resistance of a flowing fluid and it can be considered a measure of fluid friction. All fluids are viscous except superfluid. Only ideal fluids (inviscid) do not show any resistance to shear stress. Some liquids show an ideal behavior, in all other cases the behavior is between liquid and solid, being viscous and elastic. By a rheological point of view there are no differences between gases and liquids: gases are simply liquids with a lower viscosity. Instruments measuring visco-elastic properties are called rheometers, instruments which measures only the viscous flow behavior are called viscometers.

A moving fluid has different velocities and the shear stress arises between the last layer of fluid and the force that try to contrast the movement of the fluid.

Assuming two plates and a fluid between them, if we imagine to move the first plate with a force F then the fluid will be under shear stress with a velocity gradient u/y. The applied force will be

$$F = \mu A \frac{u}{y} \tag{5.1}$$

where A is the area of the plates and $\mu$ is the dynamic viscosity.

This equation lead to find the shear stress expression [39]:

$$\tau = \frac{F}{A} \tag{5.2}$$

where $\tau$ is the shear rate that in differential form becomes

$$\tau = \mu \frac{\partial u}{\partial y} \tag{5.3}$$

in the case of parallel straight and uniform flow.

$\frac{u}{y}$ that is the shear rate of deformation can be written as $\frac{du}{dy}$ that is the shear velocity.

Viscosity may depend by

- physical-chemical nature of the substance
- temperature of the substance

- pressure
- shear rate
- shear history
- electrical field

Different types of viscosity exist:

- **newtonian**: fluids which have a constant viscosity
- **shear thickening**: viscosity increases with the shear rate
- **shear thinning**: viscosity decreases with the shear rate
- **thixotropic**: substances which become less viscous if shaken, agitated or stressed
- **rheopectic**: substances which become more viscous if shaken, agitated or stressed
- **Bingham plastic**: a material that behaves as a solid at low stresses but that flows as a viscous fluid at high stresses
- **magnetorheological fluid**: a fluid that, if subjected to a magnetic field, increases its apparent viscosity becoming a viscoelastic solid

In Newtonian fluids the shear stress is proportional to velocity gradient: viscosity is constant varying velocity gradient. Because of the linear relation between the stress and the gradient, true viscosity and apparent viscosity are the same. In this case viscosity can be defined as the tangent of the slope angle of the flow curve $\tau - \frac{\partial u}{\partial y}$

In non-Newtonian fluids the shear stress is a non-linear function of the velocity gradient: viscosity varies with velocity gradient. Because of the non linear curve $\tau - \dot{\gamma}$ different viscosity values with different gradients can be calculated [40].

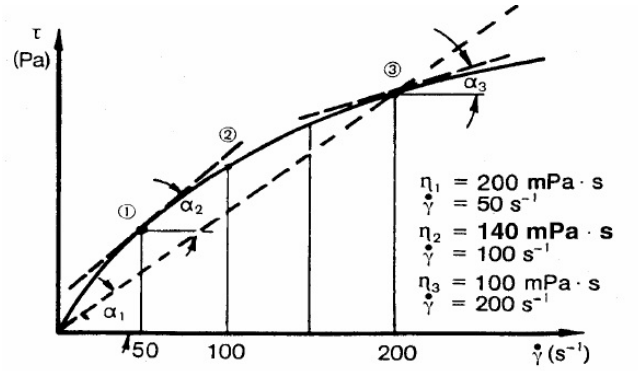


$$\eta_1 = \frac{\tau_1}{\dot{\gamma}_1}$$

$$\eta_2 = \frac{\tau_2}{\dot{\gamma}_2}$$

$$\eta_3 = \frac{\tau_3}{\dot{\gamma}_3} (= \tan\alpha_1)$$

Apparent viscosity

$$\eta_3 = \left.\frac{d\tau}{d\dot{\gamma}}\right|_3 = \tan\alpha_3$$

True viscosity

Figure 5.1: True viscosity vs. Apparent viscosity

Viscosity coefficients are defined in two ways:

- **dynamic viscosity** is also called absolute viscosity and it is measured typically in $Pas$ or poise $P$ : $1\ mPas = 1\ cP$. It is obtained as

$$\mu = \frac{\tau}{\frac{\partial u}{\partial y}} \tag{5.4}$$

- **kinematic viscosity** that is the result of the ratio between dynamic viscosity and density, typically it is measured in $cm^2/s$ or stokes $St$

Viscosity is a tensor that can be composed in two independent components giving the following viscosity coefficients:

- **Shear viscosity** describes the reaction to applied shear stress. It is obtained as the ratio of the pressure exerted on a fluid surface in lateral or horizontal direction and the change in velocity of the fluid moving down through the fluid

- **Volume viscosity** is relevant only when fluid compressibility plays a great role

Extensional viscosity describes the reaction to elongation and it is used for polymers characterization. It is a linear combination of shear and bulk viscosity.

## 5.1 Viscosity at different phases

Viscosity is determined by the number of molecules which interact. The Green-Kubo relations for the linear shear viscosity and the Evans and Morriss Transient Time Correlation Function are exact in calculating the viscosity of a dense fluid, but the use of molecular dynamics computer simulations is required.

If the substance is a gas, viscosity arises from the molecular diffusion that transports momentum between layers of flow. Basing on the kinetic theory it is stated that viscosity is independent of the pressure and it increases with temperature. The viscosity coefficient is proportional to density, mean free path and mean velocity of atoms.

In the case of liquids the forces between molecules are important. Liquids' viscosity is independent from pressure and tends to fall with increasing the temperature. Dynamic viscosities of liquids are orders of magnitude higher than dynamic viscosities of gases.

In the case of liquid mixtures the viscosity can be estimated with Refutas equation in three steps:

- the Viscosity Blending Number (VBN) is calculated for each component

- it is computed the viscosity of the mixture $VBN_{blend}$

- the kinematic viscosity is determined with:

$$\nu = exp(exp(\frac{VBN_{blend} - 10.975}{14.534})) - 0.8 \tag{5.5}$$

### Suspensions

The viscosity of slurries (suspension of solid particles in a liquid) is obtained as [41]

$$\mu_s = \mu_r \mu_l \tag{5.6}$$

where

- $\mu_s$ is the dynamic viscosity of suspension
- $\mu_l$ is the dynamic viscosity of liquid
- $\mu_r$ is the relative viscosity

The viscosity of dispersions is controlled firstly by the continuous liquid phase and then by size, shape, amount, deformability and interaction between the particles of the dispersed material [42].

In the case of very low concentration of suspended particles, the most important formula for solid spherical dispersed particles was given by Einstein:

- $$\mu_r = (1 + 2.5\phi) \tag{5.7}$$

  where $\phi$ is the phase volume, representing the volume of the dispersion occupied by the dispersed phase. For very low concentration of particles:

- $$\mu_r = 1 + 2.5\phi + 14.1\phi^2 \tag{5.8}$$

  for higher concentrations

- $$\mu_r = 1 + 2.5\phi + 10.05\phi^2 + Ae^{B\phi} \tag{5.9}$$

  from the fitting of empirical data

  From medium to high concentration of particles the Kreiger Dougherty equation is used:

- $$\mu_r = (1 - \frac{\phi}{\phi_m})^{-2} \tag{5.10}$$

  where $\phi_m$ is the maximum packaging factor.

When a dispersion is at rest, the particles are randomly dispersed throughout the continuous phase. If there is a very low shear rate there is a movement that allows the particles to move in flow direction mantaining the random distribution and high viscosity values. If the shear rate increases to high values, the particles begin to form strings and layers. This change in spatial distribution makes the movement easier, lowering viscosity.

Deformability of particles allows lower viscosity values because deformable droplets can accomodate each other: in this way $\phi_m$ is higher and the intrinsic viscosity $[\phi]$ is lower.

The shape of the particles, considering the same volume of dispersed phase, influences the thickening effect in the descending order: rods→plates→cubes/grains→spheres

In the case of amorphous materials viscosity is activated thermally [43]:

$$\mu = Ae^{\frac{Q}{RT}} \tag{5.11}$$

where Q is the activation energy, R is the molar gas constant, A is approximately a constant and T is the temperature.

Q changes from a high value $Q_H$ at low temperatures to a low value $Q_L$ at high temperatures. Amorphous materials can be classified as strong when

$$Q_H - Q_L < Q_L \tag{5.12}$$

as fragile when

$$Q_H - Q_L \geq Q_L \tag{5.13}$$

Fragility is computed by Doremus' fragility ratio:

$$R_D = \frac{Q_H}{Q_L} \tag{5.14}$$

in strong materials $R_D < 2$ , in fragile materials $R_D \geq 2$

### 5.1.1 Units

The symbol of dynamic viscosity is $\mu$ and in the SI the physical unit is the pascal-second ($Pas$)[39]. In the cgs system dynamic viscosity is measured in poise ($P$). In ASTM standards it is more commonly used the centipoise ($cP$).

Kinematic viscosity is the ratio of dynamic viscosity and density:

$$\nu = \frac{\mu}{\rho} \tag{5.15}$$

In the SI the physical unit is $m^2/s$, in the cgs it is used the stokes ($St$) or sometimes the centistokes ($cSt$). Kinematic viscosity is sometimes named as diffusivity of momentum.

Another unit that can be used is fluidity, the reciprocal of viscosity, whose symbols are $\phi$ or $F$, defined as $F = \phi = \frac{1}{\mu}$. It is measured in *reciprocal poise* ($cm * s/g$), sometimes called *rhe*.

Fluidity can be used to determine the viscosity of an ideal solution. Considering two components, $a$ and $b$, the fluidity is

$$F \approx \chi_a F_a + \chi_b F_b \tag{5.16}$$

where $\chi_a$ and $\chi_b$ are the mole fraction of component $a$ and $b$.

Also **Reyn** ( a British unit of dynamic viscosity), **viscosity index**, that measures the change of kinematic viscosity with temperature and **Saybolt Universal Seconds (SUS)** are used.

## 5.2 Measurement methods

Viscosity is measured with viscometer or rheometer. The rheometer is used when fluids can't be described by a single value of viscosity and when many parameters need to be set. It is used for liquids whose viscosity vary with flow conditions. Viscometer measures only under one flow condition. Viscosity is strongly related with temperature, especially in the case of lubricants.

In some fluids the viscosity is constant in a wide range of shear rates (Newtonian fluids). Fluids without a constant viscosity can't be described by a singular number (non Newtonian fluids).

Generally the viscosity is measured by the drag caused by relative motion between the fluid and a surface. The relative motion can be caused by an object moving in the stationary fluid or by a fluid moving to a stationary object. The Reynolds number needs to be enough small to operate in laminar conditions.

### 5.2.1 Viscometer

In this part some types of viscometer are presented.

**U-Tube (glass capillary) viscometer** It is a viscometer made of a glass U-tube at a controlled temperature [42]. In both the sides of the tubes there is a reservoir. Reservoirs are located at different heights. The liquid is in the upper bulb thanks to suction, after the fluid is allowed to go down to the other bulb through the capillary. The time taken for the gravity driven flow to move from one vertical position to another is measured. The kinematic viscosity is obtained multiplying the time by the factor of the viscometer.

**Falling Ball viscometer** It is a simple and accurate instrument for the measurement of transparent fluids from low to medium viscosity [39]. It is widely used with low viscosity Newtonian liquids. The fluid is stationary in a vertical glass tube: a sphere of known size and density can descend through the liquid reaching terminal velocity that can be measured, since the time it takes to pass two marks on the tube is known. The viscosity is calculated knowing the size and the density of the sphere, the density of the liquid and the terminal velocity using Stoke's law. The temperature is controlled with a constant temperature circulator. The measurement range is changed acting on the density or on the diameter of the ball. Calibration is obtained with a liquid of known viscosity.

The frictional force is derived for very small Reynolds number by Stokes:

$$F = 6\pi r\eta v \tag{5.17}$$

where:

- F is the frictional force
- r is the radius of the sphere
- $\eta$ is the fluid viscosity
- v is the velocity of the sphere

Terminal velocity is obtained as:

$$V_s = \frac{2}{9}\frac{r^2 g(\rho_p - \rho_f)}{\mu} \tag{5.18}$$

where:

- $V_s$ is the settling velocity of the particle
- $r$ is the Stokes radius of the particle
- $\rho_p$ is the density of the particle
- $\rho_f$ is the density of the fluid
- $g$ is the gravitational acceleration
- $\mu$ is the dynamic fluid viscosity

The roughness of the sphere is a limiting factor.

**Falling Piston Viscometer** In this instrument, known also as Norcross viscometer [44], the viscosity measurement is obtained with a piston that moves through the test liquid contained in a precise and temperature-controlled tube. Under a constant applied force, the time required to the piston to pass an assigned length of the tube is proportional to the viscosity. Values are given in seconds, SSU or centipoise. It is used in industries because of its simplicity, repeatability, low maintenance and longevity. This kind of measurement is not influenced by flow rate or external vibrations.

**Vibrational viscometer** This viscometer works by generating waves [45]. Shear waves are used in order to obtain shear condition. It can be made of a stainless steel sensor submerged in the fluid that moves back and forth microscopically at high frequency (resonance). The sensor shears through the liquid, so the energy is lost to the fluid because of viscosity. A microprocessor-controlled electronic measures the dissipated energy allowing to obtain the viscosity value.

The damping can be measured by:

- measuring the power input necessary to keep the oscillator vibrating at a constant amplitude
- measuring the decay time of the oscillation after the excitation is stopped
- measuring the frequency of the resonator as a function of phase angle between excitation and response waveforms. The higher the viscosity, the larger the frequency change .

Vibrating instruments suffer the lack of a defined shear field, making them unfit to measure the viscosity of a fluid whose flow behavior is unknown.

This type of instrument is used in industrial processes with high viscosity fluids and fluids containing fibers. Advantages are the absence of moving parts and that frequent calibration as for rotational viscometers is not needed.

**Rotational viscometer** It measures the torque required to rotate a disk or bob in a fluid at a known speed. An exact volume of a sample is sheared in a test cell where it is measured the torque required to achieve a fixed rotational speed. This viscometer exists in two forms: "cup" (also known as "Couette" ) if the cup rotates and "bob" (also known as "Searle") if the bob rotates. The cup is preferred because it prevents Taylor vortices, but it is difficult to get accurate meaurements.

**Oscillating Piston viscometer** This type of viscometer is also known as Electro-Magnetic Viscometer (EMV).

The sensor consists of a measurement chamber containing a magnetically influenced piston. The sample is introduced into the measurement chamber that is thermally controlled. Electronics cause the oscillatory motion of the piston within the measurement chamber with a controlled magnetic field. Shear stress is imposed on the liquid due to the piston travel and the viscosity is determined measuring the travel time of the piston. The viscosity is determined basing on Newton's Law of Viscosity.

**Bubble viscometer** It is used to determine quickly the kinematic viscosity of liquids like resins and varnishes [46]. The time needed for an air bubble to rise is directly proportional to the viscosity of the liquid: the faster the bubble rises, the lower the viscosity.

**Micro-Slit viscometers** This kind of viscometer has the advantages of measuring true viscosity for Newtonian and non-Newtonian fluids, eliminating air interface and sample evaporation effects, requiring a very small amount of sample volumes, showing laminar flow also at high shear rates thanks to low Reynolds number and simulating real conditions.

Some types of viscometer are calibrated on dynamic and kinematic viscosity of water at 20°C.

### 5.2.2 Rheometer

The rheometer is an instrument used to measure how a liquid or a slurry flow responds to an applied force.

There are two different kinds of rheometers:

- rotational rheometers that control the applied shear stress or shear strain
- extensional rheometers that apply extensional stress or extensional strain

#### Shear rheometer

Different types of shear rheometer are used, some of them are presented.

**Capillary rheometer** in which the liquid is forced through a tube of constant cross-section and known dimensions in laminary flow conditions. It is based on a pressure driven flow [47]. A capillary rheometer is based on gravity, compressed gas or a piston to generate pressure on the test fluid. Velocity is not zero only in the $z$ direction and there is no slip at the walls. The fluid has to be incompressible and not dependent on pressure. Flow rate and pressure drop are one fixed and the other measured. Dimensions are

known: in this way it is possible to convert the flow rate into shear rate and the pressure drop into shear stress. Varying one of the two parameters it is possible to obtain a flow curve. In Newtonian fluids the pressure drop increase linearly with flow rate. In non-Newtonian or complex fluids, because of shear thinning/thickening, the pressure drop vs. flow rate behavior needs to be analysed with Weissenberg-Rabinowitch-Mooney equation.

**Rotational cylinder** in which the liquid is placed in the annulus of one cylinder inside another [48]. One cylinder rotates at a known and set speed, determining the shear rate. The liquid drags the other cylinder, so the exerted force can be measured obtaining the shear stress. This rheometer is ideally suited for pourable liquids. The main advantage of this kind of rheometer is that the shear rate is nearly constant for large radii. The large sample volume required is the main disadvantage.

**Cone and plate** in which the liquid is placed on horizontal plate and a shallow cone is placed into it. It can consist [49] of a spring that connects the drive mechanism to a rotating cone. The resistance to rotation caused by the fluid is measured. This rheometer can be used with an oscillating mode in order to measure elastic properties.

**Linear Shear** works attaching a linear probe to the surface of the tissue: a load cell measures the shear force resulting from an applied cyclical force.

### Extensional rheometer

This kind of rheometer has encountered more problems than shear rheometer, like the shear flow given by interactions at fluid-solid interface and the need to know and control the strain history of the tested material.

This kind of rheometer works with different principles: with viscosity values between 0.01 and 1 $Pas$ are used opposed jet, contraction flow or capillary breakup rheometers. From 1 to 1000 $Pas$ are used filament stretching rheometers and above 1000 $Pas$ constant length rheometers.

**Rheotens** is based on fiber spinning and it is used with melting polymers [50]. It is based on a force transducer that measures the extensional force induced by the material pumped from a tube, causing a set of wheels to elongate the strand. This rheometer shows differences in molecular structure of different polymers.

**CaBER** is a capillary breakup rheometer built by ThermoHaake [51]. It is used to characterize polymer solutions, suspension and other materials. Two plates are stretched to a set level of strain. A small quantity of sample ($< 1$ ml) is placed between two plates. The top plate is separated from the bottom plate forming an unstable fluid filament caused by imposition of an instantaneous extensional strain on the fluid. A laser monitors the midpoint diameter of the thinning fluid filament as a function of time. It is easy to realize but analysis are more complex than with FiSER.

**FiSER** is based on a linear motion control system with real force and midpoint radius data acquisition [52, 51]. In this instrument a set of linear motors drives a fluid with an exponentially increasing velocity.

**Sentmanat** a thin layer of polymer is placed between two drums which cause a uniform extensional deformation [53]. Once the torque exerted by drums is known, it is possible to determine the stress. It has been firstly developped for uniaxial extension of polymeric materials but it can also be used for solids tensile testing or high rate fracture testing.

Other types of extensional rheometers are: capillary/contraction flow, falling plate and acoustic.

## 5.3 Rheology characterization of paraffin based fuels

A general overview on rheology of paraffin based fuel basing on some previous work is here presented. Considering that our work is based on mixtures made of waxes with additives like polyethyleneglykol, metals or metal hydrides, some previous works can give an introduction to this part of research.

The need to combine good ballistic and mechanical properties is analyzed in a work by Galfetti, Merotto, Boiocchi, Maggi and De Luca [54], where metal additives are added to pure-wax based fuels. In this study different powders and different hydrides are considered.

In this work the differences between solid and gel waxes, with and without additives are investigated. At the beginning Poly-Urethane Foam is used in order to strengthen the fuel structure, but this formulation does not give good results: the fuel is inhomogeneous and mechanical properties are not isotropic. For this reason a new structure based on thermoplastic polymers (TPE) soluble in paraffin is designed. This new formula gives good mechanical properties and homogeneous fuel.

Viscosity and storage modulus are measured with a Couette viscometer and with a plate-plate rheometer. The averaged regression rate is obtained as:

$$r_f = \frac{\Delta m}{\rho_f t_b A_b} \tag{5.19}$$

Using GW-PUF there is the need to increase its $r_f$, so melting point temperature and viscosity must be decreased. GW shows higher viscosity than SW, while adding GW with aroma lowers viscosity of an order of magnitude. PUF increases storage modulus G' .

In a formulation based on SEBS-LP fuels, adding SW causes a great increase of G. In this case the aroma's effect is less important than the effect given by SW. Adding aroma causes a steeper drop in mechanical properties near melting temperature. Complex viscosity represents the viscosity of the solid material and it is linked with the viscosity of melted materials. The use of aroma causes a decrease in complex viscosity.

At the highest mass flux reached in tests, the increase in $r_f$ values is:

- $nAl + GWP = +71\%$
- $nAl + SWP = +17\%$
- $MgH_2 + GW = +25\%$
- $MgH_2 + SW = +38\%$
- $3\%LAH + SWP = +6\%$
- $6\%LAH + SWP = +26\%$

Generally $r_f$ decreases with increasing the port area, leading to a decrease in port mass flux. This dependence is negligible because $t_b$ is small.

The blowing parameter B has a small influence, the most important parameter is the oxidizer mass flux G.

Exponent n has low values: it ranges from 0.2-0.35 for LAH formulations to 0.45-0.55 for formulations with HTPB. These fuels have a lower rate of enhancement with increasing oxidizer mass flux.

Formulations based on GWP give regression rates higher than HTPB. The highest enhancement (378%) in $r_f$ is achieved with SWP + 10% LAH. Kerosene has a good effect on GW because it decreases viscosity, increasing entrainment. GWP-based fuels give lower regression rates than SWP-based fuels. With GWP the best results are obtained with $nAl$, while with SWP the most effective additive is $MgH_2$.

Entrainment is stronger with SW because it has a lower surface tension and a lower viscosity if compared with GW. More entrainment means higher regression rate, lower particle effect on $r_f$ and Magnesium hydride full exploitation.

An analysis made by Kott [55] involves different waxes with different additives in different percentages.

Additives are used in two percentages: 10% and 40%. Waxes with 10% additives show that $T_C$ reaches the maximum value for slightly rich mixture ratio. The highest value are reached with $Al$ and $AlH_3$ , the lowest with $LiH$.

$I_{sp}$ shows a similar behavior although in this case also $BH_3 - NH_3$ presents high value.

c* shows the highest values for richer mixture than the one that shows maximum $T_C$. Both the highest c* and $T_C$ are obtained with the same formulations. A similar behavior is observed for $I_{spvac}$.

With 40% additives, $T_C$ vs. $O/F$ curves have a different behavior and higher values, although peaks are reached in the same conditions and for the same formulations. The characteristic velocity has higher values for some formulations (like $AlH_3$ and $BH_3 - NH_3$) and lower for other formulations (like $LiH$). Peaks are reached with fuel-rich conditions. The same remarks can be done for $I_{sp}$ and for $I_{spvac}$.

Viscosity decreases with increasing temperature, especially between 60 and 70°C.

Wax 1276 shows the highest viscosity, while the lowest value is obtained with wax 6003. Viscosity decreases with increasing velocity gradient, especially between 0 and 200 [1/s]. The formulation added with 10% Al shows the highest viscosity value, while the lowest value is for the formulation added with 0.8% carbon black. Particles' size is investigated: formulation with 10% Al has sizes around 30-40 $\mu m$ , sizes increase with increasing Al percentage. Using 40% $Mg$ causes bigger particles, around 40-60 $\mu m$, while using 10% $MgH_2$ gives particles size around 100 $\mu m$.

c* efficiencies are between 0.76-0.99, $I_{sp}$ efficiencies are between 0.77-0.97 (only tests with carbon black and different injectors).

### 5.3.1 Addition of nanoAl to paraffin

A research made by Teipel and Forther-Barth [56] studied the rheological behavior of HTPB/nanoAl and paraffin/nanoAl suspensions. The suspension made of paraffin oil and aluminum shows that increasing solid concentration, the shear thinning behavior increases. This non-Newtonian behavior can be caused by particle-particle interactions and by changed suspension hydrodynamic compared to monophase fluid.

At low shear rates, viscosity increases strongly as a function of concentration: interparticle forces dominate, compared to the relatively weak hydrodynamic forces. In-

creasing the shear rate, the situation changes, causing the decrease of viscosity at a given concentration. The effect of solid particles concentration on viscosity is less important at high shear rates. At high shear rates relative viscosity, defined as

$$\eta_{relative} = \frac{\eta_{suspension\dot{\gamma}}}{\eta_{paraffin}} \tag{5.20}$$

(where $\gamma$ is the deformation ), increases linearly as a function of concentration up to 25% concentration.

At low concentrations there is no difference in relative viscosity between maximum and minimum shear rate: at these concentrations there is enough distance between solid particles, so there are low interactions and a small effect on viscosity.

At low shear rates viscosity increases with increasing solid particles concentration because of quiescent structure of the particles.

At high shear rates there is a reduction in viscosity values for a given concentration.

The difference between high and low shear rates is caused by the behavior of particles in the Couette flow.

In the case of HTPB there is a Newtonian behavior up to 50% concentration. Increasing the concentration, relative viscosity increases with a linear behavior.

Viscoelastic properties are given by $G'(\omega)$ and $G''(\omega)$. At low frequencies viscous properties dominate. Both the functions increase linearly with frequency, intersecting at a characteristic frequency $\omega_i$ that varies with volumetric concentration of solid particles. The slope of storage modulus function $G'$ is greater than that of the loss modulus $G''$. Above $\omega_i$ elastic properties dominate. The structural relaxation time $\lambda$ is equal to the reciprocal of $\omega_i$:

$$\lambda\omega_i = 1 \tag{5.21}$$

In the case of paraffin $\lambda$ is higher, but in both cases $G'(\omega)$ does not depend on aluminum concentration.

### 5.3.2 Addition of molybdenum powders and alumina

Additivation of micro powders of molybdenum and alumina in liquid paraffin is the base of the research made by Beruto et al. [57] The flow behavior of particles under different shear rates is evaluated.

The global behavior is controlled by solid-liquid interface forces that depend on:

- surface diffusion
- interfacial shear viscosity
- interface solute adsorption
- interface surface gradient

Terms at solid-liquid interface are influenced by interfacial forces and particles-liquid contact surface area. Molecules of alkanes can be absorbed by molybdenum or alumina because of Van der Waals forces. A Scanning Polarization Force Microscopy is used.

Three types of additives are used:

- $Al_2O_3$ with 99.8% purity - particles with diameter equal to 7 $\mu m$

- $Al_2O_3$ with 99.7% purity - two types of particle: one with diameter about $10\mu m$ , one with diameter lower than $1\mu m$
- Molybdenum powder with 95% purity

The base fuel is liquid paraffin formed by a mixture of $C_{15} - C_{40}$ alkanes with a density of $0.85g/cm^3$.

In order to know if molybdenum particles are covered by a film of oxide, a thermobalance is used.

Dynamic contact angle is measured immersing a plate of alumina or molybdenum in liquid paraffin. Angles are measured in this way:

$$F_T = F - mg = P\gamma cos\theta - \rho gV \tag{5.22}$$

but at zero level there is no part of sample immersed, then

$$F_T = F - mg = P\gamma cos\theta \tag{5.23}$$

where

- $F_T$ is the total force measured by the instrument
- m is the mass
- P is the perimeter of the sample
- $\theta$ is the contact angle
- $\gamma$ is the surface tension of the liquid

Specific surface for the first type of particle ($I - Al_2O_3$) is $0.21m^2/g$, for molybdenum this value is $0.29m^2/g$ . Liquid - solid interface area is the same for both the suspensions.

Graphic of shear stress as a function of shear rate (Figure 5.2) shows that $I - Al_2O_3$ has a behavior that follows the Herschel - Bulkley model:

$$\tau = \tau^0 + \eta^* D^n \tag{5.24}$$

where

- $\eta^*$ is the apparent viscosity
- n is the phenomenologic coefficient
- $\tau^0$ can be neglected for concentration lower than 0.15

Van der Waals forces are stronger in molybdenum. Molybdenum and $Al_2O_3$ viscosity increases with concentration of dispersed solid particles.

In the case of molybdenum the effect of solid particles on the flow is described by Einstein's relation:

$$\eta = \eta_c(1 + \phi(\eta)) \tag{5.25}$$

where is $\eta$ is intrinsic viscosity and $\eta_c$ is the viscosity of the dispersing medium.

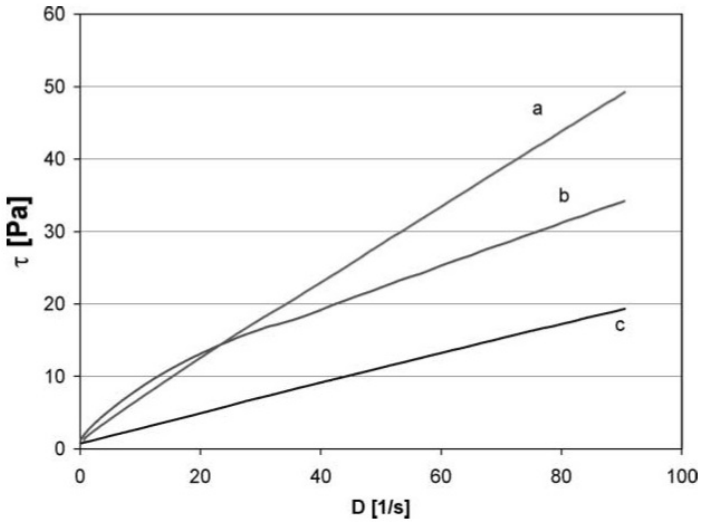


Figure 5.2: Applied stress vs. shear rate for: 10 percent Molybdenum contaminated paraffin, 10 percent Alumina contaminated paraffin, liquid paraffin

Alumina is based on Krieger - Dougherty equation:

$$\eta = \eta_c(1 - \frac{\phi}{\phi_M})^{(-[\eta]\phi_M)} \tag{5.26}$$

where $\phi_M$ is the maximum volumetric fraction of dispersed solid.
Intrinsic viscosity is defined as

$$[\eta] = \lim_{\Phi \to 0}[\frac{\frac{\eta}{\eta_c} - 1}{\Phi}] = \lim_{\Phi \to 0}[\frac{\frac{\partial \eta}{\partial \Phi}}{\eta_c}] \tag{5.27}$$

A second step is based on drops of liquid paraffin on molybdenum and alumina substrate. The droplet radius at interface is $R_i \propto D_i^{1/2} t^{1/2}$. Drop on molybdenum at the end has a contact angle near to 15°. In the case of alumina substrate, the drop has a lower height and the contact angle is near to 0°. It can be stated that the liquid paraffin drop tends to spread on alumina substrate, while it tends to stay on molybdenum substrate. For this reason it can be thought that molybdenum is covered by a thin film of oxide. Paraffin diffusion has coefficients inversely proportional to surface viscosity of paraffin. For this reason surface viscosity of paraffin at the paraffin-molybdenum interface is higher than the case with paraffin - $Al_2O_3$ (Figure 5.3).

Dynamic contact angles are calculated as:

$$\theta_i(0) = \lim_{\nu_i \to 0} \theta_i(\nu_i) \tag{5.28}$$

where $\nu_i$ is the slab speed into paraffin and $\theta_i$ is the advancing or receding angle. Values are always higher for molybdenum and advancing angles are higher than receding ones. This last is due to a thin film of paraffin that remains on the substrate while extracting it from paraffin.

The second formulation with alumina is characterized by an higher solid-liquid interface area. This formulation can have a significant production of $\tau_0$.

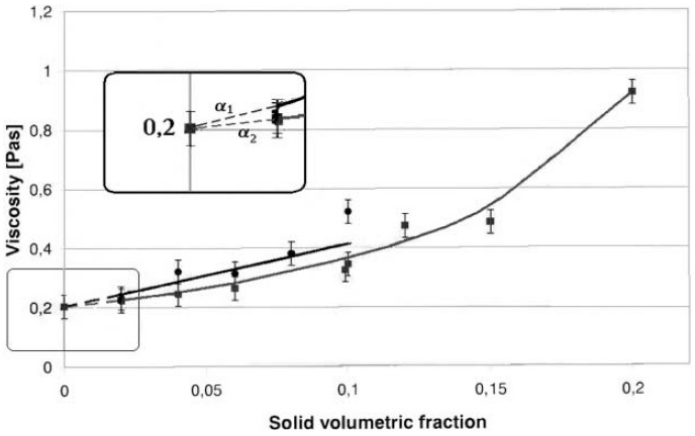


Figure 5.3: Viscosity as a function of solid volumetric fraction: squares indicate Alumina, circles indicate Molybdenum

### 5.3.3 Viscosity values

In order to give an overview on the viscosity values of different types of wax [58, 59, 60] some data are reported in Table 5.1 and Figure 5.4:

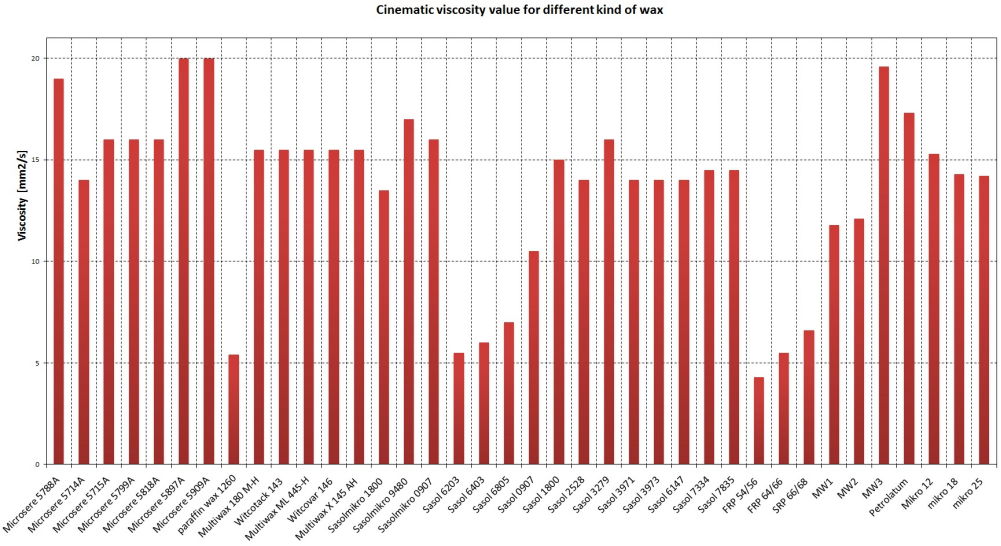


Figure 5.4: Viscosity value of some waxes at 100°C

Table 5.1: Viscocity value of some waxes at 100℃

| Substance | Viscosity [cP] |
|---|---|
| Microsere 5788A microwax | 19 |
| Microsere 5714A microwax | 14 |
| Microsere 5715A microwax | 16 |
| Microsere 5799A microwax | 16 |
| Microsere 5818A microwax | 16 |
| Microsere 5897A microwax | 20 |
| Microsere 5909A microwax | 20 |
| paraffin wax 1260 | 5.4 |
| Multiwax 180 M-H microwax | 13-18 |
| Witcotack 143 microwax | 13-18 |
| Multiwax ML 445-H microwax | 13-18 |
| Witcovar 146 microwax | 13-18 |
| Multiwax X 145 AH microwax | 13-18 |
| Sasolmikro 1800 microwax | 12-15 |
| Sasolmikro 9480 microwax | 14-20 |
| Sasolmikro 0907 microwax | 14-18 |
| Sasol 6203 paraffin | 5-6 |
| Sasol 6403 paraffin | 5.5-6.5 |
| Sasol 6805 paraffin | 6-8 |
| Sasol 0907 paraffin | 8.5-12.5 |
| Sasol 1800 paraffin | 13-17 |
| Sasol 2528 paraffin | 12-16 |
| Sasol 3279 paraffin | 13-19 |
| Sasol 3971 paraffin | 12-16 |
| Sasol 3973 paraffin | 12-16 |
| Sasol 6147 paraffin | 12-16 |
| Sasol 7334 paraffin | 13-16 |
| Sasol 7835 paraffin | 13-16 |
| FRP 54/56 microwax | 4.3 |
| FRP 64/66 microwax | 5.5 |
| SRP 66/68 microwax | 6.6 |
| MW1 microwax | 11.8 |
| MW2 microwax | 12.1 |
| MW3 microwax | 19.6 |
| Petrolatum microwax | 17.3 |
| Mikro 12 microwax | 15.3 |
| Mikro 18 microwax | 14.3 |
| Mikro 25 microwax | 14.2 |

## 5.4 Experimental Results

Viscosity tests are done using HAAKE* RheoStress 6000 Rotational Rheometer. The rheometer consist of:

- a heated plate where the substance that needs to be analysed is positioned
- the sensor, in this case a plate (plate-plate rheometer) that is spinned
- the thermocontroller that allows the setting of temperature of the heated plate
- a computer connected with the rheometer with two softwares:
  - HAAKE RheoWin 4 Job Manager that allows the setting of test and all variables like temperature, plate speed, ecc.
  - HAAKE RheoWin Data Manager that is opened after the test is done: it shows results both in graphics and in tables

The rheometer used during tests is presented in Figure 5.5, the technical data are provided in Table 5.2.

Figure 5.5: HAAKE RheoStress 6000 Rotational Rheometer

### 5.4.1 Pure waxes

Viscosity is investigated in two steps: firstly it is studied the behavior of viscosity as a function of shear rate. The curves obtained are quite flat, because pure waxes behave as Newtonian fluids. At the point where the curve is completely flat, the behavior of

Table 5.2: HAAKE RheoStress 6000 Rotational Rheometer - Technical data

| | |
|---|---|
| Torque Range | $200nNm$ - $200mNm$ |
| Speed Range (Constant Shear) | $10^{-7} - 1500\ min^{-1}$ |
| Speed Range (Constant Rotation) | $10^{-7} - 1500\ min^{-1}$ ($4500\ min^{-1}$ optional) |
| Frequency Range | $10^{-5}$ - $100\ Hz$ |
| Normal Force | 0.01 - 50 $N$ |
| Min. Lift Speed | $0.2\ \mu m/sec$ |
| Max. Lift Speed | $7\ mm/sec$ |
| Temperature Range | -60 ℃to +400℃ |
| Dimensions (D x W x H) | 15.6 x 15.6 x 30.4 $in.$ (40 x 40 x 78 $cm$) |
| Weight | $42\ kg$ |

viscosity as a function of temperature is investigated. In this case the shear rate chosen is 50 $1/s$.

Figure 5.6 shows that viscosity tends to be constant varying the shear rate. This behavior is in accord with what expected from theory for Newtonian fluids. Sasolwax 1276 shows viscosity values one order of magnitude higher than other waxes. The lowest values are shown by Sasolwax 6003.

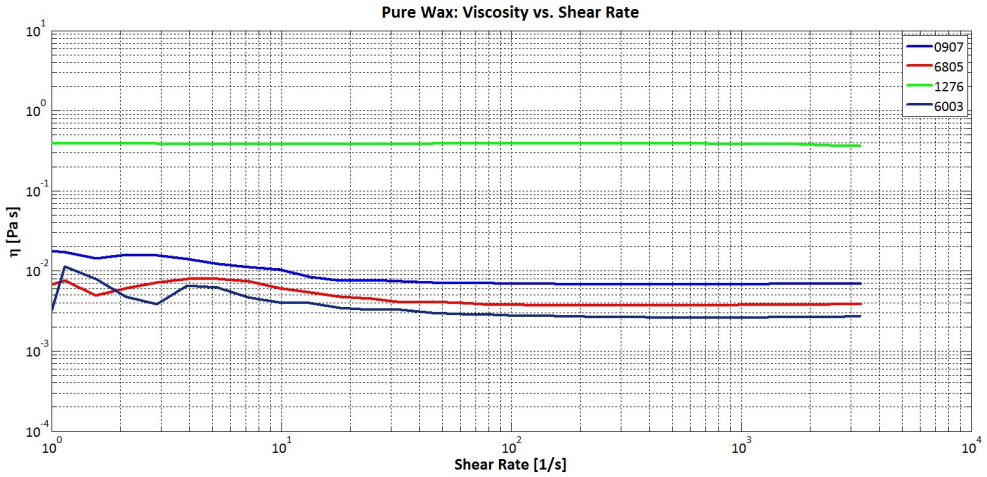


Figure 5.6: Behavior of Pure Waxes Viscosity as function of Shear Rate

After investigation of Viscosity vs. Shear Rate, the behavior of Viscosity with Temperature is shown. The temperature range varies from 200℃ to values close to the melting point: in particular to 85℃ for Sasolwax 0907, 75℃ for Sasolwax 1276 and 6805, 70℃ for Sasolwax 6003.

The Figure 5.7 and 5.8 show that viscosity increases with decreasing temperature in an exponential way. The highest values, as it could be inferred from the behavior with shear rate, are obtained by Sasolwax 1276, while the lowest values are obtained with Sasolwax 6003.

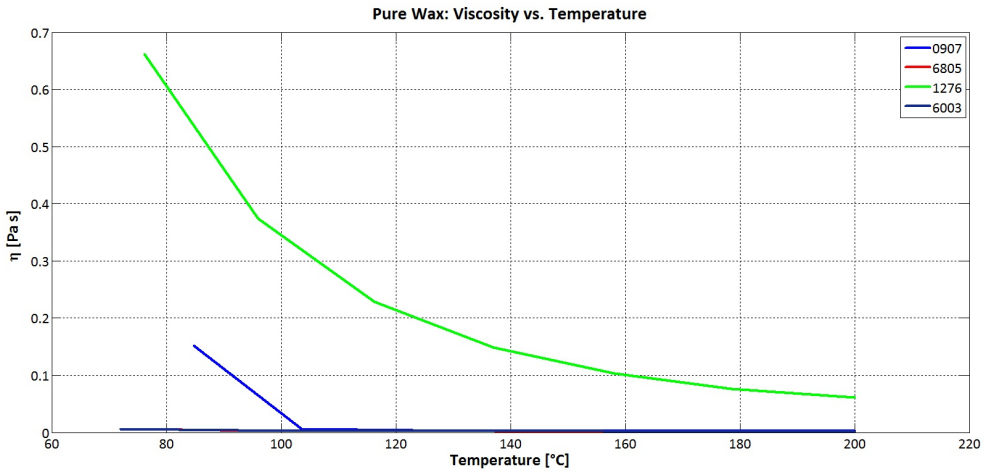


Figure 5.7: Behavior of Pure Waxes Viscosity as function of Temperature

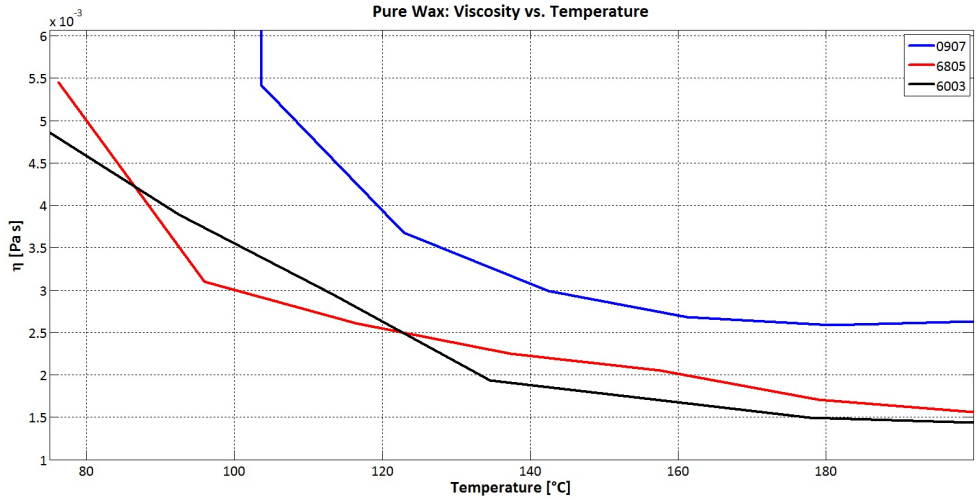


Figure 5.8: Behavior of Pure Waxes Viscosity as function of Temperature (detail)

### 5.4.2 Waxes with Additives

As done with surface tension tests, additives are used in order to modify the viscosity behavior of the pure waxes. In this part the effect of different additives on the pure waxes is analysed.

The different types of additives used are:

- 1% by wt. Poly Ethylene Co Vinyl Acetate
- 5% by wt. Poly Ethylene Co Vinyl Acetate
- 10% by wt. Poly Ethylene Co Vinyl Acetate
- 10% by wt. Poly Ethylene Glykol

- 5% by wt. Stearic Acid
- 10% by wt. Stearic Acid
- 5% by wt. SasolWax 1276
- 10% by wt. SasolWax 1276
- 1% by wt. Black Carbon
- 10% by wt. Aluminum
- 40% by wt. Aluminum

### Behavior of viscosity vs. Shear Rate

As done with pure waxes the first aspect that is investigated is the behavior of viscosity as function of shear rate. A behavior different from the pure waxes case is expected to be obtained: the particles should give to the curve a half-bell shape at low shear rates.

In these cases at low shear rates the curves are neglected because of intrinsic low viscosity of waxes and noise problem connected with the instrumentation.

In Figure 5.9 , Figure 5.10 and Figure 5.11 it can be seen that increasing the amount of Poly Ethylene Co Vinyl Acetate, the viscosity values become higher. This effect is much more visible at low shear rates in waxes which, if pure, show low viscosity values. At high shear rates the curves are flat but the higher the percentage of particles, the higher the viscosity (with a variation of one or more order of magnitude).

The curves become more bell-shaped with increasing the amount of particles.

In Figure 5.12 the behavior is similar to the one of PECVA. Sasolwax 1276 is flat because its higher viscosity is less influenced by PEG if compared with other waxes.

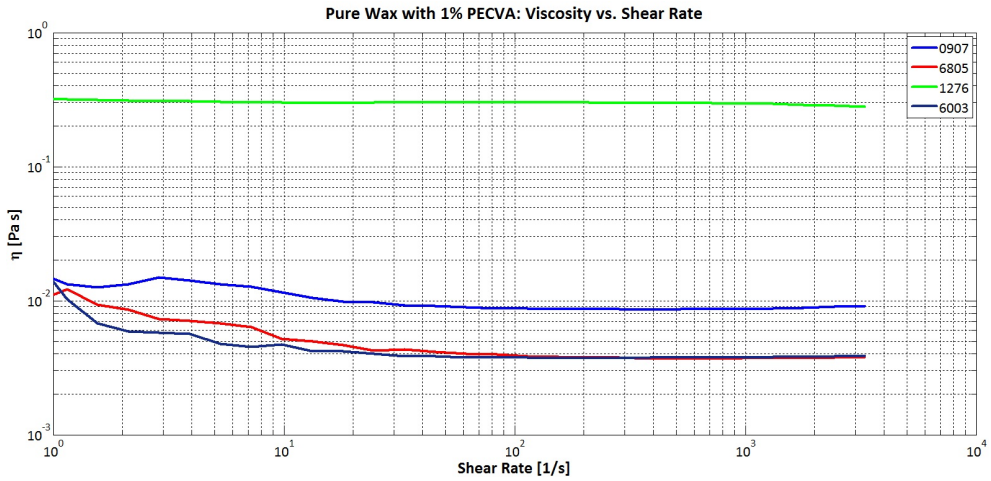


Figure 5.9: Waxes with 1% PECVA added: Viscosity vs. Shear Rate

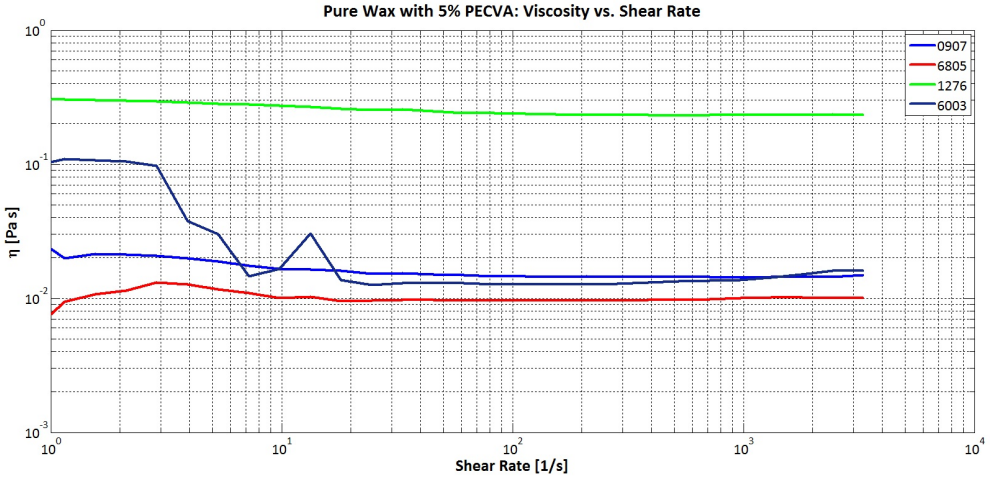


Figure 5.10: Waxes with 5% PECVA added: Viscosity vs. Shear Rate

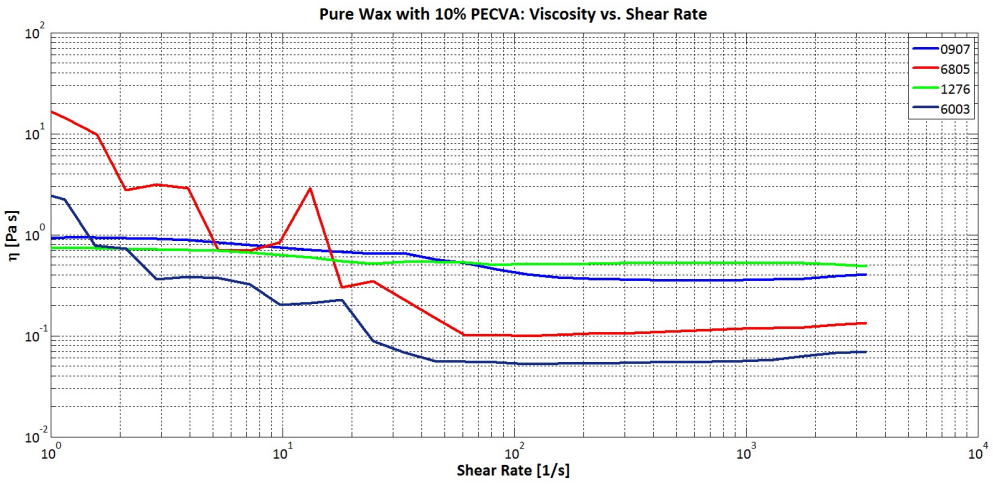


Figure 5.11: Waxes with 10% PECVA added: Viscosity vs. Shear Rate

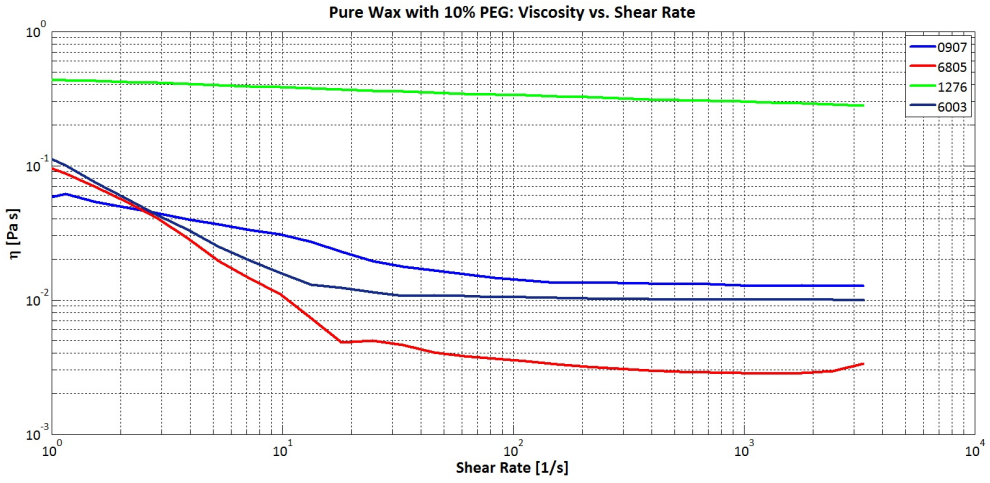


Figure 5.12: Waxes with 10% PEG added: Viscosity vs. Shear Rate

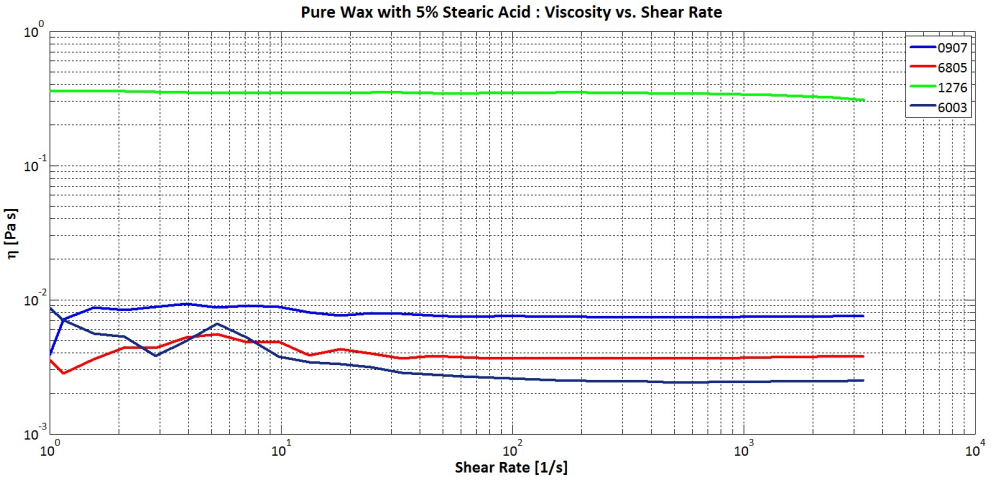


Figure 5.13: Waxes with 5% Stearic Acid added: Viscosity vs. Shear Rate

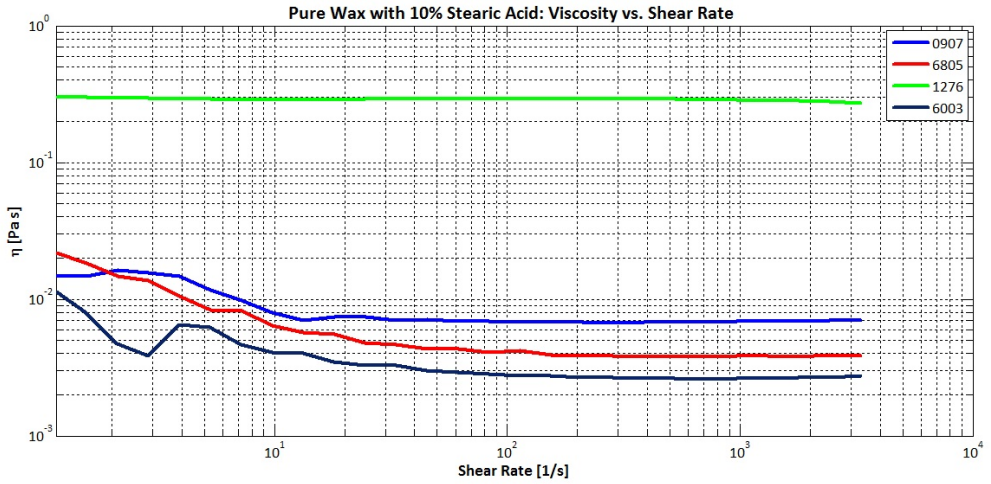


Figure 5.14: Waxes with 10% Stearic Acid added: Viscosity vs. Shear Rate

The effect of Stearic Acid is much smaller than PolyEthylene, as shown in Figure 5.13 and Figure 5.14. In fact with 5% Stearic Acid the effect on the curve is negligible, while it is visible at low shear rates with 10% Stearic Acid .

The effect of addition of 5% and 10% of Sasolwax 1276 Figure 5.15 and Figure 5.16 is relevant at low shear rates, while at higher values it becomes small.

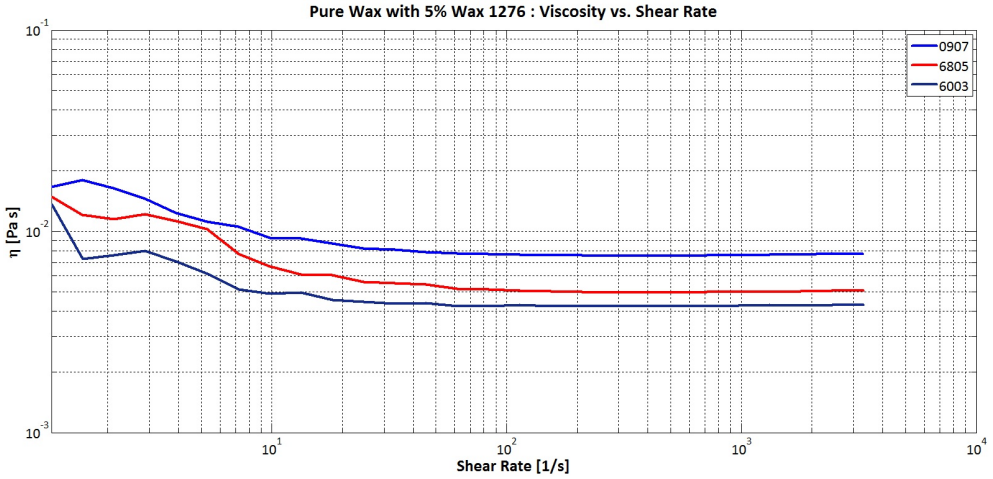


Figure 5.15: Waxes with 5% Sasolwax 1276 added: Viscosity vs. Shear Rate

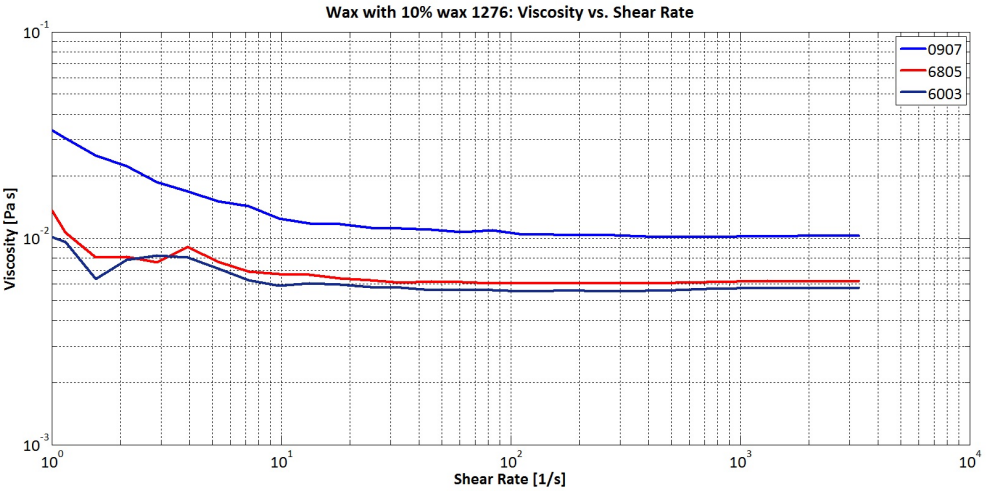


Figure 5.16: Waxes with 10% Sasolwax 1276 added: Viscosity vs. Shear Rate

Also with 1% Carbon Black the effect is small and localized in the low shear rates region, as shown in Figure 5.17.

With 10% Aluminum viscosity increases greatly at low shear rates with Sasolwax 6805 and in a moderate way with Sasolwax 0907 and Sasolwax 6003.

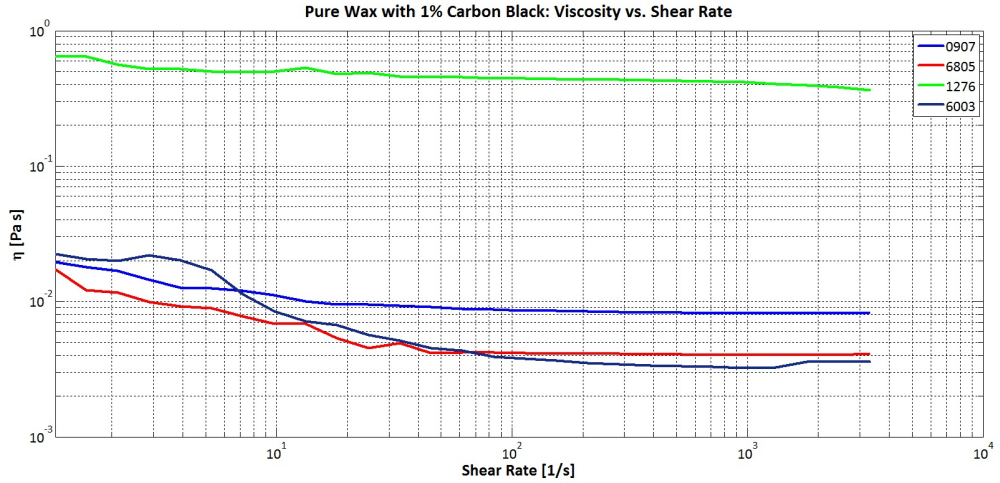


Figure 5.17: Waxes with 1% Carbon Black added: Viscosity vs. Shear Rate

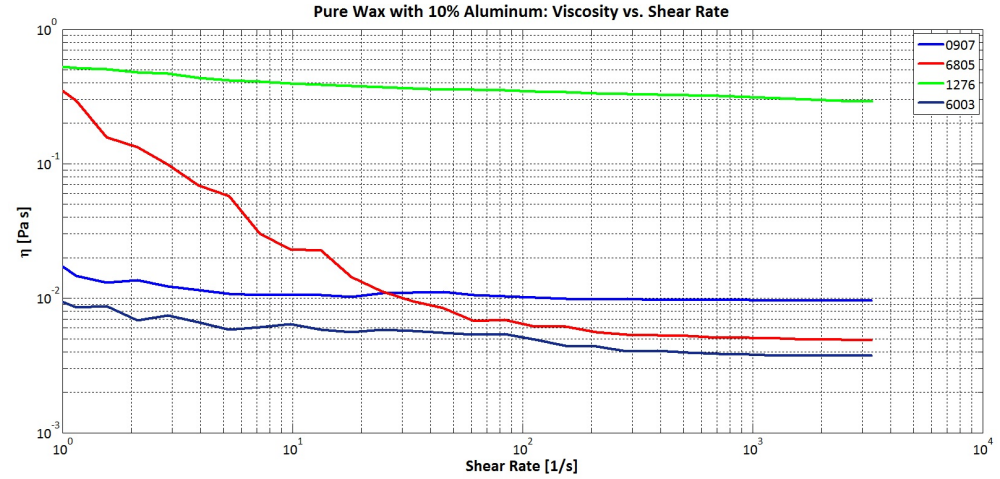


Figure 5.18: Waxes with 10% Aluminum added: Viscosity vs. Shear Rate

The addition of 10% and 40% by wt. Al shows that, increasing Aluminum content, the viscosity increases with Sasolwax 0907, Sasolwax 6003 and Sasolwax 6805 at high shear rates. Viscosity decreases with Sasolwax 1276 and Sasolwax 6805 at low shear rates.

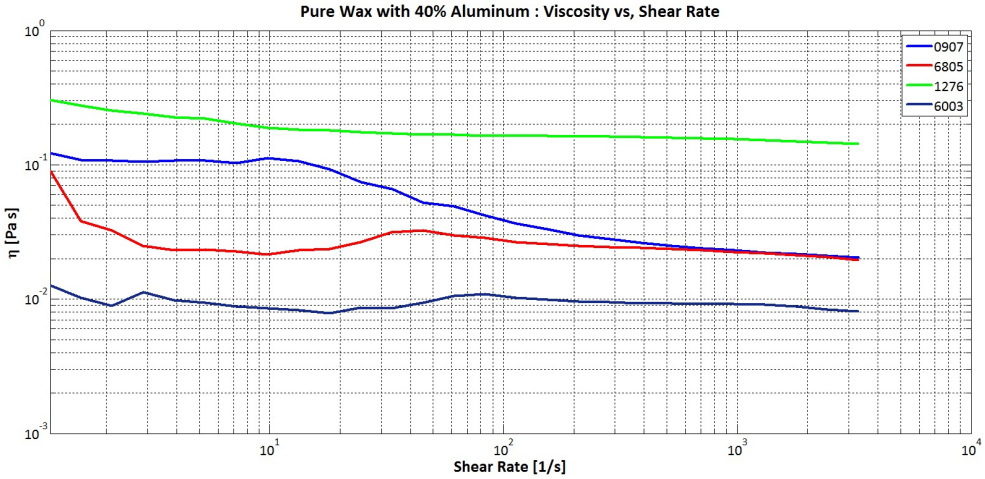


Figure 5.19: Waxes with 40% Aluminum added: Viscosity vs. Shear Rate

### Sasolwax 0907

Figure 5.20 and Figure 5.21 show an increase in viscosity values with all additives, if compared with the pure wax case. As reported in Table 5.15, the greatest increases in viscosity values are obtained with Poly Ethylene, while the lowest are shown with Stearic Acid.

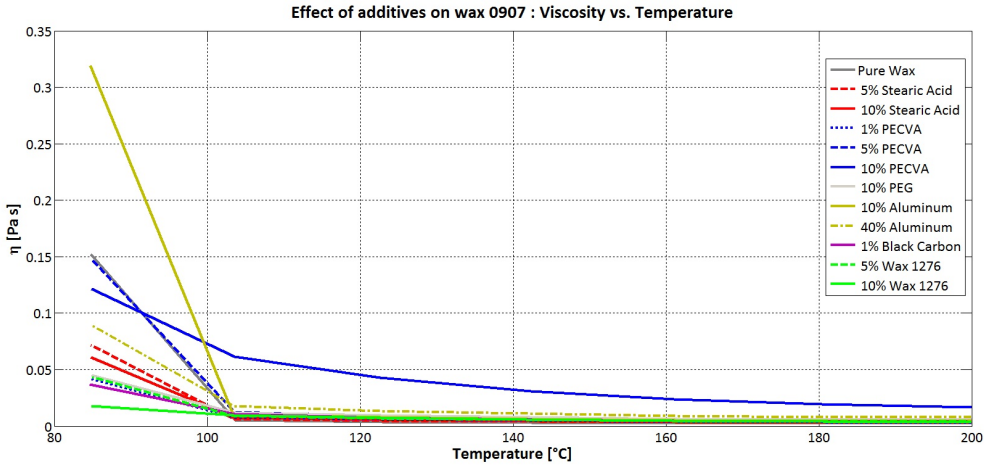


Figure 5.20: Tests with Sasolwax 0907

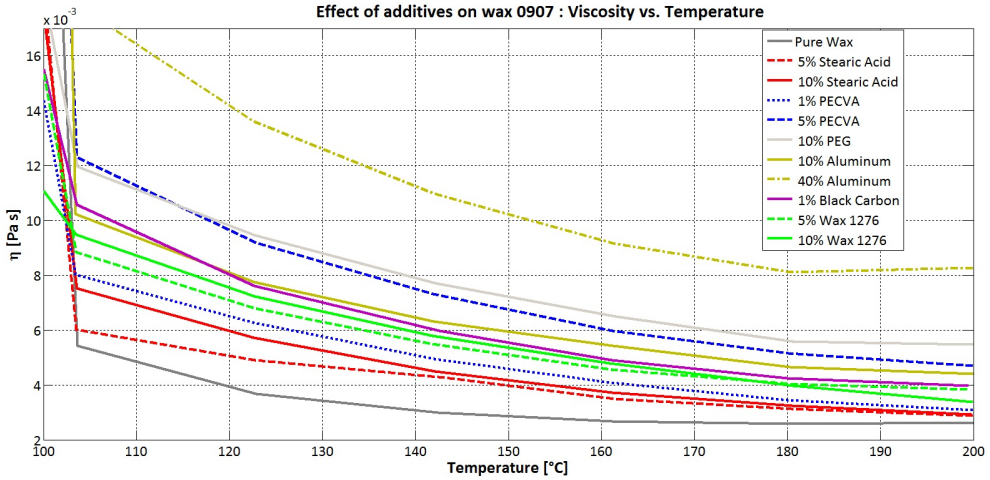


Figure 5.21: Tests with Sasolwax 0907 (detail)

In Table 5.3 , Table 5.4 and Table 5.5 variations of viscosity values, at fixed temperatures, are quoted. Variations are calculated as:

$$\Delta\eta\% = \frac{\eta_{additives} - \eta_{pure}}{\eta_{pure}} * 100 \tag{5.29}$$

Table 5.3: Variation of viscosity of Sasolwax 0907 added with PEG and PECVA compared with pure wax case

| Temperature °C | $\Delta\eta_{1\%PECVA}$ | $\Delta\eta_{5\%PECVA}$ | $\Delta\eta_{10\%PECVA}$ | $\Delta\eta_{10\%PEG}$ |
|---|---|---|---|---|
| 200.01 | + 17.62% | + 79.03% | + 527.85% | + 108.14% |
| 180.65 | + 33.58% | + 99.54% | + 638.88% | + 116.02% |
| 161.19 | + 52.09% | + 122.96% | + 788.72% | + 142.42% |
| 142.46 | + 65.85% | + 144.66% | + 934.48% | + 158.05% |
| 122.91 | + 70.66% | + 149.44% | + 1055.83% | + 156.87% |
| 103.63 | + 48.04% | + 127.01% | + 1039.22% | + 120.73% |
| 84.78 | - 72.36% | - 3.36% | - 20.13% | - 70.54% |

Table 5.4: Variation of viscosity of Sasolwax 0907 added with Stearic Acid and Sasolwax 1276

| Temperature ℃ | $\Delta\eta_{5\%Stearic}$ | $\Delta\eta_{10\%Stearic}$ | $\Delta\eta_{5\%Wax1276}$ | $\Delta\eta_{10\%Wax1276}$ |
|---|---|---|---|---|
| 200.01 | + 9.51% | + 11.19% | + 45.70% | + 28.16% |
| 180.65 | + 20.77% | + 25.05% | + 56.60% | + 53.23% |
| 161.19 | + 30.10% | + 38.91% | + 70.54% | + 78.49% |
| 142.46 | + 42.89% | + 50.06% | + 83.86% | + 94.01% |
| 122.91 | + 33.61% | + 54.79% | + 84.47% | + 96.33% |
| 103.63 | + 11.30% | + 38.66% | + 63.31% | + 74.78% |
| 84.78 | - 52.73% | - 59.90% | - 71.62% | - 88.19% |

Table 5.5: Variation of viscosity of Sasolwax 0907 added with Black Carbon, Aluminum

| Temperature ℃ | $\Delta\eta_{1\%BlackCarbon}$ | $\Delta\eta_{10\%Aluminum}$ | $\Delta\eta_{40\%Al}$ |
|---|---|---|---|
| 200.01 | + 50.80% | + 67.66% | + 214.57% |
| 180.65 | + 63.91% | + 80.23% | + 213.50% |
| 161.19 | + 83.01% | + 102.54% | + 242.31% |
| 142.46 | + 99.93% | + 111.68% | + 267.83% |
| 122.91 | + 106.83% | + 110.47% | + 270.19% |
| 103.63 | + 95.35% | + 88.88% | + 230.43% |
| 84.78 | - 75.94% | + 109.96% | - 41.75% |

Except the last point, the per cent difference in viscosity values increases with decreasing temperature.

### Sasolwax 6805

Figure 5.22 and Figure 5.23 show that the situation is similar to the one of Sasolwax 0907: viscosity values increase with all additives. As in the previous case high rises are obtained with Poly Ethylene and Aluminum, while the lowest increase is obtained with Stearic Acid.

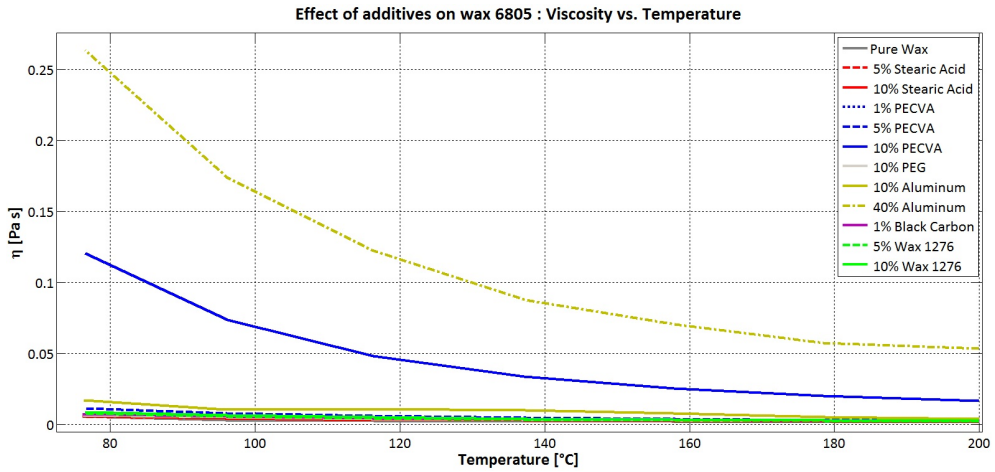


Figure 5.22: Tests with Sasolwax 6805

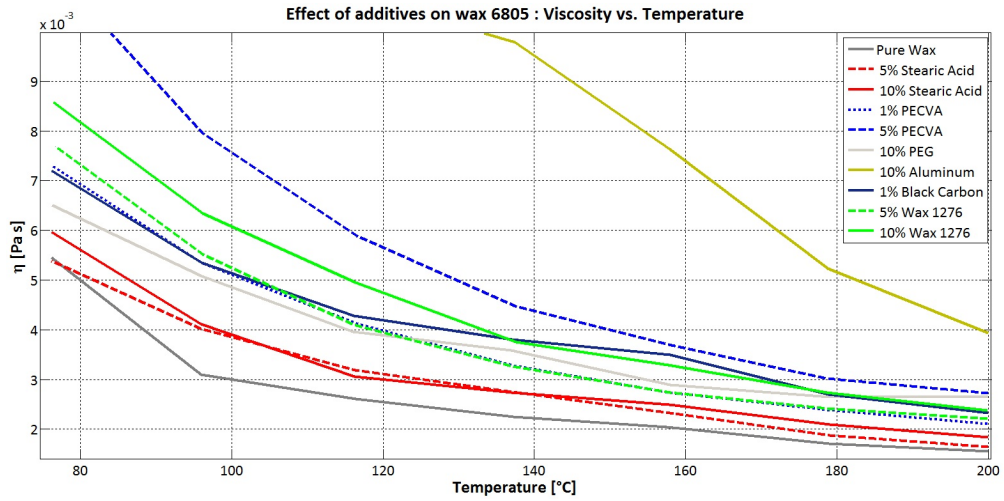


Figure 5.23: Tests with Sasolwax 6805 (detail)

Table 5.6 , Table 5.7 and Table 5.8 quote the per cent variations in viscosity values.

Table 5.6: Variation of viscosity of Sasolwax 6805 added with PEG and PECVA compared with pure wax case

| Temperature ℃ | $\Delta\eta_{1\%PECVA}$ | $\Delta\eta_{5\%PECVA}$ | $\Delta\eta_{10\%PECVA}$ | $\Delta\eta_{10\%PEG}$ |
|---|---|---|---|---|
| 199.97 | + 34.92% | + 75.03% | + 967.72% | + 69.96% |
| 178.97 | + 40.41% | + 76.95% | + 1063.05% | + 55.01% |
| 157.54 | + 33.94% | + 80.37% | + 1132.81% | + 41.50% |
| 137.29 | + 45.56% | + 98.67% | + 1397.91% | + 59.20% |
| 116.43 | + 58.05% | + 125.81% | + 1746.28% | + 51.88% |
| 95.98 | + 72.59% | + 156.47% | + 2271.33% | + 63.66% |
| 76.21 | + 33.66% | + 105.80% | + 2111.15% | + 19.23% |

Table 5.7: Variation of viscosity of Sasolwax 6805 added with Stearic Acid and Sasolwax 1276

| Temperature ℃ | $\Delta\eta_{5\%Stearic}$ | $\Delta\eta_{10\%Stearic}$ | $\Delta\eta_{5\%Wax1276}$ | $\Delta\eta_{10\%Wax1276}$ |
|---|---|---|---|---|
| 199.97 | + 5.78% | + 18.13% | + 41.59% | + 52.63% |
| 178.97 | + 10.38% | + 23.23% | + 41.52% | + 60.53% |
| 157.54 | + 13.53% | + 22.10% | + 33.84% | + 60.55% |
| 137.29 | + 22.27% | + 21.49% | + 44.89% | + 66.67% |
| 116.43 | + 22.43% | + 17.18% | + 57.13% | + 89.72% |
| 95.98 | + 29.89% | + 32.47% | + 77.94% | + 104.45% |
| 76.21 | - 1.10% | + 9.24% | + 41.02% | + 57.37% |

Table 5.8: Variation of viscosity of Sasolwax 6805 added with Black Carbon, Aluminum

| Temperature ℃ | $\Delta\eta_{1\%BlackCarbon}$ | $\Delta\eta_{10\%Aluminum}$ | $\Delta\eta_{40\%Aluminum}$ |
|---|---|---|---|
| 199.97 | + 49.10% | + 152.82% | + 3321.82% |
| 178.97 | + 58.12% | + 206.63% | + 3273.67% |
| 157.54 | + 70.85% | + 272.90% | + 3335.35% |
| 137.29 | + 68.89% | + 334.80% | + 3789.29% |
| 116.43 | + 64.00% | + 311.96% | + 4599.69% |
| 95.98 | + 72.30% | + 239.44% | + 5516.70% |
| 76.21 | + 32.03% | + 214.73% | + 4733.76% |

As with Sasolwax 0907 there is a tendency in increasing the per cent difference with decreasing temperature.

### Sasolwax 1276

In this case the situation is different from the previous cases: in fact in all tests except the one with 10% PECVA, viscosity decreases if compared with pure wax as shown in Figure 5.24 and Figure 5.25.

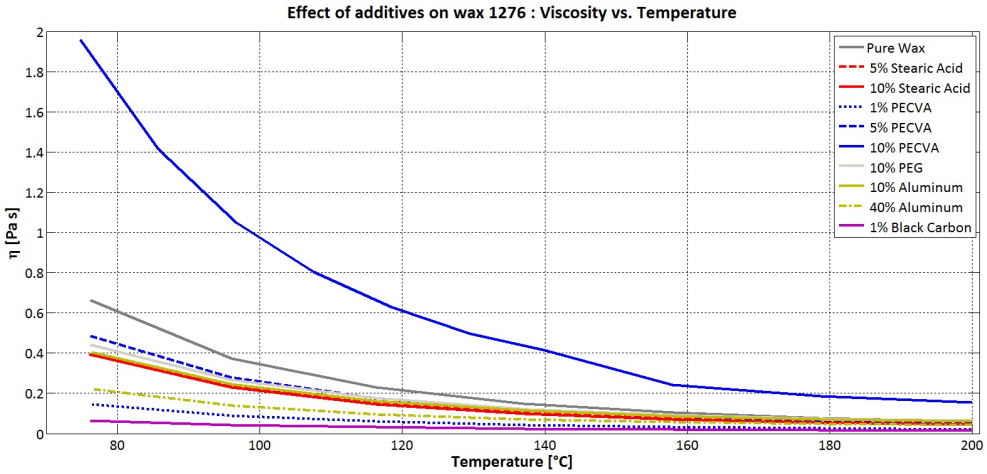


Figure 5.24: Tests with Sasolwax 1276

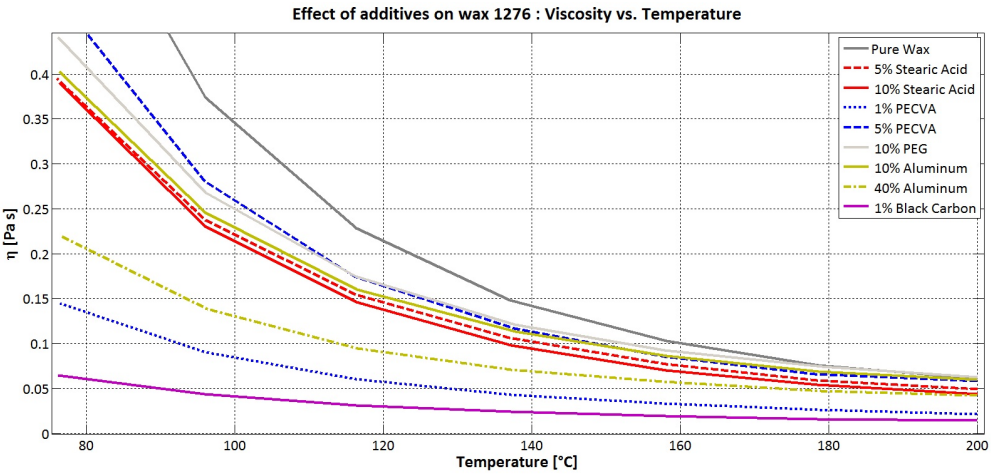


Figure 5.25: Tests with Sasolwax 1276 (detail)

Table 5.9 , Table 5.10 and Table 5.11 provide the per cent variations of viscosity between the pure wax case and the cases with additives.

With Sasolwax 1276 the per cent difference looks to increase as in the other cases, but in a much more moderate way.

Table 5.9: Variation of viscosity of Sasolwax 1276 added with PEG and PECVA compared with pure wax case

| Temperature ℃ | $\Delta\eta_{1\%PECVA}$ | $\Delta\eta_{5\%PECVA}$ | $\Delta\eta_{10\%PECVA}$ | $\Delta\eta_{10\%PEG}$ |
|---|---|---|---|---|
| 200.04 | - 64.68% | - 4.91% | + 151.93% | + 2.73% |
| 178.50 | - 65.28% | - 13.03% | + 146.30% | - 2.01% |
| 158.08 | - 67.84% | - 16.91% | + 134.47% | - 10.09% |
| 137.04 | - 70.98% | - 21.31% | + 195.41% | - 18.38% |
| 116.32 | - 73.53% | - 23.47% | + 189.29% | - 23.51% |
| 96.01 | - 75.88% | - 24.99% | + 186.44% | - 28.22% |
| 76.19 | - 78.15% | - 26.72% | + 185.52% | - 33.44% |

Table 5.10: Variation of viscosity of Sasolwax 1276 added with Stearic Acid, Black Carbon and Aluminum

| Temperature ℃ | $\Delta\eta_{5\%Stearic}$ | $\Delta\eta_{10\%Stearic}$ | $\Delta\eta_{1\%BlackCarbon}$ | $\Delta\eta_{10\%Aluminum}$ |
|---|---|---|---|---|
| 200.04 | - 19.53% | - 27.90% | - 76.78% | - 1.87% |
| 178.50 | - 21.65% | - 28.70% | - 78.68% | - 9.12% |
| 158.08 | - 24.95% | - 31.80% | - 81.54% | - 16.46% |
| 137.04 | - 27.94% | - 33.69% | - 83.84% | - 23.63% |
| 116.32 | - 32.58% | - 36.15% | - 86.34% | - 29.94% |
| 96.01 | - 36.57% | - 38.41% | - 88.36% | - 34.27% |
| 76.19 | - 40.36% | - 41.06% | - 90.22% | - 39.16% |

Table 5.11: Variation of viscosity of Sasolwax 1276 added with 40 per cent Aluminum

| Temperature ℃ | $\Delta\eta_{40\%Aluminum}$ |
|---|---|
| 200.04 | - 30.40% |
| 178.50 | - 37.28% |
| 158.08 | - 44.44% |
| 137.04 | - 52.24% |
| 116.32 | - 58.51% |
| 96.01 | - 62.96% |
| 76.19 | - 66.89% |

### Sasolwax 6003

The behavior of Sasolwax 6003 is very similar to the ones of Sasolwax 0907 and Sasolwax 6805: highest variation are obtained with Poly Ethylene and Aluminum, while the lowest are obtained with Stearic Acid and Black Carbon.

The greatest increases in viscosity values are obtained with Poly Ethylene and 40% Aluminum.

In Figure 5.26 and 5.27 these behaviors are presented.

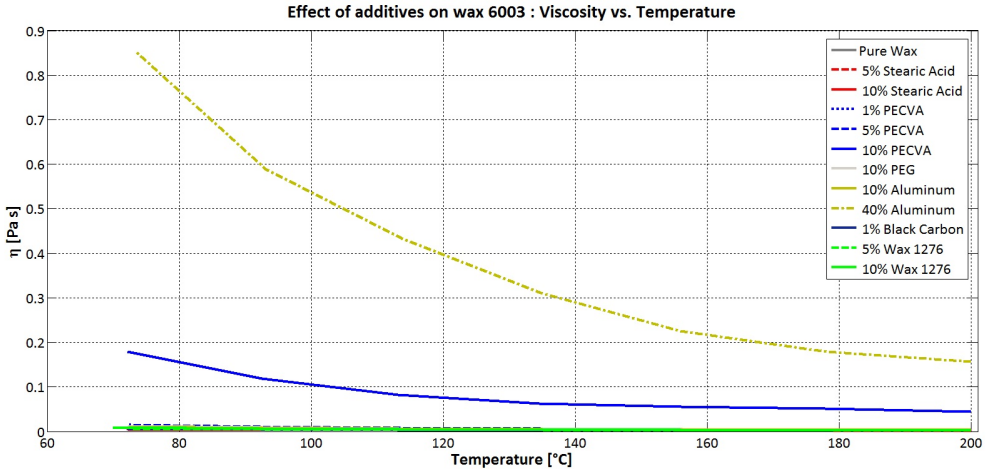


Figure 5.26: Tests with Sasolwax 6003

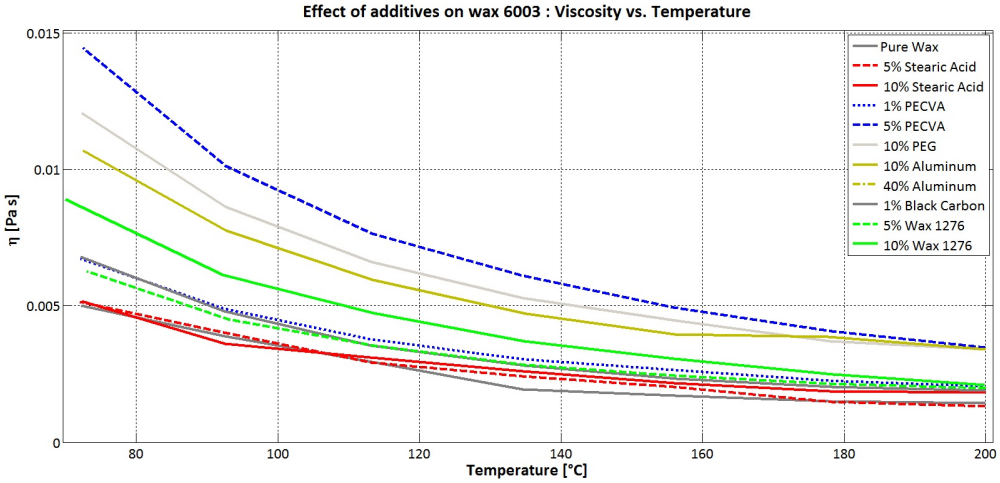


Figure 5.27: Tests with Sasolwax 6003 (detail)

Per cent variations of viscosity at recorded temperatures are shown in Table 5.12, Table 5.13 and Table 5.14.

Table 5.12: Variation of viscosity of Sasolwax 6003 added with PEG and PECVA compared with pure wax case

| Temperature ℃ | $\Delta\eta_{1\%PECVA}$ | $\Delta\eta_{5\%PECVA}$ | $\Delta\eta_{10\%PECVA}$ | $\Delta\eta_{10\%PEG}$ |
|---|---|---|---|---|
| 200.04 | + 43.69% | + 141.74% | + 3005.85% | + 138.12% |
| 178.12 | + 51.57% | + 171.21% | + 3318.50% | + 147.96% |
| 156.07 | + 54.37% | + 188.58% | + 3116.96% | + 160.55% |
| 134.97 | + 57.28% | + 215.60% | + 3139.93% | + 173.04% |
| 113.50 | + 27.74% | + 158.90% | + 2673.75% | + 123.55% |
| 93.07 | + 25.89% | + 160.35% | + 2933.84% | + 121.96% |
| 72.99 | + 34.14% | + 188.72% | + 3483.10% | + 140.83% |

Table 5.13: Variation of viscosity of Sasolwax 6003 added with Stearic Acid and Sasolwax 1276

| Temperature ℃ | $\Delta\eta_{5\%Stearic}$ | $\Delta\eta_{10\%Stearic}$ | $\Delta\eta_{5\%Wax1276}$ | $\Delta\eta_{10\%Wax1276}$ |
|---|---|---|---|---|
| 200.04 | - 8.71% | + 26.69% | + 37.98% | + 46.62% |
| 178.12 | - 1.14% | + 25.12% | + 42.75% | + 66.13% |
| 156.07 | + 18.36% | + 25.76% | + 41.84% | + 78.50% |
| 134.97 | + 24.54% | + 34.71% | + 46.54% | + 91.58% |
| 113.50 | - 0.81% | + 4.74% | + 19.79% | + 60.12% |
| 93.07 | + 3.21% | - 6.84% | + 16.10% | + 57.50% |
| 72.99 | + 2.69% | + 3.11% | + 25.04% | + 77.97% |

Table 5.14: Variation of viscosity of Sasolwax 6003 added with Black Carbon, Aluminum

| Temperature ℃ | $\Delta\eta_{1\%BlackCarbon}$ | $\Delta\eta_{10\%Aluminum}$ | $\Delta\eta_{40\%Aluminum}$ |
|---|---|---|---|
| 200.04 | + 31.08% | + 136.59% | + 10852.40% |
| 178.12 | + 36.34% | + 158.18% | + 11851.37% |
| 156.07 | + 35.72% | + 131.12% | + 13035.66% |
| 134.97 | + 44.99% | + 143.80% | + 15930.58% |
| 113.50 | + 20.09% | + 101.49% | + 14547.43% |
| 93.07 | + 23.58% | + 99.90% | + 15050.76% |
| 72.99 | + 35.84% | + 113.37% | + 16936.50% |

### 5.4.3 Comparison of all viscosity tests

Table 5.15: Variation of viscosity at 150C

| Formulation | Viscosity @ 150℃[Pa s] | $\Delta_\eta$ |
|---|---|---|
| Pure 0907 | 0.002863 | -% |
| 0907 + 1% PECVA | 0.004585 | + 60.15% |
| 0907 + 5% PECVA | 0.006746 | + 135.63% |
| 0907 + 10% PECVA | 0.028000 | + 878.00% |
| 0907 + 10% PEG | 0.007219 | + 152.15% |
| 0907 + 5% Stearic Acid | 0.003973 | + 38.77% |
| 0907 + 10% Stearic Acid | 0.004175 | + 45.83% |
| 0907 + 5% Wax 1276 | 0.005096 | + 78.00% |
| 0907 + 10% Wax 1276 | 0.005359 | + 87.18% |
| 0907 + 1% Black Carbon | 0.005542 | + 93.57% |
| 0907 + 10% Aluminum | 0.005950 | + 107.82% |
| 0907 + 40% Aluminum | 0.010200 | + 256.27% |
| Pure 6805 | 0.002125 | -% |
| 6805 + 1% PECVA | 0.002946 | + 38.64% |
| 6805 + 5% PECVA | 0.003999 | + 88.19% |
| 6805 + 10% PECVA | 0.028500 | + 1241.18% |
| 6805 + 10% PEG | 0.003157 | + 48.56% |
| 6805 + 5% Stearic Acid | 0.002487 | + 17.04% |
| 6805 + 10% Stearic Acid | 0.002587 | + 21.74% |
| 6805 + 5% Wax 1276 | 0.002939 | + 38.31% |
| 6805 + 10% Wax 1276 | 0.003466 | + 63.11% |
| 6805 + 1% Black Carbon | 0.003613 | + 70.02% |
| 6805 + 10% Aluminum | 0.008460 | + 298.12% |
| 6805 + 40% Aluminum | 0.077 | + 3523.53% |
| Pure 1276 | 0.120500 | -% |
| 1276 + 1% PECVA | 0.036900 | - 69.38% |
| 1276 + 5% PECVA | 0.097700 | - 18.92% |
| 1276 + 10% PECVA | 0.317700 | + 163.65% |
| 1276 + 10% PEG | 0.103800 | - 13.86% |
| 1276 + 5% Stearic Acid | 0.088600 | - 26.47% |
| 1276 + 10% Stearic Acid | 0.081000 | - 32.78% |
| 1276 + 1% Black Carbon | 0.020900 | - 82.66% |
| 1276 + 10% Aluminum | 0.096900 | - 19.59% |
| 1276 + 40% Aluminum | 0.0624 | - 48.22% |
| Pure 6003 | 0.001779 | -% |
| 6003 + 1% PECVA | 0.002763 | + 55.31% |
| 6003 + 5% PECVA | 0.005274 | + 196.46% |
| 6003 + 10% PECVA | 0.057300 | + 3120.91% |
| 6003 + 10% PEG | 0.004708 | + 164.64% |
| 6003 + 5% Stearic Acid | 0.002136 | + 20.07% |

Continue in the next page

Table 5.15: Variation of viscosity at 150C

| Formulation | Viscosity @ 150℃[Pa s] | $\Delta_\eta$ |
|---|---|---|
| 6003 + 10% Stearic Acid | 0.002285 | + 28.44% |
| 6805 + 5% Wax 1276 | 0.002550 | + 43.34% |
| 6805 + 10% Wax 1276 | 0.003246 | + 82.46% |
| 6805 + 1% Black Carbon | 0.002471 | + 38.90% |
| 6805 + 10% Aluminum | 0.004185 | + 135.24% |
| 6805 + 40% Aluminum | 0.249300 | + 13913.49% |

As done with surface tension, the viscosity of the mixtures is calculated at 150℃ Table 5.15.

Table 5.16: Viscosity tests set up data

| Formulation | Shear rate/Frequency | T ℃ | Rheometer Plate |
|---|---|---|---|
| Pure 0907 | 50 | 200-85 | PP 35 Ti + Rough |
| 0907 + 1% PECVA | 100 | 200-85 | PP 35 Ti + Smooth |
| 0907 + 5% PECVA | 100 | 200-85 | PP 35 Ti + Smooth |
| 0907 + 10% PECVA | 100 | 200-85 | PP 35 Ti + Smooth |
| 0907 + 10% PEG | 50 | 200-85 | PP 35 Ti + Smooth |
| 0907 + 5% Stearic Acid | 50 | 200-85 | PP 35 Ti + Smooth |
| 0907 + 10% Stearic Acid | 50 | 200-85 | PP 35 Ti + Smooth |
| 0907 + 5% Wax 1276 | 100 | 200-85 | PP 35 Ti + Smooth |
| 0907 + 10% Wax 1276 | 100 | 200-85 | PP 35 Ti + Smooth |
| 0907 + 1% Black Carbon | 50 | 200-85 | PP 35 Ti + Smooth |
| 0907 + 10% Aluminum | 50 | 200-85 | PP 35 Ti + Smooth |
| 0907 + 40% Aluminum | 500 | 200-85 | PP 35 Ti + Smooth |
| Pure 6805 | 50 | 200-75 | PP 35 Ti + Rough |
| 6805 + 1% PECVA | 100 | 200-75 | PP 35 Ti + Smooth |
| 6805 + 5% PECVA | 100 | 200-75 | PP 35 Ti + Smooth |
| 6805 + 10% PECVA | 100 | 200-75 | PP 35 Ti + Smooth |
| 6805 + 10% PEG | 50 | 200-75 | PP 35 Ti + Smooth |
| 6805 + 5% Stearic Acid | 50 | 200-75 | PP 35 Ti + Smooth |
| 6805 + 10% Stearic Acid | 50 | 200-75 | PP 35 Ti + Smooth |
| 6805 + 5% Wax 1276 | 100 | 200-75 | PP 35 Ti + Smooth |
| 6805 + 10% Wax 1276 | 100 | 200-75 | PP 35 Ti + Smooth |
| 6805 + 1% Black Carbon | 50 | 200-75 | PP 35 Ti + Smooth |
| 6805 + 10% Aluminum | 50 | 200-75 | PP 35 Ti + Smooth |
| 6805 + 40% Aluminum | 100 | 200-75 | PP 35 Ti + Smooth |
| Pure 1276 | 50 | 200-75 | PP 35 Ti + Rough |
| 1276 + 1% PECVA | 100 | 200-75 | PP 35 Ti + Smooth |
| 1276 + 5% PECVA | 100 | 200-75 | PP 35 Ti + Smooth |
| 1276 + 10% PECVA | 100 | 200-75 | PP 35 Ti + Smooth |

Continue in the next page

Table 5.16: Viscosity tests set up data

| Formulation | Shear rate/Frequency | T °C | Rheometer Plate |
|---|---|---|---|
| 1276 + 10% PEG | 50 | 200-75 | PP 35 Ti + Smooth |
| 1276 + 5% Stearic Acid | 50 | 200-75 | PP 35 Ti + Smooth |
| 1276 + 10% Stearic Acid | 50 | 200-75 | PP 35 Ti + Smooth |
| 1276 + 1% Black Carbon | 150 | 200-75 | PP 35 Ti + Smooth |
| 1276 + 10% Aluminum | 50 | 200-75 | PP 35 Ti + Smooth |
| 1276 + 40% Aluminum | 50 | 200-75 | PP 35 Ti + Smooth |
| Pure 6003 | 50 | 200-70 | PP 35 Ti + Rough |
| 6003 + 1% PECVA | 100 | 200-70 | PP 35 Ti + Smooth |
| 6003 + 5% PECVA | 100 | 200-70 | PP 35 Ti + Smooth |
| 6003 + 10% PECVA | 100 | 200-70 | PP 35 Ti + Smooth |
| 6003 + 10% PEG | 50 | 200-70 | PP 35 Ti + Smooth |
| 6003 + 5% Stearic Acid | 50 | 200-70 | PP 35 Ti + Smooth |
| 6003 + 10% Stearic Acid | 50 | 200-70 | PP 35 Ti + Smooth |
| 6805 + 5% Wax 1276 | 100 | 200-70 | PP 35 Ti + Smooth |
| 6805 + 10% Wax 1276 | 100 | 200-70 | PP 35 Ti + Smooth |
| 6805 + 1% Black Carbon | 150 | 200-70 | PP 35 Ti + Smooth |
| 6805 + 10% Aluminum | 50 | 200-70 | PP 35 Ti + Smooth |
| 6805 + 40% Aluminum | 100 | 200-70 | PP 35 Ti + Smooth |

### 5.4.4 Storage and Loss Modulus

Another point that is investigated is the behavior of Storage and Loss Modulus. The first one characterizes the elastic behavior of the wax, the second one is connected with the viscosity behavior. Storage and loss modulus are investigated under two aspects: as functions of angular velocity and as functions of temperature.

In order to investigate these properties as function of angular velocity, two steps are needed: the first is to investigate the behavior of storage and loss modulus as function of the stress $\tau$ with a fixed frequency of 1 Hz. The curve obtained in a logarithmic graph shows a flat zone: in this zone a stress $\tau$ (generally $\tau = 1Pa$) is chosen, storage and loss modulus vs. angular velocity $\omega$ are investigated.

The second kind of experiments concerns on storage and loss modulus vs. temperature: the temperature is varied from 90 to 30°C at a frequency of $1Hz$ and with a stress $\tau = 1Pa$ , in order to see the differences between the solid and the liquid phase.

#### Pure waxes

Results obtained with pure waxes are presented.

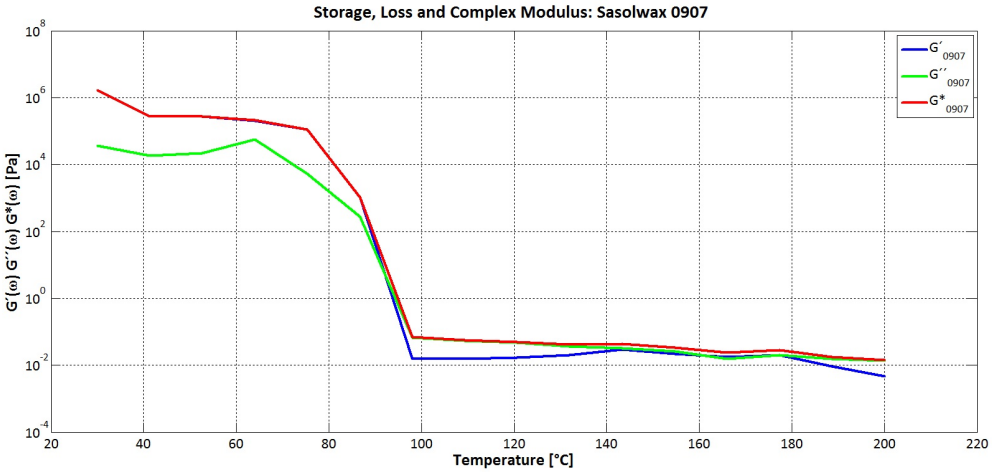


Figure 5.28: Storage, Loss and Complex Modulus as function of temperature for Sasolwax 0907

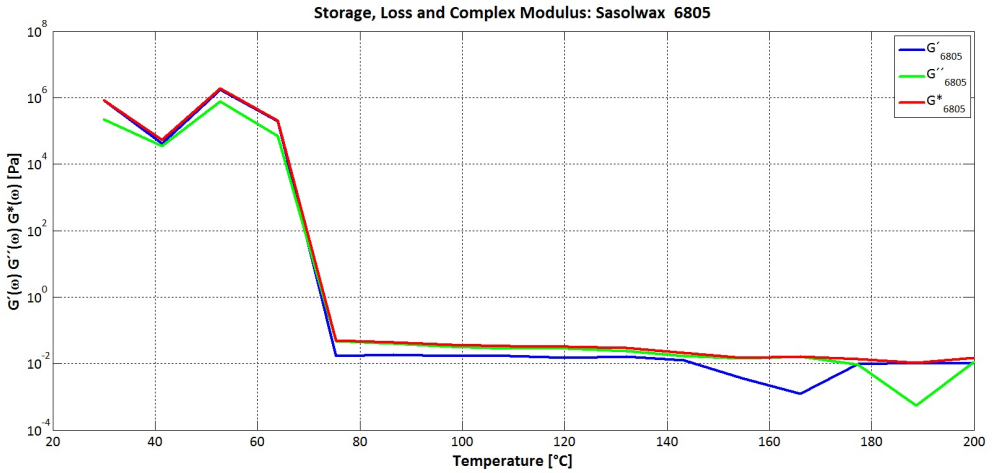


Figure 5.29: Storage, Loss and Complex Modulus as function of temperature for Sasolwax 6805

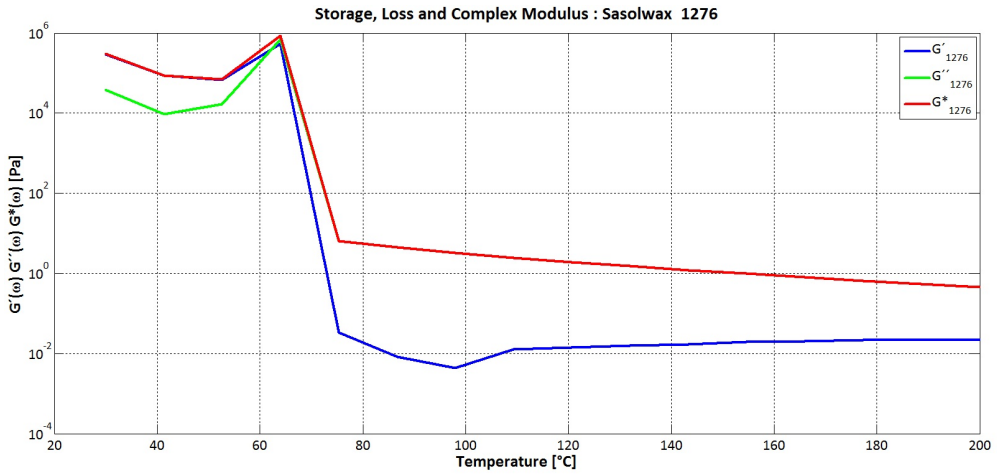


Figure 5.30: Storage, Loss and Complex Modulus as function of temperature for Sasolwax 1276

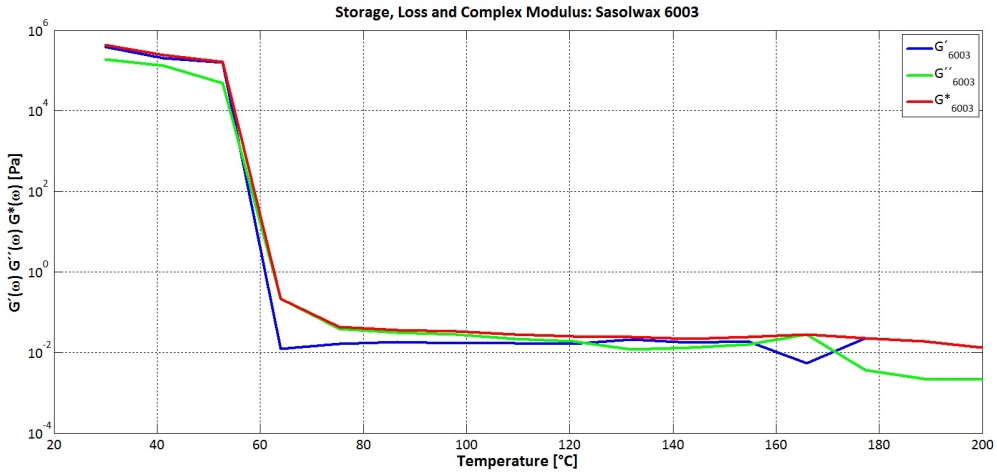


Figure 5.31: Storage, Loss and Complex Modulus as function of temperature for Sasolwax 6003

Table 5.17: Storage and Loss Modulus test set up data for pure waxes

| Formulation | f [Hz] | Stress [Pa] | T °C | Rheometer Plate |
|---|---|---|---|---|
| Pure 0907 | 1 | 1 | 200-30 | C60/2°L03 + Smooth |
| Pure 6805 | 1 | 1 | 200-30 | C60/2°L03 + Smooth |
| Pure 1276 | 1 | 1 | 200-30 | C60/2°L03 + Smooth |
| Pure 6003 | 1 | 1 | 200-30 | C60/2°L03 + Smooth |

### Waxes with additives

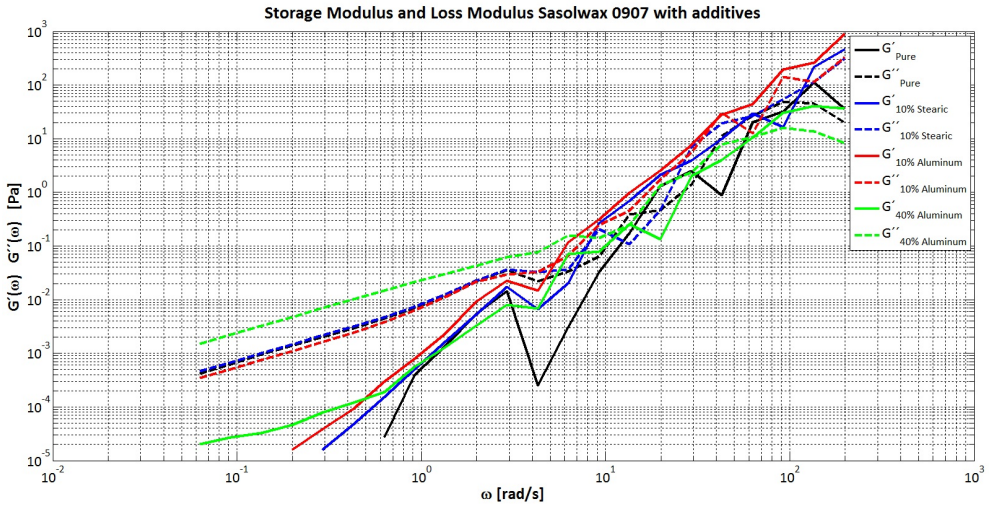


Figure 5.32: Storage and Loss Modulus as function of omega for Sasolwax 0907

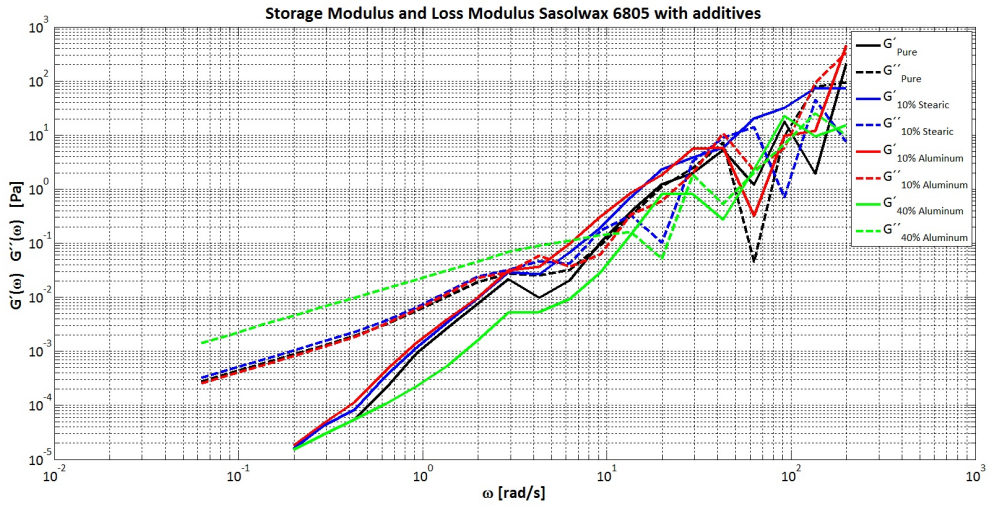


Figure 5.33: Storage and Loss Modulus as function of omega for Sasolwax 6805

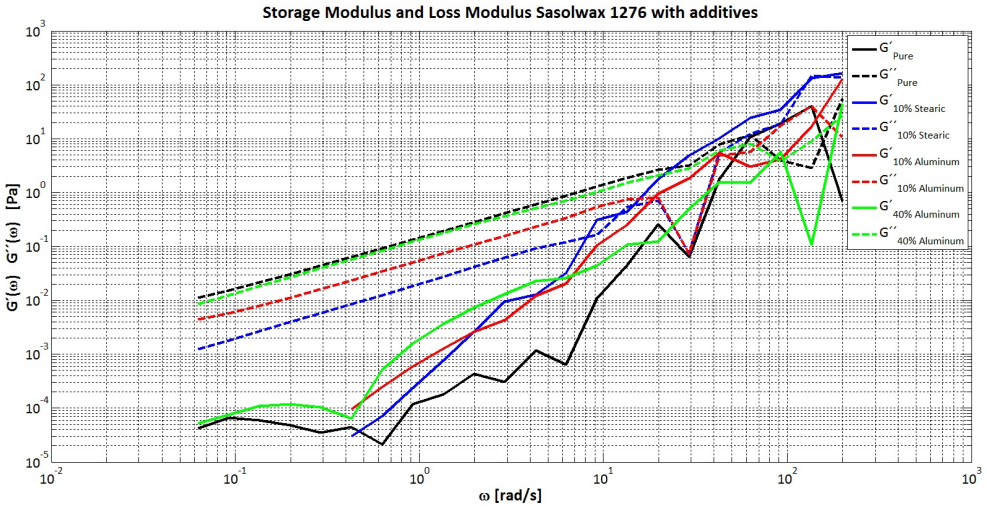


Figure 5.34: Storage and Loss Modulus as function of omega for Sasolwax 1276

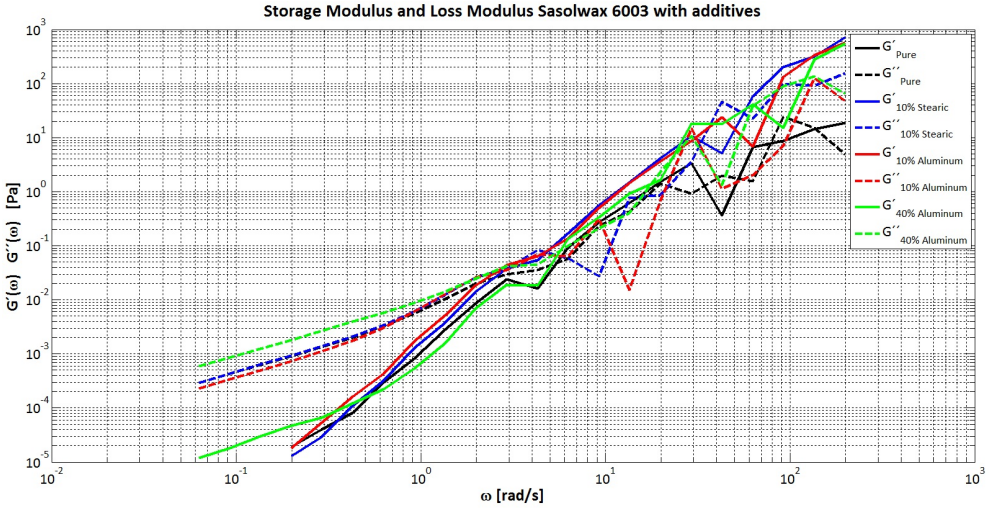


Figure 5.35: Storage and Loss Modulus as function of omega for Sasolwax 6003

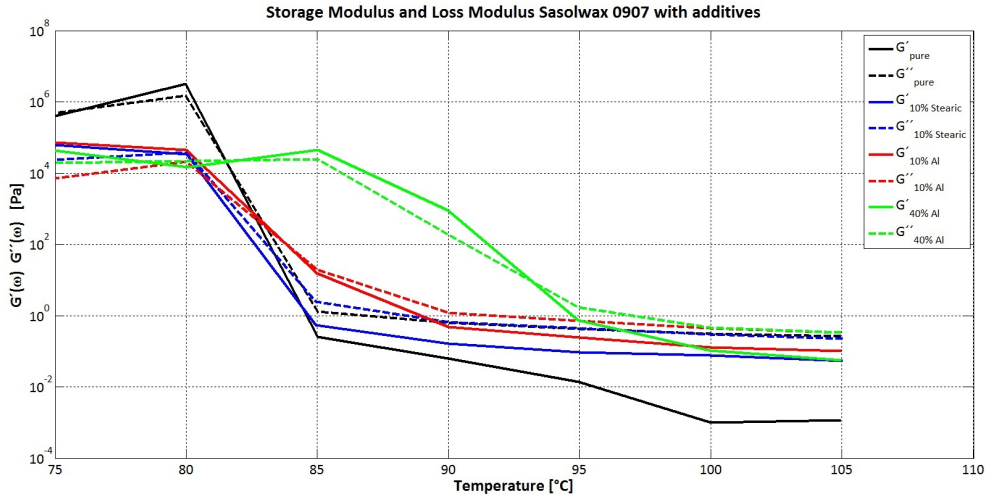


Figure 5.36: Storage and Loss Modulus as function of temperature for Sasolwax 0907 with additives

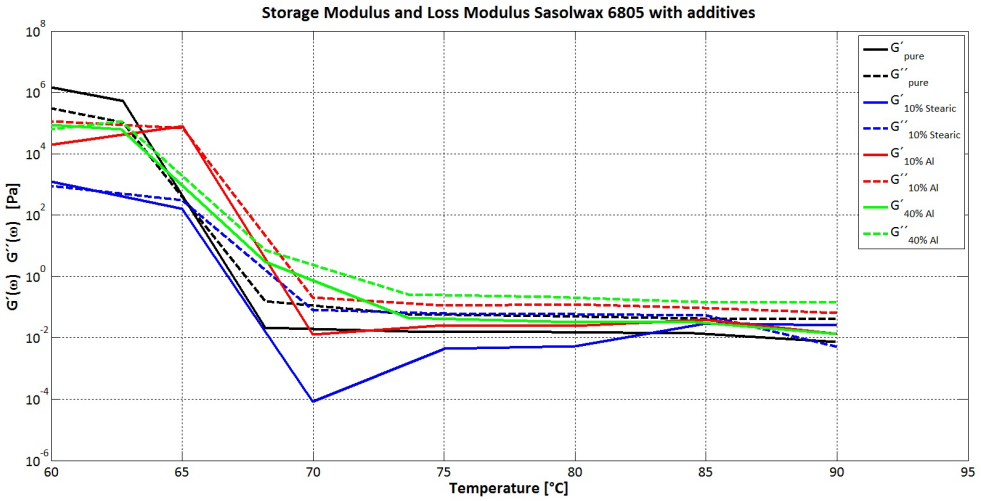


Figure 5.37: Storage and Loss Modulus as function of temperature for Sasolwax 6805 with additives

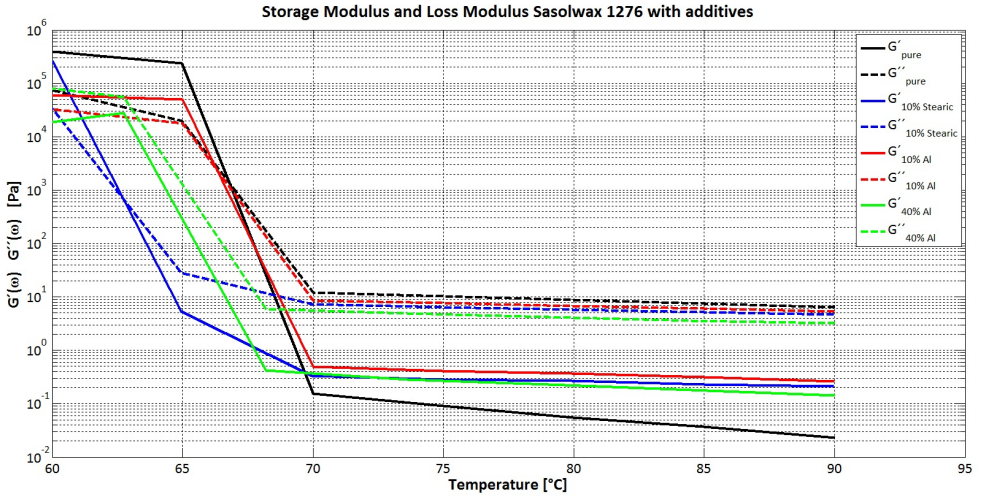


Figure 5.38: Storage and Loss Modulus as function of temperature for Sasolwax 1276 with additives

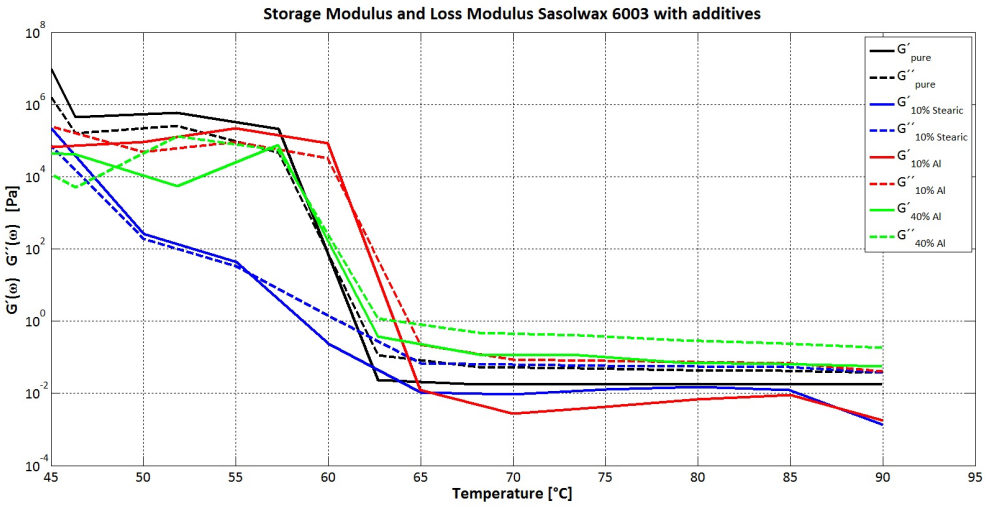


Figure 5.39: Storage and Loss Modulus as function of temperature for Sasolwax 6003 with additives

A cone plate configuration is used to measure storage, loss and complex modulus of pure waxes. A plate plate configuration is used to compare storage, loss and complex modulus of pure waxes and waxes with additives. The peak in Figure 5.39 is due to the too low viscosity of the wax measured with plate plate configuration.

Table 5.18: Storage and Loss Modulus test set up data

| Formulation | f [Hz] | Stress [Pa] | T °C | Rheometer Plate |
|---|---|---|---|---|
| Pure 0907 | 1 | 1 | 105-30 | PP 35 Ti + Rough |
| 0907 + 10% Stearic Acid | 1 | 1 | 105-30 | PP 35 Ti + Smooth |
| 0907 + 10% Aluminum | 1 | 1 | 105-30 | PP 35 Ti + Smooth |
| 0907 + 40% Aluminum | 1 | 1 | 105-30 | PP 35 Ti + Smooth |
| Pure 6805 | 1 | 1 | 90-30 | PP 35 Ti + Rough |
| 6805 + 10% Stearic Acid | 1 | 1 | 90-30 | PP 35 Ti + Smooth |
| 6805 + 10% Aluminum | 1 | 1 | 90-30 | PP 35 Ti + Smooth |
| 6805 + 40% Aluminum | 1 | 1 | 90-30 | PP 35 Ti + Smooth |
| Pure 1276 | 1 | 1 | 90-30 | PP 35 Ti + Rough |
| 1276 + 10% Stearic Acid | 1 | 1 | 90-30 | PP 35 Ti + Smooth |
| 1276 + 10% Aluminum | 1 | 1 | 90-30 | PP 35 Ti + Smooth |
| 1276 + 40% Aluminum | 1 | 1 | 90-30 | PP 35 Ti + Smooth |
| Pure 6003 | 1 | 1 | 90-30 | PP 35 Ti + Rough |
| 6003 + 10% Stearic Acid | 1 | 1 | 90-30 | PP 35 Ti + Smooth |
| 6805 + 10% Aluminum | 1 | 1 | 90-30 | PP 35 Ti + Smooth |
| 6805 + 40% Aluminum | 1 | 1 | 90-30 | PP 35 Ti + Smooth |

### Constant Stress - Constant Deformation

A comparison between measurements done with constant stress and constant deformation is done.

Two kind of pure paraffin are considered: Sasolwax 0907 and Sasolwax 1276.

As it can be noted in Figure 5.40, where data obtained with constant stress (plate 35mm) and constant deformation (plate 35mm and 60mmm) are shown, results obtained are different.

In the case of constant stress results are like expected: in the liquid phase viscous modulus is greater than elastic modulus, while in the solid phase elastic modulus is greater than the viscous one.

Using a constant deformation $\gamma$ of 5% and 1 Hz frequency the behavior is different, as expected, especially from the transition to the solid phase. In fact the viscous modulus is always greater than the elastic one. For this reason further tests should be done in constant deformation conditions.

Sasolwax 1276 shows similar results in both cases, as presented in Figure 5.41.

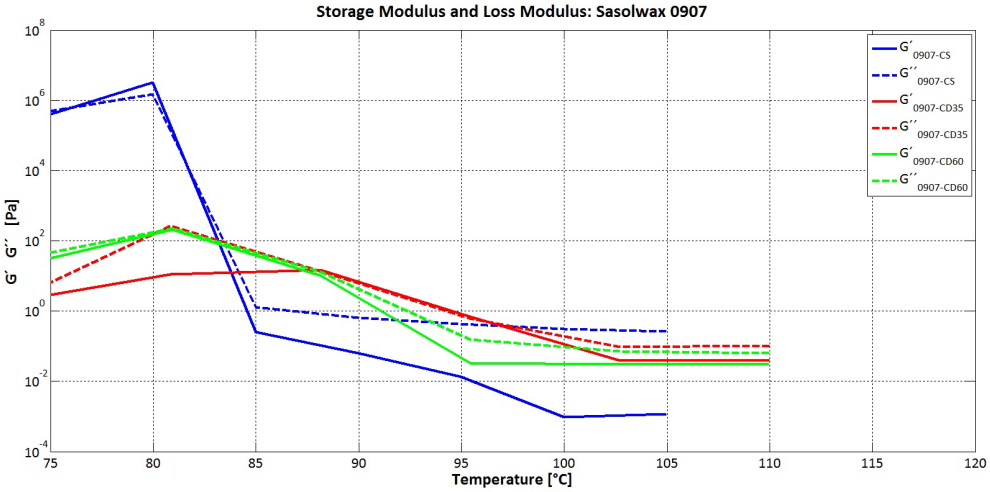


Figure 5.40: CS-CD for Sasolwax 0907

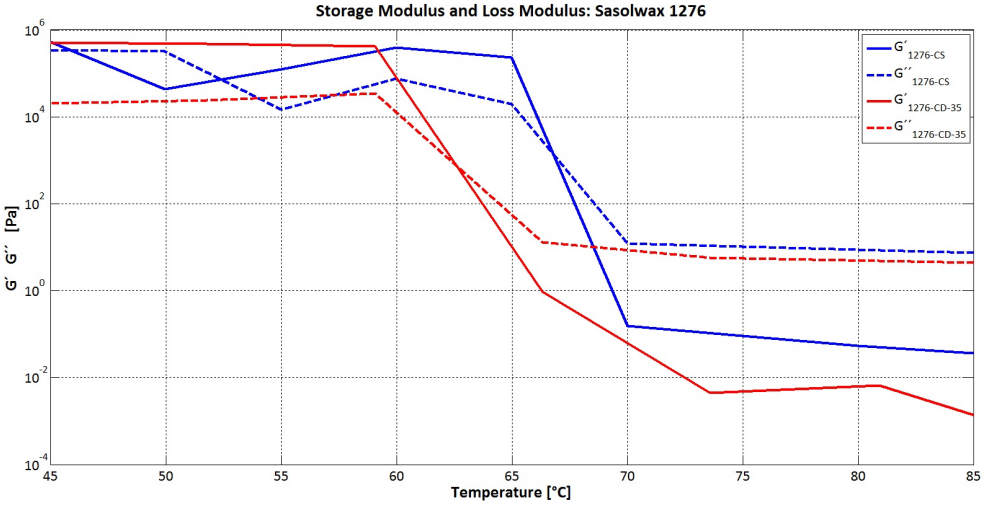


Figure 5.41: CS-CD for Sasolwax 1276

# Chapter 6

# Setup for combustion tests and performances analysis

## 6.1 Combustion facility overview

An overview of the facility for combustion tests at DLR is here reported. Work was done in order to improve the supply line system. The system, as it can be seen from Figure 6.1, is composed by:

- a combustion chamber made of two main parts: the first where the oxidizer enters and it assumes an homogeneous flow, and the second where there are the fuel slab and the ignition system.
- the igniter: located at the bottom at the beginning of the second half of the chamber. Ignition starts burning a mixture of $H_2$-$O_2$
- three main supply system: one brings hydrogen and oxygen needed for the ignition, the supply system for the oxidizer that is used during combustion and the nitrogen supply system needed to keep clean the window of the chamber and to clean and cool the chamber after tests
- the fuel is positioned at the bottom of the chamber in a parallelepiped housing with dimensions 20cm x10cm x 2cm
- the sampling probe system
- the remote control system
- the video recording camera

On the main oxygen line there is also a Coriolis mass flow meter that in Figure 6.1 is not represented.

Before starting the tests it was needed to partially renew the line: for this reason many valves and pipes on the supply lines were renewed, the chamber and the sampling probe system were already used in previous tests.

In order to have a first estimation of the values which could be obtained with the chamber, such as O/F ratio and $r_f$, some data are needed:

- the chamber section is 15cm(l) x 4.5cm(h)

- the fuel section is 10cm(l) x 2cm(h)
- the chamber section over the fuel is 10cm(l) x2.5cm(l)
- the regression coefficient are $a = 0.488$ and $n = 0.62$
- the fuel density is 850 $kg/m^3$
- the lenght of the fuel slab is 20cm
- the regression area is 20cm x 10cm

### 6.1.1 Fuels

**Preparation of the fuel**

The fuel is a slab of 20cm x 10cm x 2cm. In order to avoid the formation of cracks or inhomogeneities, the wax is cast in one time in a casing made of two parts: the lateral walls, which are removable, and a steel plate, where the wax is cast and that is fixed at the bottom of the combustion chamber.

The procedure is simply based on:

- heating in a glass 300-400 ml of wax until it melts (temperature between 90 and 105°C)
- casting the liquid wax on the steel plate
- natural cooling of the wax
- removal of the walls from the solid wax

### 6.1.2 Data analisys

**Estimation of average values for $r_f$ and $c*$**

In order to get average values of regression rate and characteristic velocity, the standard deviation of the measures is calculated.

In both cases it is assumed to have only independent variables, in this way the global error on the y variable is calculated as

$$e_y = \sqrt{(\frac{\partial y}{\partial x_1} e_1)^2 + (\frac{\partial y}{\partial x_2} e_2)^2 + .. + (\frac{\partial y}{\partial x_n} e_n)^2} \tag{6.1}$$

where $e_1, e_2, ..e_n$ are the uncertainties of the independent variables $x_1, x_2, ..., x_n$.

**Error evaluation on c***

Considering the expression of $c*$ :

$$c* = \frac{p_c A_t}{\dot{m}} \tag{6.2}$$

$$e_{c*} = \sqrt{(\frac{\partial c*}{\partial p_c} e_{p_c})^2 + (\frac{\partial c*}{\partial A_t} e_{A_t})^2 + (\frac{\partial c*}{\partial \dot{m}} e_{\dot{m}})^2} \tag{6.3}$$

leading to:

$$e_{c*} = \sqrt{(\frac{A_t}{\dot{m}} e_{p_c})^2 + (\frac{p_c}{\dot{m}} e_{A_t})^2 + (\frac{-p_c A_t}{\dot{m}^2} e_{\dot{m}})^2} \tag{6.4}$$

**Error evaluation on $r_f$**

Considering the expression of $r_f$ :

$$r_f = a(\frac{\dot{m_{ox}}}{A_{ox}})^n \tag{6.5}$$

$$e_{r_f} = \sqrt{(\frac{\partial r_f}{\partial \dot{m_{ox}}} e_{m_{ox}})^2 + (\frac{\partial r_f}{\partial A_{ox}} e_{A_{ox}})^2} \tag{6.6}$$

leading to:

$$e_{r_f} = \sqrt{(\frac{na}{A_{ox}^n} \dot{m}_{ox}^{n-1} e_{\dot{m_{ox}}})^2 + (\frac{-an\dot{m_{ox}}^n}{A_{ox}^{n+1}} e_{A_{ox}})^2} \tag{6.7}$$

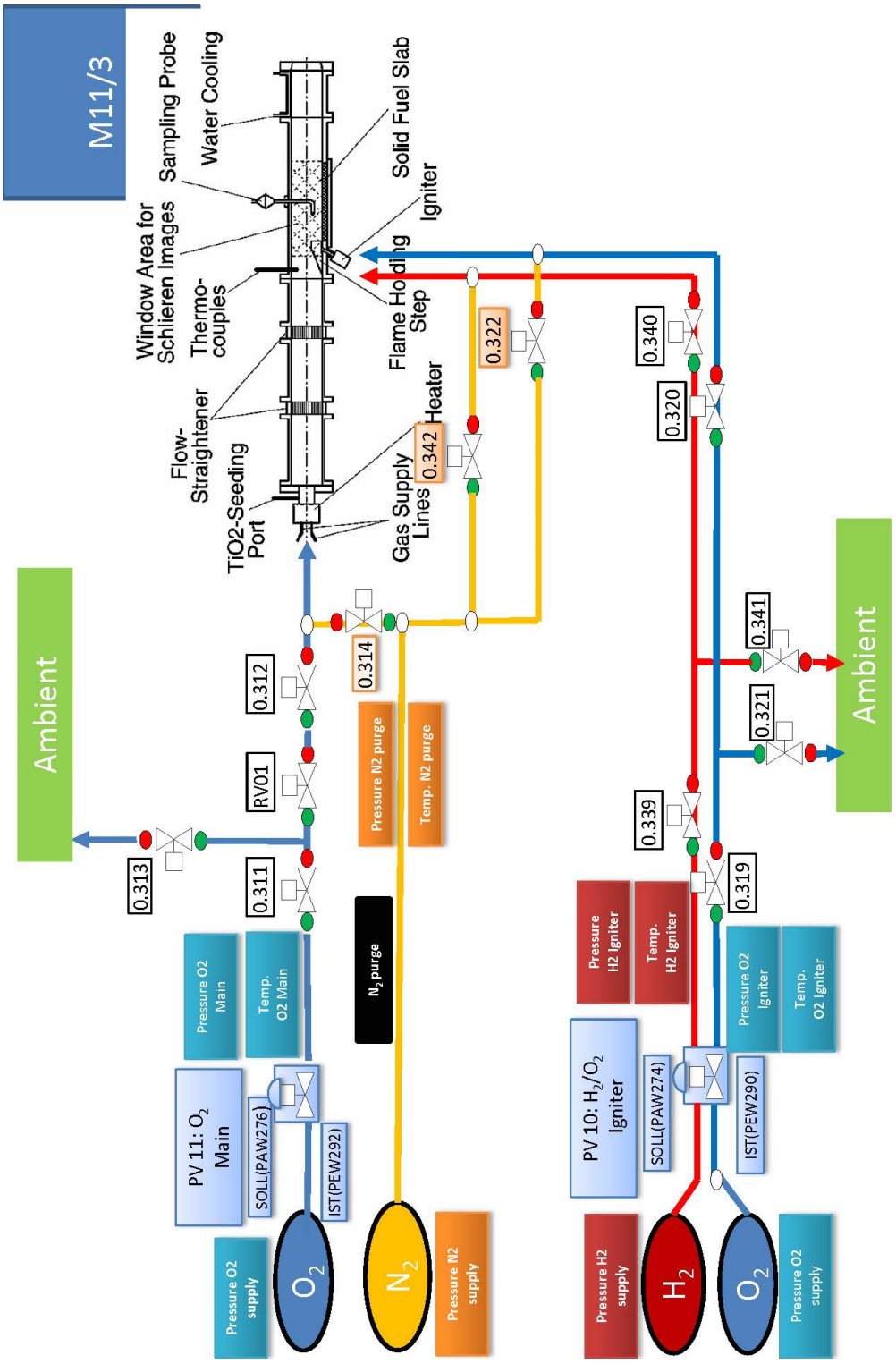


Figure 6.1: Visualization of test bench at M11

## 6.2 Combustion products analysis

A further step that should follow this work is the combustion products analysis. For this reason in this part of the work the sampling probe system, that could be used, is shown. Some analysis are done with CEA to estimate theoretically the quality of combustion and the amount of collectable Alumina.

### 6.2.1 Sampling Probe system

In order to know the combustion process and its efficiency a sampling probe system, that collects gaseous and condensed combustion products, is needed. This facility already exists and it is composed by:

- water cooled sampling probe cooled by three tubes with pressurized water
- a filter that collects the condensed phase
- remote control valve unit
- gas sampling cylinder
- vacuum pump
- pressure transducer that monitore the expansion of the probe gas flow

A scheme of the sampling probe system [9] is presented in Figure 6.2.

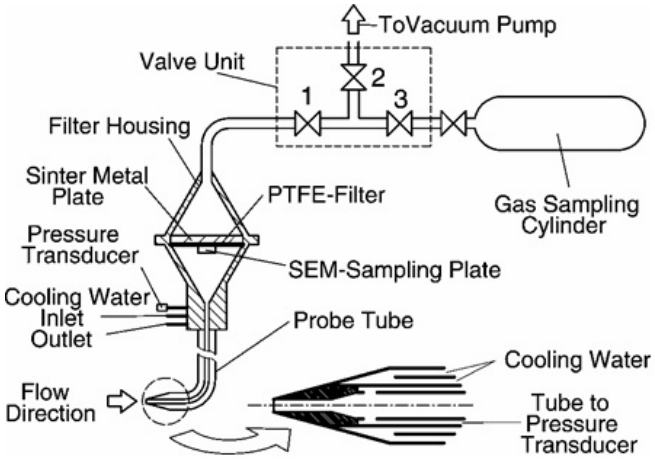


Figure 6.2: Scheme of the sampling probe system

### 6.2.2 CEA Analysis

In order to choose the hardware needed for the sampling probe system, the amount of combustion products (both gaseous and condensed ) has to be known . For this problem the NASA-program CEA (Chemical Equilibrium with Applications) is used. This program calculates chemical equilibrium product concentrations from the set of reactants and it determines thermodynamic and transport properties of the product mixture. The application that allows to solve a rocket problem is included.

In the present case the following parameters are considered:

- the chamber pressure is assumed to be 30 bar
- the $\frac{p_i}{p_e}$ ratio is assumed to be 30, considering atmospheric pressure at the exit
- the diameter of the sampling probe tube is 0.7 mm
- paraffin $C_{50}H_{102}$ with enthalpy of formation equal to -1438 $kJ/mol$ [61]
- Aluminum with a percentage ranging from 10 to 40% of the total fuel mass
- $N_2O$ as oxidizer
- O/F ratio equal to 6

With these input data the specific impulse $I_S$, the density $\rho$ at the exit and the mass fractions of combustion products are calculated. Once these data are known it is possible to calculate the total mass flow in the tube as

$$\dot{m} = \rho A_{tube} I_S \tag{6.8}$$

Knowing the total mass flow, the Alumina mass flow is obtained as product of Alumina mass fraction and total mass flow.

Two different cases are examinated: in the first case the temperature is estimated to be 3800 K, in the second case it is assigned to be 2000 K to simulate incomplete combustion.

In the following figures the values of specific impulse, density, total mass flow, Alumina mass fraction, Alumina mass flow and its mass as functions of O/F and of Aluminum percentage are shown.

### Specific Impulse

In Figure 6.3 and 6.4 the specific impulse values obtained for different Al concentrations with varying the oxidizer to fuel ratio at 2000 K and 3800 K are presented.

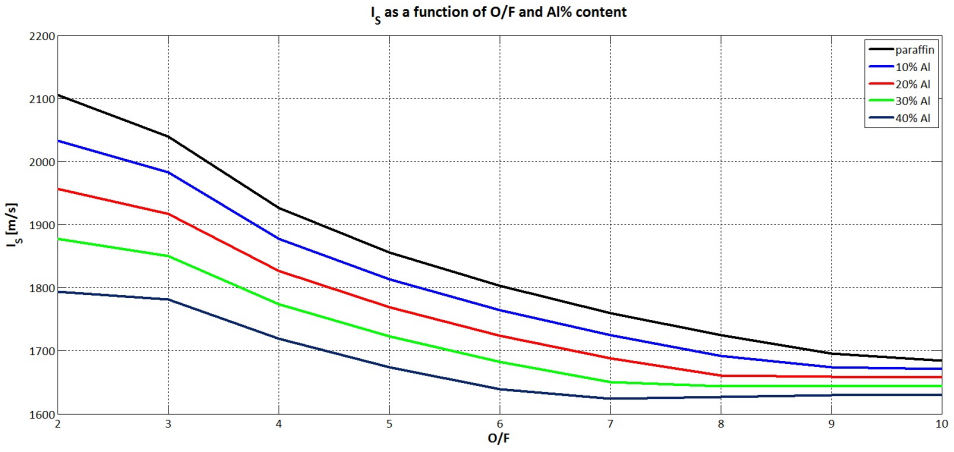


Figure 6.3: Specific impulse at 2000 K

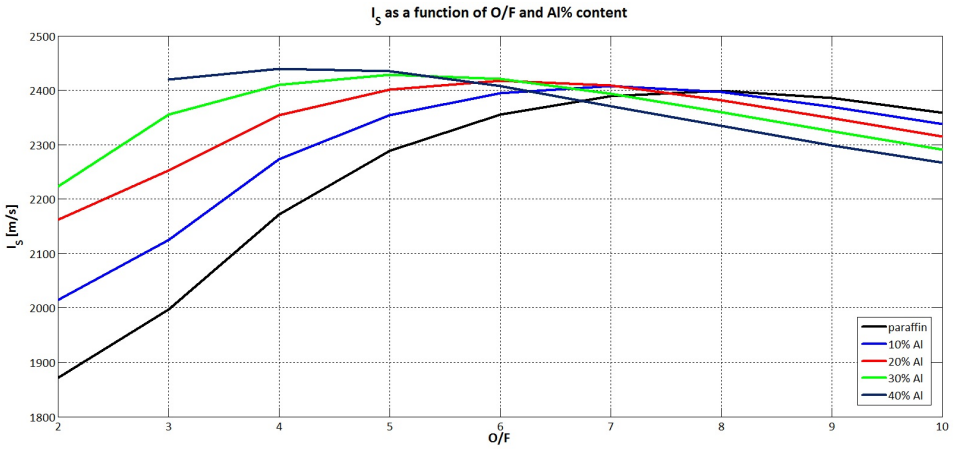


Figure 6.4: Specific impulse at 3800 K

At lower temperatures $I_S$ decreases with increasing O/F and higher values are reached with low Aluminum concentrations (the case of pure paraffin shows the higher $I_S$).

In the case with a temperature of 3800 K, specific impulse at low O/F is higher with a high Al concentration. For high O/F, $I_S$ is higher with pure paraffin.

Maximum $I_S$ values are higher at 3800 K, with a maximum for O/F=4 with 40% Al.

### Density

At 2000 K density increases monotonically with O/F and it shows the highest value with 40% Al (Figure 6.5 ).

At 3800 K the highest value is obtained with pure paraffin at the lowest oxidizer to fuel ratio. The minimum value is at O/F=6 with 40% Al. For high O/F, density values increase with Aluminum content (Figure 6.6).

Density values are higher at 2000 K, except for pure paraffin at low O/F.

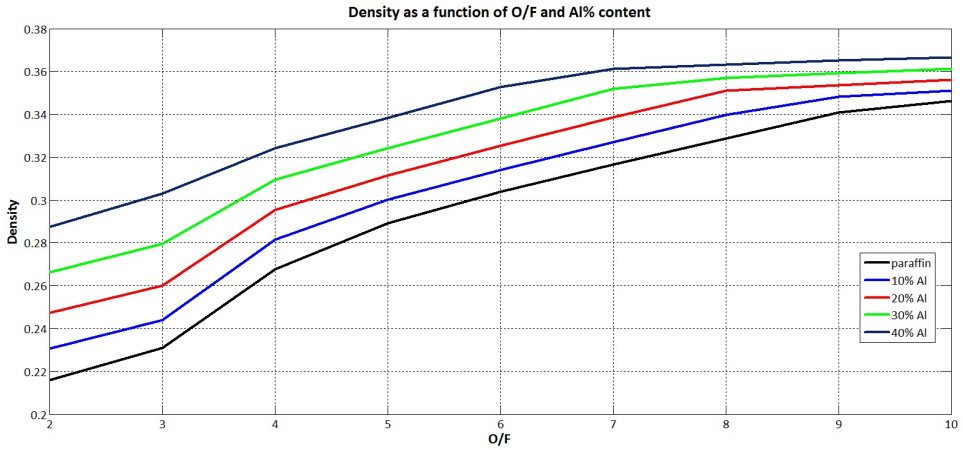


Figure 6.5: Density at 2000 K

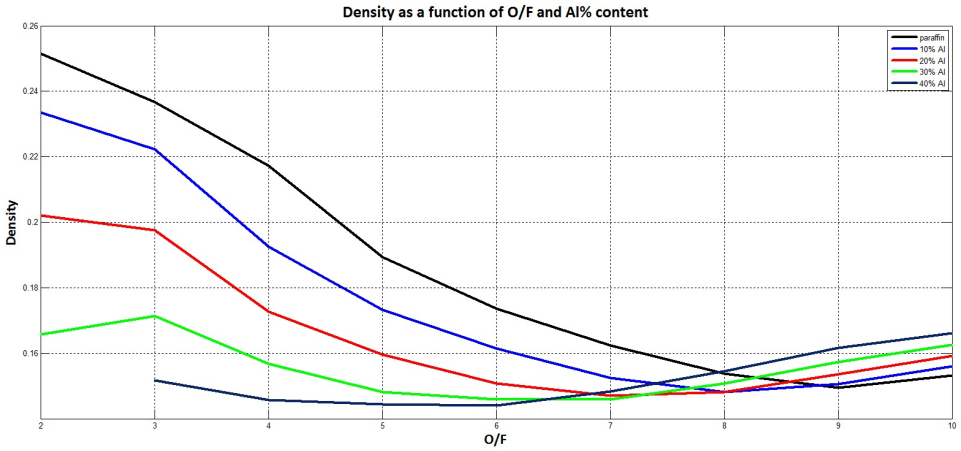


Figure 6.6: Density at 3800 K

### Mass flow rate in the tube

At 2000 K mass flow rate increases with Al% content. Values increase with O/F, strongly with low Aluminum content. Except for paraffin at low O/F, values are higher than at 3800 K (Figure 6.7 ).

At 3800 K mass flow rate values show a peak for O/F = 3 , except for the case with 40% paraffin, where the highest value is reached at O/F = 10 (Figure 6.8 ). The lowest mass flow rates are obtained for increasing OF ratio with decreasing Aluminum content. The lower the Al%, the higher the mass flow rate (except at high OF).

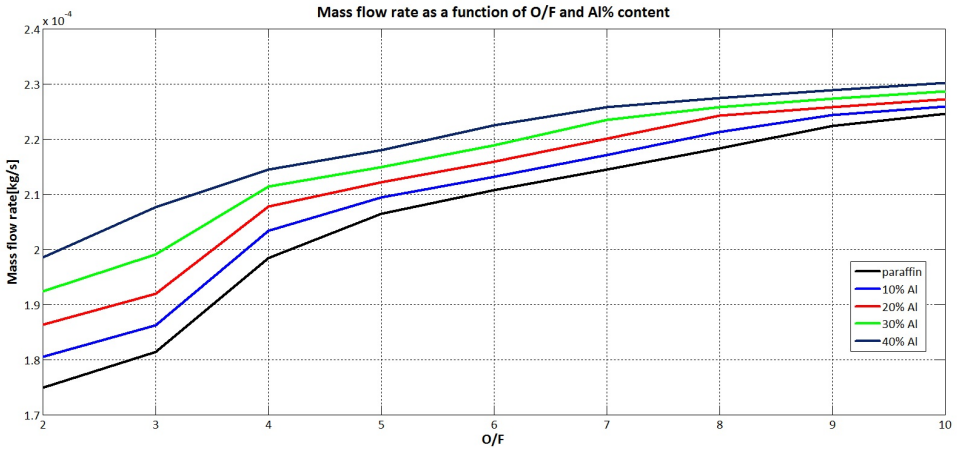


Figure 6.7: Total mass flow at 2000 K

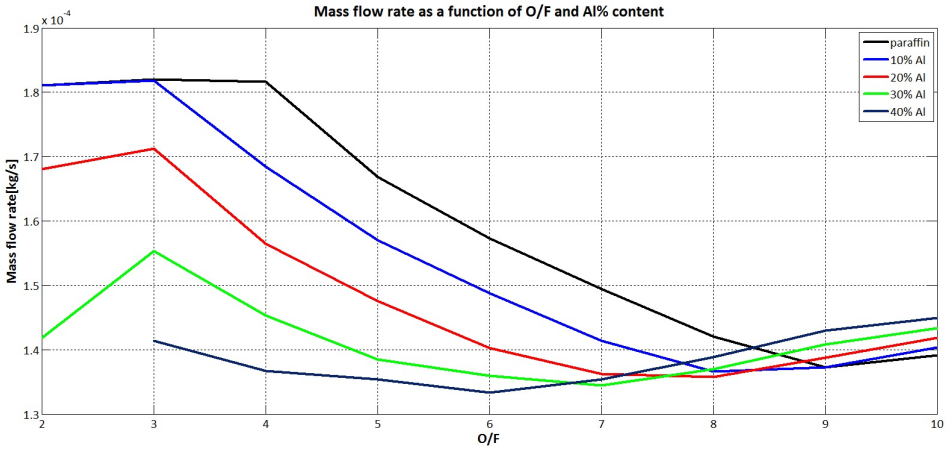


Figure 6.8: Total mass flow at 3800 K

### Alumina mass fraction

Mass fraction values are the same at 2000 K and 3800 K. Values decrease monotonically with increasing oxidizer to fuel ratio and decrease with decreasing Aluminum content (Figure 6.9 and 6.10).

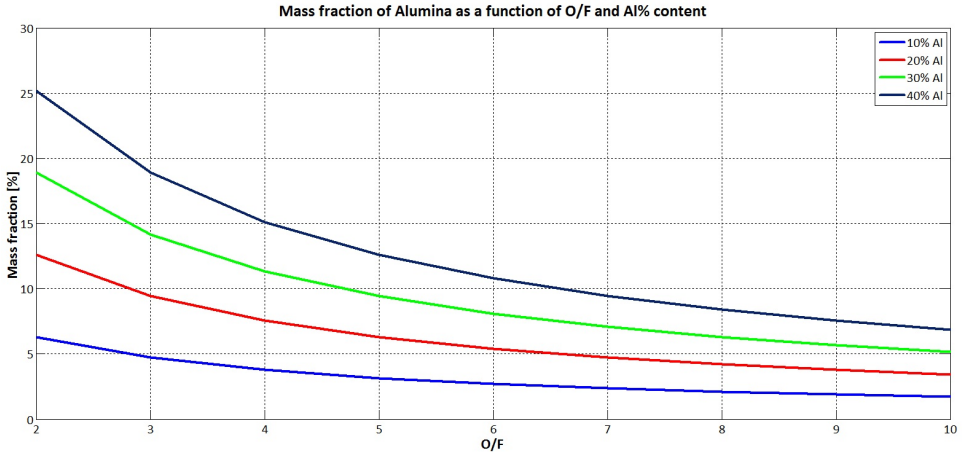


Figure 6.9: Alumina mass fraction at 2000 K

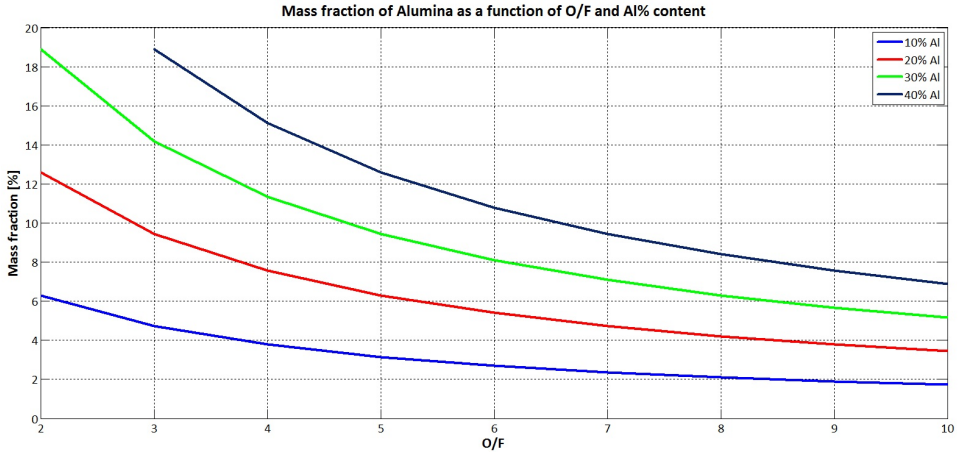


Figure 6.10: Alumina mass fraction at 3800 K

### Alumina mass flow rate

Alumina mass flow rate is higher at lower temperature. Values increase with increasing Aluminum presence and with decreasing OF (Figure 6.11 and 6.12).

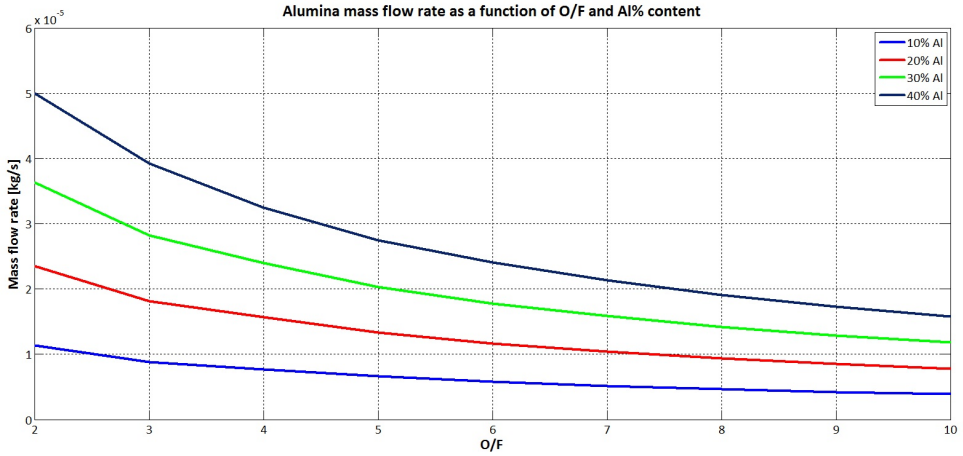


Figure 6.11: Alumina mass flow rate at 2000 K

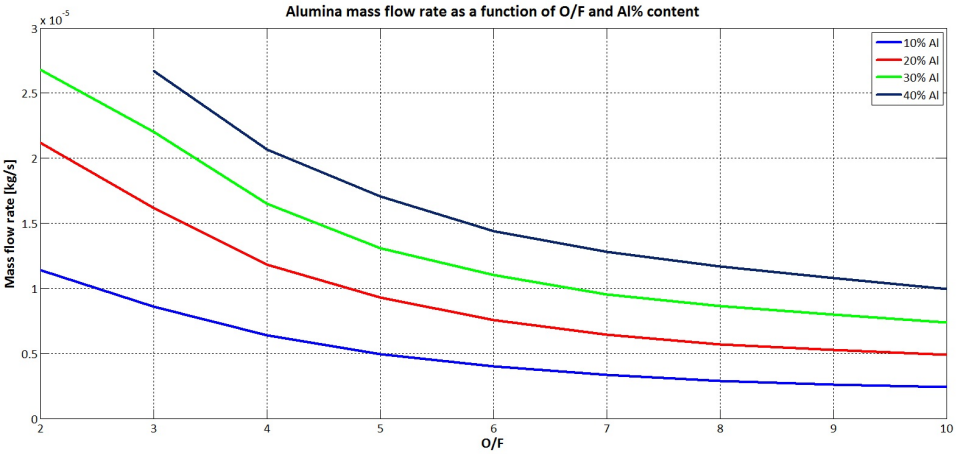


Figure 6.12: Alumina mass flow rate at 3800 K

### Combustion efficiency

In order to understand the theoretical quality of combustion process, combustion efficiency is calculated as a function of Equivalence Ratio (ER) and Oxidizer to Fuel Ratio.

The efficiency is simply obtained as the ratio of characteristic velocity c at 2000 K and at 3800 K.

In Figure 6.13 and 6.14 it is possible to see that combustion efficiency in fuel rich mixtures reaches highest values with pure paraffin, while in oxidizer rich mixtures the values increase with Aluminum percentage. The minimum value decreases with increasing Aluminum percentage. It can also be noticed that the difference from a formulation to another is higher at low O/F than at high O/F.

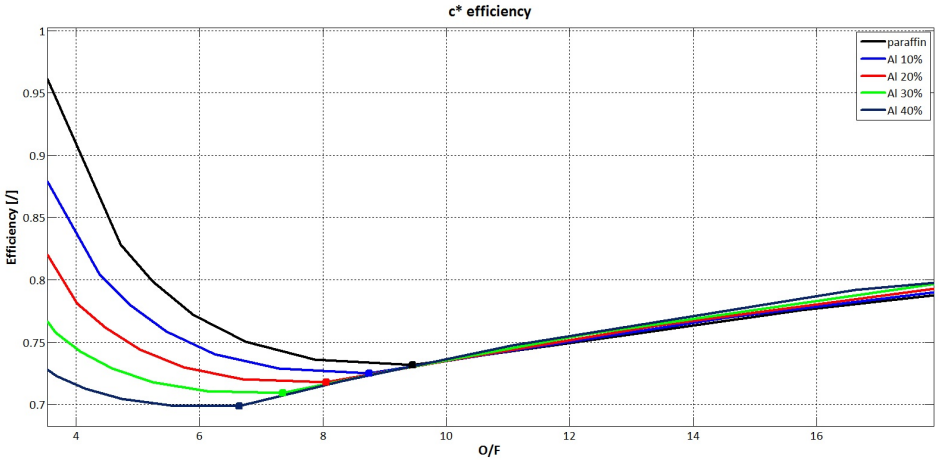


Figure 6.13: Combustion efficiency as a function of O/F

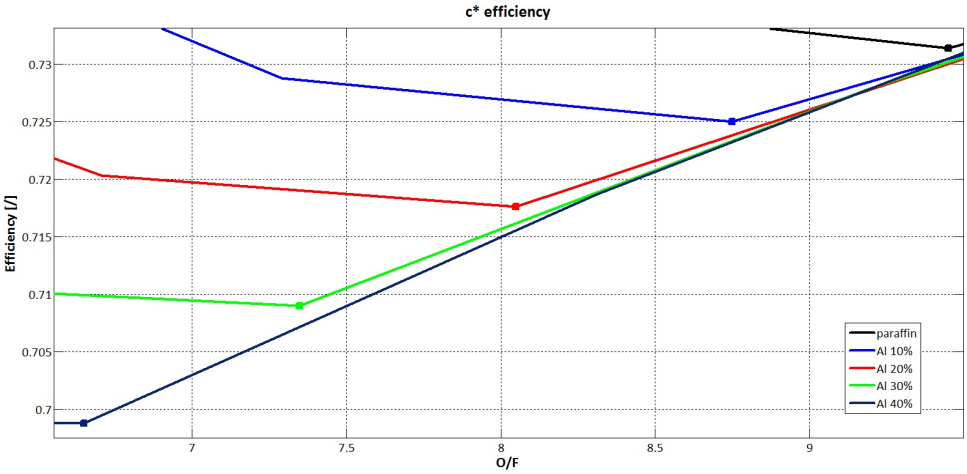


Figure 6.14: Combustion efficiency as a function of O/F (particular)

In Figure 6.15 it can be noticed that the highest efficiency values are reached at low ER for pure paraffin. Minimum values are obtained for ER = 1 .

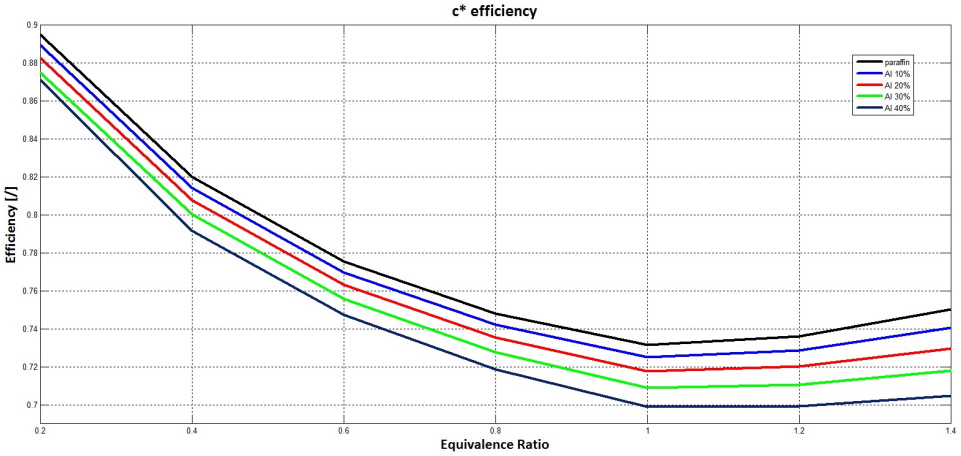


Figure 6.15: Combustion efficiency as a function of Equivalence Ratio

### Mass of collectable Alumina

The amount of Alumina that can be collected in a test is calculated as product of burning time ($t_b = 5s$) and Alumina mass flow rate.

Figure 6.16 and 6.17 show that the amount of Alumina increases with low OF ratio and with high Aluminum percentage. At lower temperatures the amount of Alumina is higher. This result needs further investigations.

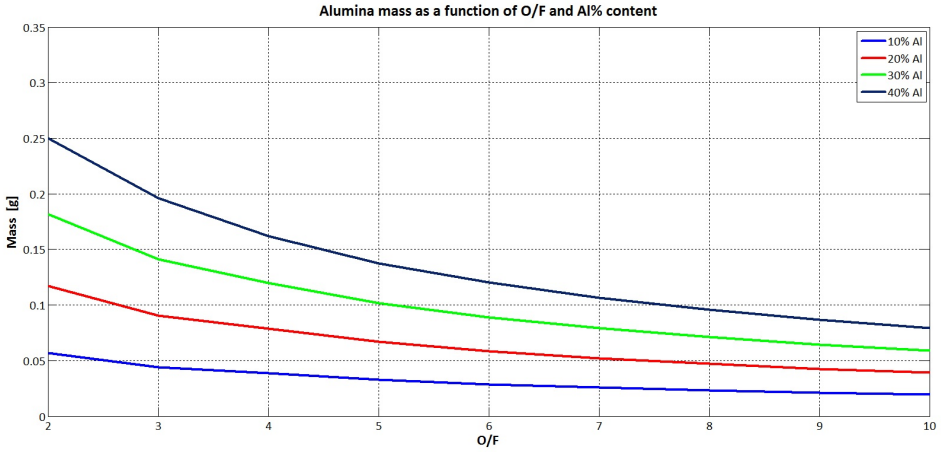


Figure 6.16: Mass of Alumina at 2000 K

These data show that the mass amount of Alumina that could be collected is very small. For this reason now we can choose between two possibilities:

- chemical analysis

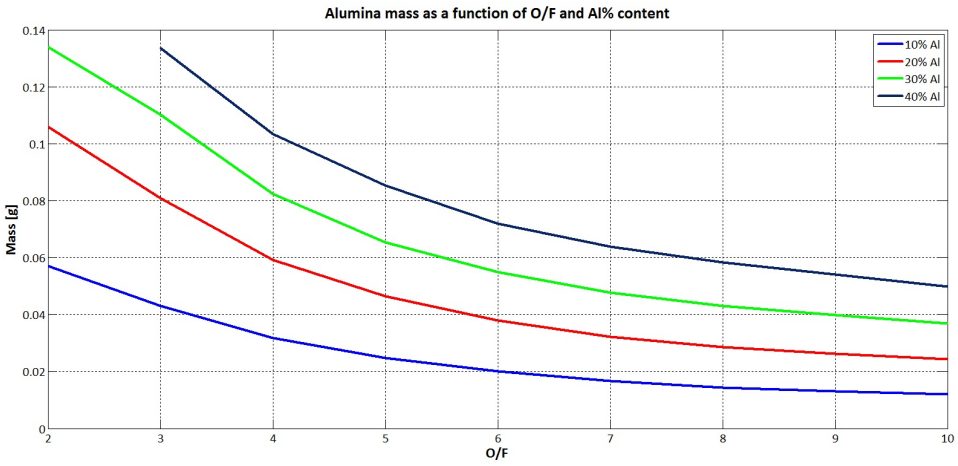


Figure 6.17: Mass of Alumina at 3800 K

- additional hardware

Chemical analysis could be titration, a laboratory procedure for quantitative analysis used to determine concentration of analytes [62]. Titration needs an analyte solution (whose concentration is unknown) and a standard solution (whose concentration is known).

$$C_a = \frac{C_t V_t M}{V_a} \tag{6.9}$$

where $C_a$ is the analyte concentration in molarity, $C_t$ is the titrant concentration in molarity, $V_t$ is the volume of titrant, $M$ is the mole ratio of analyte and reactant from the balanced chemical equation and $V_a$ is the volume of analyte.

The procedure is based on the addition from a burette of one of the two solutions till the endpoint is reached.

There are several types of titration:

- acid - base titration
- redox titration
- zeta potential titration
- complexometric titration
- gas phase titration
- assay

Endpoint is a physical change in the solution and it can be observed in different ways: with a change in the appearance of the solution or with a change in physical or chemical properties.

It could be useful to use an indicator that changes its color at the endpoint.

An example of chemical analysis is in the work made by Merotto, Boiocchi, Galfetti, Colombo, Carea, De Luca [63] where the condensed combustion products of Aluminum

and Magnesium Hydride are collected and chemically analised with Sulfuric Acid. The chemical reaction gives $H_2$ among its products: knowing the $H_2$ gas volume, the number of moles of $H_2$ produced can be determined. From the chemical balance, the number of metal moles can be obtained, and multiplying it with the metal atomic mass, the mass of metal can be determined. This corresponds to the unburnt condensed metal mass.

In this work it has been found that unburnt metal fraction decreases with increasing oxygen mass flux. The formulation with $HTPB+LP+nAl$ shows the lowest percentage of unburnt metal, followed by $HTPB+nAl$. The formulation added with $MgH_2$ shows the highest values. The difference between the two formulations with nAl is due to the fact that the formulation with paraffin has an higher regression rate. In the case of Magnesium Hydride the regression rate is similar to the case of $HTPB+LP+nAl$, the difference is that Magnesium particles burn less efficiently than Aluminum particles.

# Conclusions and future developments

Regression rate in liquefying hybrid fuels is influenced by surface tension and viscosity: a decrease in both quantities leads to higher regression rates. In this work, different formulations of waxes and additives are investigated.

The effect of additives on surface tension is more important on high density and entangled waxes, as Sasolwax 1276. In this case additives decrease the surface tension value. On the contrary, as for Sasolwax 6003, that is the lighter and not entangled wax, additives increase the surface tension value.

Viscosity is investigated as function of temperature in a range between 200°C and the melting point: Sasolwax 1276 shows an order of magnitude higher viscosity if compared with others. Viscosity increases exponentially with decreasing temperature and the highest values are shown by entangled waxes. It can be seen that, in general, additives increase the viscosity, except in the case of Sasolwax 1276.

Related to this topic, further investigations should involve the analysis of storage modulus, loss modulus and the mechanical properties of the mixtures.

Moreover, surface tension and viscosity of new types of mixtures should be examined: substances which could be tested are wax based mixtures with metals, metal hydrides and boron in different percentage.

The most important investigation that should be done in the future is the understanding of the correlation between the physical properties of the mixtures and the regression rate values. Optical investigation of combustion should be done to observe the entrainment of droplets of the different mixtures to relate entrainment with viscosity and surface tension.

Another interesting future development is the study of unburnt combustion products. For this reason, some analysis are presented in this work at chapter 5. In particular a study of the sampling probe system and some CEA analysis are performed. Future work should be focused on the treatment of combustion products with a procedure like titration that allows to estimate the unburnt products. In this way it will be possible to know which formulations are more efficient in terms of propulsion parameters.

# Bibliography


[1] M. A. Karabeyoglu and B. J. Cantwell. "Combustion of liquefying hybrid propellants: Part 2, Stability of liquid films". In: *Journal of Propulsion and Power* 18.3 (2002), pp. 621–630.

[2] M. A. Karabeyoglu, D. Altman, and B. J. Cantwell. "Combustion of liquefying hybrid propellants: Part 1, general theory". In: *Journal of Propulsion and Power* 18.3 (2002), pp. 610–620.

[3] R. A. Gater and M. R. L. L'Ecuyer. "A Fundamental Investigation of the Phenomena that Characterize Liquid Film Cooling". In: *International Journal of Heat and Mass Transfer* 13.3 (1970), pp. 1925–1939.

[4] R. Nigmatulin et al. "Entrainment and Deposition Rates in a Dispersed Film Flow". In: *International Journal of Multiphase Flow* 22.1 (1996), pp. 19–30.

[5] I. Nakagawa and S. Hikone. "Study on the Regression Rate of Paraffin-Based Hybrid Rocket Fuels". In: *Journal of Propulsion and Power* 27 (2001), pp. 1276–1279.

[6] J. J. Marano and G. D. Holder. "A General Equation for Correlating the Thermophysical Properties of n-Paraffins, n-Olefins and Other Homologous Series. 2. Asymptotic Behavior Correlations for PVT Properties". In: *Industrial Engineering Chemical Research* 36 (1997), pp. 1895–1907.

[7] G. M. Kontogeorgis and D. P. Tassios. "Critical constants and acentric factors for long-chain alkanes suitable for corresponding state applications. A Critical Review". In: *Chemical Engineering Journal* 66 (1997), pp. 35–49.

[8] M. A. Karabeyoglu, B. J. Cantwell, and J. Stevens. "Evaluation of Homologous Series of Normal-Alkanes as Hybrid Rocket Fuels". In: *41st AIAA/ASME/SAE/ASEE Joint Propulsion Conference and Exhibit*. Ed. by AIAA. AIAA-2005-3908. Tucson, AZ, 2005.

[9] H. K. Ciezki et al. "Combustion of Solid-Fuel Slabs containing Boron Particles in Step Combustor". In: *Journal of Propulsion and Power* 19.6 (2003), pp. 1180–1191.

[10] M. A. Karabeyoglu et al. "Scale-up tests of high regression rate paraffin-based hybrid rocket fuels". In: *Journal of Propulsion and Power* 20.6 (2004), pp. 1037–1045.

[11] G. Schulte, R. Pein, and A. Högl. "Temperature and Concentration Measurements in a Solid Fuel Ramjet Combustion Chamber". In: *Journal of Propulsion and Power* 3.2 (1986), pp. 114–120.

[12] J. J. Marano and G. D. Holder. "A General Equation for Correlating the Thermophysical Properties of n-Paraffins, n-Olefins and Other Homologous Series. 3. Asymptotic Behavior Correlations for Thermal and Transport Properties". In: *Industrial Engineering Chemical Research* 36 (1997), pp. 2399–2408.

[13] Vyncolit. Last visited: 20 June 2012. URL: http://www.vyncolit.net/.

[14] Jozef Bicerano. *Prediction of Polymer Properties*. Ed. by Inc. Marcel Dekker. The Dow Chemical Company, 1996.

[15] Encyclopaedia Britannica Online. Last visited: 1 June 2012. URL: http://www.britannica.com/EBchecked/topic/278278/hydride.

[16] F. Maggi et al. "Theoretical analysis of hydrides in solid and hybrid rocket propulsion". In: *International Journal of Hydrogen Energy* 37 (2011), pp. 1760–1769.

[17] B. Bogdanovic. "Catalytic Synthesis of Organolithium and Organomagnesium Compounds and of Lithium and Magnesium Hydrides - Applications in Organic Synthesis and Hydrogen Storage". In: *Angew. Chem. Int. Ed. Engl.* 24 (1985), pp. 262–273.

[18] NIST. Last visited: 1 June 2012. URL: http://webbook.nist.gov/.

[19] NIST. *NIST - JANAF Thermochemical Tables*. Last visited: 21 May 2012. URL: http://kinetics.nist.gov/janaf/.

[20] C.E. Messer. *A Survey Report on Lithium Hydride*. Tech. rep. Tufts University - United States Atomic Energy Commission, 1960.

[21] A. E. Finholt, A. C. Jr. Bond, and H. I. Schlesinger. *Lithium Aluminum Hydride, Aluminum Hydride and Lithium Gallium Hydride, and Some of their Applications in Organic and Inorganic Chemistry*. Tech. rep. University of Chicago, 1946.

[22] S. & Brinks H. & Hauback B. Lovvik O. & Opalka. "Crystal Structure and Thermodynamic Stability of the Lithium Analates LiAlH4 and Li2AlH6". In: *Physical Review B* 69 (2004), pp. 134117–1 –134117–9.

[23] P. Patnaik. *Handbook of Inorganic Chemicals*. Ed. by McGraw-Hill. McGraw-Hill, 2003.

[24] M. B. Smith and G. E. Jr. Bass. "Heats and Free Energies of Formation of the Alkali Aluminum Hydrides and of Cesium Hydride - Heat of Formation of Aluminum Chloride in Hydrochloric Acid". In: *Journal of Chemical and Engineering Data* 8 (1963), pp. 342–346.

[25] J. Graetz et al. *Aluminum hydride, AlH3, As a Hydrogen Storage Compound*. Tech. rep. Brookhaven National Laboratory, 2006.

[26] G.C. Sinke et al. "Thermodynamic Properties of Aluminum Hydride". In: *The Journal of Chemical Physics* 47 (1967), pp. 2759–2761.

[27] L.T. DeLuca et al. "Physical and Ballistic Characterization of ALH3 - Based Space Propellants". In: *European Conference for Aerospace Science (EUCASS) - Moscow*. Ed. by EUCASS. 2005.

[28] R.W. Shore S. G. & Parry. "Chemical Evidence for the Structure of the Diammoniate of Diborane II. The Preparation of Ammonia-Borane". In: *Journal of the American Chemical Society* 80 (1958), pp. 8–12.

[29] ChemSpider. *The Free Chemical Database*. Last visited: 21 May 2012. URL: http://www.chemspider.com.

[30] W. T. Klooster et al. "Study of the N-H...H-B Dihydrogen Bond Including the Crystal Structure of $BH_3NH_3$ by Neutron Diffraction". In: *Journal of the American Chemical Society* 121 (1999), pp. 6337–6343.

[31] H. K. Ciezki and B. Schwein. "Investigation of gaseous and solid reaction products in a step combustor using a water-cooled sampling probe". In: *AIAA, ASME, SAE, and ASEE 32nd Joint Propulsion Conference and Exhibit*. Ed. by AIAA. AIAA-1996-2768. Lake Buena Vista, FL, 1996.

[32] M. R. Weismiller et al. "Characterization of Ammonia Borane (NH3BH3) Enhancement to a Paraffin Fueled Hybrid Rocket System". In: *46th AIAA/ASME/SAE/ASEE Joint Propulsion Conference and Exhibit*. Ed. by AIAA. AIAA-2010-6639. Nashville, TN, 2010.

[33] Krüss. Last visited: 11 April 2012. URL: http://www.kruss.de/de/home.html.

[34] Non Newtonian Fluid Dynamics Group MIT. Last visited: 4 May 2012. URL: http://web.mit.edu/nnf/education/wettability/definition.html.

[35] Attension. Last visited: 16 May 2012. URL: http://www.attension.com/surface-tension.aspx.

[36] Kibron. Last visited: 15 May 2012. URL: http://www.kibron.com/surface-tension/measurement-techniques.

[37] DDBST. Last visited: 20 June 2012. URL: http://www.ddbst.com/en/online/Online_Calc_sft106_Form.php.

[38] Kaye and Laby National Phisical Laboratory. Last visited: 21 May 2012. URL: http://www.kayelaby.npl.co.uk/general_physics/2_2/2_2_5.html.

[39] Gebhard Schramm. *A practical approach to Rheology and Rheometry*. Ed. by Thermo Elektron (Karlsruhe) GmbH. Thermo Elektron (Karlsruhe) GmbH, 2004.

[40] P. Universita' di Pavia Mustarelli. Last visited: 23 May 2012. URL: http://chifis.unipv.it/mustarelli/lab_chifis/reologia.pdf.

[41] H. Kyung Moon. *Rheological Behavior and Microstructure of Ceramic Particulate/Aluminum Alloy Composites*. Tech. rep. MIT, 1990.

[42] H.A. Barnes. *A Handbook of Elementary Rheology*. Ed. by Cambrian Printers. The University of Wales Institute of Non-Newtonian Fluid Mechanics, Department of Mathematics, University of Wales Aberystwyth, 2000.

[43] M.I. Ojovan, K.P. Travis, and R.J. Hand. "Thermodynamic parameters of bond in glassy materials from viscosity - temperature relationships". In: *Journal of Physics: condensed matter* 19-415107 (2007), pp. 1–12.

[44] Norcross. Last visited: 23 May 2012. URL: http://www.viscosity.com/index.html.

[45] Hydramotion. Last visited: 30 May 2012. URL: http://www.hydramotion.com/tech.html.

[46] KOHSIEH. Last visited: 24 May 2012. URL: http://www.kohsieh.com.tw/.

[47] C.W. Macosko. *Rheology Principles, Measurements, Applications*. Ed. by Wiley VCH. Wiley - VCH, 1994.

[48] Polymer Nanostructures Lab Pennsylvania State University. Last visited: 6 June 2012. URL: http://zeus.plmsc.psu.edu/.

[49] Brookfield. Last visited: 30 May 2012. URL: http://www.brookfield.eu/products/rheometers/laboratory-rs-cone-plate.asp.

[50] Goettfert. Last visited: 23 May 2012. URL: http://www.goettfert.com/.

[51] Cambridge Polymer Group. Last visited: 23 May 2012. URL: http://www.campoly.com/.

[52] MIT. Last visited: 11 May 2012. URL: http://web.mit.edu/nnf/presentation/sld004.htm.

[53] Xpansion Instruments. Last visited: 23 May 2012. URL: http://www.xinst.com/results_rheology.htm.

[54] L. Galfetti et al. "Ballistic and rheological characterization of paraffin-based fuels for hybrid rocket propulsion". In: *47th AIAA/ASME/SAE/ASEE Joint Propulsion Conference and Exhibit*. Ed. by AIAA. AIAA-2011-5680. San Diego, CA, 2011.

[55] M. Kott. "Untersuchung zur Leistunssteigerung von Treibstoffen durch energetische Additive". Masterthesis. Universitat Stuttgart, 2012.

[56] U. Teipel U. & Forter-Barth. "Rheology of Nano-Scale Aluminum Suspensions". In: *Propellants, Explosives, Pyrotechnics* 26 (2001), pp. 268–272.

[57] D.T. Beruto et al. "Dispersions of micrometric powders of molybdenum and alumina in liquid paraffin: role of interfacial phenomena on bulk rheological properties". In: *Journal of the European Ceramic Society* 22 (2002), pp. 2155–2164.

[58] Sasol Wax. Last visited: 10 May 2012. URL: http://www.sasolwax.com/en/Home.html.

[59] Sonneborn. Last visited: 10 May 2012. URL: http://www.sonneborn.com/european_products/microcrystalline_waxes.htm.

[60] The International Group Inc. Last visited: 10 May 2012. URL: http://igiwax.com/igi-products/by-type/microcrystallinewax.html.

[61] M. Grosse. "Effect of a Diaphragm on Performance and Fuel Regression of a Laboratory Scale Hybrid Rocket Motor Using Nitrous Oxide and Paraffin". In: *45th AIAA/ASME/SAE/ASEE Joint Propulsion Conference and Exhibit*. 2009.

[62] University of Wisconsin - Department of Chemistry. Last visited: 15 June 2012. URL: http://chem.wisc.edu/.

[63] L. Merotto et al. "Experimental Investigation of Metallized Hybrid Rocket Fuels". In: *3rd EUCASS*. 2009.

[64] M. A. Karabeyoglu, B. J. Cantwell, and G. Zilliac. "Development of Scalable Space-Time Averaged Regression Rate Expressions for Hybrid Rockets". In: *Journal of Propulsion and Power* 23.4 (2007), pp. 737–747.

[65] G. Zilliac and M. A. Karabeyoglu. "Hybrid rocket fuel regression rate data and modeling". In: *42nd AIAA/ASME/SAE/ASEE Joint Propulsion Conference & Exhibit*. Ed. by AIAA. 2006.

# Appendix A

# Surface tension measurements

In this chapter the tables with the data obtained for the surface tension tests and the error between the linear regression curves and the experimental data are presented. The error is calculated as:

$$err_{\%} = \frac{|IFT_{experimental} - IFT_{regression}|}{IFT_{experimental}} \tag{A.1}$$

## A.1 Pure paraffin

**Sasolwax 0907**

The experimental data are:

Table A.1: Sasolwax 0907 - Experimental surface tension data

| Temperature ℃ | Surface tension mN/m | Standard dev. mN/m | Error % | Error clean % |
|---|---|---|---|---|
| 128.3 | 26.5 | 0.1 | 2.0 | 0.98 |
| 127.2 | 26.1 | 0.1 | 0.1 | 0.84 |
| 118.8 | 27.0 | 0.1 | 0.53 | 0.38 |
| 115.6 | 27.3 | 0.1 | 0.53 | 0.61 |
| 114.7 | 27.1 | 0.0 | 0.51 | 0.36 |
| 113.3 | 27.2 | 0.1 | 0.62 | 0.37 |
| 108.6 | 27.7 | 0.1 | 0.39 | 0.19 |
| 108.0 | 27.6 | 0.0 | 0.95 | 0.33 |
| 105.2 | 27.8 | 0.0 | 1.17 | 0.35 |
| 103.5 | 28.0 | 0.0 | 1.01 | 0.08 |
| 102.1 | 28.1 | 0.0 | 1.12 | 0.09 |
| 101.1 | 28.2 | 0.0 | 1.09 | 0.02 |
| 101.0 | 28.0 | 0.0 | 1.84 | 0.74 |
| 99.4 | 28.3 | 0.1 | 1.29 | 0.08 |
| 98.0 | 28.8 | 0.1 | 0.01 | 1.33 |
| 96.6 | 28.5 | 0.1 | 1.5 | 0.06 |

Continue in the next page

Table A.1: Sasolwax 0907 - Experimental surface tension data

| Temperature ℃ | Surface tension mN/m | Standard dev. mN/m | Error % | Error clean % |
|---|---|---|---|---|
| 95.4 | 31.4 | 0.1 | 7.52 | - |

The maximum error value is in the first case 7.52% and 1.33% in the second case.

**Sasolwax 6805**

The experimental data are presented in Table A.2.

Table A.2: Sasolwax 6805 - Experimental surface tension data

| Temperature ℃ | Surface tension mN/m | Standard dev. mN/m | Error % |
|---|---|---|---|
| 129.8 | 24.9 | 0.1 | 0.09 |
| 122.2 | 25.4 | 0.1 | 0.08 |
| 119.9 | 25.6 | 0.0 | 0.11 |
| 114.7 | 25.9 | 0.1 | 0.05 |
| 113.2 | 26.0 | 0.1 | 0.04 |
| 110.0 | 26.2 | 0.0 | 0.08 |
| 105.6 | 26.5 | 0.1 | 0.04 |
| 102.8 | 26.7 | 0.1 | 0.02 |
| 101.4 | 26.8 | 0.0 | 0.05 |
| 99.6 | 26.9 | 0.0 | 0.01 |
| 98.4 | 27.1 | 0.1 | 0.44 |
| 97.4 | 27.1 | 0.1 | 0.19 |
| 97.2 | 27.1 | 0.0 | 0.14 |
| 96.7 | 27.1 | 0.0 | 0.02 |
| 96.3 | 27.1 | 0.1 | 0.07 |
| 95.3 | 27.2 | 0.0 | 0.05 |
| 94.0 | 27.3 | 0.0 | 0.11 |
| 92.2 | 27.4 | 0.0 | 0.04 |
| 90.8 | 27.5 | 0.0 | 0.07 |
| 89.7 | 27.6 | 0.1 | 0.17 |
| 88.1 | 27.7 | 0.1 | 0.15 |
| 86.4 | 27.8 | 0.0 | 0.11 |
| 84.8 | 27.9 | 0.0 | 0.09 |
| 83.4 | 28.0 | 0.0 | 0.12 |
| 81.0 | 27.9 | 0.0 | 0.8 |
| 79.3 | 28.1 | 0.0 | 0.48 |
| 78.5 | 28.3 | 0.0 | 0.05 |
| 77.0 | 28.3 | 0.0 | 0.30 |
| 75.8 | 28.1 | 0.0 | 1.30 |
| 74.6 | 28.0 | 0.0 | 1.94 |

Continue in the next page

Table A.2: Sasolwax 6805 - Experimental surface tension data

| Temperature ℃ | Surface tension mN/m | Standard dev. mN/m | Error % |
|---|---|---|---|
| 73.1 | 28.3 | 0.0 | 1.20 |
| 71.9 | 30 | 0.0 | 4.27 |

The maximum error value is 4.27%.

**Sasolwax 1276**

The errors between the experimental data and the linear regression curve are reported in Table A.3.

Table A.3: Sasolwax 1276 - Experimental surface tension data

| Temperature ℃ | Surface tension mN/m | Standard dev. mN/m | Error % |
|---|---|---|---|
| 123.0 | 27.8 | 0.1 | 0.42 |
| 116.6 | 28.6 | 0.1 | 1.25 |
| 110.0 | 28.7 | 0.1 | 0.41 |
| 104.8 | 28.7 | 0.1 | 0.51 |
| 103.1 | 28.6 | 0.1 | 1.17 |
| 100.7 | 28.8 | 0.1 | 0.89 |
| 98.3 | 29.4 | 0.1 | 0.75 |
| 97.2 | 29.2 | 0.1 | 0.13 |
| 95.9 | 29.3 | 0.1 | 0.01 |
| 93.6 | 29.4 | 0.1 | 0.07 |
| 91.9 | 29.7 | 0.2 | 0.65 |
| 91.2 | 29.4 | 0.1 | 0.49 |
| 90.3 | 29.7 | 0.2 | 0.37 |
| 87.8 | 29.6 | 0.1 | 0.40 |
| 87.7 | 29.7 | 0.1 | 0.08 |
| 86.9 | 29.9 | 0.1 | 0.45 |
| 86.8 | 29.8 | 0.2 | 0.10 |
| 86.3 | 29.7 | 0.1 | 0.32 |
| 86.3 | 29.9 | 0.1 | 0.35 |
| 86.1 | 30.0 | 0.2 | 0.65 |
| 85.8 | 29.8 | 0.1 | 0.07 |
| 85.0 | 30.0 | 0.1 | 0.46 |
| 84.3 | 30.0 | 0.1 | 0.34 |
| 83.7 | 29.7 | 0.1 | 0.77 |
| 82.8 | 29.9 | 0.1 | 0.25 |
| 81.8 | 29.7 | 0.1 | 1.10 |
| 80.7 | 30.2 | 0.2 | 0.39 |
| 79.5 | 30.0 | 0.1 | 0.48 |

Continue in the next page

Table A.3: Sasolwax 1276 - Experimental surface tension data

| Temperature ℃ | Surface tension mN/m | Standard dev. mN/m | Error % |
|---|---|---|---|
| 78.4 | 30.4 | 0.1 | 0.66 |
| 75.8 | 30.4 | 0.1 | 0.22 |

Table A.3 shows that in this case errors have a different behavior: the maximum values are not necessarily located at low temperatures .

The maximum error has a value of 1.25% , lower than of Sasolwax 0907 and Sasolwax 6805.

**Sasolwax 6003**

Table A.4: Sasolwax 6003 - Experimental surface tension data

| Temperature ℃ | Surface tension mN/m | Standard dev. mN/m | Error % |
|---|---|---|---|
| 121.3 | 25.0 | 0.1 | 0.18 |
| 114.5 | 25.5 | 0.1 | 0.42 |
| 111.3 | 25.6 | 0.1 | 0.01 |
| 109.6 | 25.7 | 0.1 | 0.03 |
| 108.5 | 25.8 | 0.1 | 0.08 |
| 107.5 | 25.8 | 0.1 | 0.17 |
| 106.5 | 26.0 | 0.1 | 0.36 |
| 106.1 | 25.9 | 0.1 | 0.13 |
| 104.6 | 26.1 | 0.1 | 0.27 |
| 104.2 | 26.0 | 0.1 | 0.21 |
| 103.0 | 26.2 | 0.1 | 0.26 |
| 102.8 | 26.2 | 0.1 | 0.21 |
| 102.6 | 26.0 | 0.1 | 0.61 |
| 102.4 | 26.1 | 0.1 | 0.27 |
| 101.4 | 26.2 | 0.1 | 0.13 |
| 101.1 | 26.2 | 0.1 | 0.21 |
| 100.5 | 26.4 | 0.1 | 0.41 |
| 99.5 | 26.4 | 0.1 | 0.16 |
| 99.3 | 26.3 | 0.1 | 0.27 |
| 98.4 | 26.5 | 0.1 | 0.27 |
| 97.4 | 26.4 | 0.1 | 0.35 |
| 96.3 | 26.5 | 0.1 | 0.24 |
| 95.0 | 26.6 | 0.1 | 0.17 |
| 94.3 | 26.9 | 0.1 | 0.78 |
| 93.5 | 26.8 | 0.1 | 0.21 |
| 93.2 | 26.8 | 0.1 | 0.14 |
| 92.3 | 26.8 | 0.1 | 0.07 |

Continue in the next page

Table A.4: Sasolwax 6003 - Experimental surface tension data

| Temperature ℃ | Surface tension mN/m | Standard dev. mN/m | Error % |
|---|---|---|---|
| 92.0 | 27.0 | 0.1 | 0.60 |
| 91.4 | 26.9 | 0.1 | 0.08 |
| 90.5 | 27.0 | 0.1 | 0.24 |
| 89.6 | 27.0 | 0.1 | 0.02 |
| 88.6 | 27.0 | 0.1 | 0.21 |
| 87.8 | 27.0 | 0.1 | 0.40 |
| 86.9 | 27.2 | 0.1 | 0.12 |
| 85.9 | 27.1 | 0.1 | 0.48 |
| 84.9 | 27.1 | 0.0 | 0.72 |
| 83.7 | 27.2 | 0.1 | 0.64 |
| 83.7 | 27.4 | 0.1 | 0.10 |
| 82.8 | 27.3 | 0.1 | 0.48 |
| 82.0 | 27.4 | 0.1 | 0.30 |
| 81.5 | 27.6 | 0.1 | 0.31 |
| 81.2 | 27.4 | 0.1 | 0.49 |
| 81.1 | 27.5 | 0.1 | 0.15 |
| 81.0 | 27.6 | 0.1 | 0.19 |
| 80.2 | 27.4 | 0.1 | 0.72 |
| 79.3 | 27.7 | 0.1 | 0.16 |
| 78.2 | 27.7 | 0.0 | 0.10 |
| 77.3 | 27.9 | 0.1 | 0.42 |
| 76.2 | 27.7 | 0.1 | 0.56 |
| 75.5 | 27.8 | 0.1 | 0.36 |
| 74.6 | 27.9 | 0.1 | 0.21 |
| 74.1 | 28.0 | 0.1 | 0.04 |
| 73.3 | 28.2 | 0.1 | 0.56 |
| 72.4 | 28.2 | 0.1 | 0.36 |
| 71.8 | 28.2 | 0.1 | 0.22 |
| 70.9 | 28.3 | 0.1 | 0.37 |
| 70.4 | 28.3 | 0.1 | 0.26 |
| 69.8 | 28.4 | 0.1 | 0.47 |
| 69.1 | 28.4 | 0.1 | 0.31 |

The maximum error has a value of 0.78% .

**Comparison of Deviation between experimental data and regression curve** shows the error as a function of temperature: the main characteristic is that generally (with the exception of Sasolwax 1276) the error is higher at the lowest temperatures. Sasolwax 1276 shows the highest deviations. The best result is obtained with Sasolwax 6805, where errors are lower.

## A.2 Paraffin with additives

### A.2.1 Sasolwax 0907 with additives

#### Sasolwax 0907 + 2% Black Carbon

Results are presented in Table A.5.

Table A.5: Sasolwax 0907 added with Black Carbon - Experimental surface tension data

| Temperature ℃ | Surface tension mN/m | Standard dev. mN/m | Error % |
|---|---|---|---|
| 125.9 | 26.2 | 0.1 | 0.05 |
| 120.3 | 26.7 | 0.1 | 0.56 |
| 115.5 | 26.9 | 0.1 | 0.15 |
| 111.8 | 27.2 | 0.1 | 0.38 |
| 108.2 | 27.3 | 0.1 | 0.11 |
| 106.5 | 27.4 | 0.1 | 0.14 |
| 104.9 | 27.5 | 0.1 | 0.15 |
| 103.7 | 27.5 | 0.0 | 0.44 |
| 102.4 | 27.7 | 0.1 | 0.01 |
| 101.4 | 27.6 | 0.1 | 0.61 |
| 100.7 | 27.7 | 0.1 | 0.41 |
| 100.1 | 27.7 | 0.1 | 0.55 |
| 99.5 | 27.8 | 0.1 | 0.33 |
| 99.1 | 27.8 | 0.1 | 0.42 |
| 98.4 | 28.3 | 0.1 | 1.20 |
| 97.7 | 27.9 | 0.1 | 0.38 |
| 97.2 | 27.9 | 0.1 | 0.50 |
| 96.4 | 27.9 | 0.1 | 0.68 |
| 95.5 | 28.4 | 0.1 | 0.89 |
| 94.4 | 28.1 | 0.1 | 0.42 |
| 92.1 | 28.9 | 0.1 | 1.84 |

The maximum error value is 1.84%.

#### Sasolwax 0907 +10% Stearic Acid

The results obtained are shown in Table A.6:

Table A.6: Sasolwax 0907 added with Stearic Acid - Experimental surface tension data

| Temperature ℃ | Surface tension mN/m | Standard dev. mN/m | Error % | Error clean % |
|---|---|---|---|---|
| 125.1 | 26.0 | 0.0 | 0.51 | 1.06 |

Continue in the next page

Table A.6: Sasolwax 0907 added with Stearic Acid - Experimental surface tension data

| Temperature ℃ | Surface tension mN/m | Standard dev. mN/m | Error % | Error clean % |
|---|---|---|---|---|
| 121.2 | 26.6 | 0.0 | 1.48 | 0.35 |
| 116.8 | 26.9 | 0.0 | 1.17 | 0.48 |
| 114.4 | 27.0 | 0.0 | 0.76 | 0.32 |
| 113.8 | 27.2 | 0.0 | 1.30 | 0.92 |
| 110.7 | 27.1 | 0.0 | 0.05 | 0.13 |
| 110.7 | 27.2 | 0.0 | 0.31 | 0.24 |
| 108.3 | 27.3 | 0.0 | 0.08 | 0.08 |
| 107.6 | 27.3 | 0.0 | 0.30 | 0.07 |
| 106.8 | 27.5 | 0.0 | 0.17 | 0.48 |
| 104.0 | 27.3 | 0.0 | 1.45 | 0.86 |
| 103.9 | 27.5 | 0.0 | 0.74 | 0.15 |
| 103.4 | 27.6 | 0.0 | 0.53 | 0.11 |
| 103.2 | 27.6 | 0.0 | 0.59 | 0.06 |
| 102.8 | 27.4 | 0.0 | 1.46 | 0.75 |
| 102.7 | 27.6 | 0.0 | 0.75 | 0.05 |
| 102.2 | 27.7 | 0.0 | 0.54 | 0.21 |
| 102.1 | 27.6 | 0.0 | 0.94 | 0.18 |
| 101.4 | 27.5 | 0.0 | 1.53 | 0.69 |
| 101.3 | 27.5 | 0.0 | 1.56 | 0.71 |
| 100.3 | 27.7 | 0.0 | 1.14 | 0.20 |
| 100.2 | 27.7 | 0.0 | 1.17 | 0.22 |
| 99.9 | 27.6 | 0.1 | 1.63 | 0.65 |
| 99.5 | 27.9 | 0.0 | 0.66 | 0.34 |
| 99.1 | 27.9 | 0.0 | 0.79 | 0.26 |
| 99.0 | 27.9 | 0.0 | 0.82 | 0.24 |
| 98.5 | 28.0 | 0.0 | 0.61 | 0.49 |
| 97.8 | 28.1 | 0.0 | 0.47 | 0.69 |
| 97.7 | 28.0 | 0.1 | 0.86 | 0.32 |
| 96.6 | 28.0 | 0.0 | 1.20 | 0.08 |
| 95.9 | 28.4 | 0.0 | 0.01 | - |
| 95.9 | 29.0 | 0.0 | 2.08 | - |
| 94.6 | 31.9 | 0.0 | 10.63 | - |
| 94.3 | 28.5 | 0.1 | 0.12 | - |

The maximum error value is in the first case 10.63% and 1.06% in the second case.

**Sasolwax 0907 +10% PEG**

The results obtained are shown in Table A.7:

Table A.7: Sasolwax 0907 added with PEG - Experimental surface tension data

| Temperature ℃ | Surface tension mN/m | Standard dev. mN/m | Error % | Error clean % |
|---|---|---|---|---|
| 127.4 | 26.3 | 0.1 | 1.57 | 0.62 |
| 122.4 | 26.8 | 0.0 | 1.49 | 0.86 |
| 118.3 | 26.9 | 0.1 | 0.29 | 0.10 |
| 115.3 | 27.2 | 0.1 | 0.25 | 0.05 |
| 112.6 | 27.3 | 0.1 | 0.40 | 0.44 |
| 110.2 | 27.5 | 0.1 | 0.57 | 0.46 |
| 107.9 | 27.9 | 0.1 | 0.03 | 0.26 |
| 106.3 | 27.7 | 0.1 | 1.29 | 0.96 |
| 105.0 | 27.9 | 0.1 | 1.04 | 0.64 |
| 104.1 | 27.9 | 0.1 | 1.37 | 0.92 |
| 103.3 | 28.0 | 0.1 | 1.30 | 0.80 |
| 102.6 | 28.6 | 0.1 | 0.57 | 1.10 |
| 101.5 | 28.3 | 0.1 | 0.88 | 0.28 |
| 100.2 | 28.7 | 0.1 | 0.06 | 0.72 |
| 98.9 | 28.4 | 0.1 | 1.47 | 0.72 |
| 97.7 | 28.9 | 0.1 | 0.14 | 0.66 |
| 96.4 | 28.5 | 0.1 | 2.01 | 1.13 |
| 95.2 | 28.9 | 0.1 | 1.09 | 0.14 |
| 94.1 | 29.0 | 0.1 | 1.07 | 0.07 |
| 92.9 | 29.8 | 0.0 | 1.23 | 2.26 |
| 91.8 | 31.6 | 0.0 | 6.50 | - |

The maximum error value is 6.50% , neglecting data it is 2.26%.

### Sasolwax 0907 + 10% Poly Ethylene Co-Vinyl Acetate

The results obtained are shown in Table A.8:

Table A.8: Sasolwax 0907 added with Poly Ethylene Co-Vinyl Acetate - Experimental surface tension data

| Temperature ℃ | Surface tension mN/m | Standard dev. mN/m | Error % |
|---|---|---|---|
| 120.4 | 26.6 | 0.1 | 0.43 |
| 116.8 | 27.0 | 0.1 | 0.70 |
| 112.8 | 27.4 | 0.0 | 0.94 |
| 109.6 | 27.4 | 0.1 | 0.02 |
| 107.4 | 27.6 | 0.0 | 0.05 |
| 106.0 | 27.6 | 0.1 | 0.37 |
| 104.6 | 27.7 | 0.1 | 0.42 |
| 103.6 | 27.7 | 0.0 | 0.72 |

Continue in the next page

Table A.8: Sasolwax 0907 added with Poly Ethylene Co-Vinyl Acetate - Experimental surface tension data

| Temperature ℃ | Surface tension mN/m | Standard dev. mN/m | Error % |
|---|---|---|---|
| 102.6 | 27.9 | 0.0 | 0.29 |
| 101.8 | 27.9 | 0.1 | 0.53 |
| 101.1 | 28.0 | 0.1 | 0.38 |
| 100.6 | 27.9 | 0.1 | 0.88 |
| 100.0 | 28.2 | 0.1 | 0.01 |
| 99.7 | 28.2 | 0.1 | 0.07 |
| 99.6 | 28.3 | 0.1 | 0.25 |
| 99.4 | 28.2 | 0.0 | 0.16 |
| 98.7 | 28.3 | 0.1 | 0.01 |
| 98.1 | 28.3 | 0.1 | 0.19 |
| 97.6 | 29.1 | 0.1 | 2.43 |

The maximum error value is 2.43%.

### Sasolwax 0907 + 10% Aluminum

The results obtained are shown in Table A.9:

Table A.9: Sasolwax 0907 added with Aluminum - case 1 - Experimental surface tension data

| Temperature ℃ | Surface tension mN/m | Standard dev. mN/m | Error % |
|---|---|---|---|
| 114.9 | 26.6 | 0.1 | 0.32 |
| 111.9 | 26.9 | 0.1 | 0.04 |
| 109.6 | 27.2 | 0.1 | 0.57 |
| 107.3 | 27.3 | 0.1 | 0.37 |
| 105.1 | 27.4 | 0.1 | 0.19 |
| 104.2 | 27.6 | 0.1 | 0.69 |
| 102.9 | 27.6 | 0.1 | 0.37 |
| 102.2 | 27.5 | 0.1 | 0.17 |
| 101.7 | 27.6 | 0.1 | 0.07 |
| 101.5 | 27.5 | 0.1 | 0.34 |
| 100.7 | 27.5 | 0.1 | 0.54 |
| 100.2 | 27.6 | 0.1 | 0.29 |
| 99.7 | 27.6 | 0.1 | 0.42 |
| 98.7 | 27.7 | 0.0 | 0.30 |
| 98.1 | 27.8 | 0.1 | 0.08 |
| 97.2 | 27.8 | 0.1 | 0.30 |
| 96.1 | 27.9 | 0.1 | 0.21 |
| 95.2 | 28.0 | 0.1 | 0.07 |

Continue in the next page

Table A.9: Sasolwax 0907 added with Aluminum - case 1 - Experimental surface tension data

| Temperature ℃ | Surface tension mN/m | Standard dev. mN/m | Error % |
|---|---|---|---|
| 94.1 | 28.0 | 0.1 | 0.34 |
| 93.1 | 28.1 | 0.1 | 0.22 |
| 91.9 | 28.2 | 0.1 | 0.15 |
| 91.0 | 28.3 | 0.0 | 0.01 |
| 89.7 | 28.8 | 0.1 | 1.42 |

The maximum error value is 1.42% .

**Sasolwax 0907 + 40% Aluminum**

The results obtained are shown in Table A.10:

Table A.10: Sasolwax 0907 added with Aluminum - case 2 - Experimental surface tension data

| Temperature ℃ | Surface tension mN/m | Standard dev. mN/m | Error % |
|---|---|---|---|
| 119.5 | 26.3 | 0.1 | 0.39 |
| 115.7 | 26.5 | 0.1 | 0.00 |
| 112.7 | 26.8 | 0.1 | 0.23 |
| 110.2 | 27.0 | 0.1 | 0.23 |
| 107.7 | 27.0 | 0.1 | 0.51 |
| 104.8 | 27.3 | 0.1 | 0.25 |
| 103.4 | 27.5 | 0.1 | 0.08 |
| 102.3 | 27.6 | 0.1 | 0.12 |
| 102.2 | 27.6 | 0.1 | 0.09 |
| 100.9 | 27.6 | 0.1 | 0.28 |
| 99.8 | 27.7 | 0.1 | 0.24 |
| 98.9 | 27.9 | 0.1 | 0.22 |
| 97.7 | 27.9 | 0.0 | 0.12 |
| 96.8 | 28.0 | 0.1 | 0.02 |
| 96.2 | 28.0 | 0.1 | 0.19 |
| 95.4 | 28.1 | 0.1 | 0.06 |
| 94.2 | 28.2 | 0.1 | 0.04 |
| 93.1 | 28.2 | 0.1 | 0.35 |
| 92.2 | 28.4 | 0.1 | 0.10 |
| 91.1 | 28.4 | 0.1 | 0.21 |
| 90.2 | 28.4 | 0.1 | 0.46 |
| 88.6 | 28.7 | 0.1 | 0.15 |
| 87.2 | 28.9 | 0.1 | 0.45 |
| 85.3 | 29.1 | 0.1 | 0.62 |

The maximum error value is 0.62% .

### A.2.2 Sasolwax 6805 with additives

#### Sasolwax 6805 +1% Carbon Black

The results obtained are shown in Table A.11:

Table A.11: Sasolwax 6805 added with Carbon Black - Experimental surface tension data

| Temperature ℃ | Surface tension mN/m | Standard dev. mN/m | Error % |
|---|---|---|---|
| 124.6 | 25.3 | 0.1 | 0.08 |
| 120.2 | 25.8 | 0.1 | 0.73 |
| 116.6 | 25.9 | 0.1 | 0.20 |
| 114.2 | 26.0 | 0.1 | 0.03 |
| 111.7 | 26.2 | 0.1 | 0.10 |
| 109.8 | 26.4 | 0.1 | 0.38 |
| 108.1 | 26.5 | 0.1 | 0.33 |
| 106.5 | 26.4 | 0.1 | 0.45 |
| 105.3 | 26.6 | 0.1 | 0.01 |
| 104.1 | 26.7 | 0.1 | 0.09 |
| 103.6 | 26.7 | 0.1 | 0.04 |
| 102.9 | 26.7 | 0.0 | 0.21 |
| 102.4 | 26.8 | 0.1 | 0.04 |
| 101.6 | 26.7 | 0.1 | 0.53 |
| 100.6 | 26.8 | 0.1 | 0.41 |
| 99.5 | 27.0 | 0.0 | 0.07 |
| 98.7 | 27.1 | 0.1 | 0.24 |
| 98.0 | 27.0 | 0.1 | 0.30 |
| 97.0 | 27.0 | 0.1 | 0.55 |
| 96.4 | 27.1 | 0.1 | 0.32 |
| 95.9 | 27.2 | 0.1 | 0.07 |
| 95.3 | 27.3 | 0.1 | 0.15 |
| 94.4 | 27.3 | 0.1 | 0.07 |
| 93.3 | 27.4 | 0.1 | 0.03 |
| 92.3 | 27.4 | 0.1 | 0.21 |
| 91.4 | 27.5 | 0.1 | 0.07 |
| 90.7 | 27.6 | 0.1 | 0.13 |
| 89.9 | 27.5 | 0.1 | 0.43 |
| 89.4 | 27.7 | 0.1 | 0.18 |
| 88.3 | 27.8 | 0.1 | 0.28 |
| 87.5 | 27.8 | 0.1 | 0.08 |
| 86.5 | 27.8 | 0.1 | 0.15 |
| 85.7 | 27.8 | 0.1 | 0.34 |
| 84.8 | 27.9 | 0.1 | 0.20 |
| 84.3 | 28.0 | 0.1 | 0.04 |

Continue in the next page

Table A.11: Sasolwax 6805 added with Carbon Black - Experimental surface tension data

| Temperature ℃ | Surface tension mN/m | Standard dev. mN/m | Error % |
|---|---|---|---|
| 83.3 | 28.1 | 0.1 | 0.16 |
| 82.6 | 28.2 | 0.1 | 0.35 |
| 81.6 | 28.2 | 0.1 | 0.12 |
| 81.0 | 28.1 | 0.1 | 0.38 |
| 80.1 | 28.3 | 0.1 | 0.12 |
| 79.3 | 28.4 | 0.1 | 0.28 |
| 78.4 | 28.5 | 0.1 | 0.42 |
| 78.0 | 28.4 | 0.1 | 0.02 |
| 76.7 | 28.5 | 0.1 | 0.03 |
| 76.1 | 28.6 | 0.1 | 0.24 |
| 75.3 | 28.6 | 0.1 | 0.05 |

The maximum error value is 0.73%.

### Sasolwax 6805 +10% Stearic Acid

The results obtained are shown in Table A.12:

Table A.12: Sasolwax 6805 added with Stearic Acid - Experimental surface tension data

| Temperature ℃ | Surface tension mN/m | Standard dev. mN/m | Error % |
|---|---|---|---|
| 125.0 | 25.0 | 0.0 | 0.08 |
| 118.6 | 25.5 | 0.1 | 0.28 |
| 114.5 | 25.8 | 0.0 | 0.33 |
| 111.4 | 26.0 | 0.0 | 0.26 |
| 109.5 | 26.2 | 0.0 | 0.51 |
| 107.7 | 26.4 | 0.0 | 0.79 |
| 105.4 | 26.4 | 0.1 | 0.18 |
| 104.4 | 26.5 | 0.0 | 0.29 |
| 102.9 | 26.4 | 0.0 | 0.49 |
| 102.0 | 26.5 | 0.1 | 0.35 |
| 101.4 | 26.4 | 0.1 | 0.89 |
| 100.4 | 26.6 | 0.1 | 0.39 |
| 100.0 | 26.5 | 0.1 | 0.88 |
| 99.6 | 26.7 | 0.0 | 0.23 |
| 99.3 | 26.8 | 0.1 | 0.07 |
| 99.3 | 26.6 | 0.0 | 0.68 |
| 99.0 | 26.6 | 0.0 | 0.76 |
| 98.9 | 26.7 | 0.1 | 0.41 |

Continue in the next page

Table A.12: Sasolwax 6805 added with Stearic Acid - Experimental surface tension data

| Temperature ℃ | Surface tension mN/m | Standard dev. mN/m | Error % |
|---|---|---|---|
| 97.8 | 26.9 | 0.0 | 0.05 |
| 97.1 | 26.9 | 0.1 | 0.13 |
| 96.9 | 27.0 | 0.1 | 0.19 |
| 95.3 | 27.1 | 0.1 | 0.14 |
| 95.1 | 27.1 | 0.1 | 0.09 |
| 94.0 | 27.1 | 0.1 | 0.19 |
| 92.9 | 27.3 | 0.1 | 0.26 |
| 92.2 | 27.2 | 0.1 | 0.29 |
| 90.7 | 27.4 | 0.1 | 0.06 |
| 90.4 | 27.6 | 0.1 | 0.71 |
| 89.3 | 27.6 | 0.1 | 0.43 |
| 88.4 | 27.6 | 0.1 | 0.20 |
| 87.6 | 27.5 | 0.1 | 0.37 |
| 86.6 | 27.7 | 0.1 | 0.10 |
| 86.0 | 27.8 | 0.1 | 0.31 |
| 85.2 | 27.8 | 0.1 | 0.11 |
| 84.2 | 27.7 | 0.1 | 0.50 |
| 83.5 | 27.9 | 0.1 | 0.04 |
| 82.6 | 28.0 | 0.1 | 0.17 |
| 81.8 | 28.0 | 0.1 | 0.03 |
| 80.7 | 28.2 | 0.1 | 0.41 |
| 80.0 | 28.1 | 0.1 | 0.12 |
| 79.0 | 28.3 | 0.1 | 0.34 |
| 78.2 | 28.3 | 0.1 | 0.14 |
| 77.3 | 28.4 | 0.1 | 0.27 |
| 76.5 | 28.5 | 0.1 | 0.42 |
| 75.6 | 28.6 | 0.1 | 0.55 |
| 74.9 | 28.5 | 0.1 | 0.03 |
| 74.1 | 28.6 | 0.1 | 0.18 |
| 73.5 | 28.6 | 0.1 | 0.04 |
| 72.6 | 28.6 | 0.1 | 0.18 |
| 72.0 | 28.5 | 0.1 | 0.68 |
| 71.2 | 28.6 | 0.0 | 0.53 |

The maximum error value is 0.89% .

### Sasolwax 6805 + 10% PEG 6000

The results obtained are shown in Table A.13:

Table A.13: Sasolwax 6805 added with PEG 6000 - Experimental surface tension data

| Temperature ℃ | Surface tension mN/m | Standard dev. mN/m | Error % |
|---|---|---|---|
| 118.1 | 25.8 | 0.1 | 0.25 |
| 114.4 | 25.9 | 0.1 | 0.21 |
| 112.1 | 26.0 | 0.1 | 0.35 |
| 110.6 | 26.2 | 0.1 | 0.08 |
| 109.5 | 26.1 | 0.1 | 0.55 |
| 108.5 | 26.3 | 0.1 | 0.01 |
| 108.1 | 27.0 | 0.1 | 0.28 |
| 107.0 | 26.4 | 0.1 | 0.03 |
| 106.7 | 26.4 | 0.1 | 0.04 |
| 106.6 | 26.4 | 0.1 | 0.32 |
| 106.3 | 26.5 | 0.1 | 0.13 |
| 105.5 | 26.4 | 0.1 | 0.07 |
| 104.8 | 26.5 | 0.1 | 0.29 |
| 103.4 | 26.6 | 0.1 | 0.02 |
| 101.9 | 26.8 | 0.0 | 0.40 |
| 101.0 | 26.8 | 0.1 | 0.20 |
| 100.1 | 26.8 | 0.1 | 0.00 |
| 99.2 | 26.9 | 0.1 | 0.17 |
| 98.4 | 26.9 | 0.0 | 0.00 |
| 97.6 | 26.9 | 0.1 | 0.18 |
| 97.3 | 27.0 | 0.1 | 0.13 |
| 97.0 | 26.8 | 0.1 | 0.69 |
| 96.9 | 26.5 | 0.1 | 1.85 |
| 96.8 | 27.0 | 0.1 | 0.02 |
| 96.3 | 27.0 | 0.0 | 0.09 |
| 95.9 | 27.1 | 0.1 | 0.19 |
| 95.2 | 27.6 | 0.0 | 1.85 |
| 88.5 | 27.5 | 0.1 | 0.05 |
| 88.0 | 27.6 | 0.1 | 0.30 |
| 87.9 | 27.4 | 0.1 | 0.45 |
| 87.7 | 27.5 | 0.1 | 0.12 |

The maximum error value is 1.85%.

### Sasolwax 6805 +10% PECVA

The results obtained are shown in Table A.14:

Table A.14: Sasolwax 6805 added with PECVA - Experimental surface tension data

| Temperature ℃ | Surface tension mN/m | Standard dev. mN/m | Error % | Error clean % |
|---|---|---|---|---|
| 126.9 | 25.9 | 0.1 | 0.67 | 0.06 |
| 121.6 | 26.3 | 0.0 | 0.81 | 0.34 |
| 117.6 | 26.6 | 0.0 | 0.91 | 0.55 |
| 114.1 | 26.7 | 0.0 | 0.39 | 0.12 |
| 110.8 | 26.7 | 0.0 | 0.45 | 0.64 |
| 107.6 | 26.9 | 0.0 | 0.51 | 0.62 |
| 105.0 | 27.1 | 0.0 | 0.42 | 0.46 |
| 103.6 | 27.2 | 0.0 | 0.40 | 0.41 |
| 102.4 | 27.3 | 0.0 | 0.33 | 0.31 |
| 101.5 | 27.4 | 0.0 | 0.19 | 0.14 |
| 100.4 | 27.5 | 0.0 | 0.10 | 0.02 |
| 99.7 | 27.5 | 0.0 | 0.27 | 0.18 |
| 98.8 | 27.7 | 0.1 | 0.23 | 0.35 |
| 97.8 | 27.8 | 0.0 | 0.35 | 0.49 |
| 96.8 | 27.7 | 0.0 | 0.26 | 0.09 |
| 95.4 | 27.9 | 0.1 | 0.12 | 0.32 |
| 94.5 | 27.8 | 0.0 | 0.46 | 0.24 |
| 93.4 | 28.1 | 0.0 | 0.35 | 0.59 |
| 92.2 | 27.8 | 0.0 | 1.02 | 0.75 |
| 91.1 | 28.3 | 0.0 | 0.50 | 0.80 |
| 89.7 | 28.3 | 0.0 | 0.17 | 0.49 |
| 88.6 | 28.1 | 0.0 | 0.81 | 0.45 |
| 87.5 | 28.5 | 0.0 | 0.34 | 0.72 |
| 86.4 | 28.2 | 0.0 | 0.98 | 0.58 |
| 85.5 | 28.3 | 0.0 | 0.84 | 0.41 |
| 84.5 | 28.5 | 0.1 | 0.37 | 0.08 |
| 83.2 | 28.5 | 0.0 | 0.68 | 0.20 |
| 82.1 | 28.7 | 0.0 | 0.24 | 0.26 |
| 80.8 | 29.0 | 0.0 | 0.49 | 1.02 |
| 78.7 | 29.1 | 0.0 | 0.34 | 0.92 |
| 77.4 | 28.7 | 0.0 | 1.35 | 0.74 |
| 76.3 | 28.8 | 0.0 | 1.26 | 0.63 |
| 75.5 | 29.1 | 0.0 | 0.40 | 0.24 |
| 74.2 | 31.3 | 0.0 | 6.37 | - |
| 73.4 | 29.0 | 0.0 | 1.24 | - |

The maximum error value is 6.37% , neglecting data it is 1.02%.

### A.2.3 Sasolwax 1276 with additives

#### Sasolwax 1276 + 1% Carbon Black

The results obtained are shown in Table A.15:

Table A.15: Sasolwax 1276 added with Carbon Black - Experimental surface tension data

| Temperature ℃ | Surface tension mN/m | Standard dev. mN/m | Error % |
|---|---|---|---|
| 128.1 | 27.6 | 0.1 | 1.04 |
| 115.0 | 28.2 | 0.1 | 0.77 |
| 107.5 | 28.0 | 0.2 | 1.30 |
| 107.1 | 28.2 | 0.1 | 0.66 |
| 103.9 | 28.3 | 0.1 | 0.88 |
| 101.5 | 28.5 | 0.1 | 0.60 |
| 100.7 | 28.2 | 0.0 | 1.82 |
| 100.7 | 28.5 | 0.1 | 0.74 |
| 100.6 | 28.5 | 0.1 | 0.76 |
| 100.2 | 29.5 | 0.1 | 2.58 |
| 99.2 | 29.3 | 0.1 | 1.75 |
| 97.7 | 28.9 | 0.1 | 0.12 |
| 96.7 | 28.7 | 0.1 | 0.75 |
| 94.6 | 29.3 | 0.1 | 0.94 |
| 92.5 | 29.3 | 0.1 | 0.58 |
| 90.9 | 29.1 | 0.1 | 0.38 |
| 89.6 | 29.0 | 0.1 | 0.96 |
| 88.2 | 29.3 | 0.1 | 0.17 |
| 86.8 | 29.8 | 0.1 | 1.27 |
| 85.2 | 29.2 | 0.1 | 1.04 |
| 83.5 | 29.4 | 0.1 | 0.64 |
| 82.0 | 29.9 | 0.1 | 0.78 |
| 80.6 | 29.6 | 0.1 | 0.46 |
| 79.5 | 29.5 | 0.1 | 1.00 |
| 79.0 | 29.6 | 0.1 | 0.74 |
| 78.0 | 30.1 | 0.1 | 0.76 |
| 77.6 | 29.9 | 0.1 | 0.03 |
| 77.4 | 30.3 | 0.1 | 1.32 |
| 77.0 | 29.9 | 0.1 | 0.07 |
| 76.2 | 30.0 | 0.1 | 0.13 |
| 75.6 | 30.2 | 0.1 | 0.69 |
| 75.0 | 30.0 | 0.1 | 0.08 |

The maximum error value is 2.58%.

#### Sasolwax 1276 + 10% Stearic Acid

The results obtained are shown in Table A.16:

Table A.16: Sasolwax 1276 added with Stearic Acid - Experimental surface tension data

| Temperature ℃ | Surface tension mN/m | Standard dev. mN/m | Error % |
|---|---|---|---|
| 126.9 | 27.0 | 0.1 | 1.91 |
| 123.7 | 27.0 | 0.1 | 1.09 |
| 121.9 | 26.8 | 0.1 | 0.11 |
| 119.3 | 27.1 | 0.0 | 0.34 |
| 118.6 | 27.0 | 0.1 | 0.20 |
| 116.1 | 26.6 | 0.0 | 2.36 |
| 115.9 | 27.0 | 0.1 | 0.89 |
| 112.8 | 27.1 | 0.0 | 1.30 |
| 111.6 | 27.1 | 0.1 | 1.61 |
| 110.7 | 27.4 | 0.1 | 0.72 |
| 110.0 | 27.3 | 0.0 | 1.26 |
| 107.7 | 27.7 | 0.1 | 0.37 |
| 106.3 | 28.1 | 0.1 | 0.72 |
| 106.2 | 27.6 | 0.0 | 1.11 |
| 105.6 | 27.7 | 0.1 | 0.89 |
| 105.2 | 27.6 | 0.1 | 1.36 |
| 104.3 | 27.3 | 0.1 | 2.70 |
| 103.0 | 28.2 | 0.1 | 0.26 |
| 102.4 | 28.7 | 0.1 | 1.86 |
| 102.3 | 27.5 | 0.0 | 2.45 |
| 102.3 | 28.6 | 0.1 | 1.49 |
| 102.3 | 28.0 | 0.1 | 0.62 |
| 102.1 | 29.1 | 0.1 | 3.14 |
| 102.0 | 28.3 | 0.1 | 0.37 |
| 101.5 | 28.3 | 0.1 | 0.25 |
| 101.4 | 28.3 | 0.1 | 0.23 |
| 100.8 | 28.1 | 0.1 | 0.63 |
| 100.4 | 28.0 | 0.1 | 1.08 |
| 100.1 | 28.9 | 0.1 | 1.99 |
| 99.8 | 28.3 | 0.1 | 0.16 |
| 99.4 | 28.4 | 0.1 | 0.10 |
| 99.1 | 28.6 | 0.1 | 0.72 |
| 98.9 | 28.7 | 0.1 | 1.02 |
| 98.7 | 28.7 | 0.1 | 0.97 |
| 98.5 | 29.1 | 0.1 | 2.29 |
| 98.2 | 29.1 | 0.1 | 2.22 |
| 98.2 | 28.2 | 0.1 | 0.90 |
| 97.9 | 28.6 | 0.1 | 0.44 |
| 97.2 | 28.5 | 0.1 | 0.08 |
| 97.0 | 28.8 | 0.1 | 0.91 |
| 96.4 | 28.1 | 0.1 | 1.70 |
| 95.9 | 28.8 | 0.1 | 0.65 |

Continue in the next page

Table A.16: Sasolwax 1276 added with Stearic Acid - Experimental surface tension data

| Temperature ℃ | Surface tension mN/m | Standard dev. mN/m | Error % |
|---|---|---|---|
| 95.8 | 28.5 | 0.1 | 0.42 |
| 94.9 | 28.6 | 0.1 | 0.28 |
| 94.4 | 29.5 | 0.1 | 2.66 |
| 94.1 | 28.6 | 0.1 | 0.48 |
| 93.2 | 28.3 | 0.1 | 1.76 |
| 93.0 | 29.6 | 0.1 | 2.66 |
| 92.4 | 28.6 | 0.1 | 0.88 |
| 92.0 | 29.0 | 0.1 | 0.41 |
| 91.5 | 28.9 | 0.1 | 0.05 |
| 90.9 | 29.1 | 0.1 | 0.50 |
| 90.5 | 29.2 | 0.1 | 0.74 |
| 90.0 | 28.8 | 0.1 | 0.75 |
| 89.5 | 29.1 | 0.1 | 0.17 |
| 88.9 | 29.1 | 0.1 | 0.02 |
| 88.6 | 29.1 | 0.1 | 0.05 |
| 88.1 | 29.0 | 0.1 | 0.51 |
| 87.5 | 29.1 | 0.1 | 0.31 |
| 87.0 | 29.9 | 0.1 | 2.26 |
| 86.8 | 28.7 | 0.1 | 1.87 |
| 85.9 | 28.9 | 0.1 | 1.38 |
| 85.8 | 29.2 | 0.0 | 0.36 |
| 85.1 | 28.8 | 0.1 | 1.92 |
| 84.6 | 30.2 | 0.1 | 2.69 |
| 84.2 | 29.4 | 0.1 | 0.05 |
| 83.9 | 29.8 | 0.1 | 1.22 |
| 83.3 | 29.5 | 0.1 | 0.08 |
| 83.0 | 29.7 | 0.1 | 0.68 |
| 82.7 | 29.2 | 0.1 | 1.09 |
| 82.1 | 29.3 | 0.1 | 0.88 |
| 81.8 | 29.5 | 0.1 | 0.27 |
| 81.1 | 29.9 | 0.1 | 0.91 |
| 81.1 | 29.6 | 0.1 | 0.09 |
| 80.3 | 29.5 | 0.1 | 0.62 |
| 80.3 | 29.4 | 0.1 | 0.96 |
| 79.4 | 29.4 | 0.1 | 1.17 |
| 79.3 | 30.1 | 0.1 | 1.16 |
| 78.6 | 29.6 | 0.1 | 0.67 |
| 78.4 | 30.0 | 0.1 | 0.62 |
| 77.5 | 29.9 | 0.1 | 0.08 |
| 76.8 | 29.8 | 0.1 | 0.41 |
| 76.6 | 29.8 | 0.1 | 0.46 |
| 75.8 | 29.9 | 0.1 | 0.31 |

Continue in the next page

Table A.16: Sasolwax 1276 added with Stearic Acid - Experimental surface tension data

| Temperature ℃ | Surface tension mN/m | Standard dev. mN/m | Error % |
|---|---|---|---|
| 75.7 | 30.0 | 0.1 | 0.01 |
| 74.8 | 29.8 | 0.1 | 0.87 |
| 74.0 | 29.9 | 0.1 | 0.72 |
| 73.3 | 30.1 | 0.1 | 0.21 |
| 72.8 | 30.3 | 0.1 | 0.34 |
| 72.1 | 30.2 | 0.1 | 0.15 |
| 71.0 | 30.1 | 0.1 | 0.73 |
| 70.3 | 30.0 | 0.1 | 1.23 |
| 69.6 | 31.3 | 0.1 | 2.82 |

The maximum error value is 3.14%.

### Sasolwax 1276 +10% PEG

The results obtained are shown in Table A.17:

Table A.17: Sasolwax 1276 added with PEG - Experimental surface tension data

| Temperature ℃ | Surface tension mN/m | Standard dev. mN/m | Error % | Error clean % |
|---|---|---|---|---|
| 127.7 | 28.0 | 0.1 | 4.17 | - |
| 122.3 | 27.4 | 0.1 | 0.48 | 1.70 |
| 118.8 | 27.3 | 0.1 | 0.92 | 0.16 |
| 113.8 | 28.1 | 0.1 | 0.52 | 1.36 |
| 110.7 | 28.0 | 0.1 | 0.72 | 0.01 |
| 107.7 | 28.1 | 0.1 | 1.23 | 0.64 |
| 105.3 | 28.0 | 0.0 | 2.28 | 1.80 |
| 103.5 | 28.5 | 0.1 | 0.99 | 0.59 |
| 102.3 | 28.3 | 0.1 | 2.05 | 1.70 |
| 100.5 | 28.4 | 0.1 | 2.20 | 1.92 |
| 100.5 | 28.5 | 0.1 | 1.84 | 1.56 |
| 99.2 | 29.3 | 0.1 | 0.58 | 0.80 |
| 98.6 | 28.8 | 0.1 | 1.31 | 1.12 |
| 98.2 | 28.8 | 0.1 | 1.42 | 1.24 |
| 96.8 | 30.2 | 0.2 | 2.91 | 3.02 |
| 95.6 | 29.5 | 0.1 | 0.27 | 0.34 |
| 93.9 | 30.3 | 0.1 | 2.46 | 2.46 |
| 92.7 | 29.5 | 0.1 | 0.52 | 0.56 |
| 91.7 | 29.7 | 0.1 | 0.11 | 0.20 |
| 90.5 | 29.7 | 0.1 | 0.44 | 0.57 |

Continue in the next page

Table A.17: Sasolwax 1276 added with PEG - Experimental surface tension data

| Temperature ℃ | Surface tension mN/m | Standard dev. mN/m | Error % | Error clean % |
|---|---|---|---|---|
| 89.1 | 30.4 | 0.1 | 1.51 | 1.32 |
| 87.5 | 30.1 | 0.1 | 0.10 | 0.15 |
| 86.4 | 30.2 | 0.1 | 0.13 | 0.16 |
| 85.2 | 30.2 | 0.1 | 0.19 | 0.53 |
| 83.9 | 30.8 | 0.1 | 1.42 | 1.04 |
| 82.8 | 30.9 | 0.1 | 1.46 | 1.03 |
| 81.8 | 30.4 | 0.1 | 0.43 | 0.90 |

The maximum error value is 4.17% , in the clean case it is 3.02%.

### Sasolwax 1276 +10% PECVA

The results obtained are shown in Table A.18:

Table A.18: Sasolwax 1276 added with PECVA - Experimental surface tension data

| Temperature ℃ | Surface tension mN/m | Standard dev. mN/m | Error % | Error clean % |
|---|---|---|---|---|
| 125.7 | 29.4 | 0.1 | 4.07 | - |
| 121.1 | 28.2 | 0.1 | 0.72 | 0.50 |
| 116.9 | 28.2 | 0.1 | 1.37 | 0.28 |
| 110.1 | 28.7 | 0.1 | 0.63 | 0.22 |
| 105.8 | 28.9 | 0.1 | 0.58 | 0.13 |
| 102.9 | 29.1 | 0.1 | 0.32 | 0.29 |
| 100.1 | 29.0 | 0.1 | 1.09 | 0.57 |
| 99.8 | 29.1 | 0.1 | 0.79 | 0.27 |
| 98.1 | 29.3 | 0.1 | 0.35 | 0.10 |
| 96.2 | 29.1 | 0.1 | 1.32 | 0.93 |
| 94.8 | 29.2 | 0.1 | 1.18 | 0.83 |
| 93.0 | 29.4 | 0.1 | 0.76 | 0.47 |
| 91.4 | 29.5 | 0.1 | 0.66 | 0.42 |
| 90.4 | 29.8 | 0.1 | 0.21 | 0.42 |
| 89.9 | 29.9 | 0.2 | 0.47 | 0.66 |
| 89.8 | 29.9 | 0.1 | 0.46 | 0.65 |
| 87.3 | 30.5 | 0.2 | 2.06 | 2.08 |
| 86.7 | 30.1 | 0.1 | 0.67 | 0.76 |
| 85.7 | 30.2 | 0.1 | 0.86 | 0.92 |
| 82.7 | 30.0 | 0.1 | 0.24 | 0.27 |
| 80.4 | 30.0 | 0.1 | 0.57 | 0.67 |
| 79.5 | 30.2 | 0.1 | 0.04 | 0.16 |

Continue in the next page

Table A.18: Sasolwax 1276 added with PECVA - Experimental surface tension data

| Temperature ℃ | Surface tension mN/m | Standard dev. mN/m | Error % | Error clean % |
|---|---|---|---|---|
| 78.4 | 30.4 | 0.1 | 0.46 | 0.30 |
| 77.6 | 30.5 | 0.1 | 0.68 | 0.49 |
| 76.9 | 30.2 | 0.1 | 0.41 | 0.62 |
| 76.1 | 30.2 | 0.2 | 0.53 | 0.76 |
| 75.3 | 30.6 | 0.2 | 0.67 | 0.42 |
| 74.7 | 30.6 | 0.1 | 0.59 | 0.32 |

The maximum error value is 4.07% , in the clean case it is 2.08%.

### A.2.4 Sasolwax 6003 with additives

#### Sasolwax 6003 +1% Carbon Black

The results obtained are shown in Table A.19:

Table A.19: Sasolwax 6003 added with Black Carbon - Experimental surface tension data

| Temperature ℃ | Surface tension mN/m | Standard dev. mN/m | Error % |
|---|---|---|---|
| 127.4 | 24.6 | 0.1 | 0.47 |
| 122.9 | 25.0 | 0.1 | 0.03 |
| 119.7 | 25.1 | 0.1 | 0.45 |
| 115.6 | 25.4 | 0.1 | 0.31 |
| 113.7 | 25.4 | 0.1 | 0.79 |
| 111.6 | 25.6 | 0.1 | 0.53 |
| 109.8 | 25.8 | 0.1 | 0.20 |
| 108.2 | 25.9 | 0.1 | 0.22 |
| 107.6 | 26.0 | 0.1 | 0.02 |
| 106.2 | 26.1 | 0.1 | 0.06 |
| 105.4 | 26.2 | 0.1 | 0.24 |
| 104.6 | 26.2 | 0.1 | 0.04 |
| 103.6 | 26.2 | 0.1 | 0.20 |
| 103.3 | 26.4 | 0.1 | 0.48 |
| 102.7 | 26.4 | 0.1 | 0.34 |
| 102.1 | 26.5 | 0.1 | 0.57 |
| 100.8 | 26.4 | 0.1 | 0.13 |
| 99.0 | 26.5 | 0.1 | 0.19 |
| 97.9 | 26.6 | 0.1 | 0.08 |
| 97.6 | 26.8 | 0.1 | 0.60 |
| 95.7 | 26.9 | 0.1 | 0.51 |
| 94.3 | 26.9 | 0.1 | 0.17 |

Continue in the next page

Table A.19: Sasolwax 6003 added with Black Carbon - Experimental surface tension data

| Temperature ℃ | Surface tension mN/m | Standard dev. mN/m | Error % |
|---|---|---|---|
| 93.0 | 27.0 | 0.1 | 0.23 |
| 91.5 | 27.1 | 0.0 | 0.24 |
| 90.5 | 27.2 | 0.1 | 0.37 |
| 89.7 | 27.2 | 0.1 | 0.18 |
| 88.3 | 27.3 | 0.1 | 0.22 |
| 87.2 | 27.3 | 0.1 | 0.04 |
| 86.5 | 27.4 | 0.1 | 0.16 |
| 85.7 | 27.5 | 0.1 | 0.33 |
| 84.9 | 27.6 | 0.1 | 0.51 |
| 84.0 | 27.6 | 0.1 | 0.30 |
| 82.7 | 27.7 | 0.1 | 0.35 |
| 81.6 | 27.7 | 0.1 | 0.10 |
| 80.6 | 27.8 | 0.1 | 0.22 |
| 79.8 | 27.9 | 0.1 | 0.40 |
| 79.0 | 28.0 | 0.1 | 0.57 |
| 77.6 | 28.0 | 0.1 | 0.24 |
| 76.5 | 27.9 | 0.1 | 0.37 |
| 75.9 | 28.1 | 0.1 | 0.21 |
| 75.5 | 27.9 | 0.1 | 0.60 |
| 74.5 | 28.0 | 0.1 | 0.47 |
| 73.0 | 28.1 | 0.1 | 0.46 |
| 72.2 | 28.1 | 0.1 | 0.64 |
| 71.3 | 28.4 | 0.0 | 0.22 |
| 70.8 | 28.3 | 0.1 | 0.25 |
| 70.2 | 28.2 | 0.1 | 0.74 |
| 69.6 | 28.5 | 0.1 | 0.18 |
| 68.6 | 28.4 | 0.1 | 0.40 |
| 67.8 | 28.4 | 0.1 | 0.58 |

The maximum error value is 0.79%.

### Sasolwax 6003 +10% Stearic Acid

The results obtained are shown in Table A.20:

Table A.20: Sasolwax 6003 added with Stearic Acid - Experimental surface tension data

| Temperature ℃ | Surface tension mN/m | Standard dev. mN/m | Error % |
|---|---|---|---|
| 116.0 | 25.4 | 0.0 | 0.65 |

Continue in the next page

Table A.20: Sasolwax 6003 added with Stearic Acid - Experimental surface tension data

| Temperature ℃ | Surface tension mN/m | Standard dev. mN/m | Error % |
|---|---|---|---|
| 112.6 | 25.7 | 0.0 | 0.88 |
| 110.7 | 25.8 | 0.0 | 0.75 |
| 109.6 | 25.9 | 0.0 | 0.84 |
| 108.2 | 25.8 | 0.0 | 0.08 |
| 107.5 | 25.8 | 0.0 | 0.11 |
| 106.7 | 25.8 | 0.0 | 0.33 |
| 105.9 | 25.9 | 0.0 | 0.16 |
| 105.3 | 25.8 | 0.0 | 0.71 |
| 104.8 | 25.9 | 0.0 | 0.45 |
| 104.5 | 26.1 | 0.0 | 0.24 |
| 104.2 | 26.0 | 0.0 | 0.23 |
| 104.2 | 26.0 | 0.0 | 0.23 |
| 103.6 | 25.8 | 0.0 | 1.17 |
| 103.0 | 26.0 | 0.0 | 0.55 |
| 102.4 | 26.1 | 0.0 | 0.33 |
| 101.8 | 26.2 | 0.0 | 0.10 |
| 101.1 | 26.3 | 0.0 | 0.09 |
| 100.2 | 26.2 | 0.0 | 0.53 |
| 99.2 | 26.3 | 0.0 | 0.41 |
| 98.4 | 26.4 | 0.0 | 0.24 |
| 97.3 | 26.5 | 0.0 | 0.15 |
| 96.5 | 26.6 | 0.0 | 0.01 |
| 95.4 | 26.8 | 0.0 | 0.47 |
| 94.6 | 26.8 | 0.0 | 0.26 |
| 93.9 | 26.9 | 0.0 | 0.45 |
| 93.0 | 26.9 | 0.0 | 0.22 |
| 92.3 | 26.9 | 0.0 | 0.04 |
| 91.2 | 26.8 | 0.0 | 0.62 |
| 90.2 | 27.0 | 0.0 | 0.14 |
| 89.2 | 27.1 | 0.0 | 0.02 |
| 88.4 | 27.1 | 0.0 | 0.23 |
| 87.4 | 27.3 | 0.0 | 0.25 |
| 96.7 | 27.4 | 0.0 | 0.43 |
| 86.1 | 27.3 | 0.0 | 0.09 |
| 85.2 | 27.4 | 0.0 | 0.05 |
| 84.3 | 27.4 | 0.0 | 0.18 |
| 83.5 | 27.6 | 0.0 | 0.35 |
| 82.8 | 27.6 | 0.0 | 0.17 |
| 81.8 | 27.7 | 0.0 | 0.28 |
| 80.9 | 27.7 | 0.0 | 0.05 |
| 80.3 | 27.8 | 0.0 | 0.26 |
| 79.6 | 27.8 | 0.0 | 0.08 |

Continue in the next page

Table A.20: Sasolwax 6003 added with Stearic Acid - Experimental surface tension data

| Temperature ℃ | Surface tension mN/m | Standard dev. mN/m | Error % |
|---|---|---|---|
| 78.7 | 27.9 | 0.0 | 0.22 |
| 77.8 | 28.0 | 0.0 | 0.35 |
| 76.7 | 27.9 | 0.0 | 0.29 |
| 75.9 | 28.0 | 0.0 | 0.13 |
| 75.1 | 28.1 | 0.0 | 0.03 |
| 74.5 | 28.1 | 0.0 | 0.12 |
| 73.8 | 28.3 | 0.0 | 0.42 |
| 73.1 | 28.4 | 0.0 | 0.59 |
| 72.2 | 28.1 | 0.0 | 0.69 |
| 71.3 | 28.4 | 0.0 | 0.15 |
| 70.4 | 28.4 | 0.0 | 0.07 |
| 69.8 | 28.5 | 0.0 | 0.14 |
| 69.4 | 28.5 | 0.0 | 0.04 |
| 68.9 | 28.5 | 0.0 | 0.09 |
| 68.3 | 28.5 | 0.0 | 0.23 |
| 67.9 | 28.5 | 0.0 | 0.33 |

The maximum error value is 1.17%.

### Sasolwax 6003 +10% PEG

The results obtained are shown in Table A.21:

Table A.21: Sasolwax 6003 added with PEG - Experimental surface tension data

| Temperature ℃ | Surface tension mN/m | Standard dev. mN/m | Error % |
|---|---|---|---|
| 127.1 | 24.8 | 0.1 | 0.50 |
| 121.5 | 25.2 | 0.1 | 0.27 |
| 117.2 | 25.6 | 0.1 | 0.26 |
| 114.3 | 25.8 | 0.1 | 0.33 |
| 110.7 | 25.9 | 0.1 | 0.14 |
| 108.6 | 26.1 | 0.1 | 0.13 |
| 106.4 | 26.3 | 0.1 | 0.37 |
| 104.8 | 26.3 | 0.0 | 0.00 |
| 102.7 | 26.4 | 0.1 | 0.11 |
| 101.5 | 26.5 | 0.1 | 0.02 |
| 100.7 | 26.6 | 0.1 | 0.17 |
| 99.7 | 26.6 | 0.1 | 0.06 |
| 99.1 | 26.6 | 0.1 | 0.20 |

Continue in the next page

Table A.21: Sasolwax 6003 added with PEG - Experimental surface tension data

| Temperature ℃ | Surface tension mN/m | Standard dev. mN/m | Error % |
|---|---|---|---|
| 98.7 | 26.6 | 0.1 | 0.29 |
| 97.7 | 26.8 | 0.1 | 0.23 |
| 96.1 | 26.8 | 0.1 | 0.14 |
| 94.6 | 26.9 | 0.1 | 0.11 |
| 93.4 | 26.9 | 0.1 | 0.39 |
| 92.0 | 27.0 | 0.1 | 0.34 |
| 91.1 | 27.1 | 0.1 | 0.17 |
| 90.0 | 27.3 | 0.1 | 0.31 |
| 89.1 | 27.2 | 0.0 | 0.26 |
| 87.8 | 27.5 | 0.1 | 0.54 |
| 86.7 | 27.4 | 0.1 | 0.07 |
| 85.9 | 27.5 | 0.1 | 0.12 |
| 84.8 | 27.6 | 0.1 | 0.23 |
| 83.8 | 27.7 | 0.1 | 0.37 |
| 83.3 | 27.7 | 0.1 | 0.26 |
| 82.4 | 27.6 | 0.1 | 0.30 |
| 81.2 | 27.8 | 0.1 | 0.15 |
| 80.4 | 27.9 | 0.1 | 0.33 |
| 79.6 | 27.9 | 0.1 | 0.15 |
| 78.6 | 28.1 | 0.1 | 0.64 |
| 77.6 | 28.0 | 0.1 | 0.07 |
| 76.6 | 28.1 | 0.1 | 0.21 |
| 75.4 | 28.1 | 0.1 | 0.06 |
| 75.0 | 28.3 | 0.1 | 0.56 |
| 73.5 | 28.2 | 0.1 | 0.12 |
| 72.4 | 28.2 | 0.1 | 0.36 |
| 71.2 | 28.3 | 0.1 | 0.27 |
| 69.9 | 28.0 | 0.0 | 1.63 |
| 68.7 | 28.6 | 0.0 | 0.24 |
| 67.8 | 28.6 | 0.1 | 0.05 |

The maximum error value is 1.63%.

### Sasolwax 6003 +10% PECVA

The results obtained are shown in Table A.22:

Table A.22: Sasolwax 6003 added with PECVA - Experimental surface tension data

| Temperature ℃ | Surface tension mN/m | Standard dev. mN/m | Error % |
|---|---|---|---|
| 126.5 | 25.6 | 0.1 | 0.78 |
| 119.2 | 26.3 | 0.1 | 0.17 |
| 114.4 | 26.4 | 0.1 | 0.58 |
| 110.3 | 26.8 | 0.1 | 0.04 |
| 107.8 | 27.0 | 0.1 | 0.13 |
| 104.9 | 26.9 | 0.1 | 0.92 |
| 103.4 | 27.1 | 0.1 | 0.52 |
| 102.6 | 27.4 | 0.1 | 0.40 |
| 101.6 | 27.5 | 0.1 | 0.54 |
| 100.2 | 27.5 | 0.1 | 0.22 |
| 99.3 | 27.6 | 0.1 | 0.38 |
| 98.0 | 27.8 | 0.1 | 0.80 |
| 96.7 | 27.9 | 0.1 | 0.87 |
| 95.3 | 27.9 | 0.1 | 0.55 |
| 94.1 | 27.8 | 0.1 | 0.07 |
| 92.8 | 28.1 | 0.1 | 0.71 |
| 91.7 | 28.0 | 0.1 | 0.11 |
| 90.6 | 28.0 | 0.1 | 0.14 |
| 89.2 | 28.2 | 0.1 | 0.26 |
| 87.7 | 28.1 | 0.1 | 0.42 |
| 86.4 | 27.9 | 0.1 | 1.44 |
| 85.2 | 28.5 | 0.1 | 0.44 |
| 83.8 | 28.6 | 0.1 | 0.48 |
| 82.7 | 28.5 | 0.1 | 0.11 |
| 81.8 | 28.5 | 0.1 | 0.31 |
| 80.6 | 28.6 | 0.1 | 0.22 |
| 80.0 | 28.9 | 0.1 | 0.69 |
| 79.2 | 28.6 | 0.1 | 0.52 |
| 77.9 | 28.7 | 0.1 | 0.46 |
| 77.5 | 29.1 | 0.1 | 0.84 |
| 75.8 | 28.8 | 0.1 | 0.56 |
| 75.0 | 28.9 | 0.1 | 0.39 |
| 74.0 | 29.2 | 0.1 | 0.43 |
| 72.0 | 29.0 | 0.1 | 0.68 |

The maximum error value is 1.44%.

### Sasolwax 6003 +10% Aluminum

The results obtained are shown in Table A.23:

Table A.23: Sasolwax 6003 added with Aluminum - Experimental surface tension data

| Temperature ℃ | Surface tension mN/m | Standard dev. mN/m | Error % |
|---|---|---|---|
| 122.1 | 24.9 | 0.1 | 0.69 |
| 117.4 | 25.3 | 0.1 | 0.25 |
| 113.9 | 25.6 | 0.1 | 0.07 |
| 111.3 | 25.8 | 0.1 | 0.22 |
| 109.8 | 25.9 | 0.1 | 0.24 |
| 108.8 | 26.0 | 0.1 | 0.39 |
| 107.5 | 26.0 | 0.1 | 0.08 |
| 106.5 | 26.1 | 0.1 | 0.22 |
| 105.9 | 26.0 | 0.1 | 0.30 |
| 104.9 | 26.1 | 0.1 | 0.16 |
| 103.6 | 26.2 | 0.1 | 0.08 |
| 102.9 | 26.2 | 0.1 | 0.25 |
| 101.9 | 26.4 | 0.1 | 0.27 |
| 100.8 | 26.6 | 0.0 | 0.77 |
| 99.7 | 26.5 | 0.1 | 0.13 |
| 98.7 | 26.5 | 0.1 | 0.10 |
| 97.6 | 26.5 | 0.1 | 0.36 |
| 96.8 | 26.5 | 0.1 | 0.55 |
| 95.5 | 26.7 | 0.1 | 0.10 |
| 94.0 | 26.8 | 0.1 | 0.07 |
| 92.0 | 26.9 | 0.1 | 0.16 |
| 90.7 | 27.1 | 0.1 | 0.28 |
| 89.9 | 27.1 | 0.1 | 0.09 |
| 88.8 | 27.1 | 0.1 | 0.16 |
| 88.0 | 27.2 | 0.1 | 0.03 |
| 87.0 | 27.2 | 0.1 | 0.20 |
| 85.9 | 27.4 | 0.1 | 0.28 |
| 85.0 | 27.4 | 0.1 | 0.08 |
| 84.2 | 27.5 | 0.1 | 0.26 |
| 83.2 | 27.5 | 0.1 | 0.03 |
| 81.6 | 27.7 | 0.1 | 0.40 |
| 80.6 | 27.6 | 0.1 | 0.19 |
| 79.9 | 27.8 | 0.1 | 0.37 |
| 79.1 | 27.8 | 0.1 | 0.19 |
| 78.2 | 27.8 | 0.1 | 0.01 |
| 77.2 | 28.0 | 0.1 | 0.48 |
| 76.3 | 27.9 | 0.1 | 0.07 |
| 75.6 | 28.0 | 0.1 | 0.13 |
| 75.0 | 28.0 | 0.1 | 0.00 |
| 74.0 | 28.1 | 0.1 | 0.13 |
| 73.2 | 28.1 | 0.1 | 0.05 |
| 72.7 | 28.1 | 0.1 | 0.16 |

Continue in the next page

Table A.23: Sasolwax 6003 added with Aluminum - Experimental surface tension data

| Temperature ℃ | Surface tension mN/m | Standard dev. mN/m | Error % |
|---|---|---|---|
| 71.7 | 28.1 | 0.1 | 0.38 |
| 71.0 | 28.3 | 0.1 | 0.18 |
| 70.2 | 28.2 | 0.1 | 0.35 |
| 69.2 | 28.2 | 0.1 | 0.57 |
| 67.9 | 28.4 | 0.1 | 0.15 |

The maximum error value is 0.77%.

# Appendix B

# Rheometer Calibration

In order to show the reliability of the data obtained the calibration of the rheometer is done.

The characteristics of the fluid used in calibration are shown in Table B.1

| Thermo Fisher Scientific 082-5445-E2000 | |
|---|---|
| Dynamic viscisity @ 20°C | 1930 mPa s |
| Uncertainty | 2% |

Table B.1: Calibration fluid properties

The result of the test is shown in Figure B.1

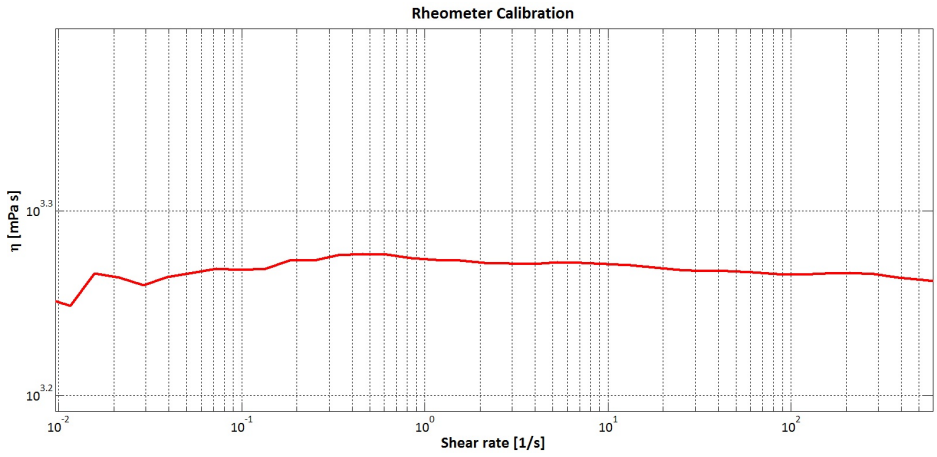


Figure B.1: Rheometer Calibration

# Nomenclature

$A_b$ burning area
$a_t$ thickness parameter
$B$ blowing parameter
$C_{B1}$ blowing correction coefficient
$C_f$ skin friction coefficient
$C_H, C_{H0}$ Stanton number with and without blowing
$c*$ characteristic velocity
$Fr$ heat transfer correction factor for surface roughness
$G$ local instantaneous mass flux
$G_{air}$ air mass flux
$H$ step height, $mm$
$h$ melt layer thickness, mm
$I_{sp}$ specific impulse
$I_{spvac}$ specific impulse in vacuum condition
$L*$ ratio of average combustion combustion chamber volume to average nozzle area

$M_w$ molecular weight of the alkane $C_nH_{2n+2}$
$\Delta m$ burned mass
$\dot{m_{ent}}$ entrainment component of mass flux from fuel surface, $kg/m^2s$
$\overline{\dot{m}_l}$ mass flow rate of liquid flowing through melt layer per unit width, $kg/ms$
$n$ carbon number
$n_0$ offset carbon number for the ABC prediction method
$O/F$ mixture ratio
$P_d$ dynamic pressure in the port, $Pa$
$R_ent$ entrainment parameter,
$R_f$ final port radii, $mm$
$R_i$ initial port radii, $mm$
$\dot{r}_{ent}$ entrainment component of the regression rate
$r_f$ fuel regression rate, $mm/s$
$\dot{r}_v$ vaporization component of the regression rate
$\dot{r}$ instantaneous regression rate, $mm/s$
$\overline{\dot{r}}$ time average regression rate, $mm/s$

$T$ temperature
$T_C$ chamber temperature
$T_m$ melting temperature
$t_b$ burn-out time, s
$x$ cartesian coordinate (streamwise direction) $mm$
$Y$ quantity predicted by the ABC method
$Y_0, Y_{\infty,0}$ ABC method parameters
$\Delta Y_0, \Delta Y_\infty$ ABC method parameters
$y$ cartesian coordinate (transverse direction) $mm$
$z$ cartesian coordinate (spanwise direction) $mm$

### Subscripts

$f$ fuel
$l$ liquid

### Greek symbols

$\alpha$ dynamic pressure exponent
$\beta$ thickness exponent
$\delta$ thermal thickness, $mm$
$\phi_{cl}$ non-dimensional classical regression rate parameter
$\mu$ viscosity, $milliPa - s$
$\rho$ density, $kg/m^3$
$\rho_s$ solid density
$\sigma$ surface tension, $milliN/m$

### Chemical formulations

$AB$ Ammonia Borane
$AlH_3$ Aluminum Hydride
$BH_3NH_3$ Ammonia Borane
$B_2O_3$ Boron Oxide
$EVA$ Ethylene-Vinyl Acetate
$GWP$ gel wax
$HDPE$ High Density Polyethylene Polymer
$HFI$ 60% isopropanol, 30%hexane, 10% tetrahydrofuran
$HTPB$ Hydroxyl Terminated Polybutadiene
$LAH$ Litium Aluminum Hydride ($LiAlH_4$)
$LiH$ Litium Hydride

$LP$ Liquid Paraffin
$MgH_2$ Magnesium Hydride
$NH_3$ Ammonia
$nAl$ nano Aluminum
$PBAN$ Polybutadiene Acrylonitrile
$PE$ polyethylene
$PECVA$ polyethylene co-vinyl-acetate
$PEG$ polyethyleneglykol
$PUF$ Polymeric Foam
$SEBS$ Styrene Polymer
$SP-1a$ Paraffin-based liquefying fuel
$SWP$ solid wax
$TiO_2$ Titanium Dioxide
$THF$ Tetrahydrofuran